Laura Marello

# Basin Architecture and Lithospheric Structure of the Barents Sea Region from Geophysical Modelling

Thesis for the degree of Philosophiae Doctor

Trondheim, June 2012

Norwegian University of Science and Technology
Faculty of Engineering Science and Technology
Department of Petroleum Engineering and Applied Geophysics

**NTNU – Trondheim**
Norwegian University of
Science and Technology

**NTNU**
Norwegian University of Science and Technology

Thesis for the degree of Philosophiae Doctor

Faculty of Engineering Science and Technology
Department of Petroleum Engineering and Applied Geophysics



ISBN 978-82-471-3644-7 (printed ver.)
ISBN 978-82-471-3645-4 (electronic ver.)
ISSN 1503-8181

Doctoral theses at NTNU, 2012:176

Printed by NTNU-trykk

*... to my family.*

# Acknowledgments

The PhD work was carried out at the Geological Survey of Norway (Norges Gelogiske Undersøkelse - NGU) in association with the Department of Petroleum Engineering and Applied Geophysics, NTNU (Norwegian University of science and technology, Trondheim). The supervisor was Jörg Ebbing (NTNU and NGU) and Laurent Gernigon (NGU) was co-supervisor.

The thesis is part of the project Petroleum-related regional studies of the Barents Sea region (PETROBAR) funded by Statoil and the Research Council of Norway (NFR) under the Petromaks programme.

§

*First of all I would like to thank my supervisor, Jörg Ebbing, who decide to take me under his wing and to guide me during this PhD. Thank you to give me the opportunity to make this experience to make me more "german organized" and independent. Thank you for the advices, for your time, for shearing your knowledge, for your patience and for your help to improve myself.*

*I own many thanks to my co-supervisor Laurent Gernigon, a source of inspiration and curiosity. Thank you to let me consult your private library. I am still impressed by the amount of references and books that I was getting every time I asked you a simple question. Thank you for all you taught me, for your time and, for the endless discussion.*

*I would like to express my gratitude to Odleiv Olesen to involve me in the "Continental Shelf" activities, to trust me and my work. Thanks for your interest in my project, for your inspiration and help.*

*Many thanks to Sofie Gradmann for guiding me "in to the deep". Thank you for adding the work in the Barents Sea to your long list of things to do. It was a nice support to share the office with you in these last months. I wish you soon reach this goal as well ;)*

*I express my gratitude to David Roberts, for his valuable help with English and scientific writing. I made treasure of your advices. Thank you also for all the references and for the valuable geological discussions.*

*Thanks to the PhD group (Cecile, Fjalar, Aziz, Albert) for shering this experience. Thank you for helping me facing difficulties, frustrations but also enjoying good satisfactions during these PhD years.*

*Thanks to the "Continental Shelf Geophysics" group and to NGU to be a scientific and creative international environment, thanks for all the seminars and discussions, source of stimulation during this PhD work. Thanks to NGU to support last months of my PhD.*

*Special thanks go to all the NGU and Trondheim friends that created a positive atmosphere around me and made my life in Norway enjoyable.*

*Thanks to Tomas Kjennerund and my new colleagues at Exploro that believe in my skills and gave me more time to finish my PhD.*

*Thanks to Carla Braitenberg who has been the initial link between Trieste (Italy) and NGU (Norway). I really think that without her I would have never started working with potential fields and I would have newer ended up in Norway.*

*Thanks to my Ex-Geo group in Trieste that shered with me the intrest in geology and that has always been an important support and link with Italy. Thanks to Manu and to all the friends that are in Italy for your psychological support that have been many times so important.*

*Difficult to find words to thank my family, if I reached this goal is thanks to your love and your support. Thanks to incorage me to always go forward and to sustain my choice to come in Norway even if that would take me far away from you.*

*Dulcis in fundo, thanks to Nicola. Thank you for making my life easier and enjoyable always, even in crazy busy time like this last months. Thanks for your patient, for your love for your neverending optimism. I really don't know how I could have done without you. I am glad that I have reached the end of the PhD. Now my free time is for you and Emil.*

*Trondheim, March 2012*
*Laura Marello*

Take a German, a French and an Italian,
put them far in to the North
and,
make them working in the cold Arctic...

This looks like the beginning of a joke, but is what really happens and it ends up in this work.

# Abstract

This thesis provided a new understanding of the lithospheric structural setting and anomalies observed in the greater Barents Sea.

The Barents Sea has been focus of attention for geological and economical reason since the 70ies-80ies. The crustal and lithospheric evolution of this area has been poorly understood and relatively challenging because it involved a large number of different processes. During its evolution, plate aggregation and orogenesis have been alternated with episodic rifting and magmatic events. The final result is the present day continental shelf area formed by a heterogeneous crust and continental mantle, dominated by structural highs, platforms and structural lows (grabens, half graben and large sag basins). Although the general structures have been well outlined, numerous problems have been encountered in understanding the structure and evolution of the basins and the crust and their relation with the geodynamic evolution. Moreover the offshore propagation of Timanian, Caledonian and Uralian structures are still disputed.

In this thesis, I have developed a new understanding of the lithospheric setting and properties of the Barents Sea using an integrated geophysical approach. The results have been obtained by combining gravity, magnetic and geoid potential fields with seismic, petrophysics and offshore observations. 3D magnetic anomalies inverse models have been developed first to define the distribution of magnetic crustal properties. The inversion results have been further integrated with 2D forward modelling and potential field analysis. The magnetic crustal units have been further refined by a 3D forward model which beside defining magnetic and density properties provided, major sedimentary interfaces, top basement, upper-lower crust boundary and Moho depth. Finally, thermal and compositional models have been constructed to constrain the nature of the lithospheric mantle.

The adopted integrated approach provides an enhanced regional understanding of the structure and devolution of the Barents Sea Four distinct Barents Sea basement types have been distinguished: Archaean-Paleoproterozoic, Timanian, Caledonian, and Uralian terranes. A distinction of the different allochthon nappes forming the Caledonian terranes is also proposed and a correlation with the onshore structures made. The crustal setting resulting from the models support the bifurcated extension model of the Caledonian into the western Barents Sea. The existence of a Svalbard micro-plate (Barentsia) has been identified as a thick and distinct crustal unit located in the northwest Barents Sea.

The southeastern Barents Sea results to be the extension of the Timan-Pechora basement terranes, that are traced further north in the North Barents Basin. The lithospheric mantle velocity anomaly under the East Barents Sea has been interpreted as a relict Paleo-Proterozoic craton accreted toward Paleo-Baltica during the Timanian event.

Thermal and compositional models of the lithospheric mantle provide also evidences of lithospheric-sublithospheric mantle interaction due to rifting and due to large magmatic events, as for example the magmatism on Svalbard and the opening of the North Atlantic.

# Contents

# Chapter 1

# Introduction

## 1.1 Thesis Objective

The innate curiosity of humanity has always pushed to exploration and discoveries. The more inaccessible and wild an area is, the bigger the challenge becomes. Exploration of the Arctic has a history that extends over more than 500 years and is still not finished today. Nowadays, the real challenges are below its surface and, within the area north of the Arctic Circle, the Barents Sea region is a focus of attention for economical, political and scientific reasons. The Barents Sea region encompasses the area of the Barents Sea shelf, the Svalbard archipelago, and the islands of Franz Josef Land and Novaya Zemlya, which lies in between the Atlantic ocean in the west, the Arctic ocean in the north, the Kara Sea and Timan-Pecora in the east and south-east and the Fennoscandian shield in the south (Fig. 1.1).

Hydrocarbon exploration in the Barents Sea has a long history. Mesozoic and Palaeozoic sediments are expected to have accumulated significant hydrocarbon quantities in the Barents Sea, where the petroleum potential has been proven with major discoveries (e.g Shtokmanovskoye, Kildinskoye, Skrugard, Havis, Norsel). In the Timan–Pechora region exploration started in the 1960s and led to the discovery of several oil fields (Fossum et al. 2001). In the Norwegian sector prior to the 1980s exploration activity included only seismic and early NGU aeromagnetic surveys, as drilling north of the 62$^{nd}$ parallel was not authorized

(Smelror et al. 2009, Olesen et al., 2010). During the last 25 years exploration in the Barents Sea increased and a substantial number of geological and geophysical data were acquired. Most of the actual knowledge is based on industrial seismic, potential field, and exploration well data. In addition, detailed information exists from continuously cored shallow boreholes on the Norwegian Barents shelf, and from several onshore studies on Svalbard, Franz Josef Land and Novaya Zemlya. Recently technological improvements (e.g. 3D seismic, high-resolution aeromagnetic surveys) provide a far better understanding of the sedimentary sequences, and deep seated basement structure (Smelror et al. 2009).

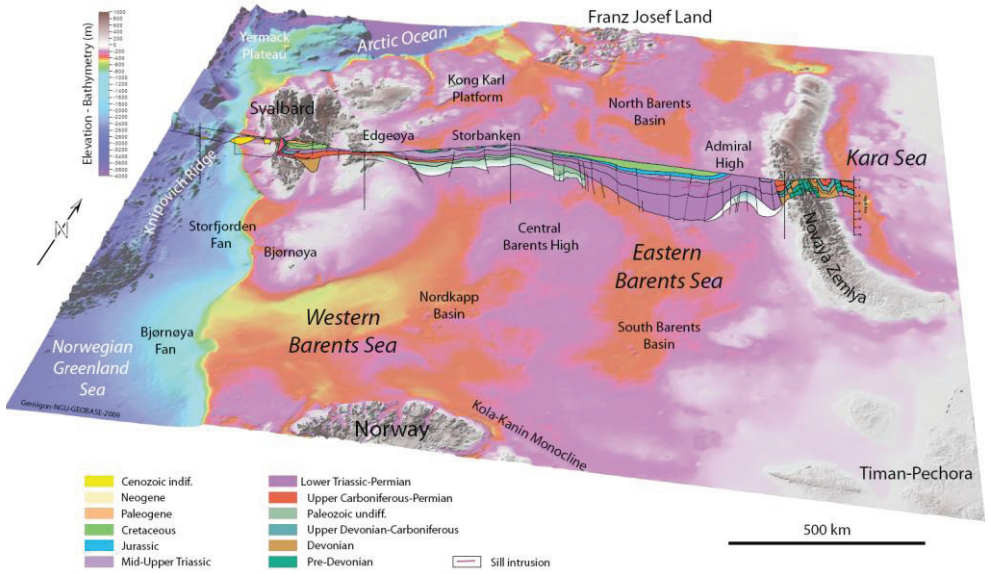


*Figure 1.1. Three-dimensional bathymetry of the Barents Sea continental shelf and regional geological profile (from Smelror et al. 2009)*

However, major parts of the region are still to be considered as exploration frontiers, and many gaps remain in our knowledge regarding the geological history and basin evolution in the Barents Sea. In that framework the PETROBAR project (Petroleum-related regional studies of the Barents Sea region) was initiated to improve our understanding of the fundamental, large-scale, processes behind sedimentary basin formation, the geological evolution of the Barents Sea region and the impact on the petroleum systems.

This PhD project is part of PETROBAR and its objective is to develop a new understanding of the regional lithospheric structure of Barents Sea region. The crustal scale study investigates the shape of the deep basins, the top basement, the Moho geometry and major lineaments. The Barents Sea setting is dominated by structural highs, deep basins and platforms. To describe the nature of the basement and to define the top basement have been main objectives of this work. The deep seated basement structures buried under the thick sedimentary packages in the basins are poorly defined due to problems encountered in using conventional seismic and due to the poor direct sampling. The interest in understanding the

shape of the sediments/basement boundaries is of geological and economical importance. It gives a better understanding of the geodynamic regional evolution and of the basin location and development. A further objective of the project was to link basin architecture with the underlying (deep) structures in the crust and upper mantle. Lithospheric mantle thermal and composition structure have been investigated and related with the geodynamic history of the region.

## 1.2 Contribution of thesis

To achieve the thesis objectives, an interdisciplinary approach is applied. Potential field methods as gravity, magnetic and geoid, are combined with seismic and petrophysical data. This has two major advantages: first local seismic, petrophysical and well data allow to constrain locally densities, magnetization and geometries and then to develop more reliable models and interpretation. Secondly the integration of local studies with regional potential fields guides the extrapolation of data and knowledge from the local study area to more remote and less explored parts. In this way, the potential field investigations offer a unique possibility to study the whole Barents Sea region at the crustal and mantle scale.

Different geophysical regional models have been developed during this work. Initially 3D inverse and 2D forward models have been designed, subsequently they have been included and further developed in a 3D forward model. In a final stage, the lithospheric mantle has been studied using thermal and petrological modelling.

The development of regional models has the advantage to study the Barents Sea shelf as a unique system. This provides new insights for the understanding of the link between the evolution of the eastern and western Barents Sea. Moreover, this offers the possibility to investigate the relation between shallow and deep structures as for example the link between basin settings and the crustal geometry and basement type, or the link between crustal setting and the structure of the lithospheric mantle.

The actual Barents Sea is the result of the aggregation of different crustal blocks. Their extension and the interaction with each other were not clearly defined previously. The thesis defines the major crustal structures and provides the distribution of petrophysical properties (e.g. densities, magnetic properties), which in turn, combined with studies of anomaly patterns, enables us to identify different crustal domains. In this context the thesis contributes to defining the link between the onshore and offshore terranes and outlines the possible extension of Timanian, Caledonian and Uralian orogenesis. The work provides new insight in the link between crustal inhomogeneities and geological terranes aggregated in the Barents Sea, and their link to the upper mantle structure.

In the thesis, the present structure of the upper mantle, as imaged by seismic tomography and analysed by potential fields, is linked to the geodynamic evolution of the Barents Sea. This confirms the existence of old cratons and the imprints of rifting and large magmatic events on the lithosphere.

## 1.3 Organization of the thesis

The thesis describes the methods, the area and the most relevant results. The gravity, magnetic and geoid potential field methods together with an introduction to their use use and different approaches of interpretation are introduced in **chapter 2.** The chapter presents also an overview of the potential field applications in the Barents Sea and focuses particularly at the top basement definitions.

**Chapter 3** outlines the geological evolution of the Barents Sea from the main orogenic events to the latest riftings and the evolution of the platform.

The study presented in **chapter 4** is from an article published in Tectonophysics (Marello et al. 2010). The paper is based on my own work with support from Jörg Ebbing and Laurent Gernigon. The main focus of the work was to investigate the magnetic properties of the entire Barents Sea basement and to define distinct magnetic domains. The study presents a magnetic field image analysis and both 3D inversion and 2D forward modeling to characterize the geometry of the top-basement and the distribution of magnetization and density. For the 3D inversion, the influence of the input parameters has been studied in detail. On a regional scale, the petrophysical parameters and not the geometry of the top-basement dominate the magnetic anomalies. The 2D models assisted in linking together the main crustal units of the Barents Sea, which are expressed by different magnetic basement characteristics. Each magnetic domain has been finally related with a common geological evolution.

**Chapter 5** presents a study submitted to Geophysical Journal International. The article is also based on my own work with support from Jörg Ebbing and Laurent Gernigon. The paper presents a 3D model that highlights the basement properties and crustal setting of the Barents Sea. The model results from the modelling of gravity and magnetic field anomalies and is based on a large number of seismic and petrophysical data. The study describes the availability and uncertainty of the individual data sets, and allows identifying different crustal blocks. Furthermore, a division of the Barents Sea in four major terranes is proposed: pre-Carboniferous basement, Timanian, Caledonian and Uralian terranes.

A manuscript ready for publication is presented in **chapter 6**. The study is based on my own work with the support of Sofie Gradman and Jörg Ebbing. In this chapter, I studied the lithospheric mantle in the Barents Sea. A recently developed thermal and compositional approach was applied to build models of the Barents Sea lithospheric mantle. The work investigates best coinciding composition and thermal structure with the observed geophysical data sets for the Barents Sea. The transition from the oceanic domain to the stable Barents Sea shelf was investigated as well as a shear-wave anomaly underlying mainly the eastern part of the Barents Sea. The origin of this fast upper mantle domain is studied with respect to composition, temperature and geometry. From the modelling, a two layered lithospheric mantle it is proposed beneath the Barents Sea with a more depleted upper part and a more fertile lower part. The formation of this layered lithosphere is discussed in the context of the geodynamic evolution of the Barents Sea.

The main conclusion of the PhD work are summarised and recommendations for further studies are provided in **chapter 7**.

The **appendix** contains a paper published in Geology (Gernigon et al 2011). The study shows an interpretation of locals, high resolution aeromagnetic surveys to detect salt diapirs. My contribution to this work is minor, and was mostly related to the definition of the deep structures along the presented profile, which has been included in the 3D model presented in chapter 5.

# Chapter 2

# Potential fields

Gravity and magnetic fields are each vector fields describing the forces that act at any point in space and time due to mass distribution in one case and magnetic distribution in the other. A vector field (F) can be characterized by its equipotential field lines, which are tangent at every point to the vector field.

If F is conservative could be defined as $F = \nabla\emptyset$. In this case F is said to be a *potential field* and $\emptyset$ is called *scalar potential* of F. In general the potential at any point is defined as the work necessary to move a unit mass or pole from an infinite distance to that point through the ambient field. Gravity and magnetic potential obeys to Laplace's Equation $\nabla^2\emptyset = 0$ in regions where there is no density and magnetic sources. Then at this condition they are harmonical and could be described mathematically by spherical harmonic (Blakely 1996).

A detailed description of potential field theory can be found in Blakely (1996), Gibson and Millegan (1998) or Jacoby and Smilde (2009) a.o.

In geophysical exploration the application of potential fields involves the measurement of the field over a target.

The measured potential field data must then be reduced to a more significant form, which represents its anomalies. The anomaly field describes the deviation from an assumed uniformity in physical properties: a perturbation from a normal, uniform, or predictable field. This in gravimetry and magnetometry is obtained by subtracting the theoretical, expected value from the observed one (Sheriff, 2006).

Anomalies are the effect of the shape, the properties and the location of the source body. Interpreting an anomaly means to define the source and to describe it with a geological model (Musset and Khan; 2000).

## 2.1 Gravity

**Historical note**

*The realization that the earth has a force of attraction surely must date back to our initial awareness that dropped objects fall to the ground, observations that first were quantified by the well-known experiments of Galileo Galilei around 1590. In 1687 Isaac Newton published his landmark treatise, Philosophiae Naturalis Principia Mathematica, in which he proposed (among others revolutionary concepts) that the force of gravity is a property of all matter, Earths included.*
*(Blakely 1996)*


*The contribution to gravity:*
*Galileo Galilei (1564-1642) = 2000 lire (former Italian currency) = 1.03 euro*
*Isaac Newton (1642-1727) = 1 pound (English currency) = 1.24 euro*

The force of gravity on the Earth is due to both to the mass of the Earth and to the centrifugal force caused by the Earth's rotation. The shape of the Earth is a product of the balance between gravitational and centrifugal accelerations. The combined accelerations create a slight flattening, forming an oblate spheroid. Mathematically it is convenient to refer to the Earth's shape as being an *ellipse of rotation (spheroid or ellipsoid)* that approximates the mean sea-level surface. The total potential of the spheroid is the sum of its self-gravitational potential and its rotational potential (Blakely 1996). The reference ellipsoid is defined and refined through the International Association of Geodesy (IAG) as the Geodetic Reference

System (e.g. Moritz, 1980). Total gravitational attraction at the reference spheroid is defined by the *Somigliana equation* (Heiskanen and Moritz 1967) and is commonly referred to as the *theoretical gravity* or *normal gravity* (Blakely, 1996).

Gravity measurements have to be reduced to obtain anomalies. This operation accounts for the theoretical gravity, elevation of the measurements above the ellipsoid, tidal effects (sun and moon), motion of the instrument and gravitational effects of an infinite sheet of intervening density (the *Bouguer slab*) and the effect of terrain in the vicinity of the measurement. The so obtained gravity anomaly (*Bouguer anomaly*) reflects density deviation in the crust and upper mantle from the value predicted (normal gravity) (e.g. Blakely, 1996; Nabighian et al. 2005).

On a gravity anomaly map, a gravity low indicates missing mass in the subsurface, while a gravity high indicates a mass surplus.

Gravity interpretation is the explanation of the gravity anomalies by modelling a density distribution. The gravity method is useful for finding buried bodies and structures that range from a few meters to hundreds of kilometres across. It can be applied in any case where the contrasts in subsurface densities produce a measurable anomaly. This depends mostly of the size of the anomaly and of the accuracy of measurement.

More in specific, a detectable anomaly exist just if there is a lateral variation in density. In the case of an infinite slab made by infinite small component masses there is no detectable anomaly, this because the sum of all the components at two distinct measured points is the same (Musset and Khan 2000).

Gravity measurements are made at a wide range of scales and geophysical purposes. Small structures like salt domes, magmatic intrusions, and faults are typical cases for study. Gravity interpretation has been used in oil exploration in any plays involving salt because of the large density contrast of salt (e. g. Huston et al., 2004), and for mapping the geometry and features of remote basins (e.g. basement geometry, high density lower crustal body, Moho shape; e.g. Pratsch, 1998; Jacques et al., 2003; Mendonca, 2004; Reynisson et al., 2009; Barrère et al., 2011). In the mining industry, the gravity technique is a common exploration tool to map subsurface geology and to help estimate ore reserves for some massive sulfide orebodies (e.g. Gibson and Millegan, 1998).

Improvements in gravimeters and in particular the advent of global positioning systems (GPS) during the past 25 years, have led to a marked improvement in the quality of gravity data. New high-resolution gravity surveys have become a prospect-level exploration tool that is particularly applicable in remote areas of transition zones that are otherwise inaccessible. Recently, moving-platforms gravity gradiometers have become available. With repeated measurements, variations can be observed both in changing structures (e.g. oil reservoirs and along fault zones). This provides scientists with new opportunities for studying dynamic processes and promise to play an important role in the future exploration (Nabighian et al., 2005).

## 2.2 Geoid

The *geoid* is the equipotential surface coinciding with the mean sea-level that is undisturbed by wind or tides. It has the property of being horizontal and at right angles to the direction of the vertical gravity acceleration everywhere. Especially near the Earth's surface, irregular distributions of masses warp the geoid so that it is not identical to the ellipse of rotation. It bulges above in the case of mass excesses (e.g. mountain ranges or buried high-density bodies) and is depressed over mass deficiencies (e.g. valleys or buried low-density bodies) (Blakely, 1996; Reynolds, 1997).

The determination of the geoid has attracted much attention within the discipline of geodesy. Both theoretical and practical problems are studied in order to improve the definition and accuracy of the geoid. More recently, a precise determination of the geoid at a regional scale has been demanded in order to transform Global Positioning System (GPS) derived heights to heights above mean sea-level (Featherstone, 1997; Eckman 1998). Many geoid solutions are now available at both global and regional scales. Recently a new model, EGM2008, has been released (Pavlis et al. 2008). This model is complete to spherical harmonic degree at 2159 order, and contains additional coefficients extending to degree 2190.

The vertical distance between the geoid and the normal ellipsoid is known as *geoid undulation* or *geoid height* and is positive if the geoid is above the ellipsoid (Turcotte and Schubert, 2002). Global geoid undulations are positive over zones with positive mass anomaly (excess of mass) while they are negative over areas with missing of mass.

The application and importance of the geoid in geophysics has been recognized for some time. Understanding the geoid and its undulation provides information about the deep-Earth mass density anomalies and near surface mass density anomalies. The use of the geoid in geophysics is described for example by Vanicek and Christou (1994), who discussed the relationships between the geoid and deep Earth mass density anomaly structure, strain and stress fields, tectonic forces, the isostatic state of oceanic lithosphere, Earth rotation, geophysical prospecting, and ocean circulation.

Following the advent of seismic mapping of mantle heterogeneities, the geoid has become a supporting role in seismic tomography to investigate plate tectonic features. For example tectonic plate motions and geoid anomalies have proven to be an important constraint in developing geodynamic models of 3-D mantle heterogeneity in terms of subducted slabs Hager (1984) or to estimate the depth to the low-density material supporting hot-spot swells (Monnereau and Cazenave, 1990).

More high resolution geoids models are used in lithospheric studies and their applications is increasing thanks to the development of new interpretations tools (e.g. Le Stunff and Ricard, 1995; Krapychev and Fleitout 2000; Afonso et al. 2008). Chapter 6 in this thesis is an example of geoid applications for lithospheric studies.

Dynamic applications of the geoid high have been also largely made as for example studies on glacial isostatic adjustment (e.g. Mitrovica et al., 2005).

## 2.3 Magnetics

Ninety percent of the Earth's magnetic field can be described as a *dipole field caused by a bar magnet* located in the centre of the Earth and almost aligned with the Earth's rotational axis (~10 degree deviation). The source of the Earth's internal magnetic field is believed to be caused by electrical currents in the Earth's fluid outer core. For exploration work, this field acts as the *inducing* magnetic field.

The remaining 10 % is related to the non-dipole field (Blakely 1996; Reynolds 1997). This part of the field is related largely to the crustal field and to a small portion by external (extraterrestrial) sources. The crustal component is associated with the magnetism of crustal rocks located at temperatures below the Curie temperature. This portion of the field contains both magnetisms caused by induction from the Earth's main magnetic field and from *remanent* magnetization. The external magnetic field is believed to be produced by interactions of the Earth's ionosphere with the solar wind. Hence, some *temporal variations* associated with the external magnetic field are correlated to solar activity (Lindsay, 1998).

The dipolar nature of the geomagnetic field necessitates taking some care in specifying the field's direction. The field is oriented vertically downward at the north magnetic pole, is horizontal (and pointing north) at the magnetic equator and points vertically upwards at the south magnetic pole. The definition of the main geomagnetic field at any point on the earth's surface requires the specification of the scalar magnitude of the total field vector (F), its orientation in dip (Inclination) and its azimuth (Declination) (Fig. 2.1).

The mathematical representation of the low spherical harmonic degree part of

**Historical note**

*De Magnete*, published in 1600 in England, is commonly recognized as the first publication of any sort which employs modern scientific principles. It is also the first treatise on geophysics. The author, William Gilbert (1540–1603), was considered to be England's most distinguished scientist during the Elizabethan era. He was physician to the queen, and he researched electricity and magnetism. His descriptions of magnets and of the Earth's magnetic field as a centered dipole are accurate, and the word *electricity* derives from his work. Gilbert alsobrought the Copernican theory of planetary motion to England.

A. Reid and R. I. Gibson

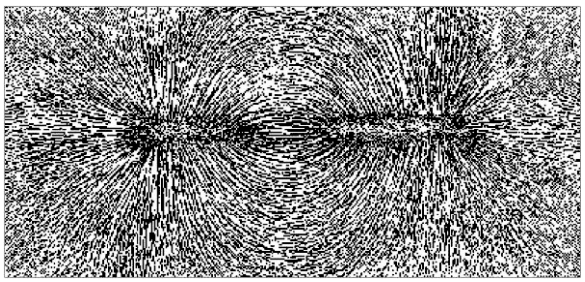

*"Magnus magnes ipse est globus terrestris"*
*(The whole earth is a magnet)*
*William Gilbert*

the geomagnetic field is determined by international agreement and is called the International Geomagnetic Reference Field (IGRF). The IGRF consist of Gauss coefficients through degree and order 10 because these low-order terms are believed to represent in large part the field of the earth's core. The geomagnetic field changes with time (e.g. secular variations, diurnal variation, effect of transient magnetic storms), and so must its mathematical description. The International Association of Geomagnetism and Aeronomy (IAGS) defines the IGRF for five-year intervals which are intended to represent the geomagnetic field for the following five-year period (Blakely 1996).

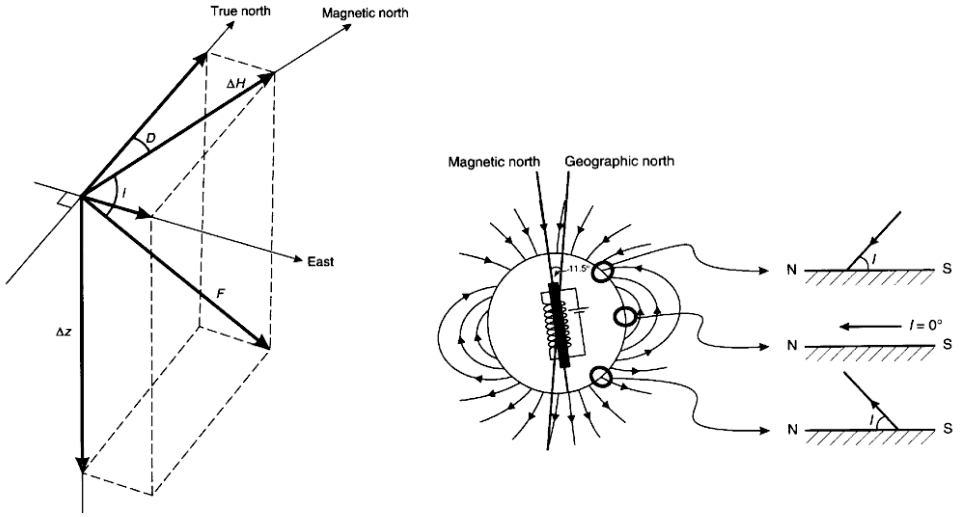


*Figure 2.1. (Left) Elements of the magnetic field: Inclination I, declination D, and total magnetic force F. (Right) Variation of the inclination with latitude (from Reynolds 1997).*

For geophysical applications the magnetic field anomaly is used, which corresponds mostly to the crustal field component then this last needs to be distinct from the total and external magnetic field components (Blakely 1996). The magnetic field anomaly is calculated from total field measurements by subtracting the magnitude of a suitable regional field, usually the IGRF model appropriate for the day of the survey. Then the residual is related to structures located in the Earth's crust (e.g. Blakely 1996; Paterson and Reeves 1985).

When a magnetic material is placed in a magnetic field, the material becomes magnetized and the external magnetising field is reinforced by the magnetic field induced in the material itself. This is known as *induced magnetisation*. When the external field is shut down, the induced magnetisation disappears, but some materials retain a permanent or *remanent magnetisation* and its direction will be fixed within the specimen in the direction of the (now disappeared) inducing field. Any rock in situ is then characterised by these two magnetisations, one induced and one remanent. The induced component will be parallel to the Earth's present field, while the remanent component may have any direction (Reeves 2009).

The magnitude of the induced magnetisation that crustal rocks acquire is proportional to the strength of the Earth's field in their vicinity, by a constant of proportionality, which is defined as the *magnetic susceptibility* of the rock. A comprehensive review of the magnetic susceptibility of rocks can be found in Clark and Emerson (1991) or Clark (1997). A wide range of values are found even within one rock type, but a simple classification would be that sedimentary rocks are usually non-magnetic, while metamorphic and igneous rocks have a wide range of magnetic susceptibilities. In particular dykes and sills of a mafic composition have a strong, remanent magnetisation.

Secondly the largest unknown is if behind the induced magnetisation there is any remanent magnetisation and how it is oriented. As well as depending on the geometry and properties of the magnetic crustal body, the shape of a magnetic anomaly is affected by the direction of the Earth's magnetic field, the direction and intensity of the body's remanent magnetism, and the orientation of the observations with respect to the Earth's field.

Magnetic measurements for exploration focus on variations in the magnetic field produced by lateral variations in the magnetization of the crust (Nabighian et al. 2005). The variation in magnetic rocks properties makes the identification of different lithotypes and the definition of their possible boundaries possible. This makes the magnetic field method applicable to a wide range of cases. Airborne and marine magnetic surveys are routinely acquired and used for petroleum and mineral exploration (Olesen et al. 2010).

The magnetic method has been largely use for mapping basement structures. More recently, new applications have increased the method's utility in all realms of exploration. Some practical examples include locating intrasedimentary faults, defining subtle lithologic contacts, mapping salt domes in weakly magnetic sediments, and better defining targets through 3D inversion (Gunn 1997; Nabighian et al. 2005). Chapter 4 and the appendix present examples how to interpret magnetic data for basement characterization and salt detection.

## 2.4 Potential field interpretation - Field analysis and modeling

The interpretation of gravity, geoid and magnetic anomalies is based on determining plausible positions and physical parameters for the geologic structures which cause these fields.

Conversion of the information which has been obtained by measurements into geologic models is a *non unique problem*. Many geophysical interpretations may fit the observed data. This statement could bring to the erroneous idea that potential field interpretations are not reliable and that no single interpretation is better in a geologic sense than any other. Different strategies are applicable to face the non uniqueness on the way to limit the number of possible solutions, and have been proven to produce significant, robust, and definitive results (e.g. Saltus and Blakely, 2011) (Fig. 2.2). Simplifying assumptions could be made about the source (e.g. petrophysical parameters are uniform throughout the body; the body is infinitely extended in one or more directions). An alternative approach would be to

attempt to find aspects about the source that are common to the entire infinite set of solutions (e.g. maximum depth of burial of any realistic source). Another way to produce more reliable potential field interpretation is using others methods to help constrain the source. If some geological information already exists for the area, then this should be used to help with the geophysical interpretation (Blakely, 1996; Reynolds, 1996).

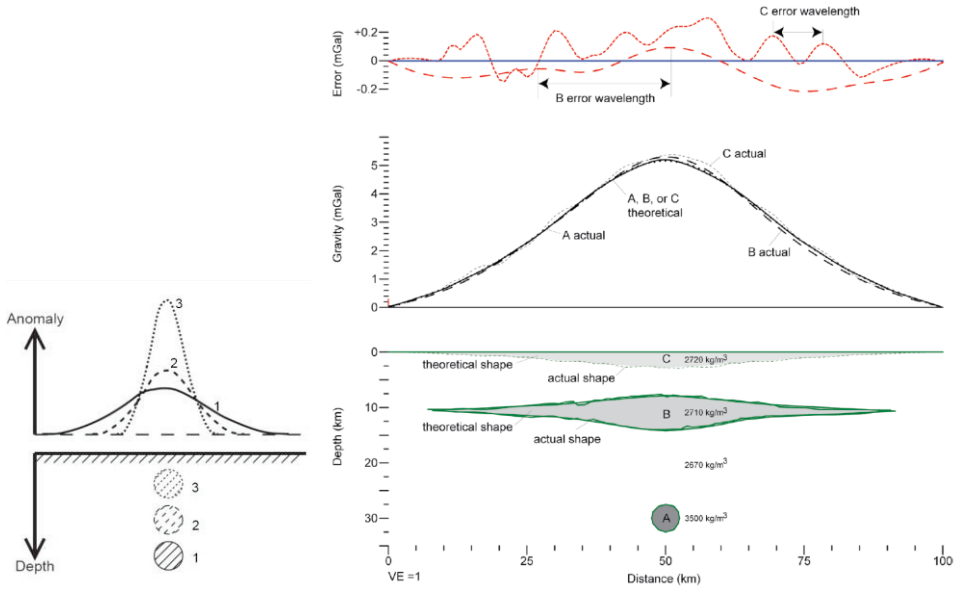


*Figure 2.2. (Left) The observed anomaly changes in width and amplitude depending on the burial depth, the shallower the source, the higher the amplitude of the anomaly, even though the body has the same shape and petrophysical contrast. This concept is the basis for separation of different anomalies. (Right) Results of two-dimensional calculation of the gravity effect of the source bodies (A, B, and C) depicted in the cross section view (bottom panel). When the smooth theoretical shape of each is used, the resulting calculated anomaly is identical in all three cases, as depicted by the smooth dotted lines labelled "A, B, or C theoretical." However, when the source bodies include some irregularity in their shape, as expected in the real world, the calculated gravity anomaly will differ from the smooth theoretical result (as shown by the "B actual" and "C actual" curves). The difference between the anomalies caused by the theoretical and actual shapes is shown by the "error" curves in the top panel. These differences will depend on the depth to source bodies as illustrated by the broad wavelength for the B error curve and the narrower wavelength for the C error curve (from Saltus and Blakely, 2011).*

Gravitational and magnetic potentials obey the principle of superposition: the gravity or magnetic potential of a collection of bodies is the sum of the effect of the individual bodies. This principle implies the need to relate the investigated feature with the related anomaly when interpreting potential fields. This process consists usually in the separation of different anomaly components and to isolate the anomaly object of the study from the others (Fig. 2.2). A separation commonly applied is between regional and residual anomalies (Spector and Grand 1970). The first reflect larger and usually deeper structures, the second correspond to smaller and shallower structures. The regional-residual separation is often a subjective process depending on the study purpose and is ultimately a matter of scale (Blakely, 1996).

Interpretation of potential fields can be distinguished in a qualitative and in a quantitative estimation of the sources parameters. The qualitative methods consist mostly of the observation of the anomaly properties to gain some preliminary information on source location or petrophysical parameters. The anomaly characteristics of interest are wavelength content, amplitude, shape, gradients, lineaments, dislocation and domains with similar characteristics. This information leads to a first indication of the source properties such as low or high density, or susceptibility, location (near surface/deep seated feature), possible dip and dip direction, possible strike (e.g. sills lineaments, faults), possible lateral offsets, or regional zonations (Reynolds 1996). To enhance these anomaly properties a large number of techniques exist, which are usually categorized as field analysis or field transformations. Mathematical operations such as convolution and correlation can filter the data, separate regional and residuals, field continuation and so on. Operations can be performed in the spatial or wave number domain. The most common field transformations are:

*Filtering* is the separation of the different wavelength components caused by sources of different size and depth (e.g. high-pass filter, low-pass filter).

*Derivatives:* first and second vertical derivatives emphasize shallower anomalies and can be calculated either in the space or frequency domains. These operators also amplify high-frequency noise, and special tapering of the frequency response is usually applied to control this problem (Nabighian 2005 and references in there). Many modern methods for edge detection and depth-to source estimation rely on horizontal and vertical derivatives (e.g. Blakely and Simpson 1986; Roest et al. 1992; Verduzco et al. 2004; Wijns et al. 2005).

*Upward and downward continuation:* data measured on a given plane can be transformed to data measured at a higher or lower elevation, thus either attenuating or emphasizing shorter wavelength anomalies. These analytic continuations lead to convolution integrals which can be solved either in the space or frequency domain (Blakely 1996; Nabighian 2005 and references in there).

*Reduction to the pole:* This method transforms the observed magnetic anomaly into an anomaly approximating measurements at the magnetic pole, where the magnetic field is vertical.

*Pseudogravity transformation:* Poisson's relation shows that gravity and magnetic anomalies caused by a uniformly dense, uniformly magnetized body are related by a first derivative. Baranov (1957) used this principle to transform an observed magnetic anomaly into the gravity anomaly that would be observed if the

distribution of magnetization were replaced with a proportional density distribution. The pseudogravity transformation is most commonly used as an interim step to several other edge-detection or depth-estimation techniques or in comparing with observed gravity anomalies (Nabighian 2005).

The quantitative phase in potential field interpretation can help quantify the depth, the shape, the size and the properties of the body which produced the anomaly. This information is obtained in two ways: first by *direct methods*, where the field data are interpreted to yield a physical model. The other is the *inverse method*, where models are generated and fitted against the observed data (Reynolds 1997).

Depth-to-source estimation techniques are diverse and estimate a first source parameter. The first early depth-to-source techniques were mostly of graphical nature and applicable only to single-source anomalies. In the 1990s, 3D automated depth-estimation methods began to appear and develop significantly. An overview of these methods is given by Nabighian et al. (2005).

A more complete estimate of the source parameters can be obtained through geophysical modelling. The modelling can be defined in 2D or 3D. In the first case the structures are defined along the profile and extend forward and backward. In some cases it is possible to specify the length of the extension and the azimuth. The more complex 3D modelling approaches have the advantage that shape and properties of the sources can be defined and changed in all three directions.

Both 2D and 3D models attempt to mathematically describe the complex geology. For that purpose a simplification is required in which the real geological situation is described by simple and elementary bodies. This permits defining simply formed models (sphere, mass-point, lines etc.) for which precise mathematical expression of the gravity/magnetic effect can be given. Alternatively the gravity/magnetic effect of more complicated models can be developed by approximating the complex geological geometry in a greater number of elementary bodies (cuboids, prisms, polyhedrons, layers). In this late approach the size and number of bodies that form the final model is a compromise between the real complex geology, the need to solve mathematical equations and the aim of the study.

In order to obtain a calculated model effect as close as possible to the observed, two approaches could be used. (a) *Inverse methods*: defined as an automated numerical procedure that defines one or more geometrical and petrophysical parameters from measured data and any prior information independent of the measured data (modified from Nabighian et al 2005). (b) *Forward methods:* in which an initial model for the sources is constructed based on geological and geophysical intuition. The model effect is calculated and compared with the observed anomaly, and model parameters are adjusted in order to improve the fit between the two anomalies. This three-step process of body adjustment, anomaly calculation and anomaly comparison is repeated until calculated and observed anomalies are deemed sufficiently alike (Blakely 1996).

All the techniques described above should ideally be combined in the interpretation of potential fields (Fig. 2.4). At the same time, it is important to use all available independent information in the interpretive process. Knowledge of the geologic and tectonic setting should be incorporated at each step of the modeling

process. Other geophysical data should be also incorporated to guide the modeling itself.

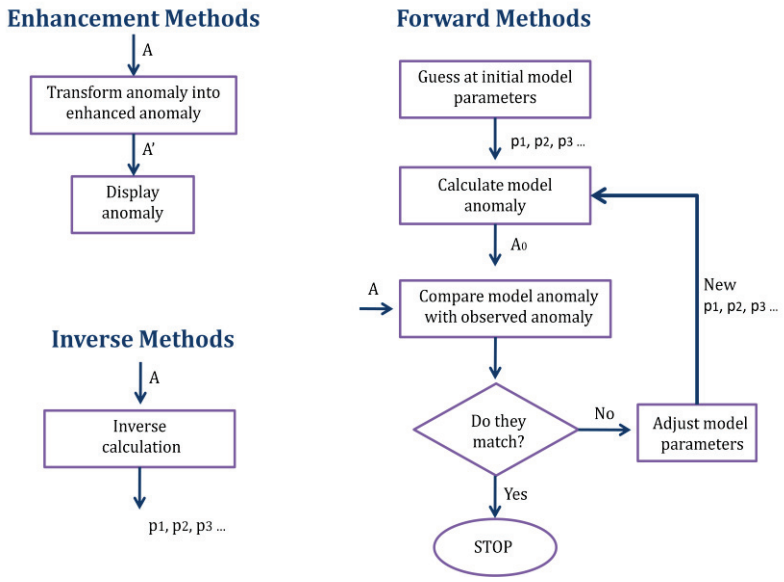


*Figure 2.4. Alternative techniques to interpret potential field data. Measured anomaly is represented by A, calculated anomaly by $A_0$ and transformed measures anomaly by A'. Parameters p1, p2, p3… are attributes to the source, such as depths, thickness, density or magnetisation (from Blakely 1996).*

The simultaneous use of different geophysical methods to build a model produces what is defined commonly as an integrated or combined model. Besides being constrained by independent information, models defined in this way have to satisfy simultaneously more than one geophysical observation (e.g. gravity, magnetic, seismic, electromagnetic). This approach limits the numbers of possible solutions. The integration of different geophysical methods is strategic for another reason. The same geological feature could be distinguished by some methods but at the same time might not produce a detectable contrast from another method (e.g. increase in seismic velocities is not always correlated with changes in magnetic properties). In this way the combination of different methods is efficient. For example, in potential field interpretation the geoid is more sensitive to deep structures (upper mantle), the gravity field to crustal thickness and structures, and the magnetic field to upper crustal bodies (e.g. shallower intrusion, faults).

## 2.5 Potential fields in the Barents Sea

Gravity and magnetic studies in the Barents Sea have a long history. The Norwegian North Polar Expedition (1893-1896) led by the Norwegian explorer Fridtjof Nansen provided the first database of the Barents Sea, including gravity

and density measurements. Since then a large number of surveys have been acquired in the region. Fig. 2.5 and 2.6 show the coverage of gravity and magnetic data for the Barents Sea.

Gravity and magnetic methods have previously shown much value for studying the Barents Sea. Some important results that have been obtained include the definition of continental-ocean transition, the mapping of the shape of the basins (top basement maps), the location of magmatic intrusions, the definition of salt structures, the location of faults and others structural lineaments, and distinction of crustal domains.

An example of gravity interpretation is given by Breivik et al. (1995), where the authors combine seismic mapping and gravity modeling and demonstrate the presence of a major rift basin with large accumulations of unmobilized salt (Ottar Basin). Grogan et al. (1998) used forward modeling of magnetic anomalies and seismic mapping to reveal the extent of the magmatic province in the offshore area to the south and east of Svalbard. Sills and dykes were identified within sedimentary sequences.

Applications on crustal studies were provided shows by Skilbrei (1995) who combined aeromagnetic, gravity, well and seismic data to locate the crystalline basement in the Southwestern Barents Sea. Fichler et al. (1997) presented a gravity study of the entire Barents Sea in which they show the importance of satellite data for regional structural mapping using image enhancement techniques.

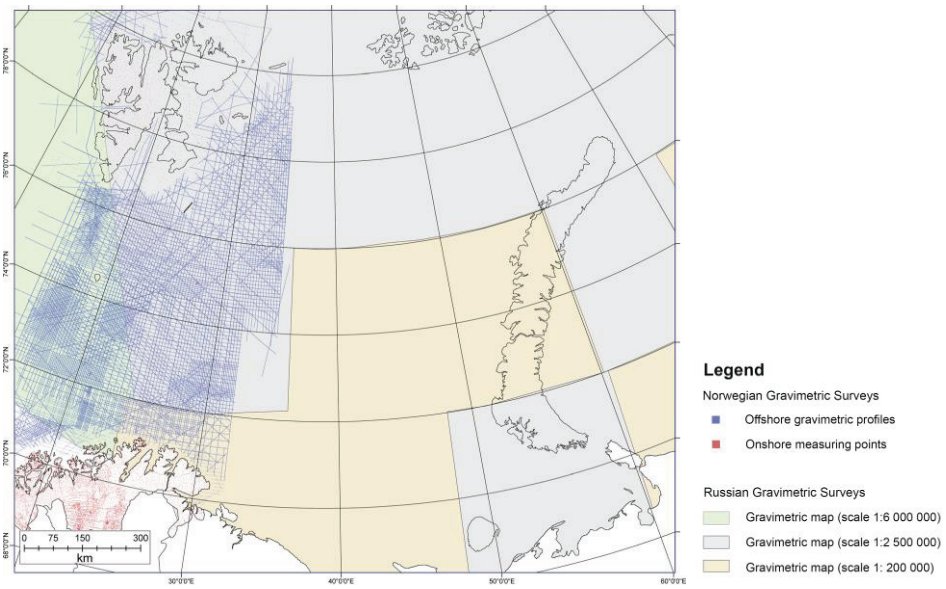


*Figure 2.5. Map of the gravity data sources. For the western Barents Sea, this map shows the station density and the ship-tracks along which gravity has been measured. For the eastern Barents Sea, the distribution of map-sheets is shown (Smelror et al, 2009; Werner et al. 2011).*

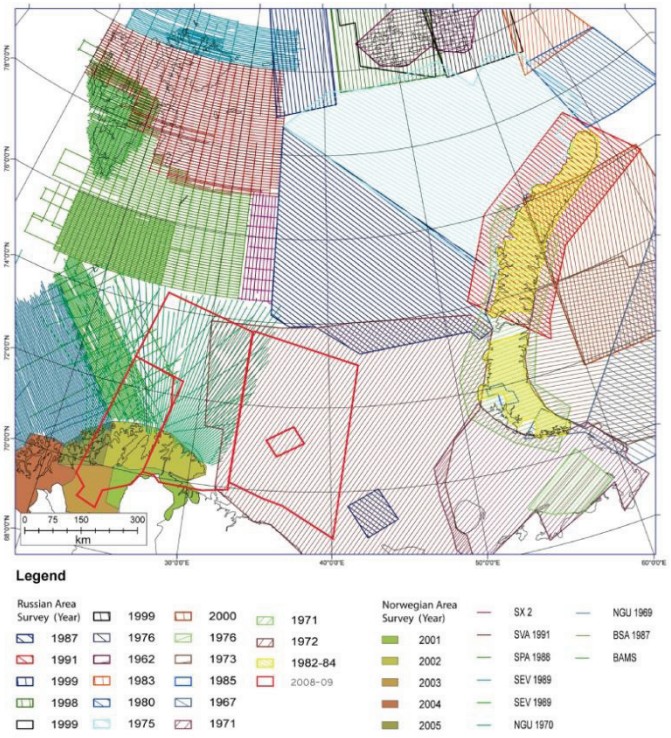


*Figure 2.6. Overview of the aeromagnetic surveys in the Barents Sea (Smelror et al, 2009; Werner et al. 2011)). Additional high-resolution surveys are displayed in the red frames (redrawn after Olesen et al. 2010).*

A large numbers of combined gravity and seismic models have been developed by Breivik et al. (1999; 2002; 2003; 2005) and provide crustal structure and density distributions along 2D profiles in the western Barents Sea. Ebbing et al (2007) presented an interpretation of the gravity anomalies in the Barents Sea by using 3D isostatic density modelling. The results provided crustal and mantle density distribution for the entire Barents Sea and underline differences between the East and the West Barents Sea shelf.

Recently, a new understanding of the offshore Caledonian terrane extension was provided by Barrère et al. (2009, 2011) using integrated 2D and 3D potential field models. Crustal geometries, densities and basement magnetic properties have been also given in their study for the western Barents Sea.

## 2.6 Integrated models and top basement ambiguities

Integrated modelling can be a powerful tool if the used data are carefully evaluated. For example the identification of the top basement in the Barents Sea is ambiguous. Conventional seismic data have certain limitations when dealing with the deepest parts of the basins. In the deep Barents Sea basins, the sediments are strongly affected by compaction and consequently the acoustic impedance is reduced and consequently the top basement difficult to resolve with seismics.

Another problem in basement imaging is associated with the presence of evaporites and carbonate layers.

The efficiency of integrated modelling is a powerful tool, but to be such require a careful check on the compatibility of the data introduced in the model as constrain. Below I discuss definitions of the top basement to clarify how to face the problem of evaluation and comparison of existent data sets during modelling.
Despite this, a variety of top basement models are available for the Barents Sea (e.g. Barrère et al. 2011; Ritzmann et al. 2007; Gramberg et al. 2001; Johansen et al. 1992; Skilbrei et al. 1991). To avoid misinterpretation when using integrated models, the definition of basement needs to be clarified. Different definitions of basement are found in the literature (e.g. Goussev and Peirce, 2010; Sheriff 2006):

1. **Geologic basement** is the surface beneath which sedimentary rocks are deposited, extending downward to the Moho boundary. In many places the rocks are igneous and metamorphic, granitized, or highly folded rock underlying sedimentary rocks (Neuendorf et al.2005; Sheriff 2006).
2. The **magnetic basement** is the upper surface of extensive heterogeneous rocks showing relatively large magnetic susceptibilities compared with those of sediments; often but not necessarily coincident with the "geologic basement" defined above (Neuendorf, Mehl and Jackson, 2005).
3. **Gravity** or **density basement** is where a very significant vertical density contrast exists (modified from Sheriff, 2006).
4. The **acoustic basement** is the deepest more-or-less continuous seismic reflector; often an unconformity below which seismic energy returns are poor or absent. Also called seismic basement (Sheriff 2006).
5. **Petroleum economic basement** is the surface below which there is no current exploration interest, even though some sedimentary units may lie deeper (Sheriff 2006).
6. **Electrical basement** is the surface below which resistivity is very high so that variations below this surface do not affect electrical survey results significantly (Sheriff 2006).

It should be noted that the locations of the top basement obtained with different methods may not coincide with one another. For example the geological and acoustic basements are not necessarily the same: if the impedance contrast is too low the seismic method will not be able to define the surface. Magnetic and seismic basements can be structurally close or coincident, or can be very different. For example, the top of tight carbonates can be defined by seismic data, but is not characterized by high magnetic properties. On the other hand, if there is no velocity contrast between the lowermost sediments and basement, the basement itself is unlikely to show a clear acoustic reflector but the magnetic contrast can be high (for example deep buried sediments with densities similar to basement).

In the integrated forward model presented in chapter 5 I define the top basement using the geological concept. This required in some case the review of previous top basement interpretations. For example Riphean metasediments (1400-800 Ma) of the Timanian-Pechora Basin are seismically distinguished from the crystalline basement underneath but considered as part of Timanian basement in the presented model (See chapter 5).

# Chapter 3

# Geodynamic Evolution and Tectonic Setting of the Barents Sea

## 3.1 The Barents Sea

The Barents Sea area is part of the Arctic region and is bounded by two passive margins defining a lithospheric transition between the Norwegian-Greenland Sea to the west and the Eurasian Basin to the north. Towards the East, the Barents Sea is delimited by Novaya Zemlya and in the south by the Baltic Shield (North Norway and Northwest Russia).

The actual Barents Sea shelf consists of complex structural features including platform areas, and basement highs and lows, and is the final result of a multiphase geodynamic evolution. Several orogenic phases have affected the structural framework (e.g. Johansen et al. 1992; Fichler et al. 1997; Gudlaugsson et al. 1998; Henriksen et al. 2011).

At the present-day, major differences are recognised in the Barents Shelf (Fig. 3.1). The East Barents Sea is dominated by a broad, elongated, deep megabasin, whereas the southwestern Barents Sea is characterised by a shallow platform and narrow grabens and half-grabens (Fig. 3.2). The northwestern and most of the

central Barents Sea form a widespread platform area (Johansen et al. 1992; Worsley, 2006; Henriksen et al. 2011).

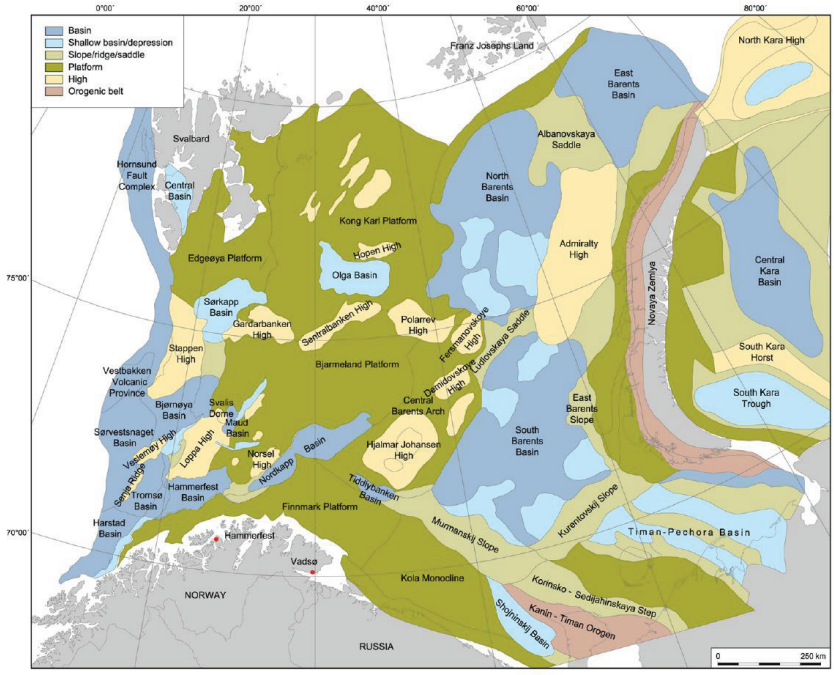


*Figure 3.1. Main structural elements of the Barents Sea (Henriksen et al. 2011)*

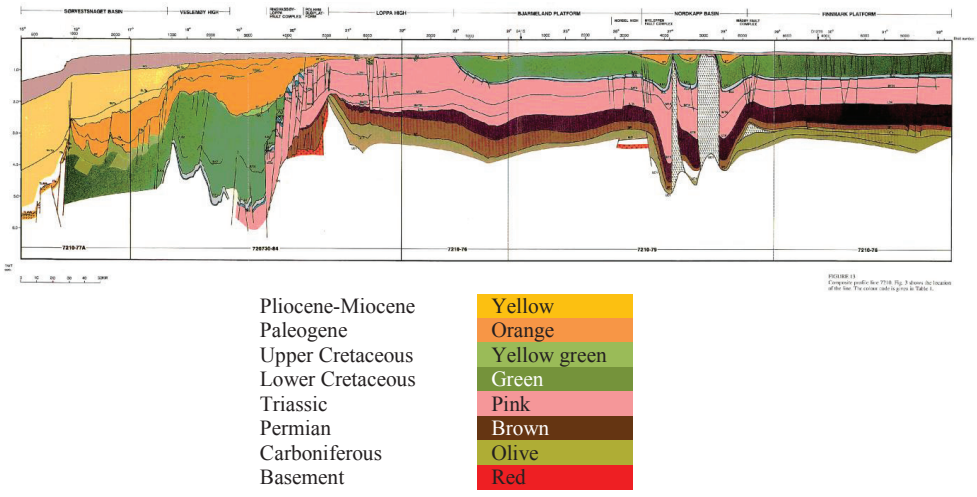


*Figure 3.2. Composite profile showing the major sedimentary structures of the western Barents Sea. On the western side of the profile, the thick sedimentary succession of Cretaceous and Cenozoic age is the consequence of Atlantic rifting leading to breakup between the Barents Sea and Greenland. In the eastern and central part, the Cenozoic formations are relatively condensed, and the southwestern Barents Sea consists mostly of a large Triassic platform locally affected by extension and halokinesis (Gabrielsen et al. 1990).*

Although the regional setting and the overall evolution of the Barents Sea have been described in many publications, the origin of many structures remains unclear. For example, the evolution of the Early Palaeozoic basins, the offshore extension of the main orogenic belts, the old plate boundaries, the composition of the crust, the locations of major magmatic intrusions, the dynamics of evaporate bodies and the formation of the megasag East Barents Basin are controversial issues. This chapter does not aim to contribute to the ongoing debate but to summarise the general ideas and concepts proposed for the tectonic and geodynamic evolution and setting of the Barents Sea.

## 3.2 Major collision phases

The Barents Sea is part of the Eurasian plate (Fig. 3.3). Its configuration is the result of the interaction between three main tectonic plates (Baltica, Laurentia and Siberia) during the last 500 Ma.


*Figure 3.3. The actual setting of the Eurasian plate. The red circle indicates the location of the Barents Sea.*

### 3.2.1 From Proterozoic extension to Timanian orogeny

During Neoproterozoic time the megacontinent Rodinia was involved in a major regime of extension, rifting and plate separation which gave birth to several smallers continents such as Baltica, Siberia, Laurentis and Avalonia. Baltica was separated from other continents by large marine areas, including the Iapetus Ocean between Baltica and Laurentia (North America, Greenland, Scotland and Northern Ireland), the Ærir Sea between Siberia and Baltica, and the Tornquist Sea between Baltica and Avalonia (the southern areas of England /Ireland and Parts of Western Europe) (Fig. 3.4). In one interpretation, refined paleomagnetic data suggest that Baltica was possibly lying in an inverted position in the Late Neoproterozoic (Torsvik et al. 1992; Torsvik et al. 1996) (Fig. 3.4).

The actual northeastern margin of Baltica in Mid to Late Riphean time (1000-635 Ma; Tonian and Cryogenian time in the International Stratigraphic Chart), was dominated by crustal extension leading to initiation of a rifted passive margin and oceanic system in which sediments were accumulating. Parts of these formations are observed onshore in Finnmark and Northwest Russia (Roberts and Siedlecka, 2002).

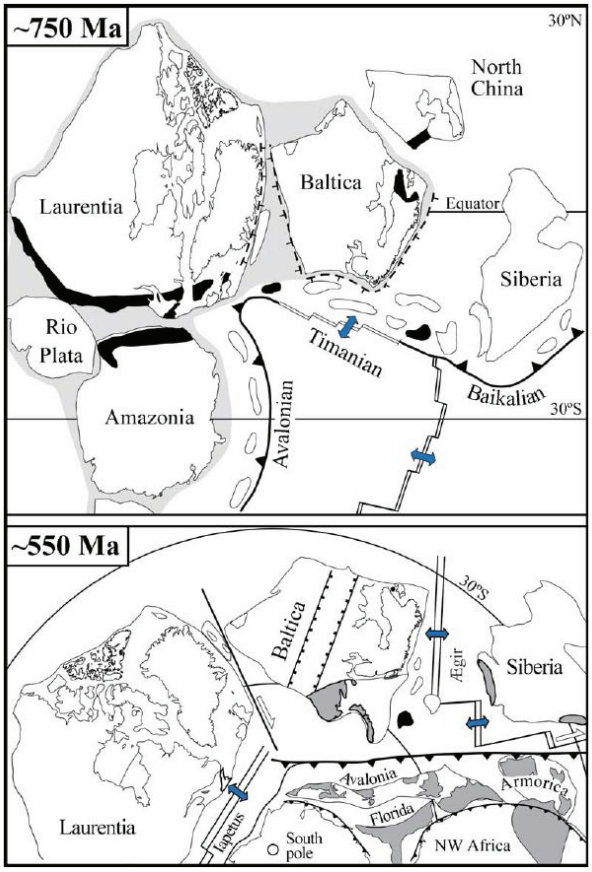


*Figure 3.4. The postulated early position of Baltica and surrounding terranes. At about 750 Ma ago, proto-Baltica was still attached to Laurentia, which was in turn attached to the South American terranes. The dispositions of Avalonian, and Timanian/Baikalian island arcs are modelled on the peri-Pacific system of today (Cocks and Torsvik, 2005). Black shaded areas-Grenvillian-Sveconorwegian-Kiabaran c. 1 Ga mobile belt. Below, Equal Area Polar Projection at about 550 Ma, modified after Hartz and Torsvik (2002), when the southern Iapetus Ocean was in existence, and when a rift-trench-strick-slip regime was initiated in the northern Iapetus (Ægir Sea). This led to an independent extension between Baltica and Laurentia. Grey areas represent the Timanian-Baikalian-Avalonian-Cadomian-Pan African mobile belt (from Cocks and Torsvik, 2005).*

A change of the tectonic regime from extensional to a compressive, active regime occurred in the *Vendian* (635-542 Ma, Ediacaran in the International Stratigraphic Chart), initiating the Timanian orogeny (Fig. 3.4, Schatsky, 1935; Getsen, 1987). During latest Precambrian to Early Cambrian time, a collage of Riphean to earliest Vendian ocean floor and island arc magmatic rocks, sedimentary assemblages, felsic to mafic plutons and blocks of crystalline basement rocks were involved in a substantial contractional collision in which complex terranes accreted against the northeastern margin of Baltica (Roberts and Siedlecka, 2002) and were united to form a much expanded terrane area in Lower Palaeozoic time (Cocks and Torsvik, 2005).

Timanian terranes today extend over a strike distance of 1800 km from the Timan Range in Northwest Russia via the Rybachi and Sredni Peninsulas of northern Kola to the northeastern part of Varanger Peninsula in Finnmark, Northeast Norway (Fig. 3.5, Roberts and Siedlecka, 2002). The lithostratigraphic successions exposed on land in the NW-SE-trending Timan-Varanger Belt lie unconformably upon the high-grade, polymetamorphic, Archaean to Palaeoproterozoic crystalline complex of the Fennoscandian (Baltic) Shield. The deeper parts of the old oceanic system are now largely concentrated in the Pechora Basin in Russia (Fig. 3.5). Deep drillholes through the Pechora Basin have penetrated pre-Palaeozoic oceanic tholeiites, subduction-related island arc volcanites and diverse plutonic bodies in the distal parts of the oceanic basinal domain (Gee et al. 2000; Roberts and Siedlecka, 2002).

This Proterozoic deformation associated with the Timanides includes fold structures and associated metamorphic fabrics. These are mostly NW-SE trending, SW-verging folds and NE-dipping cleavages or, locally, schistosities. At the southeastern end of the Timan-Varanger Belt, the NW-SE Timanian structural trend swings into near parallellism with the roughly N-S trend of the central and southern Urals (Puchkov 1997; Roberts and Siedlecka, 2002).

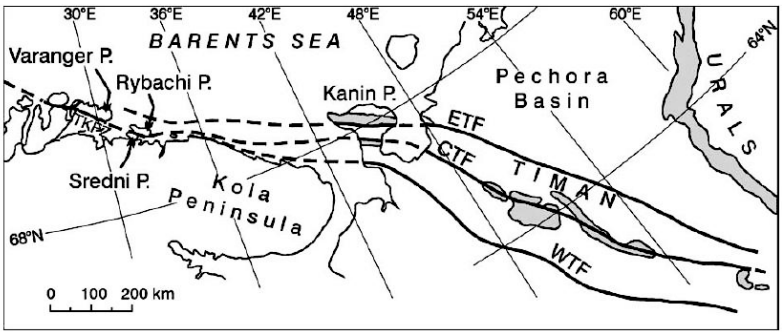


*Figure 3.5. Outline map of the Timan-Varanger Belt. CTF- Central Timan Fault, ETF-East Timan Fault, WTF-West Timan Fault, TKFZ-Trollfjorden Komagelva Fault Zone. P-Peninsula. The grey shading indicates the main areas of Neoproterozoic rock outcrops.*

Timanian terranes are known to exist under the Timan-Pechora Basin, southern Novaya Zemlya and parts of the Barents Shelf. However, their full extent and significance in the Arctic are still poorly constrained ((Olovyanishnikov et al.

2000; Roberts and Siedlecka, 2002; Pease and Scott 2009;). There is a general consensus that the basement of both the Timanian Pechora Basin and the East Barents Sea basin mainly comprises crust accreted to the East European Craton during the Late Neoproterozoic Timanide Orogeny (e.g. Gee and Pease, 2004 and references in therein).

### 3.2.2 Caledonian: Baltica and Laurentia collision

The major Iapetus Ocean began to contract in Early Ordovician time (Fig. 3.6a) and by the Early-Mid Silurian had more or less ceased to exist. At that time, Baltica began to collide with and subduct beneath Laurentia. The impact between the two plates resulted in the formation of the Caledonian mountain chain (the Caledonides), which extended from Scandinavia and Greenland as far north as Svalbard (e.g. Cocks and Torsvik, 2005; Roberts, 2003), and southwestwards into Britain, Ireland and NE Canada and the USA (the Appalachians). Consolidation of the two plates gave rise to the continent Laurussia (Fig. 3.6c)

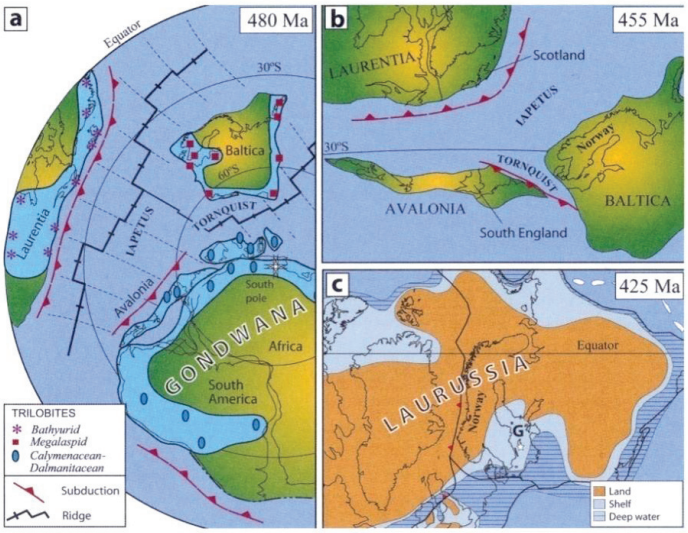


*Fig. 3.6. (a) Early Ordovician (480 Ma) reconstruction based on palaeomagnetic data from the various plates that existed at this time (e.g. Gondwana, Baltica, Laurentia). Gondwana extended from the South Pole to the Equator, Baltica was located at intermediate to high southerly latitudes (separated by the Tornquist Sea), whilst Laurentia was located close to the equator. The Iapetus Ocean and the Tornquist Sea were at their widest at this time. (b) Late Ordovician (455 Ma) reconstruction of Laurentia, Baltica and Avalonia. The Iapetus Ocean was shrinking rapidly at this time and the Taconian orogeny developed along the margin of eastern Laurentia. (c) Silurian (425 Ma) reconstruction, in which Baltica and Avalonia have collided with Laurentia and thereby formed Laurussia. The Iapetus Ocean had then closed (Torsvik and Steinberger, 2008.*

Four principal compressive and possibly transpressive events have been recorded in different parts of the Caledonian mountain belt.

- *Finnmarkian* (Late Cambrian - Early Ordovician)
- *Trondheim* (Early Ordovician)
- *Taconian* (Mid-Late Ordovician)
- *Scandian* (Mid Silurian- Early Devonian).

The *Finnmarkian* and *Trondheim* events involved scenarios of subduction with contraction/accretion between Baltica and/or an adjacent microcontinent and Iapetan arcs. Obduction of ophiolotes and primitive arcs also occurred at this time, onto either a microcontinent or, in some interpretations, Laurentia. The *Taconian* is also an arc-accretion, tectonothermal event, but it occurred along the margin of the Laurentian plate, remote from Baltica. The later *Scandian* event culminated approximately 420-400 Ma ago, and represented the closure of the Iapetus Ocean. It involved rapid subduction of the Baltican margin beneath Laurentia to depths exceeding 180 km and equally rapid exhumation (Van Roermund and Drury 1998; Terry et al. 2000; Van Roermund 2009).

The Baltica-Laurentia collision produced a progressive telescoping of the Baltoscandian passive margin and shelf successions, as well as exotic, oceanic and arc terranes derived from the Iapetus Ocean, and their eastward translation onto Archaean and Proterozoic crystalline complexes of the Fennoscandian Shield (Roberts and Gale, 1978; Torsvik et al. 1996; Roberts, 2003; Gee et al 2005, 2006). In many thrust sheets, slices of Precambrian crystalline basement have been incorporated into the developing orogen (Roberts and Gee 1985).

### 3.2.3 Caledonide orogen in the Barents Sea

The western Barents Sea has been strongly influenced by the Caledonide orogen. Caledonian terranes are observed onshore in Scandinavia and extend farther north Bjørnøya, Svalbard and possibly even as far as Franz Josef Land (e.g. Cocks and Torsvik 2005, 2011).

In the *Finnmark area*, the autochthonous Fennoscandian Shield rocks (Palaeoproterozoic and Archaean crystalline complex) are overlain unconformably by a thin Neoproterozoic sedimentary cover and then by a series of Caledonian nappes and thrust sheets. These allochtonous terranes are subdivided into a distinctive tectonostratigraphy comprising : Lower, Middle, Upper and Uppermost Allochthons (e.g. Roberts and Gee 1985; Roberts, 2003; Siedlecka *et al.* 2004; Gee et al. 2006; Gee et al. 2008 Fig. 3.7).

Taking Norway as a whole, the rocks composing the *Lower Allochthon* are Neoproterozoic to Silurian successions originally deposited in platformal palaeogeographic environments.

The *Middle Allochthon* is a predominantly metasedimentary unit that represents accumulation on the Baltoscandian outer margin and includes dolerite-intruded Neoproterozoic sandstones, some high-grade metamorphic compexes, and Precambrian crystalline nappes (Strand and Kulling, 1972; Andreasson et al. 1998; Gee at al., 2008).

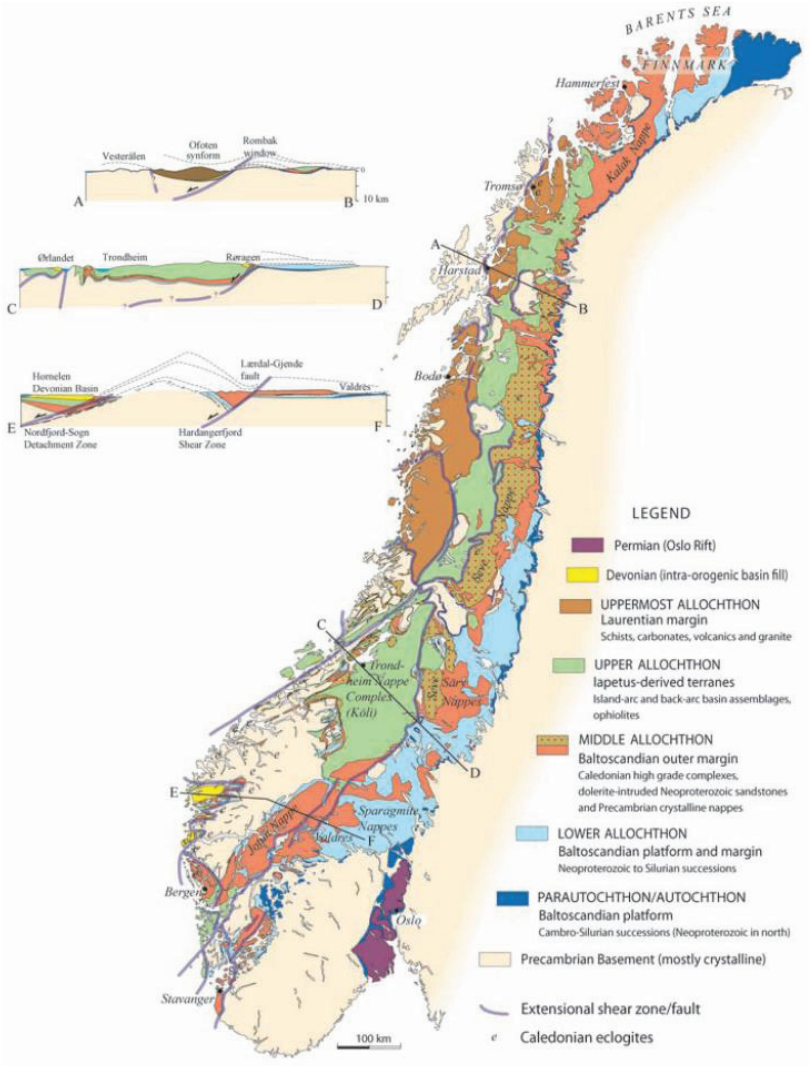


*Figure 3.7. Simplified tectonostratigraphic map of the Scandinavian Caledonides (from Gee et al. 2008)*

The *Upper Allochthon* represents remnants of oceanic crust (ophiolitic), including diverse magmatic arc and marginal basin associations from unknown locations within or peripheral to the Iapetus Ocean (e.g. Gale and Roberts, 1974; Gee, 1975; Stephens and Gee, 1985, 1989; Pedersen et al. 1988; Roberts 2003).

The *Uppermost Allochthon* is composed of more exotic elements, inferred by many to have affinities with Laurentia (Stephens and Gee, 1989; Roberts et al. 2007).

In northernmost Norway, on Varanger Peninsula, the thrust front of the Caledonide orogen truncates Timanian structures that continue nearly 2000 km southeastwards to the foreland of the Urals. Northwards from the Barents Sea coast of Finnmark, the character of the Caledonide Orogen is canceled by Late Palaeozoic and Mesozoic sedimentary basins.

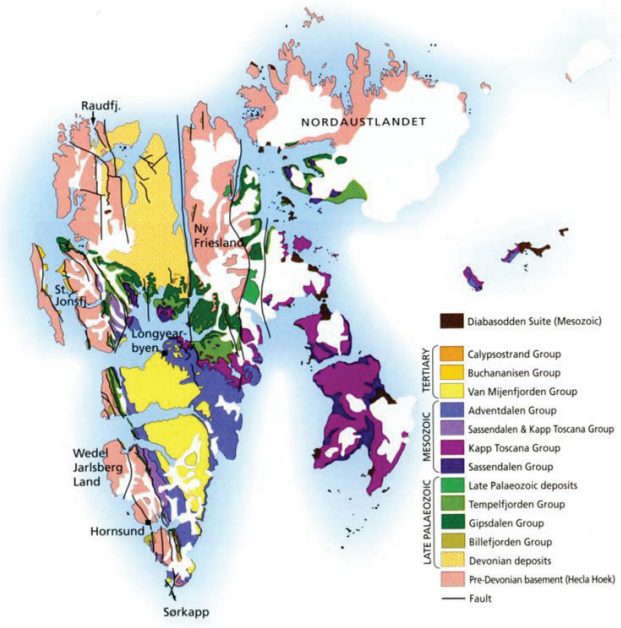


*Figure 3.8. Geological Map of Svalbard (Ramberg et al. 2008)*

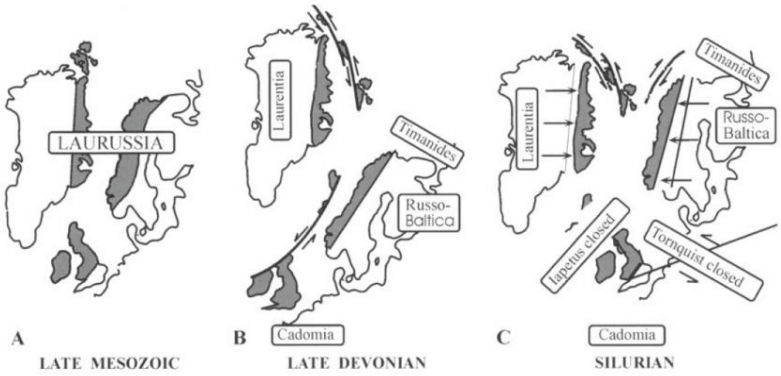


*Figure 3.9. Late Mesozoic reconstruction of the North Atlantic Caledonides; (A) an alternative hypothesis for the tectonic evolution, (B) from Harland (1997), and (C) from Gee and Page (1994). (From Gee and Teben'kov, 2004).*

The basement in *Svalbard* has been defined under the term "Hecla Hoek", which is taken to include all pre-Carboniferous rocks (Harland 1997; Fig. 3.8). Most authors agree that three blocks can be distinguished and formed the margins of Laurentia in Precambrian and Early Palaeozoic times, and were united with each other and the rest of the shelf during the development of the Caledonides in Silurian times (Cocks and Fortey 1982; Torsvik et al. 1996; Hartz and Torsvik 2002; Gee and Teben'kov 2004; Gee et al. 2006). Although marked contrasts between Svalbard's provinces have been recognised, defining the boundaries

between the different blocks has been controversial (e.g. Harland, 1997; Gee and Treben'kov, 2004). Moreover, Gudlaugsson et al. (1998) proposed that the eastern Svalbard province is part of a crustal microblock which they named the *'Barentsia craton'*.

Different hypotheses for Caledonian terrane assembly on Svalbard have been proposed (Gee and Page 1994; Harland 1997; Gee and Teben'kov, 2004; Fig. 3.9).

Harland (1985, 1997) envisaged large sinistral fault movements (around 1000 km) to explain the geological differences between the three main units and their aggregation (Fig. 3.9b). Gee and Teben'kov (2004) reviewed the pre-Caledonian location of Svalbard and argued that it represents a continuation of the northeast Greenland Caledonides, and that this part was ruptured by transform faults during the Devonian period (Fig. 3.9c).

On *Franz Josef Land*, pre-Carboniferous basement rocks have been found in the Nagurskaya borehole (Dibner 1998 and references therein). There, Precambrian successions (Ediacaran, 635-542 Ma) were found to be deformed and metamorphosed in greenschist facies, most likely during a late-Caledonian deformation event (Devonian-Carboniferous boundary). However, late-Timanian deformation has been also proposed, but this remains doubtful (Dibner 1998; Gee et al. 2006).

On *Bjørnøya* (Bear Island), Neoproterozoic basement is unconformably overlain by Late Devonian sedimentary rocks and Mid Carboniferous to Triassic carbonates. The pre-Devonian stratigraphy of Bjørnøya shows a close similarity with that of Northeast Greenland (Smith 2000) and it has been proposed that Bjørnøya was part of Laurentia (Smith and Rasmussen, 2008).

The trends of Caledonian structures in the Barents Sea are buried under a thick cover of Late Palaeozoic and younger sediments and have been considered for a long time to coincide with the trends of the younger extensional basins (e.g. Gudlaugson et al. 1998; Gabrielsen et al 1990). At the western Barents Sea margin and on Svalbard, N-S trends are dominant. These change gradually towards the south and become NE-SW oriented in the southwestern Barents Sea and in Finnmark (e.g. Doré et al. 1995; Fichler et al. 1997; Roberts and Lippard 2005). The influence that pre-existing thrusts have in the localisation of younger extensional faults has been documented in many rift basins worldwide, particularly where deep seismic reflection data are available (Dengo and Røssland 1992 and references therein). Nevertheless, recent new aereomagnetic data question the correlation between the orientation of Caledonian structures and the location of Late Palaeozoic basins (Gernigon et al. 2007; Gernigon and Brönner, 2012).

Tracing the *extension of the Caledonian* nappes from northern Norway into the offshore areas of the Barents Sea is still controversial. The classification of the thrust sheets and their offshore prolongation, especially for the Upper and Uppermost Allochthons can be considered a key to understanding the location of the Baltica-Laurentia suture offshore. Different approaches have been used to solve this enigma, but the location of the Caledonian terranes and tracing the boundary between Baltica and Laurentia has proved difficult. Roberts and Olovyanishnikov (2004) have summarised the different interpretations proposed for the plate boundaries (Fig. 3.10).

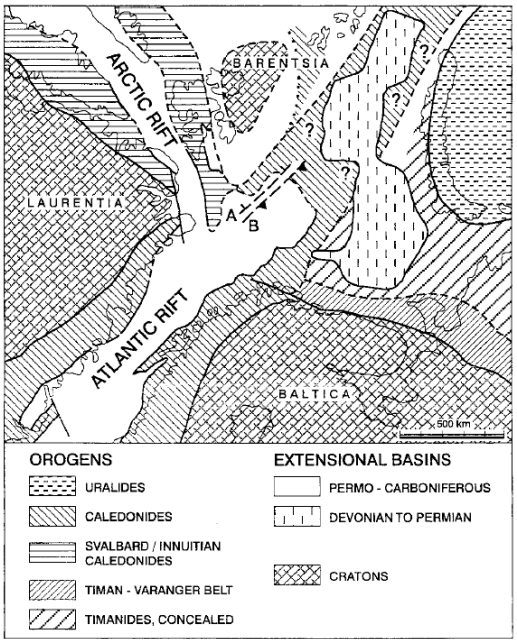


*Figure 3.10. Regional palaeotectonic setting in Late Permian time, modified and simplified from Gudlaugsson et al (1998), with small additions, showing the NE and NW branches of the Caledonides, and the distribution of the Timanide and Uralide orogens (from Roberts and Olovyanishnikov (2004). The question marks are those of Fichler et al. (1997) who regarded these particular areas of the Barents Sea as being dominated by Timanide trends. The dashed lines with tags, marked A and B, are as follows: A, Approximate trace of a zone of SE-directed thrusting, interpreted as a possible Caledonian suture (Gudlaugsson et al. 1987); B, Approximate trace of an interpreted SE-dipping Caledonian suture zone (Breivik et al. 2002). The dotted line passing between the Barentsian microplate and Franz Josef Land is part of an inferred Caledonian suture, according to Gee et al. (2000); this is believed to link up, across the Barents Sea, with the North Norwegian Caledonides.*

Harland and Gayer (1972) believed that the Caledonides swung sharply eastwards, paralleling the north coast of Kola, effectively transposed upon the Timanian trend. Siedlecka (1975) preferred a solution where the Finnmark Caledonides continued in a northeasterly direction across the Barents shelf into the sea area between Franz Josef Land and northern Novaya Zemlya, separating a Barents craton to the northwest (later called Barentsia; Gudlaugsson et al. 1998) from a Pechora craton (part of Baltica) to the southeast. In her model, Siedlecka also recognised a branch of the Caledonides extending towards western Svalbard, reflecting an inferred triple junction of pre-Iapetus Ocean rifting origin.

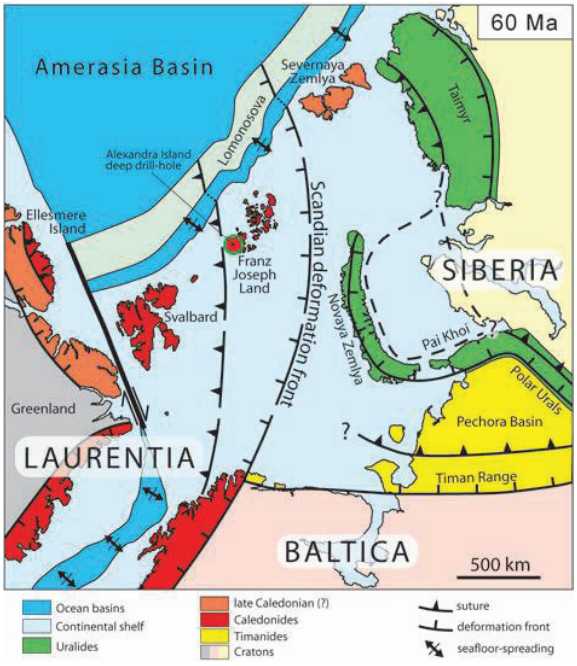


*Figure 3.11. Arctic Caledonides, showing the relationships between the Caledonides, Timanides and Uralides and the cratons of Laurentia, Baltica and Siberia at the time of opening of the North Atlantic Ocean and the Eurasian basin (from Gee et al. 2008).*

In other interpretations, both Ziegler (1988) and Nikishin et al. (1996) favoured a northwestward swing of the Caledonian grain, linking up with the Innuitian fold belt via the Caledonide terranes on Svalbard. Over the years, abundant seismic and refined, potential field data have tended to support Siedlecka's (1975) view of a bifurcation of the Caledonides (Gudlaugsson et al. 1987, 1998; Doré 1991; Johansen et al. 1994; Fichler et al. 1997; Breivik et al. 2002; Fig. 3.10). Although favouring this bifurcate model, Fichler et al. (1997) restricted the northeasterly trending branch of the Caledonides to the SW Barents Sea, noting that NW–SE-trending gravity highs cause the NE–SW trend to terminate in central areas of the Barents Sea.

From the same area of the SW Barents Sea, Gudlaugsson et al. (1987) reported deep-seismic reflection profiles that revealed a pattern of reflections consistent with E- to SE-directed thrusting at middle and lower crustal levels. It was speculated that this W- to NW-dipping feature might represent the main Caledonian suture, an interpretation supported by Doré (1991). More recently Breivik et al. (2002, 2005) presented OBS data from roughly the same part of the SW Barents Sea, which in their interpretation denote the existence of a SE-dipping Caledonian suture between Barentsia and Baltica (Fig. 3.10). More recent studies based on the integration of geophysical data, have revieved the concept of a unique Caledonian arm and Caledonian suture. Gee et al. (2000, 2006, 2008), for example, have suggested that a possible suture extends from the Scandinavian Caledonides

northwards through the Barents Sea between eastern Svalbard (Kvitøya) and Franz Josef Land (Fig. 3.11).

Ritzmann and Faleide (2007b) investigated the offshore continuation of Caledonian structures into the western Barents Sea. They interpret the crustal unit to the west of the Loppa High as fragments of Laurentia, and the Loppa High as representing the collision zone between Baltica and Laurentia. Barrère et al. (2011), however, locate the boundary between Baltica and Laurentia west of Loppa High and propagating northwards between Svalbard and Franz Josef Land.

Ritzmann and Faleide (2007b) investigated the offshore continuation of Caledonian structures into the western Barents Sea. They interpret the crustal unit to the west of the Loppa High as fragments of Laurentia, and the Loppa High as representing the collision zone between Baltica and Laurentia. Barrère et al. (2011), however, locate the boundary between Baltica and Laurentia west of Loppa High and propagating northwards between Svalbard and Franz Josef Land.

Recent models based on new high-resolution aeromagnetic data have proposed a tectonic scenario in which arc-shaped Caledonian nappes swing anticlockwise from a NE-SW orientation close to the Varanger Peninsula and reorientate to a clear NNW-SSE/NW-SE trend across the Nordkapp Basin and the Bjarmeland Platform (Gernigon and Brönner, 2012). This model does not support any north eastward prolongation of the Caledonides towards the eastern Barents Sea but suggest a lateral escape and flow of the nappes in the southwestern Barents Sea in late Caledonian time.

### 3.2.4 Uralian: Laurussia and Siberia collision

After the Caledonian event, another orogenic episode affected the eastern part of the Barents Sea. In Early Carboniferous time, transpressional reactivation of the faults initiated a major tectonic change and the closure of the Uralian Ocean by eastward subduction under the Siberian craton (e.g. Puchkov, 2002; Cocks and Torsvik, 2006) (Fig. 3.12).

The subduction and subsequent collision between the Laurussian continent (Baltica, Laurentia, Avalonia and fragments of the Rodinia continent) and western Siberia contributed to the generation of the supercontinent *Laurasia* (Laurentia, Baltica, Siberia, Kazakhstania, North China, and the East China cratons). The active margin phase propagated northwards and reached the eastern Barents Sea in the Late Carboniferous to Early Permian. The continent-continent collision culminated in the latest Permian-earliest Triassic and created the Ural mountain chain with its younger northern extension, Novaya Zemlya (Johansen et al. 1992; Faleide et al. 1993; Otto and Bailey 1995; Torsvik and Cocks 2004). The north Urals truncate the grain of the NW-SE trending Timanides and swing northwestwards into the Pai-Khoi–Vaigach–Novaya Zemlya fold-and-thrust belt (Puchkov 1997; Gee et al. 2006). Evidence for the continuation of the classical Uralide Orogen northwards into the Barents shelf and eastwards to Taimyr has been proposed by many authors (e.g. Bogdanov et al. 1996; Gee et al. 2006).

The largest structures in the East Barents Sea reflect arcuate shape of Novaya Zemlya and are generally attributed to the Uralian deformation (Korago et al. 2004). The major structural elements of the Novozemelsky fold belt (Fig. 3.13) are striking parallel on the island (Korago et al. 2004).

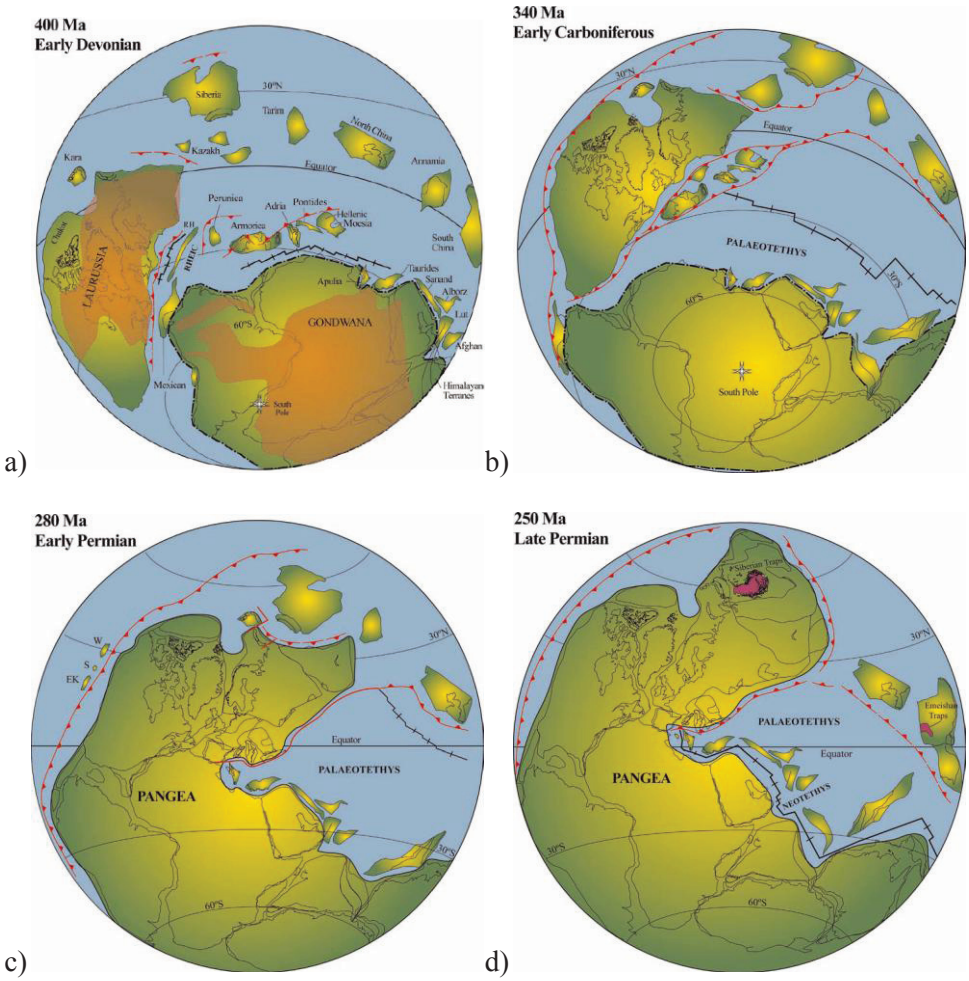


*Figure 3.12. Palaeozoic reconstruction of the Southern Hemisphere (a) Early Mid-Devonian (Emsian, 400 Ma), showing the Old Red Sandstone continents in Laurussia and Gondwana; terrane names are labelled. The outline of the Rheno-Hercynian (RH) Terrane is arbitrary. (b) Early Carboniferous (Tournaisian, 340 Ma) reconstruction. (c) Early Permian (Asselian, 280 Ma), extensive glacial deposits (not shown) covered much of the Southern Hemisphere. W: Wrangellia–Alexander Terrane; S: Stikinia Terrane; EK: Eastern Klamath Terrane. (d) Permo-Triassic boundary (250 Ma) showing the flood basalts in Siberia and China. Spreading centres are shown as black lines, subduction zones as red lines with ticks, and transform faults as red lines with no extra ornament. The alternately dashed and dotted black line marks the limit of the 'core' Gondwana (after Cocks and Torsvik, 2006).*

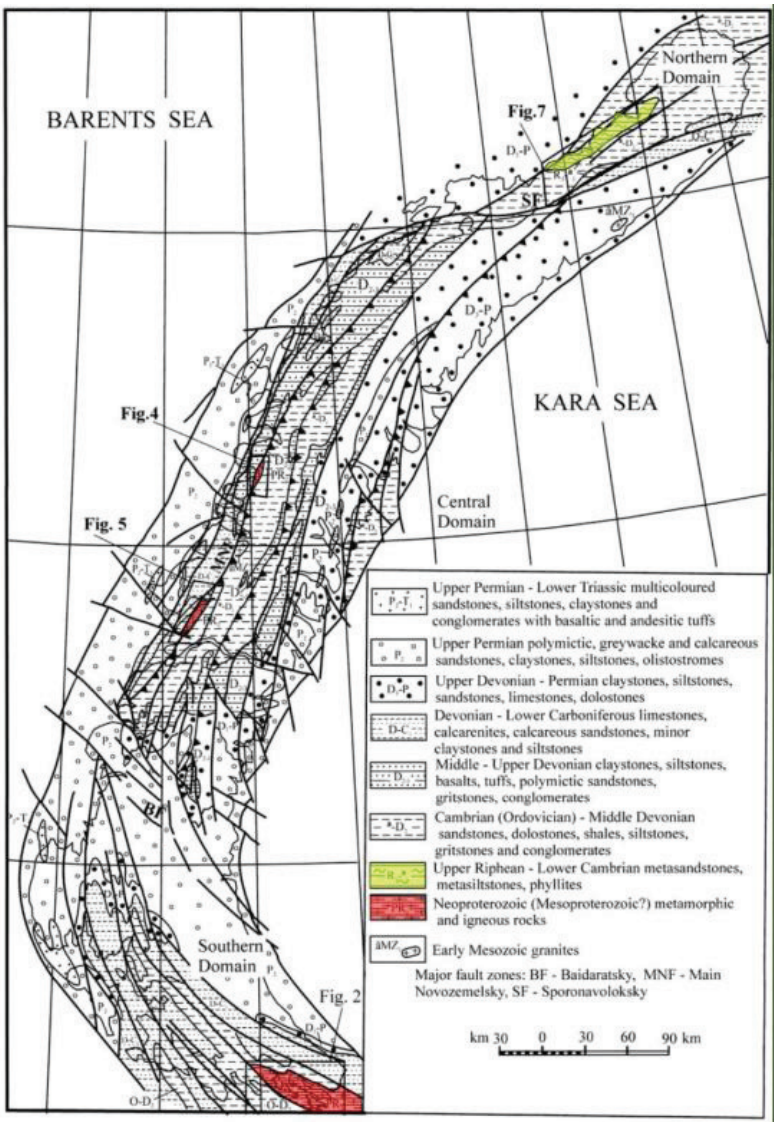


*Figure 3.13. Simplified geological map of the Novaya Zemlya archipelago and adjacent offshore areas (from Korago et al. 2004).*

On Novaya Zemlya, the Early Palaeoproterozoic basement is characterised by marbles, quartzites, shales and amphibolites (Korago et al. 1992, Ivanova et al. 2011). Neoproterozoic and perhaps older metamorphic and igneous rocks are exposed in four main localities on the Novaya Zemlya archipelago. Korago et al. (2004) provided a review of these outcrops and an organisation of the geology into three domains: (1) a Southern Domain with Neoproterozoic basement, recently re-dated as Late Carboniferous by Pease and Scott (2009); (2) a Central Domain with probably older basement; and (3) a Northern Domain with unknown basement including a continuous sedimentary succession from Neoproterozoic to Early Palaeozoic (Korago et al. 2004). The major NW-SE trending Baidaratsky fault

zone (Fig. 3.13) is considered to separate the Southern Domain from Central and Northern Domains. The southern area is interpreted as a peripheral part of the Neoproterozoic Timanian (Baikalian) fold belt. Farther to the northeast, across the Baidaratsky fault zone, lies a broad area of conceivably older basement, including the Central and Northern Domains and possibly the Franz Josef Land archipelago (Korago et al. 2004).

Ophiolites, island-arc and back-arc associations, and high-P glaucophane-bearing eclogites can be traced into the Polar Urals up to the coast of the southernmost Kara Shelf but not farther north (Brown at al., 2002; Dobretsov and Sobolev, 1984; Gee et al. 2006). The ophiolites possibly represent the location of the Uralian suture between Baltica and Siberia.

### 3.2.5 East Barents Basin and buried crust

The formation of the 16-20 kmdeep basin located in the East Barents Sea has beencontroversial and a debate is still going on to attempt to explain the thick sedimentary cover and the mechanism that triggered the rapid subsidence (Fig 3.14).

More recent studies have involved multiple phases of extension to explain the basin formation and its subsidence (Johansen *et al.* 1992; Otto and Bailey 1995; O'Leary *et al.* 2004; Stephenson et al, 2006; Ivanova et al. 2011). O'Leary *et al.* (2004) distinguish three extensional episodes in the South Barents basin, (1) Ordovician-Silurian rifting, associated with the opening of the Uralian Ocean along the eastern margin of Baltica; (2) Mid-Late Devonian extension; and (3) a Late Permian-Early Triassic (300-240 Ma) extension with accumulation of more than 7 km of sediments (see also Otto and Bailey 1995). O'Leary *et al.* (2004) also point out the similarity in structures and sedimentary thicknesses between the North and South Barents basins. However, the standard McKenzie concept that is usually applied to rift basin development cannot be easily applied there (e.g. Semprich et al, 2010).

It has also been proposed that the basin which lies just west of Novaya Zemlya is a foreland basin associated with the Uralian orogeny (e.g.Gramberg 1988; Ziegler 1989; Petrov et al. 2008).

A contractional event is recorded in the eastern Barents Sea (e.g. Johansen *et al.* 1992; Nikishin *et al.* 2002; Bungum *et al.* 2005), but the timing, magnitude and mechanism of the compressive movement are not well constrained (Otto and Bailey, 1995; Torsvik and Andersen 2002).

Different models have been proposed to explain the coexistence of basin formation and compressional tectonics. Artyushkov (2005, 2010) has identified a high-grade metamorphic layer below the seismic Moho, which has been interpreted to be the result of phase-changes (garnet granulite or eclogite formation). He also argued that the East Barents Sea did not experience any significant stretching and that the main subsidence can be linked to a compressional regime in the Permo-Triassic. Dobretsov and Polyansky (2010) challenged the model of basin formation by eclogitisation of mafic crust as suggested by Artyushkov and suggested an explanation based on recent models of a two-layered lithosphere (Huismans et al. 2001) that predict the main extension in the mantle lithosphere rather than in the crust, and which then leads to the production of deep continental basins. Semprich

et al. (2010) proposed a model of deflection of the lithosphere (buckling) to explain the displacement of the crust mantle boundary to greater depths. This provides the most suitable conditions for phase transitions, leading to a partial or complete high densification of the pre-existing lower crust. This process, combined with the sedimentary loading, creates the scenario for the rapid subsidence.

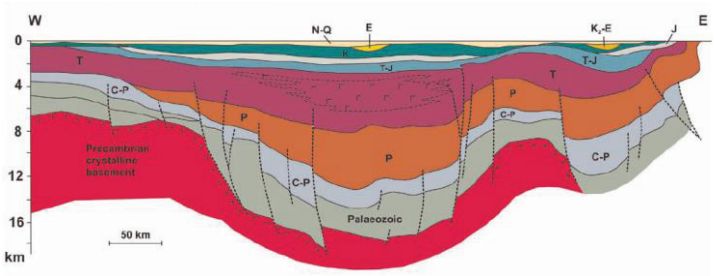


*Figure 3.14. Geological model from seismic and well data (Bogatski et al, 1996) along the East Barents Basin with inferred intrabasinal volcanic rocks marked with a Γ symbol and Precambrian (crystalline) basement with ' +'. The thickness of the sedimentary successions in the East Barents Sea Basin exceeds 15-18 km. The total sedimentary thickness decreases into the Timan-Pechora Basin, to a maximum of 7-8 km (Belyakov 1994; Lobkovsky et al 1996; Bogolepova and Gee 2004). Mesozoic sediments are up to 10 km in thickness. Thick Permian and Triassic deposits (locally 6-8 km) are recorded and illustrate the effect of high subsidence that involved the region at the time. Numerous sill intrusions affect the Triassic formations and can be linked with the Early Cretaceous volcanism recorded on Franz Josef Land and Svalbard (Maher, 2000). The deepest Late Palaeozoic sediments expected could represent a prolongation of the rift system documented in the Timan-Pechora Basin (for location and a more detailed description, see Stephenson et al. 2006).*

The deeper crustal structures beneath the sedimentary cover are characterised by a crustal thickness of around 32–35 km, 10 km less than the average Barents Sea crustal thickness (e.g. Ivanova et al. 2011). This infers that rifting has occured but its timing remains unclear as the basement rock types and their interpretation are controversial.

In the South Barents Basin, the basement is consodered to comprise continental crust that accreted to the East European Craton during the Neoproterozoic Timanide Orogen (e.g. Gee & Pease 2004, and references therein). Further to the north, Caledonian basement is postulated but it is still unclear how far it extends (e.g Gee et al. 2006). Precambrian basement rocks have been proposed to be present in the northern platform areas (Johansen et al. 1992).

Zonenshain at al., (1990) proposed a "windows of oceanic crust" within the underlying crystalline crust, of uncertain origin: either a Iapetus or a Uralian Ocean. On the basis of crustal densities and weak magnetic spreading anomalies,

Apolonov et al. (1996) proposed that a remnant oceanic basin of Devonian age could underlie the East Barents Sea Basin. Artyushkov (2005), on the other hand, dismissed the idea that oceanic crust could be present below the thick sedimentary cover. In a recent model, Ivanova et al. (2011) interpreted the upper consolidated crust of most of the Barents Sea as consisting of Archaean-Proterozoic basement, including metamorphic and intrusive rocks. The southeastern part has been correlated by these authors with granite-gneiss amphibolites, migmatite and volcanic formations of the Pechenga Greenstone Belt that crop out on the Kola Peninsula (Gramberg et al. 1988). North of the East Barents Sea, the basement is substantially complicated by faults and magmatism, probably formed in association with rifting (Ivanova et al. 2011).

## 3.3 Post-orogeny: platforms and rifting evolution

The *Late Palaeozoic and Mesozoic* evolution of the Barents Sea was mostly dominated by extensional tectonics. Important tectonic controls have been imposed by the ongoing interplay of varying factors along the shelf margins including the compressive Uralide development to the east and the proto-Atlantic rifting to the west. The progressive rifted margin initiation and final breakup of the Norwegian-Greenland Sea and Euramerican Polar Basin have, thus, also contributed to the complex mechanisms that shaped the Barents Sea (Worsley 2006).

Rift episodes have been documented in Middle-Late Devonian, Carboniferous, Permian, Triassic and Late Jurassic-Early Cretaceous time and in particular in the western Barents Sea where a complex system of grabens or half-graben basin developed during these periods (e.g. Gabrielsen et al. 1990; Johansen et al. 1992).

However, it is far to say that, the cumulative effects of the earlier collisional events, and their resultant structures, have played an important role in influencing the location, orientation and history of the younger sedimentary basins (Fichler et al. 1997; Gudlaugsson et al. 1998; Faleide et al. 1993; Johansen et al. 1992; Gernigon and Brönner, 2012).

### 3.3.1 Late Silurian-Early Devonian Caledonian collapse

Widespread extension and the formation of Devoian basins followed the Scandian orogenic climax and are recognised throughout much of Scandinavia, particularly in western and central Norway (Roberts, 1983; Andersen, 1998; Fossen, 2000, 2010). The gravitational collapse with back-sliding of the nappe pile involved major, low-angle-ductile detachments relating to top-W to –SW shear (e.g. Osmundsen et al. 1998, 2003; Braathen et al. 2000). Gudlaugsson et al. (1998) proposed a post-Caledonian extensional collapse in the western Barents Sea, but at the same time emphasised the poorly understood nature of the stress regime operating in Devonian times in the offshore area. Johansen et al. (1992) argue for possible graben formation in the southwestern Barents Sea at that time. On Svalbard, Skilbrei (1991), Chorowicz (1992), and Manby and Lyberis (1992) interpreted the Devonian graben of Spitsbergen as a post-orogenic basin.

Some authors have provided evidence for a regional subsidence leading to the formation of a large interior sag basin which they interpret as the first stage in the

formation of a rift system in the southwestern Barents Sea (Gabrielsen et al. 1990; Bugge et al. 1995; Larssen et al. 2005). However, no sedimentary rocks of pre-Late Devonian age have been penetrated by boreholes in the southwestern Barents Sea (Johansen et al. 1992).

In the Timan–Pechora Basin, the Ordovician to Devonian tectonic development was characterised by the formation of NW-SE trending highs and depressions (Fossum et al. 2001), resulting from the reactivation of Timanian lineaments (Johansen et al. 1992). These deep Devonian basins developed in an extensional tectonic regime and are also characterised by widespread mafic magmatism (Apolonov et al. 1996; Lobokovsky et al 1996; Gee et al. 2000; Smelror et al. 2009; Drachev et al. 2010). Early to Mid Devonian extension has also been proposed in the East Barents Basin leading to the formation of graben and half-graben systems (Johansen et al. 1992; Ivanova et al. 2011).

### 3.3.2 Late Devonian-Carboniferous

The Late Devonian to Mid Permian period the western Barents Sea was characterised by widespread intracratonic rifting and then by the development of a regional, post-rift, carbonate platform with local evaporitic basins (Larsson et al. 2005; Worsley, 2006). In the East Barents Sea this was a quiet tectonic period (Johansen et al. 1992).

The Devonian rifting in western Barents Sea was followed by rapid uplift and extensive erosion of the hinterland high. However, there is little detailed information available about basins developed at this stage (Gabrielsen et al. 1990, Gudlaugsson et al. 1998). The rifting phase is related to the very earliest stage of initiation of the Atlantic rift system between Norway and Greenland. A major rift pulse is inferred for the Mid Carboniferous in the Atlantic rift and in the SW Barents Sea (see Gudlaugsson et al. 1998 and references therein; Fig. 3.15a). This event established an asymmetric crustal extension dominated by a strike-slip transfer setting with horst and graben development (Gudlaugsson et al.1998; Johansen et al. 1992). Major basins that formed at that time are the Tromsø, Bjørnøya, Hammerfest and Nordkapp basins (see Fig. 3.1; Dengo and Røssland, 1992; Faleide et al. 1993; Gabrielsen et al. 1990).

Development of fault-bounded basins commenced on Svalbard and Bjørnøya by the end of Devonian time (Steel and Worsley 1984; Gudlaugsson et al. 1998) and extension continued during the Carboniferous (Dengo and Røssland 1992; Worsley 2006).

In the southeastern Barents Sea, major rifting occurred in Late Devonian-Early Carboniferous time, coeval with basaltic volcanism (Drachev at al. 2010). Otherwise, a relatively quiet tectonic regime with stable subsidence dominated throughout Carboniferous and Early Permian times (Johansen et al. 1992). The eastern Barents-Kara Sea region was probably a shallow-water province dominated by carbonate sedimentation (Smelror et al. 2009; Henriksen et al. 2011). Althought, the nature of the strata in the deep Barents Basin is not well known due to a lack of well data, carbonate rocks and shales predominate (Drachev et al. 2010). A north- or northwestward extension of the basin may possibly have occurred in the Late Devonian and Early Carboniferous may possibly have taken place (Johansen et al 1992).

In the *Late Carboniferous,* the sea areas expanded, dominated by carbonate shelf conditions, and also reached into the western Barents Self (Gudlaugson et al. 1998). The climate changed from tropical to arid and large amounts of evaporate deposits were formed (Larssen et al. 2005, Johansen et al. 1992). Salt deposits have been proposed to mark the end of rifting and the beginning of thermal subsidence (Dengo and Røssland, 1992).

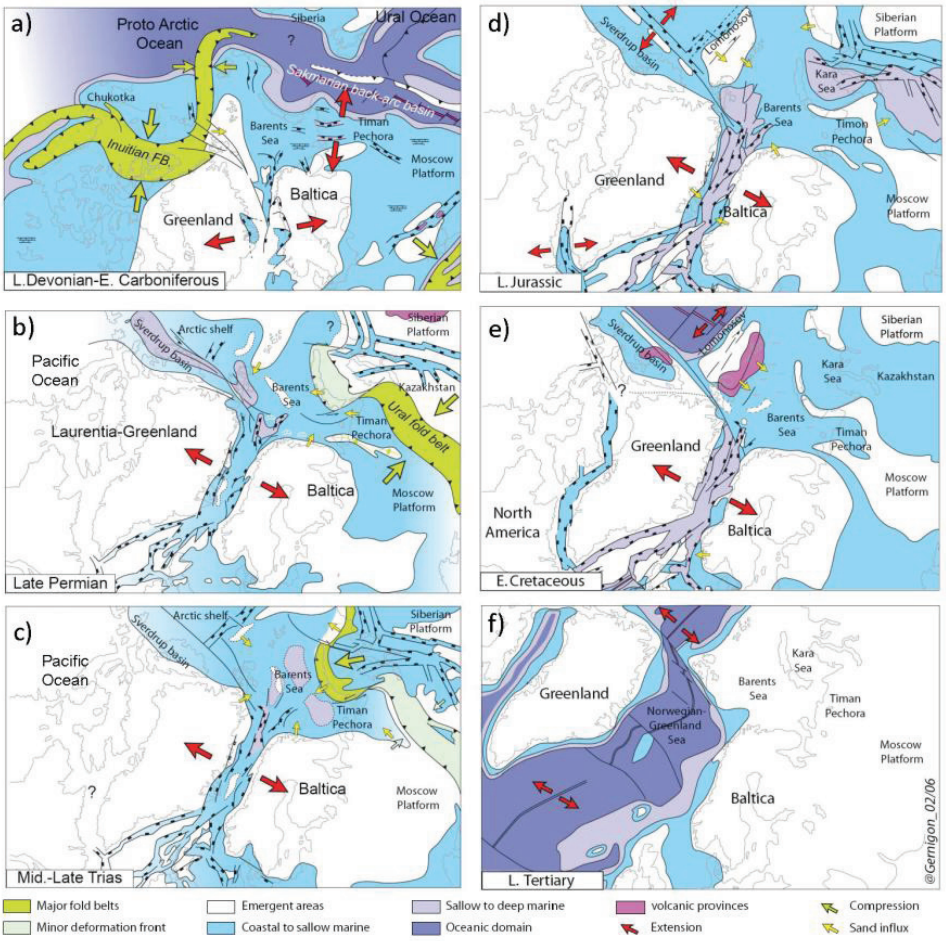


*Figure 3.15. Schematic cartoon of the geodynamic evolution of the Barents Sea regions (L. Gernigon in Smelror et al. 2009)*

### 3.3.3 Permian

In *Early Permian time*, the southwestern Barents Sea continued to subside forming a widespread carbonate shelf environment dissected by a mosaic of shallow basins and highs (e.g. Stemmerik and Worsley 2005). The central and eastern parts of the western Barents Sea experienced regional subsidence in the Late Carboniferous with development of a regional sag basin (Gudlaugsson et al. 1998). The regional sag was probably related to the closure of the Uralian Ocean along the eastern margin of Baltica.

The western Barents Sea was separated from the eastern area by structural highs (Dorè 1995). The climate changes created conditions of high-frequency and high-amplitude, eustatic sea-level changes. During major low stands, halite deposition took place, whereas during sea-level highs the entire shelf areas were flooded and shallow-water platform carbonates developed (Worsley et al. 2006; Smelror et al. 2009, Henrikssen et al. 2011).

In the *Late Permian* (Fig. 3.15b) the region was subject to a major transgression across an extensive marine shelf, with different shallow- and deep-marine depositional environments. A sudden climate change occurred during the Late Permian leading to temperate conditions (Worsley et al. 2006; Smelror et al. 2009). The closure of the Uralian Sea during the Late Permian to Early Triassic period placed the Barents shelf in a distal foreland position in relation to the Ural Mountains. Sediment loading reactivated some normal faults in the basement and increased the withdrawal of salt, accompanied by the local development of basement-detached normal faults (Dengo and Røssland, 1992; Gabrielsen et al. 1992; Nilsen et al. 1995).

In the southeast Barents Sea, rapid subsidence and sedimentation dominated the Late Permian but its association with crustal extension or other mechanisms has a long been a source of debate (see section 3.2.4).

### 3.3.4 Triassic

Rapid subsidence started in the Late Permian and continued throughout Triassic time, when average accumulation rates of the siliciclastic sediments gradually, decreased (Johansen et al. 1992). The greater subsidence rates were located in the South Barents Basin and in the eastern part of Franz Josef Land. This resulted in a continuous sedimentation of non-marine, near-shore and minor shallow-marine deposits derived from the newly formed Uralian orogen (Smelror et al. 2009; Mørk 1999). Meanwhile, the western Barents Sea was tectonically more quiescent and characterised by a passive regional subsidence and a shallow-water siliciclastic shelf. Active faults are found along the western margin, where the Loppa High was uplifted and eroded at this time, anf fault, movements have also been recorded in the Bjarmeland and Finnmark platforms (Ziegler, 1988; Gabrielsen et al. 1990; Smelror et al. 2009). On the Svalbard Platform, little Triassic tectonic activity has been recorded (Johansen et al. 1992).

The *Middle Triassic* (Fig. 3.15c) was characterised by a central marine shelf bordered by land areas to the northwest, east and south. Organic-rich mudstone accumulated in an enclosed, restricted, anoxic basin in the west. To the east, non-marine deposition was replaced by the accumulation of near-shore sediments (Smelror et al. 2009).

The *Late Triassic was* generally marked by an overall regional regression in the entire Arctic region. The Barents Sea formed an extensive regional coastal plain and flood-plain area (Smelror et al. 2009).

### 3.3.5 Jurassic

In Jurassic times, another rifting episode was initiated and involved the western Barents Sea. Block faulting occurred in the Mid Jurassic and increased during the

Late Jurassic to Early Cretaceous period, terminating with the formation of major basins and highs (Gabrielsen et al. 1990)

During Jurassic, the central part of the East Barents Sea megabasin continued to subside with decreasing subsidence rates. Continental and marine-shelf deposition was characteristic of Early and Mid Jurassic time.

In the latest *Early Jurassic*, a global sea-level rise led to the establishment of shallow-marine conditions in the eastern and western Barents Sea.

In the *Mid Jurassic,* regression occurred and reached its maximum. The central areas of the Barents Sea were uplifted and exposed to erosion and a depositional gap is observed over most of the western Barents Shelf. Marine environments were restricted to the western and the eastern areas.

However, the eastern flank of the East Barents Basin was uplifted and affected by erosion during most of Jurassic time (Drachev et al. 2010). In the *Late Jurassic* (Fig. 3.15d), transgression reached its maximum and an extensive marine shelf covered most of the Barents Sea (Johansen et al. 1992). At this time renewed crustal extension between Greenland and Norway initiated an uplift of the Loppa High together with the Stappen, Sentralbanken, and Hopen highs and the Hjalmar Johansen Dome (Smelror et al. 2009). To the north, latest Jurassic evolution was accompanied by magmatic activity (Johansen et al. 1992) followed by a general northerly uplift accompanying breakup and opening of the present polar Euramerican Basin (Worsley 2006). At this time, the East Barents Basin become a starved basin accumulating organic-rich marine sediments (Drachev et al. 2010).

The Jurassic/Cretaceous transition also saw the cataclysmic meteor impact which formed the Mjølnir crater in the Central Barents Sea, an impact that may have had some influence on the regional depositional environment (Worsley 2006).

### 3.3.6 Cretaceous

The Cretaceous period in the western Barents Sea commenced with intensive rifting and subsequent subsidence, whilest in the east the subsidence and accumulation rates were moderate (Johansen et al. 1992).

Structural development in this period was complicated in the West Barents Sea. Rapidly subsiding basins (i.e., the Harstad, Tromsø and Bjørnøya basins) where decoupled from the rest of the Barents Shelf during the Early Cretaceous rifting events (Smelror et al. 2009). On the other hand, indications of local Early Cretaceous inversion are found (Gabrielsen et al 1990).

In the *Early Cretaceous* (Fig. 3.15e), the opening of the Amerasia Basin in the Arctic Ocean caused uplift and gentle tilting in northern parts of the Barents-Kara region that controlled the sedimentation over large areas during this period (Smelror et al. 2009, Johansen et al. 1992). At this time, most of the Barents Sea was an open shelf with structural highs and platforms separating the basins (Smelror et al. 2009). On Svalbard and Franz Josef Land, the vertical tectonic movements were accompanied by significant volcanic activity (Grogan 1998; Fig. 3.15e). The magmatism has been associated with a Large Igneous Province linking Greenland, Svalbard, Franz-Josef Land and adjacent shelf areas before the continental breakup and ocean basin formation (Maher 2001).

In the *Late Cretaceous,* major rifting led to continental break up between the Barents Sea and Greenland in the Amundsen Basin (Faleide et al. 2008).

### 3.3.7 Cenozoic

The breakup history of the Norwegian-Greenland Sea and subsequent sea floor spreading had a great effect on the Cenozoic geological evolution of the Barents Sea (Johansen et al. 1992).

Sea-floor spreading began in the Norwegian-Greenland Sea as a sheared margin in the *Early Eocene* (Myhre at al. 1982). Most of the deformation occurred west of the Loppa High and Senja Ridge, reactivating, pre-existing faults (Dengo and Røssland 1992; Faleide et al. 2008). The basins of the westernmost Barents Shelf continued to subside and received significant amounts of sediment from the local highs (e.g. Stappen High, Loppa High), and from the eastern and northern parts of the shelf that in the meantime were uplifting (Johansen et al. 1992; Smelror et al. 2009). The Harstad Basin, Tromsø Basin, Sørvestsnaget Basin, Vestbakken volcanic province and the areas west of the Knølegga and Hornsund Fault Zones, were principal areas of clastic deposition. Up to several kilometres of sediments were probably removed from the north-western part of the shelf during the Cenozoic (Ryseth et al. 2003; Faleide et al. 1996).

Compressive Paleogene-Neogene deformation associated with a dextral stress field occurred and led to the development of the Spitsbergen Fold- and-Thrust Belt (Eldholm et al. 1987; Saalmann and Thiedig, 2001), and to compressive structures in the west Bjørnøya region. To the east there is little evidence of compressive deformation in the Barents Sea during the Cenozoic (Smelror et al. 2009; Buiter and Torsvik, 2007; Otto and Bailey, 1995).

From *Mid Miocene* time to the present, the western Barents Sea has been regionally uplifted (Dengo and Røssland, 1992).

In the *Neogene,* deposition was dominated by thick clastic wedges that shed off the newly formed western shelf margin as a response to glaciation/deglaciation of the shelf itself (Worsley 2006).

## 3.4 Summary

The Barents Sea shelf is the result of the Neoproterozoic and Palaeozoic assembly of plates and microblocks. The configuration and evolution of the original plates (Precambrian) is still not clear, largely due to the limitations of paleomagnetic methods and analysis. The plate aggregation occurred through collisional events resulting in the Timanian, Caledonian and Uralian orogeneses. The Caledonide influence is recorded in the northwest Barents Sea by N-S structural trends and in the southwest by NE-SW lineaments. The Timanian dominated the structural grain of the southeast Barents Sea with easternmost NW-SE trends that also extend towards the north. The Uralian orogeny involved the easternmost part of the Barents Sea shelf with trends that follow the shape of Novaya Zemlya.

The post-orogenic evolution is dominated by several phases of rifting and may involved a variety of processes: post-orogenic collapse, active rifting, sedimentary loading, thermal subsidence, foreland basin development due to orogeny, phase transition, and the influence of the Atlantic rifting.

Cretaceous and Cenozoic magmatism in the North Barents Sea, East Barents Sea and on Svalbard is characterised by lava flows and several sill intrusions that contributed to the complex tectonostratigraphic evolution of the area.

In the following chapters I will analyse the structure of the basement and lithosphere of the Barents Sea and discuss its links with the geological history described above.

# Chapter 4

# Magnetic basement characterization

*The content of this chapter is published in: Marello, L.; Ebbing, J; Gernigon, L. 2010. Magnetic basement study in the Barents Sea from inversion and forward modeling. Tectonophysics **493**, 153–171.*

In this work we have investigated the basement in the Barents Sea region and its relationship to the magnetic anomalies observed. Besides magnetic field image analysis (incl. pseudo-gravity), we performed both 3D inversion and 2D forward modelling to characterise the geometry of the top-basement and the distribution of magnetisation and density. For the 3D inversion, the influence of the input parameters has been studied in detail, and large uncertainties have been encountered over some areas. On a regional scale, the petrophysical parameters and not the geometry of the top-basement dominate the magnetic anomalies. The 2D models assist in linking together the main crustal units of the Barents Sea, which are expressed by different magnetic basement characteristics. Based on our inversion and modelling work we have compiled a map which shows the different basement domains and their structural trends. The map allows us to interpret the possible extension of Timanian, Caledonian and Uralian magnetic terranes in the area.

## 4.1 Introduction

The Barents Sea is an area of increased interest from both scientific and economic points of view and a detailed knowledge of the basement is of major importance in understanding the evolution of sedimentary basins and their petroleum systems (e.g. Johansen et al., 1993; Doré and Vining, 2005, and references therein). However, only a few studies have been carried out at the regional scale of the Barents Sea (Johansen et al., 1993; Fichler et al., 1997; Gramberg et al., 2001; Ebbing et al., 2007; Ritzmann et al., 2007). Consequently, the overall basement setting of the study area, which reflects its tectonic history, is still poorly understood and unclear over vast areas. Seismic and density models for the basement constrain the deep structures only locally (e.g. Breivik et al., 2003; Ivanova et al., 2006; Kostyuchenko et al., 2006) and, in places, show large differences. For example, the top-basement geometry of the Eastern Barents Sea published by Gramberg et al. (2001) and Johansen et al. (1993) shows locally discrepancies of up to 8 km. The absence of an integrated top-basement model is not just a consequence of the lack and/or sparse distribution of seismic reflection and refraction data (Morozova and Pavlenkova, 1995; Gramberg et al., 2001; Ritzmann et al., 2007), but is also due to the complex geology of the Barents Sea. The Barents Shelf is dominated by basement highs and a large number of deep sedimentary basins (Fig. 4.1). In the deepest part of these basins, sediments are strongly affected by compaction reaching densities close to those of the basement rocks, which therefore result in decreases in both the acoustic impedance contrast and the signal-to-noise ratio. Under such conditions, seismic and gravity data lead to large uncertainties in estimating the deeply buried top-basement. Furthermore, the presence of salt (e.g. Nordkapp Basin, Svalis Dome) as well as shallow magmatic intrusions (e.g. East Svalbard, Franz-Josef Land Platform) can locally complicate the estimation of depth to top-basement by means of potential field modelling.

The magnetisation contrast between sedimentary and basement rocks is usually high and therefore an interpretation of the magnetic field is generally effective in basement studies. In the Western Barents Sea and the Southeast Barents Sea (Timan Ridge, Pechora Basin, Fig. 4.1), magnetic methods have previously been applied in studying the basement (Olesen at al., 1990, 2010; Skilbrei, 1991; Johansen et al., 1993; Kostyuchenko et al., 1999; Barrère et al. 2009) but none have considered the entire Barents Sea.

In the present study, we have investigated the top-basement geometry and the magnetic basement properties of the Barents Sea by testing and evaluating previous studies (e.g. Johansen et al., 1993; Gramberg et al., 2001). Besides image processing, we have applied inverse modelling and carried out sensitivity tests. The inversion results have then been integrated along four profiles with existing seismic and gravity data. We used 2D forward modelling to refine the magnetic properties along the profiles, which were then linked together to illustrate the main crustal units of the Barents Sea associated with the different magnetic basement domains. Finally, the known tectonic setting was compared with the different magnetic patterns and the location of magnetic basement blocks in order to investigate the link between the magnetic anomalies and the geology.

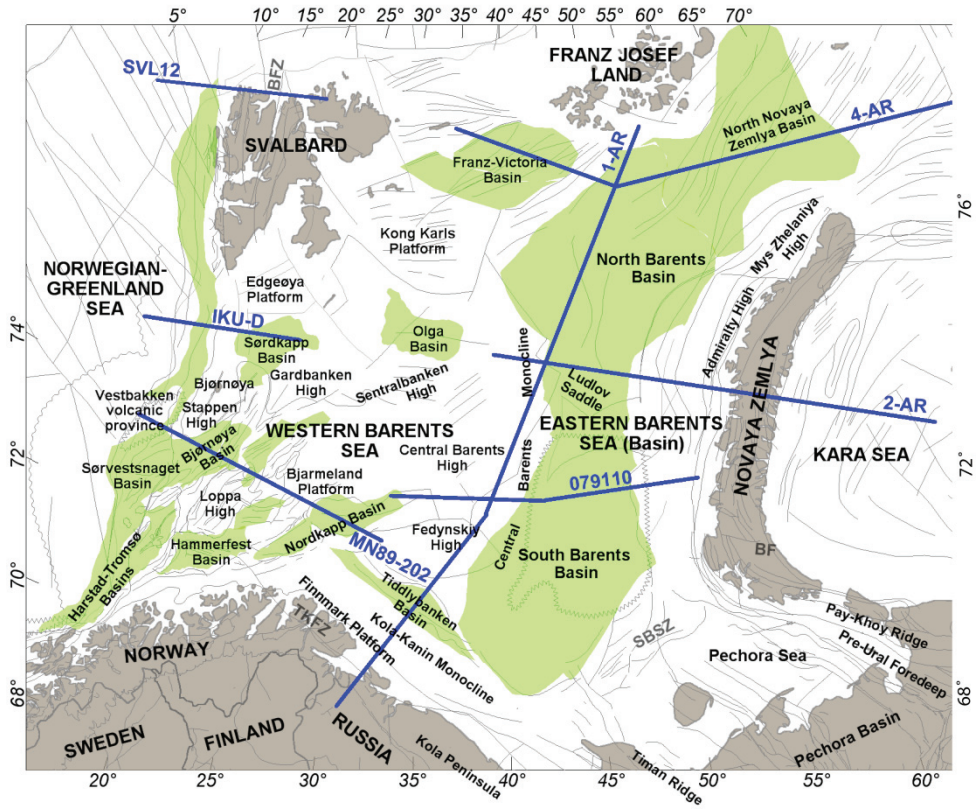


*Figure 4.1. Barents Sea structural map (Gabrielsen et al., 1990; Johansen et al., 1993). The locations of the main basins are highlighted in green. The major fault notations are: BFZ= Billefjorden Fault Zone; TKFZ=Trollfjorden-Komagelva Fault Zone; SBSZ=South Barents Fault Zone; BZ= Baidaratsky Fault Zone. The blue lines show the locations of the 2D seismic transects.*

## 4.2 Geology and tectonic setting

The present-day basement structure of the Barents Sea is the final result of a complex tectonic history. Through geological time, the Baltica, Laurentian and Siberian plates, and smaller continental blocks, have collided and interacted during three major orogenic events (Timanian, Caledonian and Uralian).

The oldest orogenic phase, *Timanian* (Ediacaran age), in which complex terranes accreted against the presentday northeastern margin of Baltica, is today recorded in the Southeast Barents Sea (Timan Range, Pechora Basin, extreme Northeast Norway, South Novaya Zemlya) as fold structures and associated metamorphic fabrics. The general Timanian structural trends have a NW-SE orientation. The Novaya Zemlya fold belt represents an assemblage of three tectonic domains; its southern area with Neoproterozoic basement is believed to be

a peripheral part of the Timanian fold belt (Pease and Scott, 2009). The other two domains, north of the Baidaratsky fault zone (Fig. 4.1), are believed to be part of a broader area (may include the northeastern part of Svalbard and Franz Josef Land) of older basement, perhaps of Mesoproterozoic age (Korago et al., 2004). Today, there is a general agreement that the Timanian trends extend into the South Barents Basin (Olovyanishnikov et al., 1997; Roberts and Siedlecka, 2002) but exactly how far north and west is still a matter of debate.

The subsequent *Caledonian Orogeny* involved mostly the western Barents Sea region, Svalbard and mainland Norway. It started in Late Cambrian time when Baltica, Siberia and Laurentia began to converge, until the Iapetus Ocean finally closed and Baltica and Laurentia collided in Mid Silurian-Early Devonian time (Roberts and Gee, 1985). Caledonian nappes dominate the geology of northern Norway (Roberts, 2003), locally with major, mafic-ultramafic and plutonic complexes (Robins and Gardner, 1975; Corfu et al., 2006; Roberts et al., 2006). Offshore, the original character and extent of the Caledonide Orogen is concealed by overlying Late Palaeozoic and Mesozoic sedimentary basins. Farther north, the Caledonian bedrock is exposed on the islands of Bjørnøya and Svalbard. There, the Caledonian structural trends are dominated by N-S orientations that gradually change towards the south to become NE-SW oriented in the southwestern Barents Sea and Finnmark (Skilbrei, 1991; Doré, 1995; Fichler et al., 1997; Doré and Vining, 2005; Roberts and Lippard, 2005). The thrust front of the Caledonide Orogeny truncates the Timanian trend in northeasternmost Norway and near-offshore areas. The suture zone between the Baltican and Laurentian plates can be traced from Lyngen in northern Norway, into the Southwestern Barents Sea, where it is still poorly constrained and the subject of much discussion (Breivik et al., 2002; Ritzmann and Faleide, 2007; Gee et al., 2008; Barrère et al., 2009).

The Late Silurian-Early Devonian time interval is dominated by the main Caledonian (Scandian) orogeny followed by extensional collapse, recognised throughout much of Scandinavia and in parts of the western Barents Sea (Roberts, 1983, 2003; Gudlaugsson et al., 1987; Andersen, 1988; Skilbrei, 1991; Fossen et al., 2000).

The youngest orogenic phase, the *Uralian event* (Early Carboniferous-Late Permian/Triassic) led to closure of the Uralian Ocean and subsequent collision between Laurussia (Baltica and Laurentia) and western Siberia. It affected mostly the Eastern Barents Sea region, generated the Pay-Khoy Ridge and Novaya Zemlya fold belt (Puchkov, 1997) and most likely later influenced the formation of the Eastern Barents Sea Basin ( e.g., Ziegler, 1989; Buiter and Torsvik 2007). The Uralian structural trends run approximately parallel to the island of Novaya Zemlya.

By Late Devonian-Early Carboniferous time, the rifting between Greenland and Norway had been initiated. This event affected the Western Barents Sea and major basins (e.g. the Tromsø, Bjørnøya, Hammerfest and Nordkapp basins) formed at that time (see Fig. 4.1). In Late Carboniferous time, active crustal extension initiated a transition into a slowly subsiding interior sag.

The Carboniferous-Permian-Triassic evolution of the Eastern Barents Sea is also debated. It has earlier been assumed that the basins located near western Novaya Zemlya were mostly foreland basins associated with the Uralide orogeny

(Ziegler, 1989). However, some authors have claimed that the evolution of the Eastern Barents Sea could be the result of more complicated dynamic processes involving different rifting events, compressional phases and major subsidence due to mineral changes in the lower crust (Otto and Bailey, 1995; Aplonov et al., 1996; Nikishin et al., 2002; O'Leary et al., 2004; Artyushkov, 2005; Buiter and Torsvik, 2007). During Late Jurassic-Cretaceous time, renewed crustal extension between Greenland and Norway was initiated and this event strongly affected the Western Barents Sea. During the Early Cenozoic, tectonic activity involved the progressive northward opening of the North Atlantic and Arctic Oceans, subsequent to the early initiation of sea floor spreading (Early Eocene) when the western margin of the Barents Sea developed as a sheared margin (Faleide et al., 2008). From mid-Miocene time to the present, the Western Barents Sea has been regionally uplifted and eroded (Dengo and Røssland, 1992).

Magmatic intrusive and extrusive events add to the complexity of the Barents Sea tectonic scenario. Svalbard contains a record of magmatic rocks dating back to the Mesozoic. Lower Cretaceous basaltic rocks associated with the Arctic Large Igneous Province are known in Svalbard, Kongs Karl Land and Franz Josef Land (Bailey and Rasmussen, 1997). Sills are considered to extend into the central and northern parts of the Russian Barents Sea and could be part of the same Lower Cretaceous event (Maher, 2001; Meyer et al., 2007). Paleogene (Harland et al., 1997), Miocene and Pleistocene (Prestvik, 1978; Harland and Stephens, 1997) magmatic activities are also recognised offshore north of Svalbard (Yermak Plateau).

## 4.3 Database

### 4.3.1 Magnetic data

The magnetic data (Fig. 4.2) used are from a recent compilation integrating Russian and Norwegian datasets (Smelror et al., 2009; Olesen et al., 2010). The surveys over the Norwegian Barents Sea and Svalbard have been acquired by the Geological Survey of Norway and TGS-NOPEC. In the Eastern Barents Sea, most of the data were collected by VNIIOkeangeologia (formerly NIIGA-Research Institute for Arctic Geology), Polar Geophysical Expedition NPO "Sevmorgeo" and FGUP "Sevmorgeologia". The mean least square grid errors of the compiled datasets are in the order of 11-14 nT (Smelror et al., 2009).

### 4.3.2 Gravity data

The Free Air Gravity data used are available from the Arctic Gravity Project (http://earth-info.nga.mil/GandG/wgs84/agp/index.html). The Bouguer anomaly (Fig. 4.2) has been calculated from the free-air anomalies using a reduction density of 2670 kg/m$^3$ onshore and 2200 kg/m$^3$ offshore. The topography correction was calculated using the International Bathymetric Chart of the Arctic Ocean (IBCAO) database (Jakobsson et al., 2008) released in April 2008.

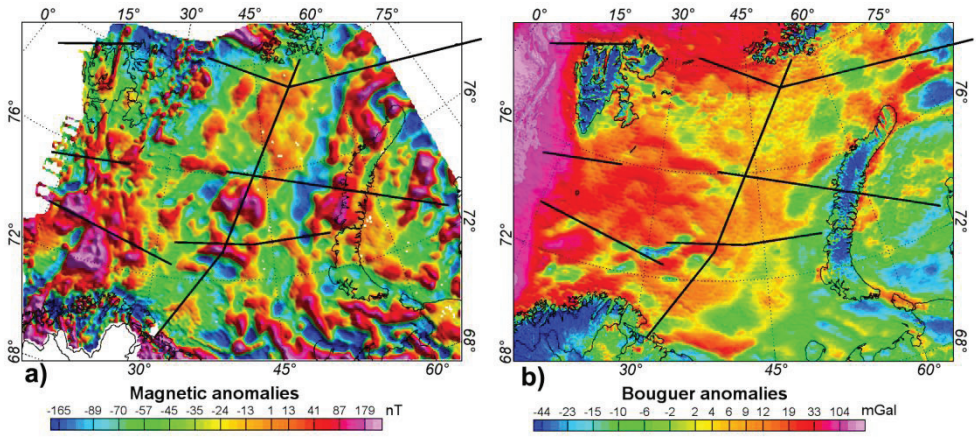


*Figure 4.2. a) Total magnetic field anomaly (Smelror et al., 2009). b) Bouguer anomaly map from Arctic Gravity Project 2008. The black lines show the paths of the seismic profiles.*

### 4.3.3 Petrophysical data

Petrophysical parameters were gathered from the literature (Åm, 1975; Olesen et al., 1990, 2010; Skilbrei, 1991; Barrère et al., 2009). These publications show that the susceptibilities of the basement rocks can range between 0.0005 and 0.3 SI whilst the susceptibilities of the overlying sediments remain only in the order of 0.0003 SI, one to three orders of magnitude lower. The range of susceptibilities for the basement depends on its composition and varies typically from 0.005-0.01 SI for the Caledonian basement, 0.01-0.1 SI for the Precambrian basement, to higher values for basement intruded by mafic plutonic rocks (Barrère et al., 2009; Olesen et al., 2010). Susceptibility values for Uralian and Timanian basement rocks are not available. A few measurements are also available on Franz Joseph Land (Dibner, 1998). For the remaining region, we used average susceptibilities that consider the collected direct information and the general petrophysical data for basement rocks. The general range of susceptibilities for igneous rocks is between 0.001 and 0.1 SI on average; between 0.0005 and 0.5 SI for metamorphic rocks and 0.00001- 0.0002 SI for sedimentary rocks (Clark, 1997).

The densities used for the sedimentary cover and the bedrock are based on direct measurements of samples (Olesen et al., 1990, 2010); or result from the conversion of seismic velocities to densities using general laws and previous models (Breivik et al., 1995, 2003; Mjelde at al., 2002; Ivanova at al., 2006; Ritzmann et al., 2007; Barrère et al., 2009). The average crustal densities are estimated to be in the range of 2700-3000 kg/m$^3$. The mantle densities reflect the thermal and compositional change from the oceanic (around 3260 kg/m$^3$) to the continental domain (around 3290 kg/m$^3$) (Breivik et al., 2003; Hacker et al., 2003; Simon and Podladchikov, 2008).

### 4.3.4 Seismic information

The seismic data available for the Barents Sea include commercial and public domain seismic data (Johansen et al., 1993; Ritzmann et al., 2007), and references

therein). For this study we used recently interpreted seismic lines (Fig. 4.1) including the western MN89-202 and eastern 079110 lines (Smelror et al., 2009), the OBS line IKU-D (Breivik et al., 2003), the northern Svalbard (N-SVL) profile (Geissler, 2001; Ritzmann, 2003; Faleide et al., 2008) , and the 1-AR, 2-AR and the 4-AR Arctic Regional Russian transects (Ivanova et al., 2006; Roslov et al., 2008, 2009). To constrain the crustal structures, in particular the boundary between crust and mantle, we employed the Barents50 model (Ritzmann et al., 2007) that defines the Moho geometry with 50 km resolution, and the recent compilation for the "Moho depths of the European Plate" (Grad et al., 2009) that extended the previous Barents50 model towards the Baltic Shield and the oceanic domain.

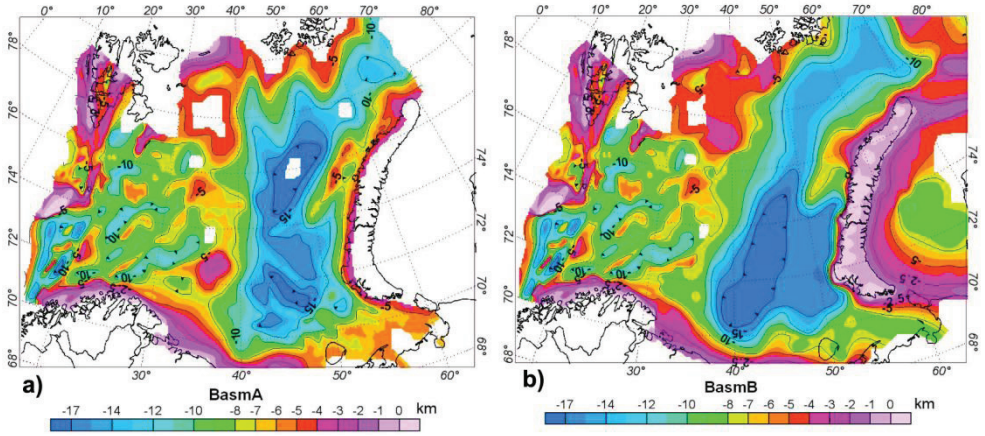


*Figure 4.3. Different top-basement models for the Barents Sea. a) BasmA from Skilbrei et al. (1991) (Western Barents Sea) and Johansen et al. (1993) (Eastern Barents Sea). b) BasmB from Skilbrei et al. (1991) (Western Barents Sea) and Gramberg et al. (2001) (Eastern Barents Sea). The contour lines spacing is 2.5 km.*

### 4.3.5 Top-Basement models

The Barents Sea basement is very inhomogeneous and reflects different kinds of rocks. Under the definition of basement we include the Archaean-Palaeoproterozoic crystalline complexes, the Neoproterozoic magmato-sedimentary Timanian assemblages, the Caledonian nappes, the Uralide terranes and large mafic intrusions.

One of the first, regional, top-basement models for the Western Barents Sea (See Fig. 4.1 and 4.3) was published by Skilbrei (1991, 1995), based on magnetic depth estimates integrated with local indications of top-basement deduced both from seismic profiles and well data.

For the Eastern Barents Sea we considered two regional compilations (Fig. 4.3). The first one published by Johansen et al. (1993) presented magnetic depth estimates integrated with seismic profiles; the second (Gramberg et al., 2001) involved a combination of seismic data with magnetic and gravity observations. Although there are similarities between these depth estimations, major differences

exist in the extension and location of the deepest areas in central parts of the Eastern Barents Sea (Fig. 4.3). Whilst Gramberg et al. (2001) interpreted the Eastern Barents Sea Basin as a huge single depression, striking parallel to Novaya Zemlya, the depth interpretation of Johansen et al. (1992) emphasises a number of NW-SE-aligned, and small-scale features with a trend similar to that of many Timanian faults. In the central part of the Barents Sea, large differences also exist between the two compilations. Johansen et al. (1993) defined the surface at an approximately 8 km shallower depth than in the compilation by Gramberg et al (2001). To define a refined and coherent top-basement that covers the entire Barents Sea, we have combined the Western Barents Sea top-basement with the Eastern Barents Sea compilations (Fig. 4.3). In this work we will refer to the top-basement defined by Skilbrei et al (1991) to the west and by Johansen et al. (1993) to the east as *BasmA* and the model combining the estimation of Skilbrei et al. (1991) and Gramberg et al. (2001) as *BasmB*.

## 4.4 Magnetic field interpretation

The main magnetic effect of the Barents Sea reflects a combination of top-basement topography (i.e., tilted blocks, undulation of erosion surfaces) and intra-basement sources (i.e., high-magnetic plutons, high-magnetic metamorphic complexes). Local magmatic intrusions in the form of sills and/or dykes characterised by high-magnetic properties are responsible for high-frequency anomalies. Sedimentary rocks are seen to be low-magnetic and usually give only an insignificant contribution to the magnetic anomalies (Clark, 1997; Gibson and Milligan, 1998; Mørk et al., 2002). Therefore, the main sources of the magnetic anomalies are expected to depend on the basement setting and its magnetic properties.

### 4.4.1 Magnetic field analysis

By analysing the data it is possible to sub-divide the field into different wavelength components that, theoretically, can be linked to sources at different depths. For the field analysis we used the Discrete Fast Fourier Transformation algorithm (Geosoft, 2005b), which applies the method of Bhattachatyya (1966). The FFT transformation for potential fields may lead to edge effects; this, in particular, is due to the pronounced effect of the anomalies located at the borders of a grid area. To avoid such effects, we expanded the original grids by a minimum of 30%.

In the first step, wavelength filtering of the magnetic field was used to enhance geological structures at different depth levels. The high-pass filtering of the data is expected to highlight shallower sources and small structures (faults, salt diapirs, minor intrusions). Considering the Barents Sea as a whole and the low grid resolution (which is 5 km), the definition of the tectonic structures mostly reflects the main basin architecture and does not allow any precise identification of the smaller subtle structures. On the contrary, low-pass magnetic filtering was used to highlight regional structures that represent mid to upper crustal variations in basement terranes. Different wavelength cut-off filters (25, 50, 70, 100 and 125

km) were used to isolate the short, the long and the intermediate wavelength patterns (e.g. Fig. 4.4a and 4.4b). The resulting high-pass filtered map enhances the trends of the high-frequency anomalies, while the low-pass filtered magnetic map illustrates areas dominated by a high-magnetic signal (e.g. Western Barents Sea, Central Barents Sea, and North Novaya Zemlya) and a low-magnetic signal (e.g. Northwest Barents Sea, and part of Northeast Barents Sea).

Further correlations between tectonic units and magnetic anomalies can be established using tilt-derivative (TDR); this derivative calculation has the property of being positive over a source and negative elsewhere (Miller and Singh, 1994; Verduzco et al., 2004). That is particularly useful for mapping basement structures because it enhances the geometrical contrast in the internal basement. Moreover, TDR highlight magnetic anomaly lineaments and allow us to distinguish areas characterised by different patterns (Fig. 4.4c).

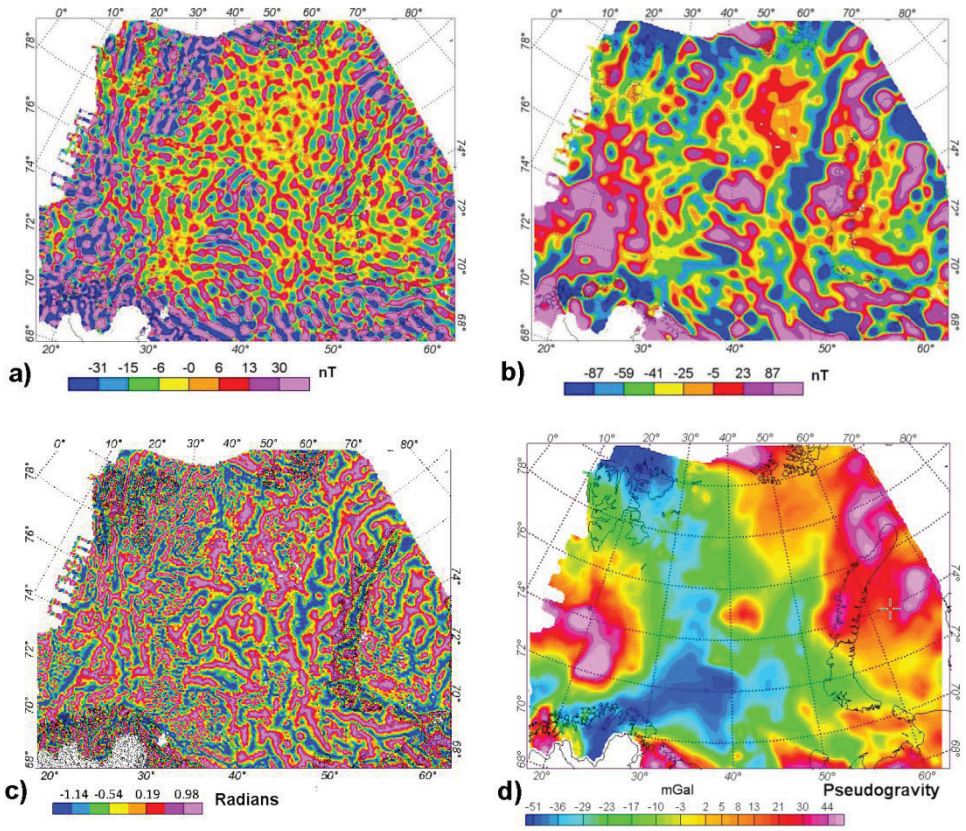


*Figure 4.4. Results of magnetic field analysis. a) high-pass filtered magnetic field (70 km cut-off wavelength). b) low-pass filtered magnetic field (70 km cut-off wavelenght). c) tilt-derivative map. d) pseudo-gravity map.*

| Domains | Tilt-derivative and high-pass filter trend direction | Low-pass filter and pseudogravity | Possible origin |
|---|---|---|---|
| **MSE Southeast Barents Sea** | NW-SE in the most southeastern area. E-W farther north. N-S, vicinity of Novaya Zemlya. | NW-SE high regional anomalies | Timanian structures. South Novaya Zemlya is considered to be part of that domain. |
| **M1 Central South Barents Sea** | NW-SE and E-W lineaments. | Prominent high regional anomaly Low pseudo-gravity response of the Barents Sea | Origin of high anomaly and its relation between trends and surrounding domains have to be investigated. The high anomaly character changes to the north and south, suggesting that this area is an independent domain. Appears to coincide with the prolongation of Timanian structures. |
| **M2 Central Barents Sea** | NNW-SSE lineaments that swing to NE-SW in the central Barents Sea. | Clear long-wavelength high anomaly and pseudo-gravity | Unknown. |
| **MW Westernmost part of the Barents Sea** | The trend swings from NE-SW near the Norwegian coast to NW-SE towards the north and to N-S in the vicinity of Svalbard | Highest regional anomaly. Distinct low pass and pseudo-gravity. | Local pseudo-gravity maxima and higher anomaly are related to basement high. The anomaly trends are most probably reflecting Caledonian structures. |
| **M3 Northwest region east of Svalbard** | High-frequency anomalies and characteristic tilt-derivatives NNE-SSW oriented | | Anomalies related to shallow sill intrusions (Cretaceous magmatism). |
| **MN Northeast Barents Sea** | Small range of anomalyvariations. Sharp peaks in the high-pass filtered map. In the TDR, trends are not easy to recognise. | Only the fairly high pseudo-gravity signature allows to define this region as a separate domain | Difficult to relate to a specific event. |
| **ME Northeastern part of the Barents Sea** | The high-frequency anomaly broadly follows the outline of northern Novaya Zemlya | Distinct high pseudo-gravity | Probably reflect the Uralian setting. Pseudogravity coincides with Bouguer gravity. |

*Table 4.1. Qualitative analysis results of the magnetic anomalies. Summary of the characteristics of the main magnetic domains (Fig. 4.5); structural patterns, regional magnetic signatures and possible origin.*

The pseudo-gravity (Baranov, 1957) enhances anomalies associated with deep magnetic sources. This technique is useful for the interpretation of major magnetic provinces as it simplifies anomaly patterns and focuses on large-scale features (Blakely and Simpson, 1986; Jeffrey, 2000). A comparison of the pseudo-gravity (Fig. 4.4d) with the Bouguer gravity anomaly (Fig. 4.2) allows us to discuss the

correlation between the magnetic and the gravity sources. Just a few magnetic anomalies, for example in the northern part of Novaya Zemlya and in the Western Barents Sea, do correlate and point to probable same sources for the magnetic and gravity anomalies.

The major results of the qualitative analysis are summarised in Fig. 4.5 and Table 4.1.

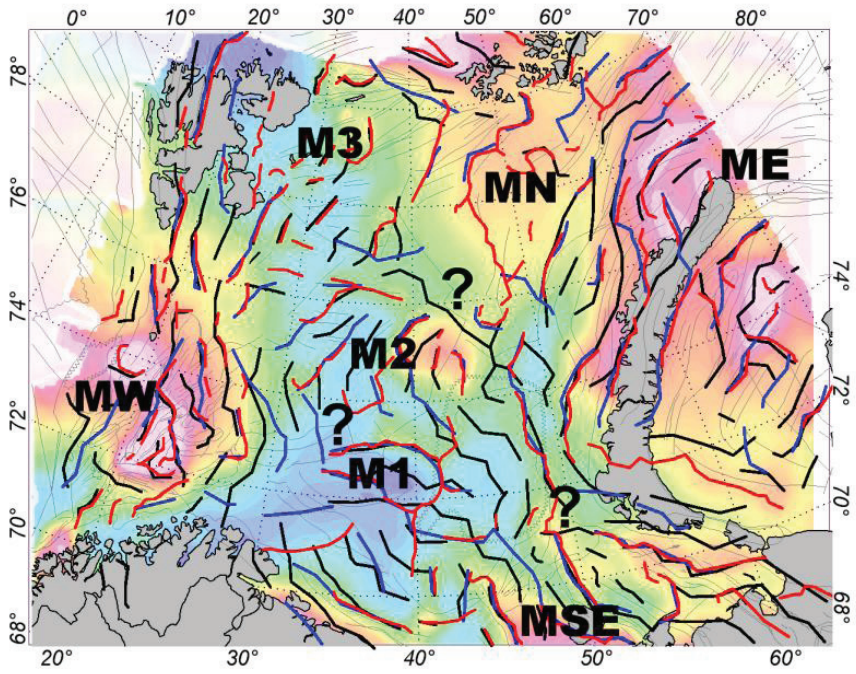


*Figure 4.5. Magnetic anomaly regions defined from the magnetic field analysis. On the map, the peaks of the filtering and tilt derivatives are displayed; in red the tilt-derivatives, in blue the high-pass filter at 120 km and in black the high-pass filter at 70 km. In the background, the pseudo-gravity map helps to define the magnetic anomaly regions.*

## 4.5 3D modelling and inversions

### 4.5.1 Magnetic modelling approach

Qualitative analysis provides just a first and rough estimation of the source parameters. A 3D magnetic model was constructed to further study the effect of the basement on the magnetic anomalies. The actual knowledge of the geological structure under investigation (e.g. top-basement, crustal structure) was adopted to define the initial magnetic model and to reduce its uncertainties. The definition of the magnetic properties takes into account the petrophysical data and assesses all previous studies (Olesen et al., 1990, 2010; Skilbrei, 1991; Dibner, 1998; Mørk et al., 2002) (see Table 4.2).

| Layers | Susceptibility (SIx$10^{-3}$) | Boundary layer |
|---|---|---|
| | | 0 km constant grid |
| Water | 0 | |
| | | Bathymetry[1] |
| Upper sediments | 0.31 | |
| | | 8 km constant grid |
| Lower sediments | 2.51 | |
| | | Top basement[2] |
| Upper crust | 12.6-37.7 | |
| | | 25 km constant grid |
| Lower crust | 5.03 | |
| | | Moho [3] |
| Mantle | 0.63 | |

*Table 4.2. Model parameters used in this study. They consisted of 6 layers with constant magnetic properties; each layer was defined by a rectangular surface grid with 5 x 5 km resolution. 1= IBCAO model (Jakobsson et al., 2008); 2= BasmA (Johansen et al., 1993; Skilbrei, 1991) and BasmB (Gramberg et al., 2001; Skilbrei, 1991); 3= combination of Barents50 (Ritzmann et al., 2007) and "Moho depth of the European Plate" (Grad et al., 2009).*

Due to the lack of direct constraints especially offshore, simplification of the magnetic properties was assumed during the modelling. The magnetisation usually comprises two components: the induced ($M_{ind}$) and the remanent ($M_{rem}$) magnetisation. The susceptibility of a rock is given by the ratio $M_{ind}/H$, which is a scalar quantity since the magnetisation is essentially parallel to the Earth's applied magnetic field (H). However, information on $M_{rem}$ is poor or non-existent for the Barents Sea and the orientation of the paleomagnetic field is not constrained. Beause of this limitation, we have chosen to revise our definition of the susceptibility. Instead of a real rock susceptibility, we here refer to a pseudo-total susceptibility ($\chi_{tot}$) defined as follows:

$$\chi_{tot} = \frac{M_{rem}}{\mathrm{H}} + \frac{M_{ind}}{\mathrm{H}} = \chi_{rem} + \chi$$

This pseudo-remanent susceptibility ($\chi_{rem}$) is a normalised parameter that considers the contribution of an artificial remanent magnetic field, which, for simplification, is assumed to be parallel to the present-day magnetic field. In this way, we do not neglect the remanence and we simplify the variables that produce the anomalies by one magnetic property. The relative importance of the remanent magnetisation and induced magnetisation is given by the *Koenigsberger ratio* (Q). Its range depends on the variety of rock types present (Clark, 1997), and estimates for the Western Barents Sea basement have been published (Barrère et al., 2009) and considered in this work. For granulites, a rock type expected in deep crust, a $\chi_{tot}$ approximation is valid, as Q is small (Clark, 1997) and $M_{rem}$ can be neglected. However, basalts and igneous complexes may have higher Q and here we have to accept a higher error using the $\chi_{tot}$ approximation.

The 3D crustal structure of the Barents Sea has been defined using GMSYS-3D (Popowski et al., 2006) and the model was defined by a number of stacked

surface grids with a physical property distribution defined for each layer. To explain the magnetic anomalies in terms of lateral susceptibility variation in the basement, we performed susceptibility inversion using the GMSYS-3D inversion routine. Calculations are performed in the wave number domain using the Parker algorithm (Parker, 1972). The approach assumes that the magnetic response of the layer chosen for the inversion is caused by a series of vertical, square-ended prisms of infinite depth extent (in our model the prisms have a 5 x 5 km base).To calculate the model anomalies we defined the Earth's magnetic field in our area. The Barents Sea geomagnetic field input (H) is derived from the International Geomagnetic Reference Field (IGRF), and an average total intensity of 54700 nT, a declination of 16.5˚ and an inclination of 80.5˚ have been calculated.

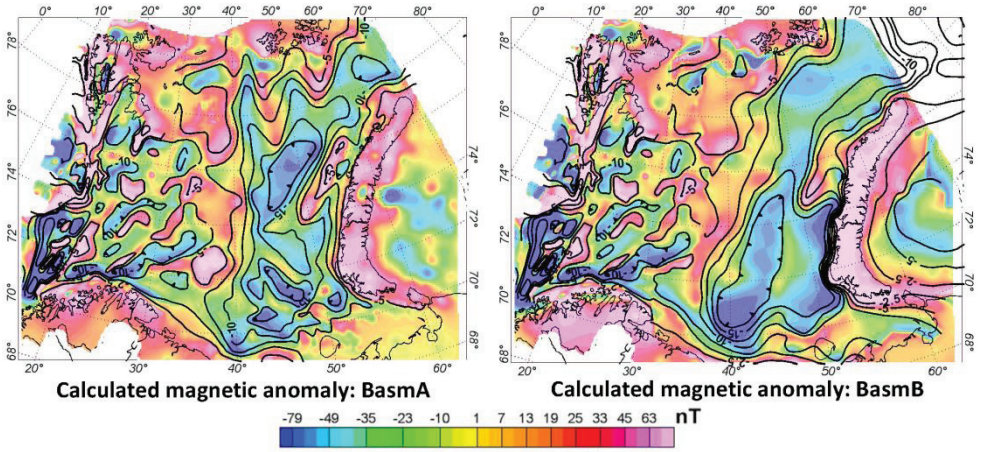


*Figure 4.6. Calculated magnetic anomalies assuming two top-basement models (BasmA and BasmB) and a homogeneous magnetisation distribution in the basement (0.025 SI). The contours represent the top-basement depths at every 2.5 km.*

## The initial 3D model

To study the relationships between top-basement geometry and magnetic anomalies we have calculated the magnetic field anomaly for two models composed of layers of constant susceptibility (Table 4.2) but differing top-basement geometries (BasmA and BasmB), as shown in Fig. 4.3.

A boundary at 8 km depth was introduced in order to differentiate the sediments into an upper and a lower layer. This distinction considers the possibility that metamorphic processes could take place at greater depths (up to 20 km) in some basins, thus generating a metasedimentary succession characterised by different magnetic properties (Clark, 1997).

A boundary between upper and lower crust is also assumed at 25 km. The lower crust gives only a small contribution to the magnetic anomalies for two main reasons; first, the rocks at depths greater than 25 km could eventually reach temperatures close to the Curie temperature, which involves a loss of the rock

magnetisation; and second, due to the large source distances, the effects of deep crustal sources become smoother.

The magnetic response of the model computed for both cases is represented in Fig. 4.6. The large contrast between the low-magnetic sedimentary rocks and the underlying high-magnetic basement makes the calculated magnetic anomaly particularly sensitive to the top-basement geometry. A clear correlation between the calculated anomalies and the basement morphology can be observed. Structural highs are producing strong positive magnetic anomalies, and deep basins generate strong negative magnetic anomalies. A comparison between the calculated magnetic effects and the observed magnetic anomaly (Fig. 4.2) demonstrates large misfits; the residual standard deviations (Table 4.3) are quite large for the two basement models (more than 100 nT).

| Model tests set up | Top Basement | Misfit Min (nT) | Misfit Max (nT) | Mean Value (nT) | Misfit Standard Deviation (nT) |
|---|---|---|---|---|---|
| Initial model (homogeneous basement) | BasmA | -766.8 | 1211.7 | -6.1 | 105.3 |
| | BasmB | -662.7 | 1201.7 | -6.3 | 107.6 |
| Susceptibility inversion test input: 25.1 SI*$10^{-3}$ | BasmA | -101.4 | 170 | -3.4 | 21.1 |
| | BasmB | -296.6 | 164 | -3.0 | 22.5 |
| Susceptibility inversion test input: 37.7 SI*$10^{-3}$ | BasmA | -103.9 | 205.6 | -3.3 | 23.6 |
| | BasmB | -279.5 | 197.5 | -2.7 | 25.4 |
| Susceptibility inversion test input: 12.57 SI*$10^{-3}$ | BasmA | -98 | 136.4 | -3.5 | 19.6 |
| | BasmB | -313.7 | 136.5 | -3.3 | 20.7 |
| Low-pass filtered magnetic field | BasmA | -78.37 | -173.5 | -4.4 | 22.5 |
| | BasmB | -191.6 | 163 | -4 | 23.8 |
| Upward-continued magnetic field | BasmA | -113 | 174.3 | -5.8 | 24.4 |
| | BasmB | -253.7 | 163.3 | -5.3 | 25.6 |
| All basement magnetic | BasmA | -93.3 | 187.1 | -2.4 | 19.3 |
| | BasmB | -273.1 | 177.9 | -1.8 | 20.1 |

*Table 4.3. Statistics on magnetic residuals (differences between observed and calculated anomalies) for the different susceptibility inversion tests.*

## The basement susceptibility inversion

The variation of magnetic properties in the entire Barents Sea basement is not well defined, notably due to the lack or impossibility of direct rock sampling. To evaluate the basement susceptibility distribution, we have applied inversion techniques and tested the influence of different source parameters (e.g. top-basement, maximum depths of magnetic basement) on the inversion results.

The lateral susceptibility variation in the basement has been calculated assuming an initial setting as defined in Table 4.2. During the first inversion, all the geometries and parameters have been fixed except for the susceptibility of the upper basement layer. We have carried out the first two tests by considering both

top-basement models (Fig. 4.3). The initial susceptibility (before inversion) was set to 0.025 SI, which is considered a good estimation of the average susceptibility based on the types of rock expected in the study area and on the acquired petrophysical data onshore. After inversion, the calculated results (Fig. 4.7) show large variations in the basement susceptibility for both types of top-basement geometry. The residuals of the two models show a standard deviation of 21-23 nT (Fig. 4.7, and Table 4.3). To understand the actual influence of the top-basement geometries on the inversion result, we have compared the main differences between the two top-basement models (Fig. 4.8a) with the differences in susceptibility obtained after inversion (Fig. 4.8b).

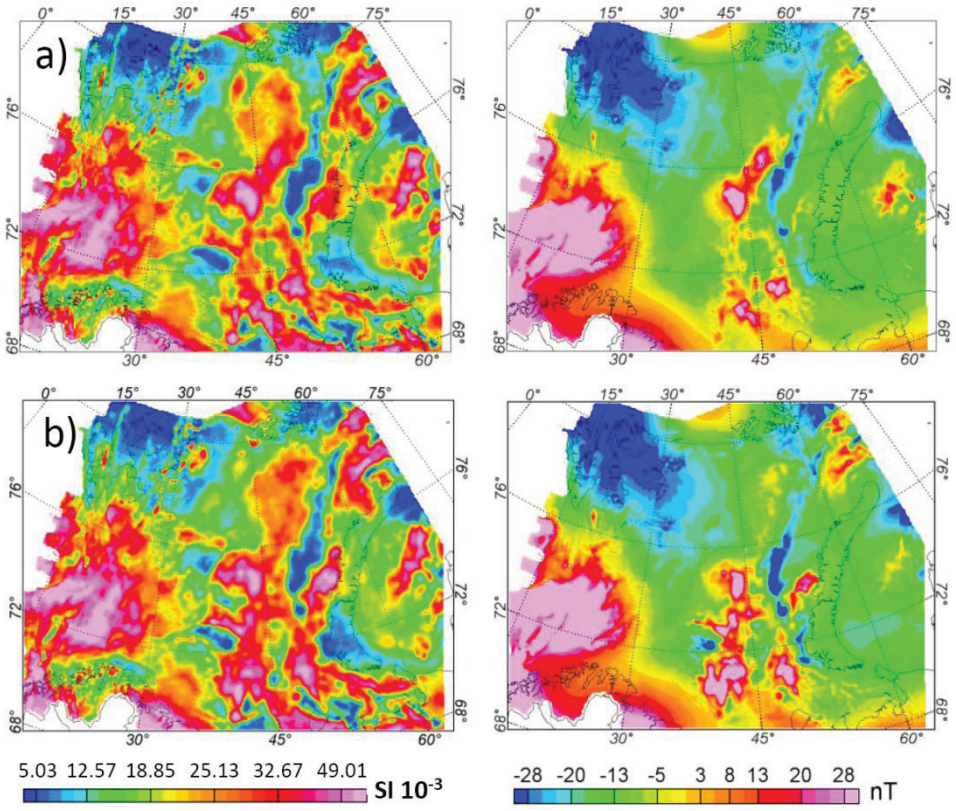


*Figure 4.7. Susceptibility inversion tests results. a) Distribution of basement susceptibilities obtained by inversion using the BasmA and input parameter of 0.025 SI. On the right the respective residual. b) Distribution of basement susceptibilities obtained by inversion using the BasmB and input parameter of 0.025 SI. On the right the respective residual.*

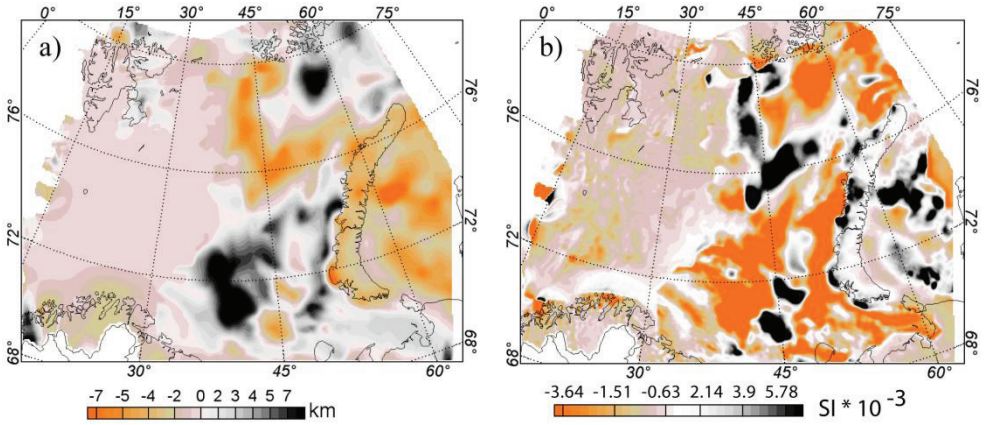


*Figure 4.8. Differences between the two top-basement compilations and their influences on the inversion result. a) Top-basement differences between BasmA and BasmB. Negative values mean that BasmA is deeper. b) Differences between the susceptibility results calculated using the total magnetic field for the two top-basement cases (Fig. 4.7a and 4.7b). In the case where the model BasmA has a deeper top-basement (negative differences), larger susceptibilities are needed to justify the anomalies. On the contrary, where a shallower top-basement is involved (positive differences), a smaller susceptibility is required to reproduce the same anomaly.*

The susceptibility range for the basement recorded from the sampled petrophysical data onshore is expected to be quite large due to the great variation in basement rock types. Consequently, the choice of the initial value is an oversimplification for the whole Barents Sea region. The use of a higher or lower initial susceptibility for the basement implies, respectively, an increase or decrease of the magnetic contrast between sedimentary successions and basement. To understand the influence of the initial susceptibility on the inversion results, we ran further inversions adopting different initial input values (0.0377 SI and 0.0126 SI). The main difference in these results is seen in a shift of the magnetic properties. This reflects the fact that magnetic anomalies are a consequence of the susceptibility contrast. The approach used of varying the susceptibility in each prism generates magnetic contrasts which are relative to the initial parameter. At the end of the inversion, the average value of the magnetic properties obtained is always close to the initial value. Table 4.3 shows the main characteristics of the residuals. This test shows that the results of the inversion do not change significantly when the magnetic contrast between sediments and the basement varies due to the choice of the initial susceptibility.

We have studied how the presence of short-wavelengths produced by noise, aliasing, levelling or other artefacts could influence the inversion. We have compared the calculated inversion obtained using the total magnetic field as input with the inversion results of the magnetic field devoid of the short-wavelength

(below 25 km, see Fig. 4.9 and Table 4.3) and upward-continued magnetic field (up to 5 km, see Fig. 4.9b and Table 4.3).

The initial simplification assumes that the rocks below 25 km do not have a strong influence on the magnetic anomalies either because of the large source distance or potentially the lack of magnetic properties due to high temperature, which nevertheless could not be the case everywhere. To study the potential influence of the lower crust, further inversion tests were also computed considering an extreme case where the entire crystalline crust from top-basement to Moho has high-magnetic properties (0.025 SI). A model employing a completely magnetic crust generates smoother contrasts and smaller variations in the results (Fig. 4.9c and Table 4.3).

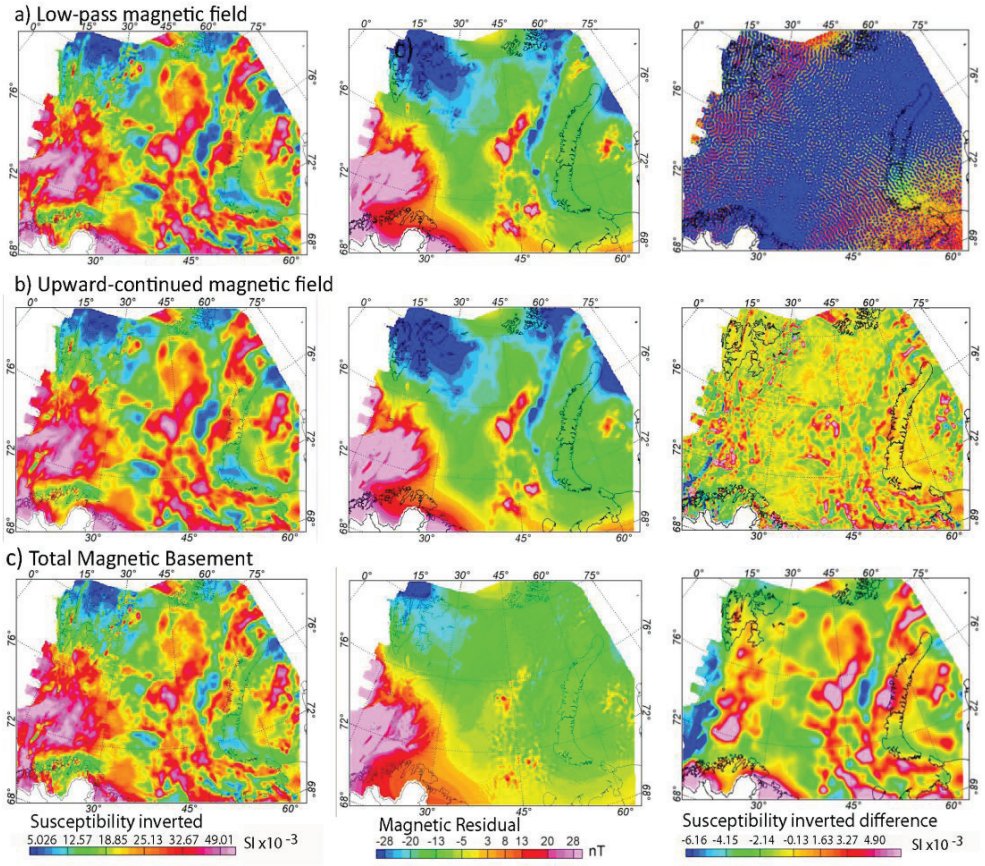


*Figure 4.9. Sensitivity tests using the BasmA model. Left column shows the inversion susceptibility results using different input parameters: a) 25 km low-pass filtered magnetic field and a magnetic crust above 25 km, b) 5 km upward-continued magnetic field and a magnetic crust above 25 km, c) the total magnetic field assuming a total magnetic crust. Middle column shows the residuals calculated for the three cases. Right column, differences between the susceptibility inversion results displayed in figure 7a and the one displayed here on the left for the three cases.*

| Sensitivity test | Influence in susceptibility results |
|---|---|
| High-frequency anomalies: Low-pass filtered magnetic field | from -2,5 to 2,5 SIx$10^{-3}$ |
| High-frequency anomalies: Upward-continued magnetic field | from -5,6 to 5 SIx$10^{-3}$ |
| All basement magnetic | from -7,5 to 5 SIx$10^{-3}$ |
| Top-basement uncertainty: max 8 km shallower | around -3,8 SIx$10^{-3}$ |
| Top-basement uncertainty: max 6 km deeper | around 6 SIx$10^{-3}$ |

*Table 4.4. Implications of the uncertainty parameters for the inversion results.*

### 4.5.2 Inversion tests: sensitivity results and discussions

The inversion techniques allowed a first estimation of the magnetic distribution of the basement. The calculated anomalies of a model characterised by homogeneous magnetisation distribution in the layers for both BasmA and BasmB are strongly influenced by the top-basement geometries (Fig. 4.6). The Barents Sea anomalies are quite large and positive (approximately from -150 to +250 nT) in areas where there are no large top-basement variations (e.g. Central Barents Monocline), and strongly negative in regions dominated by structural highs (e.g. Admiralty High, Fig. 4.2). These anomalies are considered to be the result of different magnetic properties in the basement. For example, the Admiralty High is expected to be a non-magnetic basement block, to justify the negative anomaly. Similarly, the large anomalies in the Central Barents Monocline are expected to be produced within a basement dominated by variable magnetic properties. Moreover, the range of anomalies produced using BasmA (approximately from -76 to 78 nT) and BasmB (approximately from -120 to120) is quite small compared with the observed range of the total magnetic anomalies (approximately from -180 to 350 nT). These observations point towards a heterogeneous basement structure.

The inversion tests carried out on the magnetic models allowed us to estimate the lateral susceptibility variations in the Barents Sea basement. In Table 4.4, the sensitivities of the parameters applied in the inversion are summarised. The tests have shown that the range of absolute values obtained from the inversion does not depend to any great extent on the initial susceptibility. The short-wavelength anomalies, which may be a consequence of either shallower high-magnetic sources (e.g. sills) or noise, could influence the calculated basement susceptibility by ±0.005 SI. The upward continuation, besides removing the short-wavelength, in general smoothes the anomalies and consequently the magnetic contrasts that result from the inversion are less sharp (Fig. 4.9b).

The deep boundary between the magnetic and the non-magnetic basement has a regional influence on the calculated lateral magnetic variation of the basement. The deeper this boundary is, the smaller are the susceptibility contrasts, indicating that a thicker magnetic basement requires low-magnetic properties to produce a

large-amplitude anomaly. In the same way, a larger volume of low-magnetic rocks does not require particularly low-magnetic properties to explain the observed anomalies (Fig. 4.9c and Table 4.4). The sensitivity of the calculated susceptibility to the top-basement is summarised in Table 4.4.

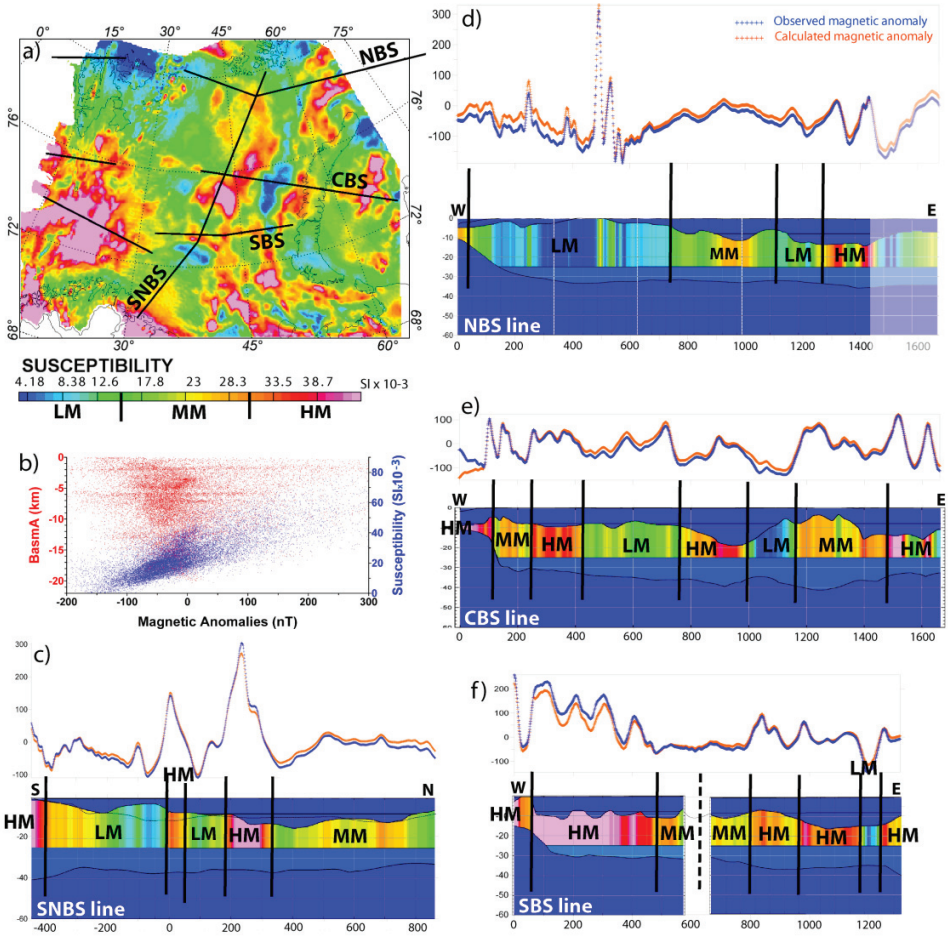


*Figure 4.10. Susceptibility inversion chosen as reference results. The model considers the total magnetic field inverted with a starting susceptibility of 0.025 SI, a magnetic basement above 25 km, a maximum standard deviation of 10 nT and a maximum of 9 iterations. a) Basement susceptibility map with the path of the seismic lines; High-Magnetic blocks (HM), Low-Magnetic blocks (LM) and Medium-Magnetic blocks (MM). b) plot of top-basement depths (BasmA) in relation to the magnetic anomalies and the susceptibility inverted toward the magnetic anomalies. The four transects show the results of the inversion along the same seismic profiles; c) South-North Barents Sea (SNBS) line; d) North Barents Sea (NBS) line; e) Central Barents Sea (CBS) line; f) South Barents Sea (SBS) line.*

Considering the range of the susceptibility results and the influence of uncertain parameters, the errors on the inversion results in the Barents Sea have been estimated to be around 30%. Despite these uncertainties, the results show a regional distribution of the magnetic properties which is consistent in all the tests and has to be considered as a first indication of magnetisation distribution in the study area. To define the main magnetic crustal units, and as an aid in further geological discussion, we focused on one specific model and considered the estimated range of errors.

The results displayed in Fig. 4.10 show that the inverted susceptibility correlates well with the anomalies (Fig. 4.10b), whereas the top-basement geometry does not show any correlation. The influence of the top-basement uncertainty on the inversion (maximum of 6 SI $10^{-3}$) will not be enough to perturb the correlation. This clearly indicates that the susceptibility is the predominant parameter which controls the regional magnetic anomalies in the Barents Sea. Further analysis has shown that the magnetic basement properties and the top-basement are not related parameters, and they play an independent role in the distribution of magnetic anomalies in the Barents Sea.

Examining the northern regional profile NBS (Fig. 4.10d), we can recognise positive high-frequency anomalies which are typically the effect of shallower sources (e.g. sills in the sediments). The inversion routine in this example is over-fitting the results and explains these anomalies in terms of lateral variations in the magnetic properties of the basement. This example shows that high-frequency basement susceptibility variations are not always reasonable, such that the results of the inversion have to be assessed at a larger scale and used to define possible regional magnetic domains. An initial organisation of the crust into several regional domains is defined from the inversion tests, also displayed in Fig. 4.10, and includes high-magnetic basement (HM), low-magnetic basement (LM) and medium-magnetic basement (MM).

## 4.6 Combined forward modelling

To validate the inversion results and to investigate the top-basement geometry, additional 2D forward models have been built combining seismic, gravity and magnetic data. Four profiles crossing the Barents Sea have been chosen on the basis of the existing seismic database. The initial geometries were set based on the same models that we adopted for the 3D magnetic model (Table 4.2) and have been locally refined taking into account published seismic transects. The main sedimentary packages, Cenozoic/Mesozoic and Palaeozoic sedimentary successions, were distinguished in the seismic profiles and are associated with different densities and susceptibility. The division into magnetic domains deduced from the 3D inversion (Fig. 4.10) was adopted in defining the main crustal units of the initial model. Density modelling has been carried out to study more accurately the geometries of the crust (e.g. top-basement, upper-lower crust boundary, Moho) by investigating the most reasonable density distribution that is able to explain the observed anomaly field and to be compatible with seismic and magnetic models.

The choice of the initial density parameters has been summarised in paragraph 4.3.3. The densities of the sedimentary package and of the mantle are fixed and consistent between all the transects, and the parameters of the basement have been changed in the expected range in order to explain the medium- to long-wavelength anomalies. The model geometry was refined and the physical parameters were tested by using the GMSYS software, applying the method of summation of irregular polygons modified after Talwano (1973). The results of the E-W lines (Fig. 4.11, 4.12 and 4.13) were integrated using the N-S line (Fig. 4.14) in order to make sure that all the profiles are coherent with each other.

### 4.6.1 South Barents Sea line – SBS line

The southern transect (SBS line, Fig. 4.11) is based on the interpretation of major seismic reflectors along two seismic sections MN89-202 and 079110 (Fig. 4.1) (Smelror et al. 2009) and refines the 3D inversion results displayed in Fig. 4.10f.

Along this profile, the top-basement is mostly the result of modelling since seismics constrain only in depth as far as the top Permian. The basement is lying at around 3 km at Stappen High, and is deepest at more than 12 km at Bjørnøya Basin, Nordkapp Basin and at the South Barents Basin (Fig. 4.11). The boundary between upper magnetic and lower non-magnetic crust is quite flat in the east, but in the west there is a thinning of the upper crust and the presence of higher densities and a high-magnetic shallower crust.

Four main crustal units (Fig. 4.11) can be distinguished: 1) a western magnetic province, 2) a central low-magnetic province, 3) a high-magnetic region beneath the South Barents Basin which is also dominated by quite high densities, and 4) a very low-magnetic basement in the east close to Novaya Zemlya. The high-magnetic western province is characterised by a highly magnetic basement, from the bottom of the basin to the Moho and by quite low densities in the upper crust. The magnetic contribution of the lower crust to the west is also necessary to justify the high-magnetic anomalies, and assuming a susceptibility in the upper crust in the expected range (Table 4.2) the shallowing of the lower crust is the most realistic configuration to balance the Bjørnoya Basin.

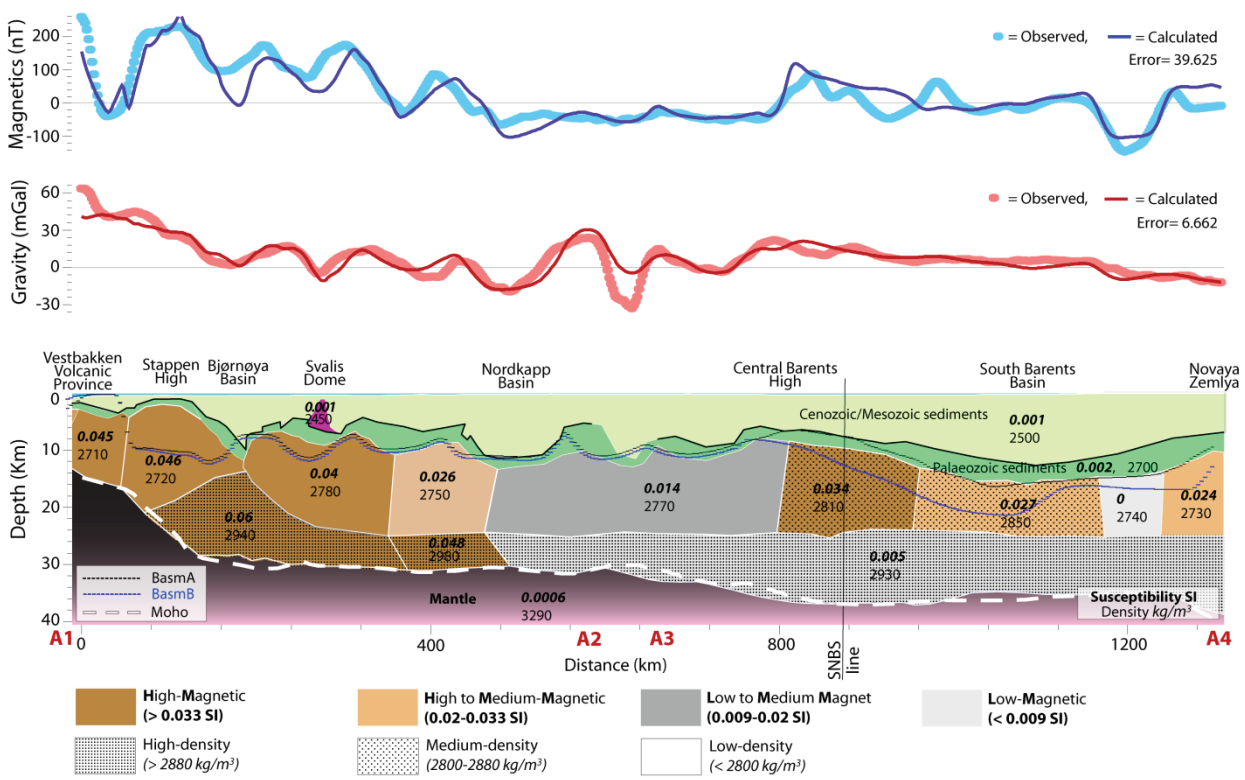


Figure 4.11. Forward modelling results along the South Barents Sea line (SBS line). See Fig. 4.15 for location (red annotation) and 10f for inversion results used as starting set up. Susceptibilities (in SI) are displayed in bold, and densities (kg/m3) in italics. The initial top-basement (BasmA and BasmB) and the initial Moho (Grad et al. 2009) are shown for comparison. The boundaries of the bodies constrained in the seismic data are displayed (in black) when they have been kept fixed during the modelling. White line shows the geometry which has been changed during the modelling. The intersection with the SNBS line is also displayed.

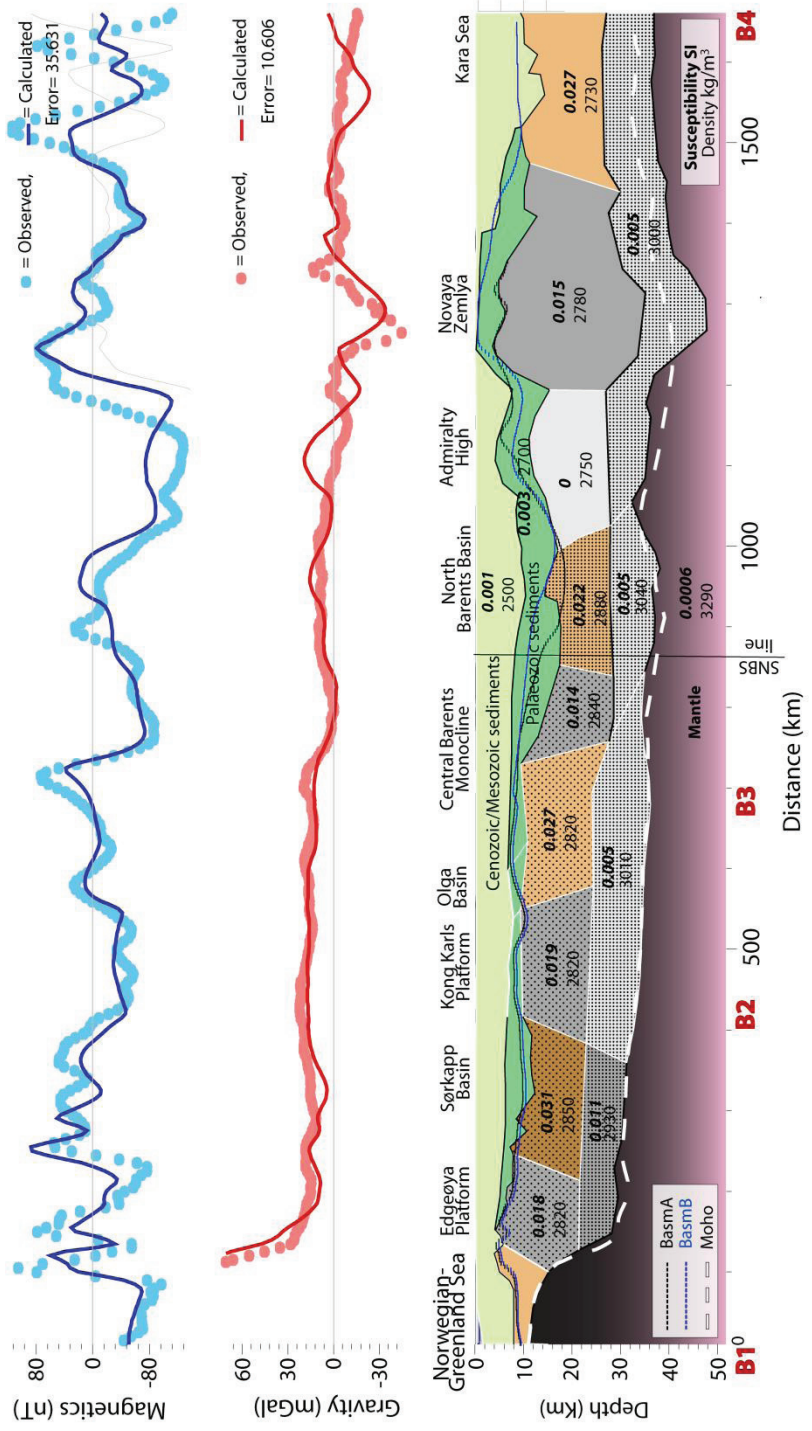


*Figure 4.12. Forward modelling along the Central Barents Sea line (CBS line). See Fig. 4.15 for location (red annotation) and 10e for inversion results. The other symbols and descriptions are in Fig.4.11.*

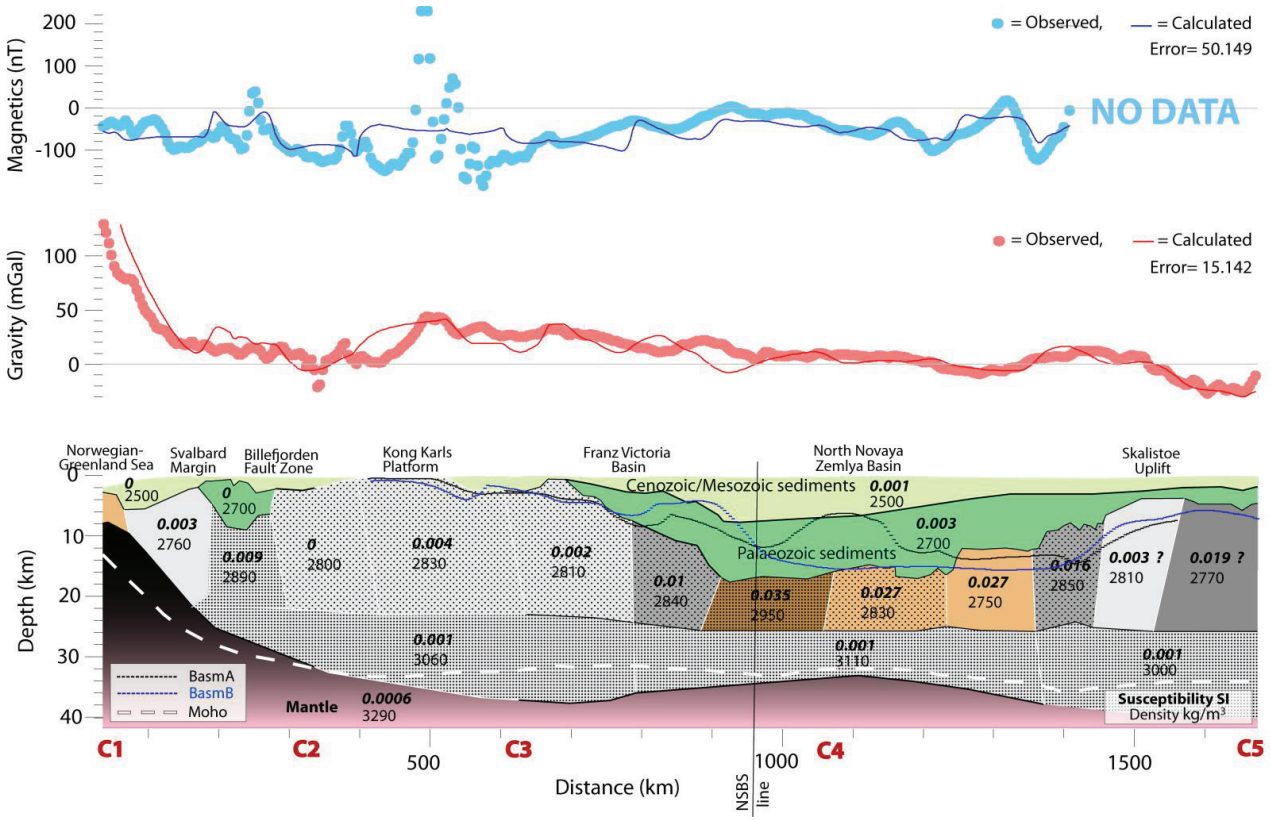


*Figure 4.13. Forward modelling along the North Barents Sea line (SBS line). See Fig. 4.15 for location (red annotation) and 10d for inversion results. The other symbols and descriptions are in Fig.4.11.*

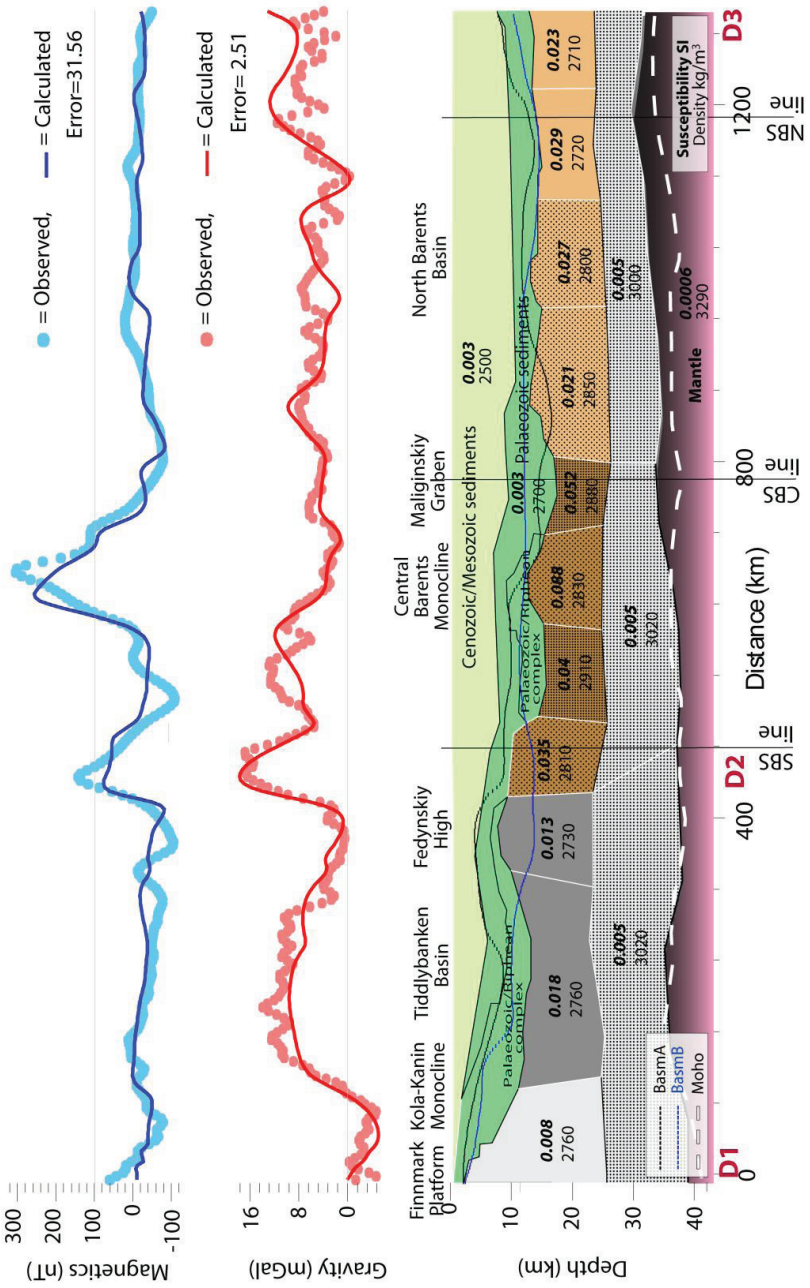


*Figure 4.14. Forward modelling along the South-North Barents Sea line (SNBS line). See Fig. 4.15 for location (red annotation) and 10c for inversion results. The other symbols and descriptions are in Fig. 4.11.*

### 4.6.2 Central Barents Sea line – CBS line

The central transect (CBS line) is based on a combination of recently published refraction profiles (Breivik et al., 2003; Ivanova et al., 2006; Roslov et al., 2009) and of our 3D inversion results (Fig. 4.10e). The modelling was complicated by large border effects of the magnetic and gravity signal that disturb the model laterally. The original 2-AR seismic line is located just at the northern edge of the central Barents Sea magnetic high, and its westward prolongation lies at the southern edge of two isolated magnetic highs (Fig. 4.2).

The majority of basement geometries have been kept fixed during the modelling where they are constrained by the seismic data (Fig. 4.12). The depth to top-basement ranges from around 4 km (Novaya Zemlya) to 18 km (North Barents Basin). The boundary between upper magnetic basement and lower crust is flat in the western province, whereas in the Eastern Barents Sea a thicker upper basement beneath Novaya Zemlya is deduced from our modelling and agrees with previous seismic studies (Ivanova et al., 2006; Roslov et al., 2009). The Moho depths are reduced to 33–37 km within the North Barents Basin and increase to 48 km beneath Novaya Zemlya.

The magnetic crustal units consist of a western magnetic province characterised by medium susceptibilities even in the lower crust (Fig. 4.12) and by medium densities in the upper crust. The upper basement from Kong Karls Platform to the margin of the North Barents Basin is mostly dominated by low-magnetic properties. A local high-susceptibility value between the Olga Basin and the Central Barents Monocline represents the edge effects of high anomalies close to the transect. The basement block beneath the North Barents Basin, adjacent to the largest Central Barents Sea anomaly (Fig. 4.2), has high magnetic properties are and high densities. That is probably an artificial effect due to lateral anomaly influence. The eastern province (Admiralty High and Novaya Zemlya) has low-magnetic properties and quite low densities. The lower crust in the Central and Eastern Barents Sea is almost non-magnetic. The boundary between magnetic and non-magnetic crust is quite flat in the Western Barents Sea (around 23 km) but deepens towards the east (around 30 km under Novaya Zemlya).

The Moho is quite flat in the west; in the east it is constrained by reflection seismic data and shows a deep root below Novaya Zemlya.

### 4.6.3 Northern Barents Sea line – NBS line

The northern profile is based on the northern Svalbard profile (Geissler, 2001; Ritzmann, 2003; Faleide et al., 2008) and on the refraction study 4-AR (Roslov et al., 2008; 2009) to the east. The seismic data constrain the deep geometries of the basement and Moho that have mostly been kept fixed in the forward modelling. The inversion results used as initial susceptibility are shown in Fig. 4.10d.

The top-basement varies considerably from shallower depths in the west (4-6 km) to depths in the order of 16-18 km towards the east. The thickness of the crust also changes laterally; it is thinnest near the Norwegian-Greenland Sea (around 10 km) and becomes thicker beneath the North Novaya Zemlya Basin (around 20 km), and even thicker below the Kong Karls Platform and in proximity to the Skalistoe Uplift (Fig. 4.13). The interface between upper and lower crust is quite flat.

The Moho is located at around 38 km depth beneath the Kong Karls Platform and Skalistoe Uplift. It shallows to around 33 km under the North Novaya Zemlya Basin and rises to around 9 km depth beneath the Norwegian-Greenland Sea.

The magnetic basement results show less magnetised rocks in the west but exhibit high-magnetic properties in the western part of the North Novaya Zemlya Basin (Fig. 4.13). The eastern part of the North Novaya Zemlya Basin seems to be dominated by medium- to non-magnetic basement. The easternmost part of the transect is not covered by magnetic data. The magnetic residual standard deviation along this section is the highest observed (50 nT) in the study area. The largest differences between the observed and the calculated field are located on the eastern side of Svalbard (Kong Karls Platform). It is well known that the region has been affected by magmatism at shallow depths (Grogan et al., 1998; Meyer et al., 2007). Magmatic intrusions have strong magnetic properties and can locally produce strong signals that have not been assessed in our regional basement study.

### 4.6.4 South-North line –SNBS line

The last transect modelled (SNBS line) follows the location of the 1-AR regional seismic transect (Ivanova et al., 2006). Our final modelled geometry follows the seismic interpretation. The inversion results considered as a starting point are displayed in Fig. 4.10c.

With the exception of the Fedynskiy High, the top-basement is relatively flat and occurs at depths in the range of 14-17 km (Fig. 4.14), The boundary between the upper magnetic and lower non-magnetic basement is almost horizontal at around 26 km. The Moho does not show any large variations, but generally shallows towards the north.

Three major basement domains are distinguished along the transect (Fig. 4.14), referred to here as the southern, central and northern domains. The basement located south of the Fedynskiy High shows low densities and quite low-magnetic properties. Medium to high densities and a high-magnetic distribution are interpreted in the central part of the transect, with the northern part of this central domain characterised by a magnetisation that is significantly higher than in the southern part. The basement farther north appears to have densities that decrease gradually towards the north, whilst the magnetic properties do not show large variations and are quite high (Fig. 4.14).

### 4.6.5 Forward modelling results

The forward modelling along the four transects gave a reasonable fit to the anomalies with residuals at around 35 nT and 9 mGal for the magnetic and gravity anomalies, respectively.

Modelling the SNBS line allowed us to integrate the E-W lines and thereby reach a consistent result. Whereas the SBS and CBS lines were nicely interconnected, discrepancies were found at the intersection between the SNBS and NBS lines (Fig.4.13 and 4.14).

The results of the forward models are quite consistent with the initial inversion models, and discrepancies exist only locally. The SBS line (Fig. 4.11) shows the most consistency (Fig. 4.10f). The CBS line (Fig. 4.12) agrees with most of the inversion results (Fig. 4.10e), but the high-magnetic block located between the

Olga Basin and the Central Barents Monocline is shown to be more magnetic in the forward modelling. On the contrary, the block beneath the North Barents Basin is less magnetic than in the inverted model. The discrepancies between the inversion results and the forward modelling are attributed to an edge effect of high anomalies close to the profile (Fig. 4.2) that cannot be removed in the 2D forward modelling, but must be addressed in a 3D model. The magnetic properties along this transect differ from the inversion results, e.g., in the proximity of Novaya Zemlya the thick modelled crustal block needs a lower magnetisation than in the thinner upper basement defined in the inversion (Fig. 4.10e and 4.12). The NBS and SNBS lines show the largest differences in the susceptibility results in comparison with those in the inverted ones, especially in the North Novaya Zemlya Basin along the NBS line (Fig. 4.13), in the Central Barents Monocline and along the southern part of the SNBS line (Fig. 4.14). In these regions, the forward models show higher susceptibilities (see Fig. 4.10c and 4.10d for comparison) and also delineate a top-basement that is significantly different to that in the BasmA and BasmB used in the inversion, which appears to be the main reason for the two different magnetic results. The forward modelling defines thinner and deeper magnetic basements, characterised by higher magnetic properties.

The four 2D models allowed us to test the validity of the existing top-basement models. From the results it is not possible to consider BasmA or BasmB as being more reliable than the other for the entire Barents Sea area. Each model fits some areas better than others.The Western Barents Sea top-basement (Skilbrei, 1991) is mostly consistent with our result along the CBS line (Fig. 4.12) but it shows a large difference along the SBS line in the area of the Stappen High (Fig. 4.11). At that specific location, our top-basement is lying at around 3 km depth, 6 km shallower than in the starting model.

In the Eastern Barents Sea the BasmA model fits nicely with the SBS line results (Fig. 4.11), but a mismatch is observed with the NBS line (Fig. 4.13). Particularly in the North Novaya Zemlya Basin (Fig. 4.13) the basement BasmA is not realistic (around 8 km shallower) and the results of our modelling explain the gravity and magnetic anomalies without requiring the presence of any basement high. Along the CBS (Fig. 4.12) and SNBS lines (Fig. 4.14), significant differences of the order of 6 km exist. The presence of a high top-basement at the Fedynskiy High and Admirality High appears to be less prominent in our model.

The BasmB model in the Eastern Barents Sea proposed depths consistent with our results along the Central Barents Monocline in both SBS and CBS lines, but in the South Barents Basin the model seems to be too deep along the SBS line (Fig. 4.11). The BasmB model here is at around 20 km depth that would imply the presence of c. 10 km of Palaeozoic sedimentary rocks beneath almost 10 km of recorded Mesozoic sediments, which does not fit either with our gravity and magnetic models or with previous studies (Otto and Bailey, 1995; O'Leary et al., 2004). Along the CBS line (Fig. 4.12), the BasmB is shallower by about 4 km at more than one location. Along the NBS line (Fig. 4.13) it is also too shallow near the Franz-Victoria Basin and too deep towards the east. Along the SNBS line (Fig. 4.14), discrepancies of around 6 km are found especially in the southern and central parts of the profile.

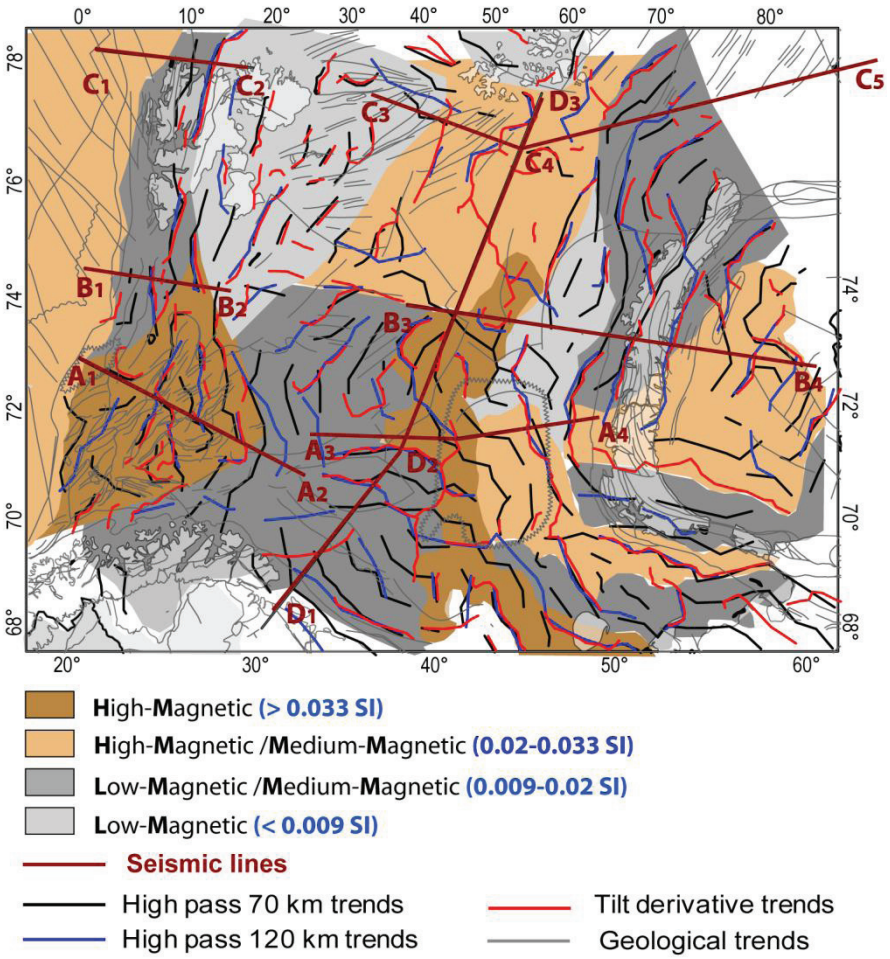


*Figure 4.15. Map of the susceptibility domains proposed for the Barents Sea.*

## 4.7 Discussion and interpretation

The results obtained along the four transects were extrapolated between the lines and considered in the light of the information that we gained from the inversion results and image processing. In this way, we were able to assess the regional distribution of the susceptibility in the Barents Sea basement. Fig. 4.15 shows the various basement blocks or domains that are dominated by similar susceptibilities. The following characteristics are recognised.

Four types of susceptibility magnetic basement are defined.

The Western Barents Sea high-magnetic block has an upper and lower basement which are both magnetic.

The two Central Barents Sea highs are considered to be parts of two distinct magnetic domains running between the Central Barents Monocline and the Eastern Barents Basin.

The low-magnetic basement east of Svalbard is part of a shallow, thick platform.

The North Barents Basin and the South Barents Basin seem to be two separate and independent magnetic regions.

The western flank of the Eastern Barents Basin is characterised by a high-magnetic basement.

The eastern flank of the Eastern Barents Basin is characterised by a low-magnetic basement.

In the Southwest Barents Sea and in Svalbard, there are good correlations between the magnetics (MW magnetic anomaly domain, Fig. 4.5 and 4.15) and tectonic lineaments (Fig. 4.1) whereas in the northern area of the Loppa High and the Bjarmeland Platform the magnetic trends do not accord with the previous tectonic interpretation of the main faults (Gabrielsen et al., 1990). One possible explanation for such a discrepancy may be attributed to the fact that the earlier interpretation considered only the main, post-Permian, basin-bounding structures. Instead, we consider that the magnetic lineaments are likely to have been generated by older and/or deeper basement structures which could have had different orientations. On Svalbard, in the southwestern Barents Sea and in western Finnmark, tectonic lineaments (Doré, 1995; Fichler et al., 1997; Roberts and Lippard, 2005) broadly correspond with the N-S and NE-SW orientations of the main magnetic lineaments (MW patterns Fig. 4.5) and are considered to reflect Caledonian structures. The minor NW-SE trends in the MW domain could eventually be explained as relict Timanian structures or even a deflected Caledonian structural grain. This interpretation of the magnetic signature is in agreement with Gernigon et al. (2007) and Barrère et al. (2009) who described elbow-shaped magnetic trends associated with a lateral deflection of Caledonian structures in the Western Barents Sea.

The largest Western Barents Sea magnetic high is the combined effect of high-magnetic properties and a shallow basement (Fig. 4.11, 4.12 and 4.15). Both Ritzmann and Faleide (2007) and Barrére et al. (2009) recognised that the source rocks in the basement of this domain could be the Archaean to Palaeoproterozoic, mafic and felsic, medium- and high-grade metamorphic rocks that extend offshore from Northeast Norway and Northwest Russia. The pseudo-gravity high together with the gravity high in the west indicates that the high-magnetic crust should also be characterised by high densities. The coinciding magnetic and gravity anomalies could be interpreted either as a metamorphic core complex formed during exhumation of lower crustal rocks along low-angle detachment zones (Barrère et al., 2009) or as magmatic intrusions. The high-magnetic and high-density, shallower, lower crust block found along our SBS line (Fig. 4.11) under the Bjørnøya Basin could be an example of exumation or magmatism, or both.

The Central Barents Sea domains (M1, M2 Fig. 4.5 and 4.15) are located at the transition between the Eastern and Western Barents Sea, where there are important changes in the tectonic setting and style of basin development. The NW-SE and E-W lineaments of M1 appear to coincide with the prolongation of Timanian structures as defined in the Timan Ridge, Pechora Sea and southern Novaya Zemlya (e.g. Baidaratsky Fault, Fig. 4.1) (Roberts and Siedlecka, 2002; Korago et al., 2004). The Kola-Kanin Monocline (Fig. 4.1) has a NW-SE magnetic trend that

extends farther north until it is truncated by NE-SW magnetic lineaments (Fig. 4.5). In the Finnmark Platform, these NE-SW trends reflect the thrust front of the Caledonide Orogen which truncates the older NW-SE structures of the Timanian terrane. We can thus assume that in the M1 domain the NE-SW magnetic trends are produced by Caledonian structures whereas the NW-SE trends are ascribed to the Timanian orogeny.

The high-magnetic anomalies over the Central Barents Monocline are mostly the effect of high-magnetic crustal blocks, and not of shallower basement topography (Fig. 4.11, 4.12 and 4.15). The forward model and the image processing illustrate that the two central magnetic anomalies probably reflect the presence of distinct high-magnetic blocks (Fig. 4.14). The southern block, running from the southern Central Barents Monocline towards the south, is less magnetic (a maximum of 0.4 SI) than the northern one (a range of 0.5-0.079 SI). The Central South Barents Sea is characterised by an inverted low susceptibility (Fig. 4.10) and basement blocks obtained from the forward modelling which have low-magnetic properties (Fig. 4.14). These properties, together with the different magnetic anomalies enhanced by the field analysis, especially from the pseudo-gravity (Fig. 4.5), suggest that the two high anomalies in the Central Barents Sea probably have different origins. A possible explanation is that the southern high anomaly (near the Fedynskiy High, located in the M1 domain in Fig. 4.5) is related to either Timanian or Caledonian basement, whereas the northern one (located in the M2 domain in Fig. 4.5) remains of unknown origin. The seismics along the 1-AR profile (Ivanova et al., 2006) show the Riphean complex below the Finnmark Platform to extend farther to the north (Fig. 4.14). Whether or not the complex is related to the source of the magnetic anomalies is still unclear. We can only speculate that the high-magnetic block that produces the largest, central Barents Sea, magnetic and gravity high is an exhumed or intruded block characterised by high-magnetic properties and high densities. The presence of either ancient or Devonian oceanic crust (Zonoenshain et al., 1990; Aplonov et al., 1996) can also be considered.

In the Southeast Barents Sea, the NW-SE-oriented magnetic anomalies correlate with the tectonic lineaments (MSE in Fig. 4.5, and 4.15) and relate to the Timanian Orogeny (Roberts and Siedlecka, 2002). Two blocks of high-magnetic crust trend NW-SE and are separated by a non-magnetic basement block (Fig. 4.10), also coinciding in orientation with the Timanides. Kostyuchenko at al. (2006) have described the magnetic anomalies of the northeast margin of the East European Craton where the NW-SE magnetic trend has been explained as the effect of Palaeoproterozoic and Archaean, high-magnetic complexes situated in the sub-surface (Timan Range and East Pechora Basin, Fig. 4.1) and distinct from the thick, turbidite-dominated successions that are associated with the Timanide orogen (Gee and Pease, 2004; Roberts et al., 2004). The turbiditic low-magnetic successions are flanked in the eastern part of the Pechora Basin by an equally prominent boundary to a highly magnetic, NW-SE-trending belt that is known from drillcores to be dominated by Riphean volcanoclastic successions and a Neoproterozoic magmatic complex (Kostyuchenko et al., 2006). The high-magnetic basement found with the inversion in the Southeast Barents Sea is considered to reflect either the volcanoclastic successions or the Palaeoproterozoic/Archaean basement. Forward modelling has not been carried out

in this part of the Barents Sea and the magnetic trends defined by field analysis become more erratic offshore, making it difficult to verify a relationship with the tectonic lineaments. However, the offshore extension of the Timanian trend can be estimated from our inversion results and it can therefore be assumed that the Timanian Proterozoic basement extends no further than the South Barents Sea line (at around 73˚N, Fig. 4.10).

The tectonic subdivision of Novaya Zemlya into three major domains (Korago et al., 2004), the southern domain considered to be a peripheral part of the Late Neoproterozoic Timanian fold belt, and the other two without Timanian influence north of the Baidaratsky Fault, is consistent with our magnetic interpretation. The pseudo-gravity (Fig. 4.4d and 4.5) also enhances the differences between the two northern domains and the southern one. Moreover, the magnetic patterns in the south are orientated parallel to the Timanian lineaments (Fig. 4.1 and 4.5), whereas in the two northern regions the setting is coinciding with the major Uralian trends (Gee and Pease, 2004; Korago et al., 2004), which can be the effect of Uralian thrusting. In central and northern Novaya Zemlya, the high-magnetic anomalies are considered to be the effect of a thick upper crust, defined on the basis of a seismic model (Ivanova et al., 2006; Roslov et al., 2009), that requires no high magnetisation to explain the anomalies. The significance of the low-magnetic basement block, in terms of rock type and its relation with Uralian thrusting or Siberian basement is still not clear.

The North and the South Barents Basins appear to be dominated by different characteristics. The field analysis distinguishes different patterns and different regional anomalies and pseudo-gravity between the North and the South Barents Basins (Fig. 4.5). The magnetic properties of the basement are found to be different between the Northern and the Southern areas, and between the western and the eastern parts of the Eastern Barents Sea using both inversion and forward modelling methods (Fig. 4.15). The origins of such different basement blocks and the roles that they have played in the evolution of the basins are not yet understood.

The Northeast Barents Sea area is quite distinctive from its surrounding by the presence of a pseudo-gravity high that coincides with a Bouguer anomaly high (Fig. 4.2 and 4.4d); and the magnetic lineaments are recognised to follow the Uralian trends (Fig. 4.1 and 4.5). The forward modelling shows that the Northeast Barents Sea is dominated by a deep basin and a crust with high-magnetic and high-density properties. Whether this basin is the continuation of the North Barents Basin or a separate basin is not clear, but the scenario of a basement beneath the basin dominated by high magnetisation in the west and lower magnetisation in the east is similar to the situation along the South and Central Barents Sea lines (Fig. 4.11 and 4.13). This could be an argument in support of the idea that the North Barents Basin swings into the Northwest Barents Sea following the Novaya Zemlya structural setting.

The region East of Svalbard lies close to the continental shelf forming the oceanic transition zone. There, a series of small-scale anomalies (M3, Fig. 4.5) are considered to be the effects of sill intrusions related either to the Cretaceous magmatic event (Grogan et al., 1998) or Paleogene-Neogene events (Prestvik, 1978; Harland et al., 1997; Harland and Stephens, 1997). Similar sills are expected to occur farther to the east and also in the deep North Barents Basin.

## 4.8 Conclusions

The qualitative analysis of the magnetic anomalies allows us to distinguish regions in the Barents Sea characterised by different magnetic signals.

The 3D magnetic models defined by homogeneous layers produce magnetic anomalies strongly affected by the top-basement geometry, but the smaller range of calculated anomalies compared with that of the observed field and the large residuals indicate the presence of an inhomogeneous magnetic basement.

A large number of estimations of the lateral susceptibility distribution in the basement have been made using inversion. Around 30% of uncertainty is to be expected for most of the results. However, a clear correlation has been found between the magnetic anomalies and the distribution of the susceptibilities. The top-basement geometry, however, shows no clear correlation with the magnetic anomalies. This implies that the magnetic properties of the basement and not its geometry is the dominating factor for the distribution of magnetic anomalies on the regional scale of the Barents Sea.

The forward models are consistent with the inversion results and allow us to refine the existing top-basement models and to estimate their validity.

A further integration of our results has resulted in the compilation and interpretation of the susceptibility basement domain map. In the Western Barents Sea, the N-S magnetic trends that swing NE-SW towards the south are associated with Caledonian structures, and the high-magnetic basement block dominated by high densities is considered to be exhumed and/or intruded lower crust. The basemen to the South Central Barents Sea remains somewhat controversial but is considered to have been affected by the Caledonian or more probably Timanian orogenies. The NW-SE lineaments of the Southeast Barents Sea and in the Central South Barents Sea are recognised as Timanian structures, and the magnetic basement in these areas is considered to be composed of Palaeoproterozoic and Archaean complexes or Neoproterozoic volcanoclastic successions. The distinction between the southern Novaya Zemlya domain affected by Timanian deformation structures and the central and northern Novaya Zemlya terranes influenced by the Uralian orogeny is supported by our study. The North and the South Barents Basins are underlain by different magnetic basement blocks that provide indications of differing origins for the two basements and of a probable propagation of the North Barents Basin towards the Northeast Barents Sea.

The study has provided new information on the magnetic properties and structures of the Barents Sea basement. Future work should be directed toward reducing the uncertainties surrounding the top-basement geometries and to better estimate the magnetic parameters, in particular of the susceptibilities in the Uralian and Siberian basement. Moreover, we are developing a more refined 3D model that will be useful for confirming the

susceptibility distribution in the basement domains and will also be conducive to an improved geological interpretation.

## *Acknowledgements*

*The study was carried out as part of the PETROBAR project (Petroleum-related regional studies of the Barents Sea region) funded by Statoil and the PETROMAKS programme of the Research Council of Norway. We thank Jan Inge Faleide and Yuri Roslov for their help regarding the interpretations of the Regional Arctic Transects. We are very grateful to David Roberts for editorial review before manuscript submission. We thank the editor Hans Thybo and two anonymous reviewers for the comments which helped to improve the manuscript.*

# Chapter 5

# Basement inhomogeneities and crustal setting

*The content of this chapter is submitted for publications in: Marello, L., Ebbing, J., Gernigon, L., 2012. Basement inhomogeneities and crustal setting in the Barents Sea from a combined 3D gravity and magnetic model. Geophys. J. Int. (submitted).*

We present a new 3D geophysical model for the Barents Sea that highlights the basement properties and crustal setting. The model results from the modelling of gravity and magnetic field anomalies and is based on a large number of seismic and petrophysical data. The set up consists of: a water layer, sedimentary units that incorporate density variations associated with depth and time of deposition (Cretaceous-Cenozoic, Triassic-Jurassic, Late Palaeozoic and deeply buried sediments), upper and lower basement, and an upper mantle. The upper crust is considered as the major source of the magnetic anomalies and has been divided into a number of units dominated by constant densities and magnetisation, which show a good correlation with the main structural elements of the Barents Sea. The Southwest Barents Sea crust is an aggregation of allochthonous Caledonian terranes and autochthonous Archaean and Palaeoproterozoic complexes. We interpret the different crustal blocks in terms of distinctive lower, middle, upper and uppermost Allochthonous terranes that can be linked with the major nappes

onshore. The North Barents Sea is distinguished from the rest of the shelf by its low-magnetic properties and its large crustal thickness. These differences are compatible with a geodynamic scenario in which Svalbard formed an independent crustal block (Barentsia) that was located between Baltica and Laurentia and became attached to the rest of the shelf during the Caledonian orogeny. To the east, the basement underlying the large mega-sag East Barents Basin, is an assemblage of Precambrian rocks deformed during the Timanian and Uralian orogenies. The basement is characterised by an alternation of high-magnetic and low-magnetic units that mimic the arcuate shape of Novaya Zemlya. In the Southeast Barents Sea, the crustal units are linked to the onshore geology of the Timan-Pechora region and are mostly the result of Timanian orogenesis.

## 5.1 Introduction

The Barents Sea represents a large part of the Arctic region and extends between the Norwegian-Greenland Sea, the Arctic Ocean margin, Novaya Zemlya and the Norwegian-Russian mainland (Fig. 5.1).

The geodynamic evolution and crustal setting of the Barents Sea have been in focus for the last few decades due to its petroleum potential (e.g. Johansen et al, 1992; Gautier et al. 2009; Henriksen at al. 2011). Several new regional models have been proposed in recent years (e.g. Ritzmann et al. 2007; Barrère et al. 2011) discussing the complexity of the area and emphasising the need for further integrated studies.

The Barents Sea is characterised by structural styles which differ between the west and the east (Johansen et al. 1992; Henriksen et al. 2011). The top basement in the Barents Sea has previously been estimated in a number of studies (Skilbrei, 1991; Johansen et al. 1992; Gramberg et al. 2001; Ritzmann et al. 2007; Barrère et al. 2009) that locally point out differences in the order of ±8 km (Marello et al. 2010). The large differences can be explained (1) by the difficulties involved in estimating the top of the deeply buried basement using seismic and gravity data, and (2) by the definition of the top basement itself. In the deepest basins, sediments are strongly affected by compaction and their densities can approach those of the underlying basement rocks. This results in a decrease of both the acoustic impedance contrast and the signal-to-noise ratio. Furthermore, the presence of salt (e.g. Nordkapp Basin, Svalis Dome) and shallow magmatic intrusions in the basins (e.g. East Svalbard or in Triassic strata in the East Barents Basin) locally complicate the estimation of the depth to top basement. The second difficulty is directly related to the concept of top basement. Depending on the target of the study area and methods used, the definition and location of the basement surface can be different.

Besides the precise location of top basement surface, the location other aspects remain uncertain. The mechanisms involved in basin formation are unknown in many places (e.g., East Barents Basin, Palaeozoic basin locations). The nature of basement also plays an important role in basin initiation and a better understanding of its crustal composition will help us to understand the evolution of the Barents Sea shelf.

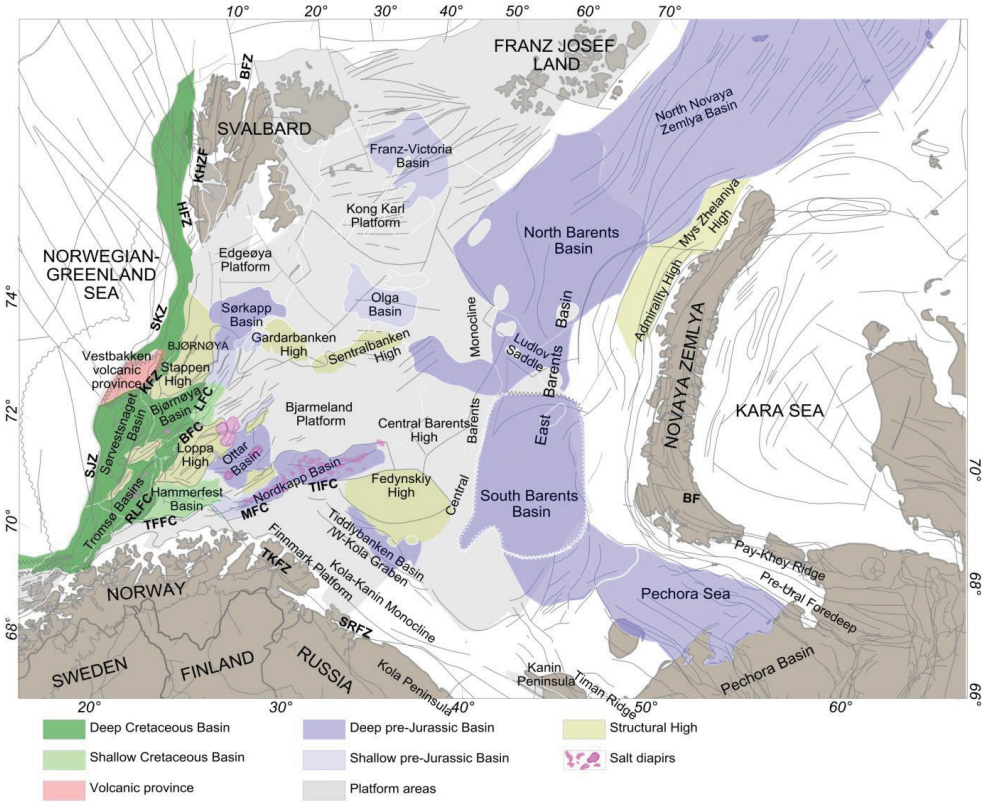


*Figure 5.1: Barents Sea structural setting map with basins, structural highs, and platform areas displayed. The abbreviations denote to the major fault complexes: SJZ: Senja Fracture Zone; RLFC: Ringvassøy-Loppa Fault Complex; TFFC: Troms-Finnmark Fault Complex; MFC: Måsøy Fault Complex; TIFC: Thor Iversen Fault Complex; BFC: Bjørnøyrenna Fault Complex; KFZ: Knølegga Fault Zone; SKZ: Sørkapp Fault Zone; HFZ: Hornsund Fault Zone; KHFZ: Kongsfjorden-Hansbreen Fault Zone; BFZ: Billefjorden Fault Zone; BF: Baidsratsky Fault Zone; SRFZ: Sredni-Rybachi Fault Zone; TKFZ: Trollfjorden-Komagelva Fault Zone.*

As direct offshore sampling and logging of the basement are limited, crustal properties must consequently be studied using indirect geophysical methods. The distributions of densities, susceptibility and seismic velocities, allow us to distingush individual areas that can have specific geological histories.

In this study, we present a 3D forward model for the entire Barents Sea region, in which we define densities and magnetisation for the crust. The model defines the major geometries and allows for a division of the Barents Sea basement into regions with homogeneous properties related to distinctive rock types and geological evolution. The relationship between the nature of the basement blocks, the crustal thickness and basins are discussed in order to provide a better understanding of the evolution of the Barents Sea.

## 5.2 The Barents Sea region: basement evolution

The Barents Sea continental shelf formed by the aggregation of different crustal terranes that evolved during three major orogenic events: Timanian, Caledonian and Uralian. Subsequently, a large number of rifting episodes took place which led to the complex intracratonic setting that we see today.

The latest Neoproterozoic to Early Cambrian Timanian event involved the Southeast Barents Sea region; the Timan-Pechora Basin, southern Novaya Zemlya and areas offshore in the Barents Shelf (Fig. 5.1). However, its full extent and significance offshore is still poorly constrained (Olovyanishnikov et al. 2000; Roberts and Siedlecka, 2002; Pease and Scott 2009). The Timanian orogenic deformation and metamorphism telescoped and accreted Neoproterozoic magmato-sedimentary assemblages against the northeastern margin of Baltica, generating NW-SE-trending, SW-vergent folds and a NE-dipping pervasive cleavage (Roberts and Olovyanishnikov, 2004). In this work, the term Timanian basement terranes include the Precambrian sedimentary successions, the volcano-sedimentary and igneous rock units, island arcs and other ocean-floor magmatic rocks involved in the Timanian orogeny.

The western Barents Sea has been strongly influenced by the Caledonian orogeny, which began in the Early Ordovician and culminated with the collision of Laurentia and Baltica in Mid Silurian to Early Devonian time (Roberts 2003; Gee et al. 2008). The Caledonian influence is recorded in northwesten part of the West Barents Sea by N-S structural trends and in the southwest by NE-SW structures (Dengo and Røssland 1992; Gudlaugsson et al. 1998; Faleide et al. 2008), although this last trend is actually now disputed in the light of new aeromagnetic data (Gernigon et al. 2008; Gernigon and Brönner 2012). On the Norwegian mainland, the basement is an assemblage of two different types of terrane: the autochthonous rocks of the Fennoscandian Shield (Palaeoproterozoic and Archaean crystalline complexes), and the Caledonian allochthons, which represent the remnants of a Baltoscandian rifted margin system including shelf successions, oceanic and arc units, and exotic rocks with Laurentian affinities (Roberts, 2003). The allochthons are subdivided into four major groups: Lower, Middle, Upper and Uppermost (Roberts and Gee 1985; Siedlecka et al. 2004; Gee 2005; Nystuen et al. 2008). The Caledonian basement in Finnmark, northernmost Norway extends into the Barents Sea shelf but its nature and geometry beneath the younger sedimentary cover are still not clear (e.g. Ziegler 1988; Doré, 1991; Gudlaugsson et al. 1998; Ritzmann and Faleide 2007; Faleide et al. 2008; Gee et al. 2008; Gernigon et al. 2008; Barrère et al. 2009, 2011).

On the Svalbard archipelago, three crustal blocks can be distinguished. Most authors agree that Svalbard formed the margin of Laurentia in Precambrian and Early Palaeozoic times. During the development of the Caledonides in Silurian time the three domains were united with the rest of the shelf (Cocks and Fortey 1982; Torsvik et al. 1996; Hartz and Torsvik 2002; Gee and Teben'kov 2004; Gee et al. 2006). Different hypotheses for Caledonian terrane assembly on Svalbard have been suggested and the actual extent of the Caledonide terranes towards the east is controversial (Harland 1985, 1997; Cocks and Torsvik 2011; Gee and Teben'kov 2004). The eastern Svalbard terranes have been also interpreted as an

old microcrustal block lying between Laurentia and Baltica and later involved in the Caledonian collision (Gudlaugsson et al. 1998). Here, we use the term Caledonian basement to comprise all the pre-Carboniferous rocks on Svalbard that form the autochthon and the allochthons involved in the orogeny.

A third orogenic event involving the East Barents Sea - the Uralian event - started in the Early Carboniferous with eastward subduction of the Uralian Ocean beneath the Siberian craton (Churkin et al. 1981). The subsequent continental collision between Laurussia (Baltica and Laurentia) and Siberia in the Early Permian produced overthrusting towards the west (Otto and Bailey 1995), and generated the Ural mountain chain. The west-vergent fold-and-thrust belt on Novaya Zemlya is considered to be the northern extension of the Urals (Puchkov 2002). The largest structures in the East Barents Sea reflect the arc-shaped geometry of the island and are attributed to the Uralian deformation (Korago et al. 2004). The Uralian basement terrane in our study includes the pre-Carboniferous rocks that were formed at the Uralian margin and the rocks with oceanic affinities that were deformed during the Late Palaeozoic and Early Mesozoic orogeny.

These three collisional events combined to establish the structural framework that controlled the subsequent Palaeozoic and Mesozoic evolution of the Barents Sea (Doré 1991; Johansen et al. 1992; Punchkov 2002). The Late Palaeozoic and Mesozoic tectonic history was dominated by several rifting episodes that culminated with the opening of the Norwegian–Greenland Sea (Gabrielsen et al. 1990; Johansen et al. 1992, 1994; Faleide et al. 1993; Smelror et al. 2009).

In the Early Cretaceous, a significant magmatic event occurred in the northeast of Svalbard (Grogan et al. 1998), the intrusion are part of the so-called Arctic Large Igneous Province linking Greenland, Svalbard, Franz Josef Land and adjacent shelf areas (Maher 2001). In addition, numerous Early Cretaceous sills affected the Triassic sediments in the East Barents Basin (Ivanova et al. 2011). An additional complexity was provided by the Cenozoic uplift. This event resulted in the emergence of the Svalbard Platform and initiation of erosional processes (Dimakis et al. 1998).

The present day Barents Sea is divided into three major structural areas: (1) The West Barents Sea, which is dominated by a complex system of grabens or half-grabens, (2) an extensive platform region which extends towards the eastern and northern parts of the shelf, and (3) a large sag basin which occupies the greater East Barents Basin (Fig. 5.1).

## 5.3 Data

Acquisition of magnetic data in the arctic started already with the early explorers like Nansen (e.g. Smelror, 2011). We use gravity and magnetic data which have been collected over the past 50 years in many parts of the Barents Sea (e.g. Skilbrei 1991, 1995; Olesen et al. 2010; Werner et al. 2011). In addition, with the available petrophysical and seismic data, these data-sets can be used to describe the crustal structure of the Barents Sea in a consistent way. In the following paragraphs, we describe the individual data-sets, which we used for the potential field modelling and interpretation.

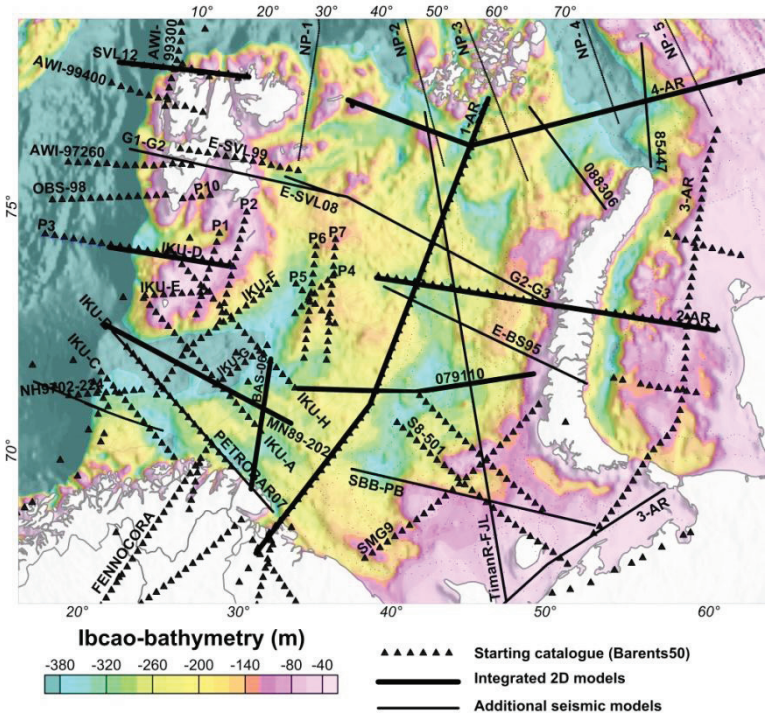


Figure 5.2: Topography/bathymetry from IBCAO (Jakobsson et al. 2008), and location of seismic profiles. Triangles indicate the catalogue included in Barents 50 (Ritzmann et al. 2007); the thick black lines are regional transects that have been the base for regional models (Marello et al. 2010); the thin black lines indicate additional seismic models used in this study (see Table 5.1 for a complete overview and references).

### 5.3.1 Bathymetry and topography

We use the data of the International Bathymetric Chart of the Arctic Ocean (IBCAO; Jakobsson et al. (2008). The model has been compiled using information from contour, grid, point and track data, and has a resolution of 2 x 2 km. The Barents Sea is not characterised by large depth variations and the sea depth ranges from -40 to -380 m (Fig. 5.2).

| Seismic lines | Characteristics | References |
|---|---|---|
| **West Barents Sea** | | |
| NH9702-224 | Ocean Bottom Seismometer (OBS) | Mjelde et al. 2002 |
| PETROBAR07 | OBS | Clark et al. 2009 |
| MN89-202 | Reflection seismic data (until the top Permian) | Marello et al. 2010 |
| IKU-A; IKU-B; IKU-C; IKU-D; IKU-E; IKU-F; IKU-G; IKU-H | Multichannel seismic reflection profiles down to the Moho. Locally combined with OBS. | Gudlaugsson et al. 1987; Faleide et al. 1993; Gudlaugsson and Faleide 1994; Sanner 1995; Breivik et al. 1998; Breivik et al. 2003; Ritzmann and Faleide 2007; Barrère et al. 2009. |

| | | |
|---|---|---|
| P1; P2; P10 | OBS | Breivik et al. 2005 |
| P4 ; P5 ; P6 ; P7 | OBS | Breivik et al. 2002 |
| G1-G2; G2-G3 | Combined geological profile | Sigmond and Roberts 2007 |
| OBS-98 | OBS | Ljones et al. 2004 |
| AWI-97260 | Seismic refraction data | Ritzmann et al. 2002; Faleide et al. 2008 |
| AWI-99400 | Seismic refraction data | Faleide et al. 2008, Ritzmann et al. 2004 |
| AWI-99300 | Seismic refraction data | Ritzmann and Jokat 2003 |
| SVL12 | Deep seismic experiments | Geissler 2001; Faleide et al. 2008 |
| E-SVL99 | | Høgden 1999 |
| E-SVL08 | | Minakov et al. 2011 |
| Bas06 seismic lines | | Gernigon et al., 2008 |
| FENNOLORA | Long-range seismic refraction profile | Guggisberg et al., 1991 |
| **East Barents Sea** | | |
| SEbaltica | Deep seismic sounding (DSS) | Kostyuchenko et al. 2006 |
| 3-AR | Refraction deep seismic and reflection-common-depth point seismic | Ivanova et al. 2011 |
| SMG9 | Seismic refraction and reflection data. | Neprochnov et al. 2000; Gubaidulin et al. 1993. |
| S8-501 (DSS-82) | Deep seismic sounding (DSS) | Neprochnov et al. 2000; Tulina et al. 1988; Morozova et al. 1995. |
| 079110 | Reflection-seismic data (until the top Permian) | Marello et al. 2010 |
| TimanR-FJL.xyz SBB-PB | Seismic constraint in depth (until the top Ordovician-Silurian) | Ostisty and Fedorovsky 1993; Johansen et al. 1992 |
| E-BS 95 | Regional seismic profile | Otto and Bailey 1995; Johansen et al. 1992 |
| 2-AR | Refraction deep seismic and reflection-common-depth point seismic | Ivanova et al. 2006; Ivanova et al. 2011 |
| 4-AR | Refraction deep seismic and reflection-common-depth point seismic | Ivanova et al. 2011 |
| 1-AR.xyz | Onshore and offshore wide-angle reflection/reflaction data. Three components OBS and MCS reflection study. (Refraction deep seismic and reflection-common-depth point seismic) | Ivanova et al. 2006; 2011; Verba and Sakoulina, 2001; Sakoulina et al. 1999. |
| 85447; 088306 | Seismic constraint in depth (until top Permian) | Shipilov and Vernikovsky 2010 |
| NP-1<br>NP-2<br>NP-3<br>NP-4<br>NP-5 | | Minakov et al. 2012 |
| BSWS2009 | | Ritzmann and Faleide 2009 |
| LineII-EBB Line15PS | Seismic constraint in depth (until top basement) | Stephenson et al. 2006 |

*Table 5.1: 2D seismic constrains data. The location of the profiles is displayed in Fig. 5.2*

### 5.3.2 Gravity data

Gravity data for the area are available from different sources. Here, we use the Arctic Gravity Project (ArcGP) data-set[1]. The compilation provides free air anomalies. We calculated the complete Bouguer anomaly (Fig. 5.3a) applying standard corrections (e.g. Blakely 1996). The water depth is replaced with bedrock of a constant density of 2200 kg/m3 and the onshore topography with a density of 2670 kg/m3. The standard deviation of the ArcGP is around ±5 mGal in the West Barents Sea and Southeast Barents Sea, and around ±8 mGal in the Northeast Barents Sea (Forsberg et al. 2007).

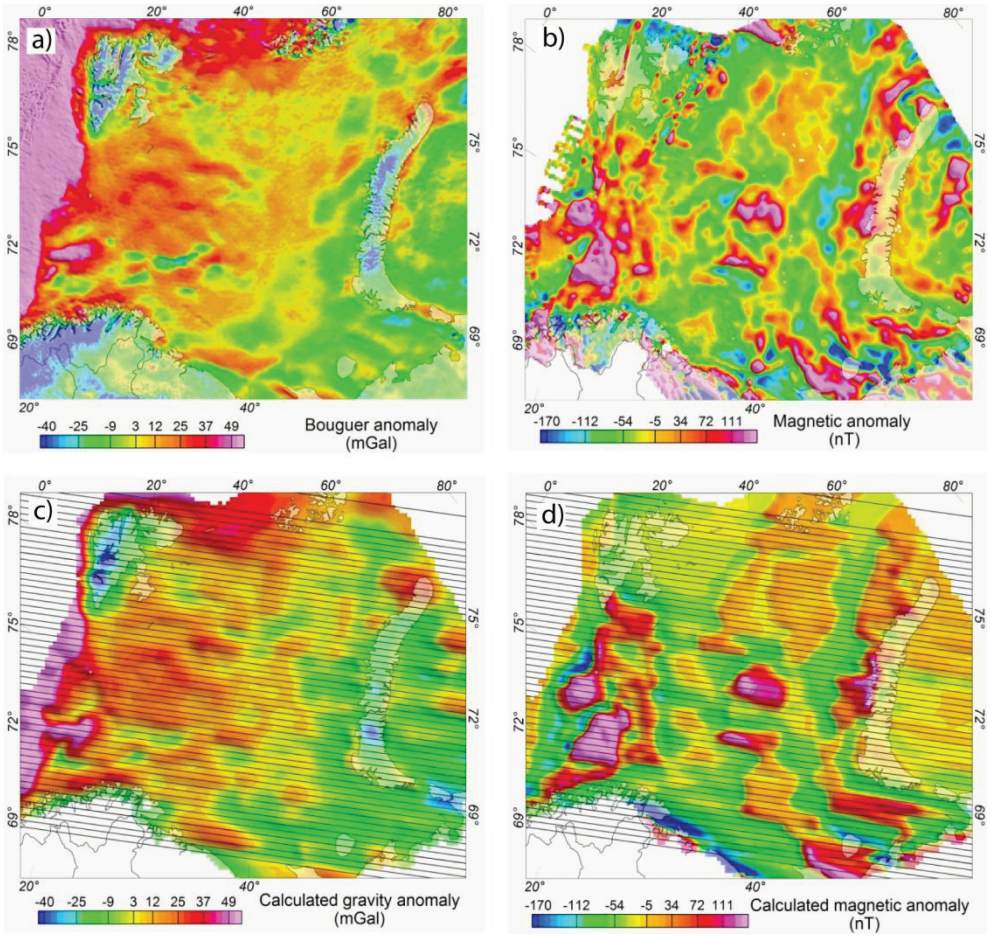


*Figure 5.3: a) Bouguer anomaly. Reduction density is 2200 kg/m$^3$ offshore and 2670 kg/m$^3$ onshore. b) Magnetic anomaly. c) Modelled gravity anomaly.. d) Modelled magnetic anomaly. Black lines in c,d show the locations of the sections defining the geometry of the 3D model.*

[1] http://earth-info.nga.mil/GandG/wgs84/agp/

### 5.3.3 Magnetic data

The magnetic data (Fig. 5.3b) are based on a compilation integrating released Russian and Norwegian aereomagnetic survey data (Smelror et al. 2009; Olesen et al. 2010; Werner et al. 2011). The mean least square errors of the aeromagnetic surveys are in the order of 11-14 nT (Werner et al. 2011).

### 5.3.4 Seismic profiles

The seismic data used in this work include both reflection and refraction data, and the horizon interpretation is mostly based on previous publications summarised in Table 5.1 and shown in Fig. 5.2. The Southwest Barents Sea is the area with the best coverage of deep seismic profiles. The northwestern boundary of the shelf is covered by data that define most of the sedimentary successions and locally provide information about the seismic top basement. There are a few seismic profiles in the eastern Barents Sea, but the interpretation of the crustal architecture is still controversial. For example, the studies by Ivanova et al. (2006, 2011) and Roslov et al. (2009) show quite different interpretations along the same seismic transect. Reflectors in the deep crust have been interpreted independently as a shallow Moho (Roslov et al. 2009) or as a lens of high-velocity lower crust (Ivanova et al. 2006, 2011).

### 5.3.5 Regional models

Besides seismic data, a large number of earlier compilations were used to gain insights into the deep crustal geometries and to provide geological and geophysical input during the modelling. Moreover, various horizons have been compiled and used to constrain the geometry of the model. The data are summarised in Tables 5.2 and 5.3.

A regional seismic velocity distribution for the Barents Sea has been adopted from the Barents50 model, a crustal model based on seismic refraction and seismic reflection profiles in the Barents Sea. The lateral resolution has been estimated at 50 km, and in addition to the velocities the seismic model defines the geometries of 3 sedimentary and 2 crustal layers (Ritzmann et al. 2007). The crustal model also provides more refined velocity information along the regional seismic profiles with its 25 km sampling distance (Fig. 5.2).

Depths to the base Cretaceous and top Permian surfaces were provided by Statoil. The base Cretaceous dataset covers most of the Barents Sea, while the top Permian covers part of the central Barents Sea and the Southwest Barents Sea.

Pre-existing top basement models are available for the western Barents Sea (Skilbrei et al. 1991; Barrére et al. 2010), the eastern Barents Sea (Gramberg et al. 2001), and for the entire Barents Sea (Johansen et al. 1992; Ritzman et al. 2007). The accuracy of the models differs from region to region (Table 5.3).

For the depth to Moho, we considered two recent compilations: the BARENTS50 model (Ritzmann et al. 2007) and the compilation for the Moho depths of the European Plate (Grad et al. 2009). The latter is partly based on Barents50, but extends towards the Baltic Shield and the oceanic domain. The lateral resolution of the new compilation is around 10 x10 km and the depth

uncertainties in the study region are estimated at ±3km along the edge of the shelf and in the Southwest Barents Sea, and at around +/-4 km in the remaining regions.

| | | Ottar Basin-Nordkapp Basin | SW-Barents Sea (IKU-C) | Sørvestsnaget Basin (NH9702-224) | Central West Barents Sea (IKU-D) | S Svalbard | SW Barents Sea PERTOBAR07 | SW Barents Sea | |
|---|---|---|---|---|---|---|---|---|---|
| | | Breivik et al. 1995 | Breivik et al. 1998 | Mjelde et al. 2002 | Breivik et al. 2003 | Breivik et al. 2005 | Clark et al. 2009 | Barrère et al. 2009, 2011 | |
| | | | | | | | | Caledonian Nappes | Archean-proterozoic |
| Sediments, Cenozoic-Cretaceous | Vp | 1800-2750 | 1800-2200 | 1900-4700 | 1800-4500 | 3200-3600 | 1040-4500 | | |
| | ρ | 1800-2140 | 1800-2000 | 2050-2400 | 2000-2490 | | | 2300-2450 | |
| | μ | | | | | | | 0 | |
| | Q | | | | | | | | |
| Sediments, Jurassic-Triassic | Vp | 3700-4600 | 3000-5200 | 5700-5900 | 4500-5450 | 4000-5450 | 4500-5000 | | |
| | ρ | 2340-2500 | 2200-2600 | 2430-2600 | | | | 2550 | |
| | μ | | | | | | | 0 | |
| | Q | | | | | | | | |
| Sediments, Palaeozoic | Vp | 5200-5500 | >5200 | | 5650-6000 | 5100-6000 | 5000 | | |
| | ρ | 2610-2660 | >2600 | 2620-2750 | | | | 2600 | |
| | μ | | | | | | | 0 | |
| | Q | | | | | | | | |
| Upper Crust | Vp | 6000 | 6100 | 6200-6900 | 6000-7000 | | 6000-6500 | | |
| | ρ | 2770 | 2800 | 2750-2820 | 2793 | 2793-2915 | | 2750 | 2750-2800 |
| | μ | | | | | | | 0.0001-0.01 | 0.010-0.2 |
| | Q | | | | | | | Q>1 | Q<1 |
| Lower Crust | Vp | >6600 | | 6900-7900 | | | 6500-7000 | | |
| | ρ | 2930 | | 2930 | 2880 | | | 2950 | |
| | μ | | | | | | | 0.0001 | |
| | Q | | | | | | | 0 | |
| Deep crustal body | Vp | >8000 | | 7400 | | | | | |
| | ρ | 3330 | | | | | | 3100 | |
| | μ | | | | | | | 0.0001 | |
| | Q | | | | | | | 0 | |
| Oceanic crust | Vp | | | | 6750-7250 | | | | |
| | ρ | | | 2800-2950 | 2900-2950 | 2900-2950 | | | |
| | μ | | | | | | | | |
| | Q | | | | | | | | |
| Mantle | Vp | >8000 | >8000 | | 8000 | | 7500 | | |
| | ρ | 3330 | 3200 | 3180-3220 | 3240-3330 | 3330-3340 | | 3300 | |
| Mafic intrusion | Vp | | | | | | | | |
| | ρ | | 3330-3340 | | | | | 3000 | |
| | μ | | | | | | | 0.015-0.05 | |
| | Q | | | | | | | Q<1 | |

*Table 5.2: Summary of previous Barents Sea studies which estimated density (ρ, kg/m3), P-wave seismic velocity (Vp, m/s), susceptibility (μ, SI), and Königsberger ratio (Q, ratio of remanent to induced magnetisation).*

| | | SE Svalbard (P4, P5, P5, P7) | W Svalbard (AWI-99400) | NW Svalbard (AWI-99300) | W Svalbard (OBS-98) | All Barents Sea | SE-Barents Sea (S8-501; SMG9) | SE-Barents Sea (1-AR-S8-501) | 1-AR, 2-AR, 3-AR, 4-AR |
|---|---|---|---|---|---|---|---|---|---|
| | | Breivik et al. 2002 | Ritzmann et al. 2004 | Ritzmann and Jokat 2003 | Ljones et al. 2004 | Ritzmann et al. 2007 | Neprochnov et al. 2000 | Morzova et al. 1995 | Roslov et al. 2009; Ivanova et al. 2011 |
| Sediments, Cenozoic-Cretaceous | Vp | 3200-4050 | 1800-3800 | >2000 | >2900 | 1800-3600 | | >2500 | >2600 |
| | ρ | >2260 | 2100-2400 | >2000 | | 2050-2590 | | >2000 | 2600 |
| | μ | | | | | | | | 0.013 |
| | Q | | | | | | | | |
| Sediments, Jurassic-Triassic | Vp | 4000-4950 | | | | 4000-5450 | | | |
| | ρ | | | | | 2380-2590 | | | 2600 |
| | μ | | | | | | | | 0.013 |
| | Q | | | | | | | | |
| Sediments, Palaeozoic | Vp | 5100-6000 | 5000-6200 | <4800 | <4150 | 4500-6000 | | <5600 | <5800 |
| | ρ | <2670 | 2600-2750 | <2100 (?) | | 2640-2710 | | <2740 | 2670 |
| | μ | | | | | | | | 0.013 |
| | Q | | | | | | | | |
| Upper Crust | Vp | 6300-6700 | 6400-6600 | 5200-6650 | 5700-6650 | 6200-6600 | 6200-6600 | 5600-6500 | 6000-6600 |
| | ρ | 2820-2890 | 2750-2900 | 2700-2850 | | 2770 | | 2800-2950 | 2770-2860 |
| | μ | | | | | | | | 0.006 |
| | Q | | | | | | | | |
| Lower Crust | Vp | | 6700-6900 | 6300-7000 | 6600-6800 | | 6600-7000 | 6300-7300 | 6600-7200 |
| | ρ | 2910-2990 | 2950-3000 | 2900-3000 | | | | 2950-3060 | 2980-3050 |
| | μ | | | | | | | | 0.126 |
| | Q | | | | | | | | |
| Deep crustal body | Vp | | | | | 7100-7600 | | | |
| | ρ | | | | | 2980-3050 | | | 2320 |
| | μ | | | | | | | | 0.088 |
| | Q | | | | | | | | |
| Oceanic crust | Vp | | | | 3500-7250 | | | | |
| | ρ | | | | | | | | |
| | μ | | | | | | | | |
| | Q | | | | | | | | |
| Mantle | Vp | 8000-8500 | >7900 | >8100 | 7600-8000 | | 8000 | > 7700 | |
| | ρ | 3330-3450 | 3240-3300 | 3300 | | 3300 | | 3320 | 3320 |
| Mafic intrusion | Vp | 6300-6400 | | | | | | | |
| | ρ | | | | | | | | 2850 |
| | μ | | | | | | | | 0.1 |
| | Q | | | | | | | | |

*Table 5.2 (continuos from previous page).*

| Grid horizons | Resolution | References |
|---|---|---|
| Bathymetry (IBCAO) | 2 km | Jakobsson et al. 2008 |
| Base Cretaceous | 0.5 km | Statoil |
| Top Permian | 2 km | Statoil |
| Top basement all Barents Sea (Barents50) | 50 km | Ritzmann et al. 2007 |
| Top basement all Barents Sea | ? | Johansen et al. 1992 |
| Top basement West Barents Sea | 5 km | Skjlbrei et al. 1991 |
| Top basement West Barents Sea | >10 km | Barrère et al 2011 |
| Top basement East Barents Sea | ? | Gramberg et al. 2010 |
| Moho (Barents50) | 50 km | Ritzmann et al. 2007 |
| Moho | 10 km | Grad et al. 2009 |
| Moho W-Barents Sea | >10 km | Barrère et al. 2011 |
| Barents 1D | 25 km on profiles | Ritzmann et al. 2007 |

*Table 5.3: Regional layer constraints.*

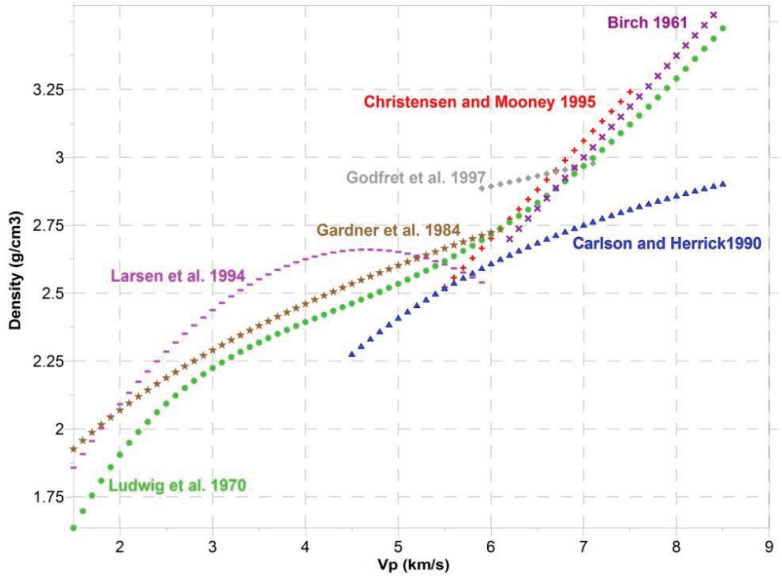


*Figure 5.4: Summary of velocity-density relations. Their application is limited to a certain type of rock as follows: Ludwig et al. 1970 for sedimentary and crystalline rocks; Larsen et al. 1994 for shale rocks; Gardner et al. 1984 for sedimentary rocks; Carlson and Herrick 1990 for oceanic crust; Godfret et al. 1997 for basalts, diabase and gabbros; Christensen and Mooney 1995 for crystalline rocks, and Birch 1961 for diabase, gabbro and eclogite rocks.*

### 5.3.6 Petrophysical indirect estimations

While densities can be indirectly calculated by conversion of seismic velocities to densities, magnetic parameters cannot be estimated from other geophysical data. Only a limited number of studies have presented interpretations of the magnetic field and estimates of magnetic properties (See Table 5.2).

Initial density estimates are made from conversion of velocities from seismic refraction and reflection studies to densities using empirical relations as presented in Fig. 5.4. Depending on the relationship used and the type of basement rock, very different densities can be estimated for the same velocity.

Table 5.2 provides a summary of seismic velocities, densities and magnetic parameters used in previous studies. In Fig. 5.5 we organize the density and seismic velocity values according to their lithology and geographic location. For sedimentary layers the variations are relatively large, which reflects the gradual increase from top to bottom within each layer. Such an increase is mostly explained by increased sediment compaction with depth (e.g. Athy 1930). In the basement the density range is more limited, and regional differences can be observed. Crust densities versus velocities are plotted in Fig. 5.5b and a general increase of densities occurs with an increase of velocities, but no simple linear or exponential relationship can be established. To find a statistically meaningful relationship more sample points would be needed.

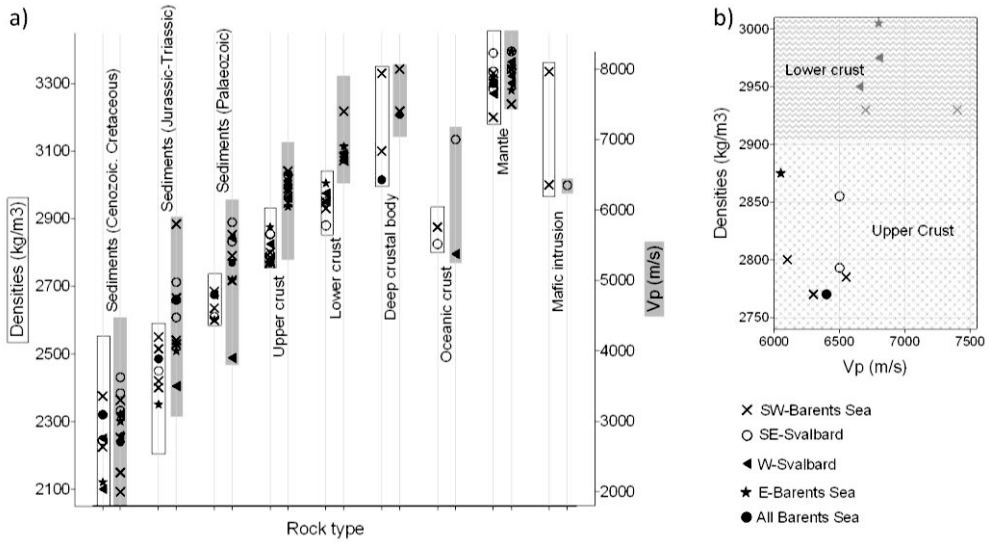


*Figure 5.5. Densities and velocities from previous models (see Table 5.2). a) Each symbol corresponds to an average value estimated from available literature. The data are classified by regions and by rock type. The white boxes represent the density range; the gray the seismic velocities range. b) The upper crust and lower crust densities are plotted versus velocities.*

### 5.3.7 Petrophysical samples

Petrophysical data from samples or boreholes are sparse for the Barents Sea. Samples of the sedimentary layers are available from well data (e.g. Tsikalas 1992; Dibner 1998), which confirm the density increase with burial depth. Only a few measurements of the offshore basement density exist (Dibner 1998, Slagstad et al. 2008), whilst for onshore Norway a large database has been established from abundant rock samples (e.g. Olesen et al. 2010). A distinction between some of the

Caledonian nappes can be made between rocks of the higher-density Upper Allochthon (2800-2850 kg/m3) and the lower-density lower, middle, and uppermost allochthonous terranes (2650-2750 kg/m3). Densities of the autochthonous terrane are established to be around 2700-2800 kg/m3.

A few susceptibility and remanence measurements of the basement are available for the western Barents Sea (Åm 1975; Olesen et al. 1990, 2010; Skilbrei 1991; Slagstad et al. 2008) and for Franz Josef Land (Dibner 1998).

From onshore data, one can establish average magnetic properties for the Caledonian terrane and extend the results to the offshore domain. The autochthonous Archaean and Palaeoproterozoic complexes have extremely high magnetic properties (> 0.01 SI), whereas the Lower Allochthon is non-magnetic (< 0.0003 SI), the Middle Allochthon is poorly magnetic (0.001-0.003 SI) and the Upper and Uppermost allochthons are moderately magnetic (0.001-0.01 SI) (Olesen et al. 2010).

Magnetic properties for sediments in the offshore domain have been reported only for the West Barents Sea (Dibner, 1998; Olesen et al. 2010) and are up to two orders of magnitude lower than those of the magmatic and metamorphic rocks forming the basement.

Magnetic measurements for Uralian and Timanian basement rocks are not available. For these regions, we adopt average susceptibilities that consider the estimated values for the western Barents Sea and the general petrophysical data for basement rocks (Hunt et al. 1995; Clark 1997).

Remanent magnetisation has been measured for the crystalline bedrock of Norway (Slagstad et al. 2008; Olesen et al. 2010), and the direction of the natural remanent magnetisation was, in general, found to be parallel to the direction of the present-day Earth's field. The Q-values (Königsberger ratio of remanent to induced magnetisation) are generally low (in the order of 0.5), but mafic and ultramafic rocks commonly show high Q-values. On Franz Josef Land (Fig. 5.1), the few measurements of remanent magnetisation that have been published (Dibner 1998) show high magnetic properties for igneous rocks and high remanence for dykes and associated basaltic sheets and sills. The observed vector direction of remanence in basalts and dolerite coincides with the present-day magnetic field direction.

## 5.4 The modelling process

An integrated forward modelling process is adopted in this study. Gravity and magnetic fields are modelled simultaneously, and are constrained by seismic profiles and petrophysical data. Modelling has been carried out using the IGMAS (Interactive Gravity and Magnetic Application System) modelling package (Götze and Lahmeyer 1988; Schmidt and Götze 1998, 1999). IGMAS uses polyhedrons with triangulated surfaces as an approximation for the complex 3D geology. A constant density, susceptibility and remanent magnetisation are ascribed to each polyhedron. The geometry is defined along parallel vertical sections with a separation of 25 km in the study area (Fig. 5.3c and 5.3d). IGMAS triangulates the geometry between the sections and calculates the potential field effect of the model

at a designated station location. Afterwards, the model is adjusted by matching the modelled field effect to the observed data by trial and error.

In order to use absolute densities, a reference model was constructed to represent the density of the lithosphere. The reference model was defined by three layers: the upper crust (from 0 to -15 km: 2670 kg/m3), the lower crust (from -15 to -32 km: 2850 kg/m3), and the upper mantle (from -32 to -300 km: 3270 kg/m3). This reference model reflects the average structure of the regional Barents50 model (Ritzmann et al. 2007).

For the calculation of the magnetic field, we defined a geomagnetic reference field based on the Definitive Geomagnetic Reference Field (DGRF). Over the Barents Sea, the magnetic field is varying in total intensity (53500-57000 nT), declination (5˚-35˚) and inclination (79˚-85˚). For the model, we considered a regional mean value of total intensity of 55000 nT, with a declination of 18.5˚ and inclination of 81˚. The use of a variable magnetic reference field affects the regional characteristics of the calculated fields only to a minor degree. Magnetic anomalies reduced to the pole, often, are used to avoid the complex calculation of the anomalies using the non-vertical Earth magnetic field. We estimated differences between calculated anomalies using a mean value of the reference field in one case, and continuous magnetic anomalies reduced to the pole in another case, and discrepancies were around ~2nT. This error is very small as compared with the uncertainties of the final model.

### 5.4.1 Initial model set up

The initial model consists of three different sedimentary layers, two crustal bodies and the mantle. The first calculated field from the initial model was quite different from the observed field. To improve the fit, we first refined the geometry in order to constrain the structure of the crust as well as the existing data would allow, and then we interactively adjusted the model.

### 5.4.2 Sedimentary cover

The upper boundary of the model, bathymetry, was taken from Jakobsson et al. (2008) (Fig. 5.2), and the geology on the seabed is based on the geological map in Sigmond and Roberts (2007). The continent-ocean transition zone (COT) was delineated from the analysis of the magnetic anomaly pattern.

The geometrical and sedimentary set-up considers the major seismic horizons (Table 5.3) and has been refined in a second phase along the available 2D seismic lines (Table 5.1 and Fig. 5.2). The density distribution in the sedimentary basins can be related to compaction, grain composition, time of deposition and metamorphic grade (e.g. a change from greenschist to amphibolite facies). In our model we study the influence of two dominant parameters, age and burial depth, as described below.

Two major reflectors can be traced regionally in the Barents Sea, the base Cretaceous and the top Permian. These boundaries correspond to a clear velocity contrast and density change. Accordingly, we define sedimentary units with constant densities corresponding to (1) the Cretaceous-Cenozoic, (2) the Jurassic-Triassic, and (3) the Late Palaeozoic successions. In addition, a deep sedimentary body has been introduced in the model in the East Barents Basin at depths below

approximately 10-12 km, where burial metamorphism is considered to have significantly altered the physical rock properties. Therefore, the use of the constant Palaeozoic sediment density was not logical here. For the same reason, the Cenozoic-Cretaceous sedimentary package of the West Barents Sea has been divided into an upper and a lower unit in the deepest sedimentary basin (Bjørnøya Basin, Tromsø Basin, Sørvestsnaget Basin). Fig. 5.6a shows the gravity contribution of the sedimentary layers so defined. The densities for each sedimentary unit are given in Table 5.4.

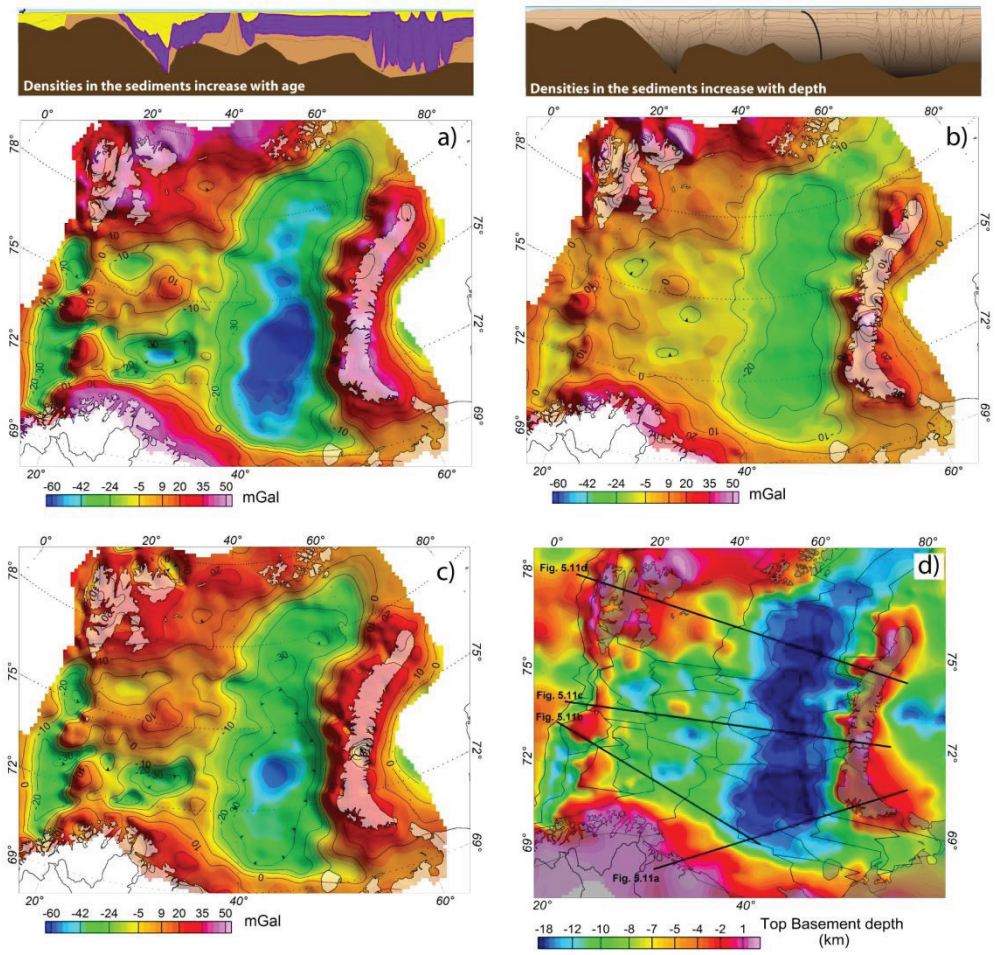


*Figure 5.6. Gravity contribution of the sediments: a) calculated using densities that increase with age of the sedimentary cover. Constant densities are used for sediments with the same age; b) calculated using depth-dependent densities. Constant densities are used for sediments at the same depth. c) Differences between the gravity effect of the sediments calculated in the two set-ups. d) Top basement model with the outline of the upper crustal blocks. See text for details.*

Fig. 5.6b displays the gravity effect of a sedimentary cover with densities defined according to burial depth. In this alternative model, sediments at the same depth have the same density. In the uppermost 4 km the sediment density increases with depth as observed in borehole data (Tsikalas 1992). For the sediments between 4 and 6 km the increase of densities with depth has been extrapolated, and for the deepest sediments a constant value of 2690 kg/m3 has been applied.

Both set-ups produce a gravity effect that is strongly influenced by the total thickness of the sedimentary successions. However, the gravity effect of the first model (Fig. 5.6a) is more sensitive to the internal discontinuities associated with the principal seismic reflectors. Large negative anomalies occur over the deep Jurassic basins (e.g. Tromsø Basin, Sørvestsnaget Basin, Ottar Basin and Nordkapp Basin), and over the East Barents Basin, whilst larger positive anomalies are located on structural highs (e.g. Stappen and Loppa Highs). The second model produces smaller anomalies that are, in general, less sensitive to the sedimentary thickness (Fig. 5.6c). Below 6 km depth, the density of the sedimentary layers is almost identical to the underlying basement, producing almost no contrast and no significant gravity effect. This can be clearly seen in the gravity difference between the two approaches (Fig. 5.6c). The largest difference is associated with the deepest basins (e.g. East Barents Basin, Nordkapp Basin). Consequently, we performed some sensitivity tests to estimate the impact that different density distributions in the sediments could produce on crustal geometries. In these tests the gravity differences obtained by the two approaches (Fig. 5.6c) were considered as gravity residuals to be explained by crustal thickness variations. We estimate that differences of 20 mGal, (Fig. 5.6c) affect the modelling in terms of crustal thickness by around 5 km.

### 5.4.3 The crustal model

The modelling of the crust was the main focus of this work, and in particular we aimed at defining the crustal geometry and its properties.

Top basement and Moho were defined following the pre-existing regional models (Table 5.3) and later refined by incorporating 2D seismic profiles (Table 5.1 and Fig. 5.2). The distinction between upper and lower crust was introduced depending on the reflectivity and velocities from the seismic profiles (Table 5.1 and Fig. 5.2). The crossing points of the original profiles show some disagreements due to the accuracies of the different techniques and modelling approaches used. At those points the definition of the geometry was guided by the potential field residuals and designed in such a way to be coherent with the neighbouring setting.

The Barents Sea shelf is characterised by a relatively small range of gravity anomalies ±40 mGal (with the exception of the Loppa and Stappen highs) that show a good correlation with the distribution of basins in the West Barents Sea (Fig. 5.1 and 5.2a). However, in the East Barents Sea, where the large sag basin is located there is no correlation with the observed negative gravity anomaly. This situation could imply either that no density contrast exists between the lower part of the sedimentary package and the basement, or that the low-densities in the basin are isostatically compensated by high densities in the crust (e.g. mantle upwelling, or high-density lower crust). This ambiguity in interpreting the density distributions could be partly solved by the use of magnetic field. Sedimentary

compaction does not alter the magnetisation significantly and, consequently, the sediment/basement magnetic contrast remains a detectable magnetic boundary.

For that reason, our initial subdivision of the crust into different basement units has been based on a first interpretation of the magnetic anomalies (Marello et al. 2010). The magnetic anomalies of the Barents Sea, besides being sensitive to the top basement geometry and sedimentary/basement contrast, are influenced mainly by the magnetic properties of the upper crystalline crust (Marello et al. 2010).

The magnetic field modelling was focused on fitting general trends to the magnetic signature, and neglecting high-frequency anomalies generated by intra-sedimentary sources (e.g. sill intrusions). For each magnetic domain defined by Marello et al. (2010) a density value has been attributed, taking into consideration existing seismic velocity and density models (see Table 5.2 and Fig. 5.4 and 5.5).

The final organisation of the basement blocks derives from the results of tested and modified model set-ups and simultaneously reducing the gravity and magnetic residuals. To this end, we managed to create a simple crustal organisation that was compatible with all the geophysical constraints. The lateral boundaries of the different domains were considered to have a large degree of freedom, whereas the top basement and Moho were modified only where no constraints existed.

A lower crustal body has been defined (Fig. 5.8b) based on seismic results beneath the East Barents Basin (Ivanova et al. 2006, 2011) in order to evaluate the different theories regarding the deep crustal setting of the East Barents Sea (see section 5.3).

### 5.4.4 Regional long-wavelength gravity model: upper mantle density variations

The long-wavelength gravity anomalies are mostly attributed to the crustal thickness and the density distribution in the uppermost mantle. The regional gravity anomalies highlight a strong regional E-W trend attributed to the continental break-up and spreading of the North Atlantic Ocean. If a homogeneous upper mantle is assumed, the calculated gravity field is much larger on the oceanic side than the observed gravity anomalies. A range of different approaches has been used to explain that misfit (e.g. O'Reilly et al. 1998; Breivik et al. 1999; Kimbell et al. 2004, 2010; Ritzmann et al. 2009).

We address this issue here by means of an oceanic mantle body that approximates the mantle change from a continental to an oceanic domain. Its upper part accounts for the density decrease related to lateral temperature variation (Breivik et al. 1999; Kimbell et al. 2004), while its lower part reflects a negative velocity anomaly observed on seismic tomography (Levshin et al. 2007). The densities of the oceanic mantle are chosen based on petrophysical models (e.g. Bonatti and Michael 1989; Hacker et al. 2003). Remaining long-wavelength gravity residuals over the shelf are accredited mostly to the Moho geometry and have been addressed by adjusting this surface within the range of the uncertainties provided by the seismic model (Fig. 5.10d).

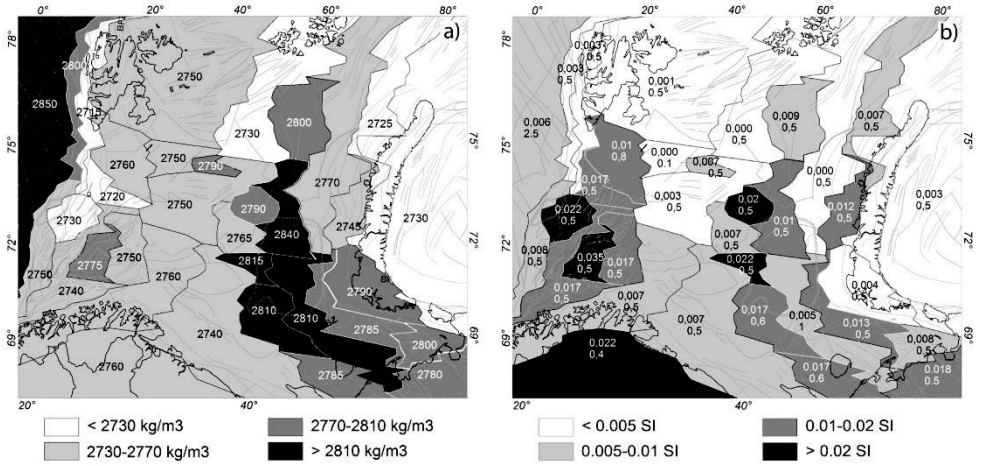


*Figure 5.7: Upper crustal properties: a) Density distribution; b) Magnetic susceptibilities (upper number) and Q-ratio (Königsberger ratio) (lower number).*

| Model unit | Density ($kg/m^3$) | Susceptibility (SI) | Q Ratio (SI) |
|---|---|---|---|
| **Cenozoic-Cretaceous sediments (upper and lower)** | 2350-2450 | 0 | 0.3-0.4 |
| **Jurassic - Triassic** | 2500 | 0 | 0.3 |
| **Palaeozoic** | 2650 | 0 | 0.3 |
| **Deep sediments** | 2730 | 0 | 0.3 |
| **Oceanic Crust** | 2850 | 0.006 | 2.5 |
| **Continent-oceanic transition crust** | 2750-2800 | 0.01-0.003 | 0.5 |
| **Upper crust (28 blocks)** | 2715-2840 | 0.029-0.00004 | 0.3-1.5 |
| **Lower crust (3 blocks)** | 2940-3000 | 0.007-0.00006 | 0.4 |
| **Lower crustal body** | 3050 | 0 | 0 |
| **Upper mantle** | 3280 | 0.003 | 0 |
| **Rift anomaly mantle** | 3220 | 0 | 0 |

*Table 5.4: Petrophysical model results.*

## 5.5 Modelling results

The densities and magnetic properties of the final model are summarised in Table 5.4. To reduce the ambiguity in potential field modelling, the integration of a large number of data that constrain the geometry or physical model parameters is of fundamental importance. The model presented was defined progressively with a careful iterative stepwise modelling procedure. We mostly rely on the accuracy of the constraints and on the geological meaning of the model to avoid an over-fitting of the observed anomalies. The largest uncertainty in the model remains in the northern part of the shelf. The basement blocks defined between Svalbard and Franz Josef Land are quite large. Refinements to these blocks are limited due to a lack of geophysical constraints and the difficulty in determining precisely the shallow sources (sills and dykes) responsible for high-frequency anomalies.

The sedimentary cover is defined by units with constant densities and almost non-magnetic properties, and with a geometry which is based on the identified major seismic reflectors. Each sedimentary unit is characterised by sediments of similar age (Table 5.4). On the continental shelf, upper and lower crusts have been distinguished. The spatial extension of the upper crustal units and their physical properties are presented in Fig. 5.7. The densities clearly differentiate the West Barents Sea (dominated by lower densities) from the East Barents Sea (dominated by higher densities). The magnetic property distribution in the upper crust allows us to differentiate three major areas: (a) a higher magnetic basement in the Southwest Barents Sea; (b) a non-magnetic crust in the northwestern part of the shelf; (c) and an alternation of magnetic and non-magnetic blocks under the East Barents Sea Basin. Towards the margin, a transitional crustal block and the oceanic crust are defined from the bottom of the sedimentary cover to the Moho (Fig. 5.8).

The lower crust is divided into three blocks. The densities are slightly lower for the two western blocks (2940 kg/m3) than for the eastern lower crust (3000 kg/m3). The magnetic properties are close to zero for the East and Northwest Barents Sea areas, while the Southwest Barents Sea has a magnetic lower crust (with a susceptibility of around 0.005 SI).

The final calculated gravity field (Fig. 5.3c) has a correlation coefficient of 0.88 with the observed field (Fig. 5.3a) and a standard deviation of ±11.5 mGal. This is higher than the accuracy of the gravity compilations (Forsberg et al. 2007), but if we consider only the wavelengths within the resolution of our model, the fit is reasonably good. Local structures (e.g. salt diapirs in the Nordkapp Basin; sill intrusions to the east of Svalbard), cannot be addressed properly with the set-up of our regional model. The largest gravity differences between calculated and observed fields are located onshore Svalbard and Novaya Zemlya, and these may be attributed to local near-surface density variations or they could represent an effect of permanent ice cover not incorporated in the model. The ice cover can locally have an effect in the order of 30 mGal, with a maximum of 45 mGal over the islands of Svalbard and Novaya Zemlya (e.g. Ebbing et al. 2007). The calculated magnetic field of our model explains, with a reasonable fit, the observed regional anomalies (Fig. 5.3b and 5.3d). The long-wavelength anomalies are modelled assuming a basement origin; short-wavelength anomalies associated with intra-basement magnetic sources would require a detailed modelling of local structures which is too complex to incorporate in the current regional model. The four largest magnetic anomalies located over the Loppa High, the Stappen High and the double anomaly over the central part of the Barents Sea are all well reproduced by the model. In the northwestern part of the Barents Sea, high-frequency magnetic anomalies are observed and are most likely related to intra-sedimentary magmatic intrusions (Grogan et al. 1998). These particular anomalies make it difficult to distinguish between local and regional magnetic anomalies and thus complicate the modelling and interpretation in this region.

The final 3D model set-up is displayed in Fig. 5.6c, 5.7, 5.8 and 5.11. The model defines densities and magnetic properties for the crust and upper mantle, as well as key crustal horizons for the region, i. e. the crust-mantle boundary (Moho), top of the lower crust, top basement and the major boundaries of sedimentary

successions (Fig. 5.6d and 5.7). Thickness maps have been calculated from the model and are shown in Fig. 5.9.

### 5.5.1 Depth to top basement

The boundary between sediments and basement in our model coincides with a seismic velocity jump recorded along 2D lines and a density contrast from +50 to +200 kg/m3 (depending on the age of the sedimentary strata and the basement type). The top basement from density modelling and seismic interpretations almost coincides with the uppermost limit of the magnetic sources, suggesting a surface close to the real crystalline basement.

The top basement map (Fig. 5.6d) reflects the structural setting of the entire continental shelf. The Southwest Barents Sea is dominated by large variations in the top basement geometry. Two major structural highs, the Loppa High and Stappen High, are recognised where the basement rises to a depth of 2-3 km and crops out on Bjørnøya. Depths to basement reach almost 12 km beneath the Harstad-Tromsø Basin, Sørvestsnaget Basin, Nordkapp Basin, and Sørkapp Basin and in the southern part of Sentralbanken High. In the Northwest Barents Sea, the basement is relatively flat and shows maximum depths of c. 8 km. In proximity to the Svalbard archipelago, the basement is quite shallow cropping out locally (northeast of Svalbard and west of the Kongsfjorden-Hansbreen Fault Zone (KHZF in Fig. 5.1, Harland 1997; Gee and Teben'kov 2004).

In the eastern Barents Sea, the basement geometry follows a unique and large regional structure; the East Barents Basin with a maximum depth reaching more than 18 km.

### 5.5.2 Boundary between upper and lower crust

The boundary between upper and lower crust (Fig. 5.8a) coincides with a jump in seismic velocities, a density contrast of +150 to +220 kg/m3, and a decrease in the magnetic properties in our model.

The geometry of this boundary is fairly flat with depths in the range 22-28 km. The top of the lower crust is locally relatively deep, e.g. in proximity to the Loppa High, below the Kola-Kanin Monocline, to the southeast of Svalbard, and beneath Novaya Zemlya and the Pechora Basin, whereas it is shallower in the western and northern parts of the shelf.

### 5.5.3 Lower crustal body

A lower crustal body has been inferred to exist beneath the Barents Sea Basin in order to validate the seismic interpretations that proposed either a lens of "mantle mixture" in the lower crust (Ivanova et al. 2006, 2011) or an uplift of the mantle under the basin (Roslov et al. 2009). Fig. 5.8b displays the location of the body. The density of this body (3050 kg/m3) is similar to that of the lower crust (3000 kg/m3), and its thickness is in the order of 1.5 km up to a maximum of 2.5 km. These characteristics make the existence of the proposed body doubtful and almost insignificant in terms of gravity modelling, as such a small density contrast is below the resolution of the model and within the range of uncertainties of seismic interpretation.

### 5.5.4 Crust-mantle boundary (Moho)

The modelled Moho depth (Fig. 5.8b) reaches a maximum beneath the Fennoscandian mainland (40-45 km) and southern Novaya Zemlya (45 km). The Moho is relatively shallow in the western Barents Sea where it rises to a minimum depth of 12 km, reflecting the transition from the continental shelf to the oceanic domain. Despite this large variation, the depths to Moho over the Barents Sea shelf are fairly uniform. In the Southwest Barents Sea, the depths are around 30-33 km with a local deepening below the Loppa High down to 35 km. In the northwestern areas and in the East Barents Sea, the crust-mantle boundary is located at 33-37 km depth. Beneath the mega-basin of the East Barents Sea, our model suggests a 2-3 km upwelling of the mantle.

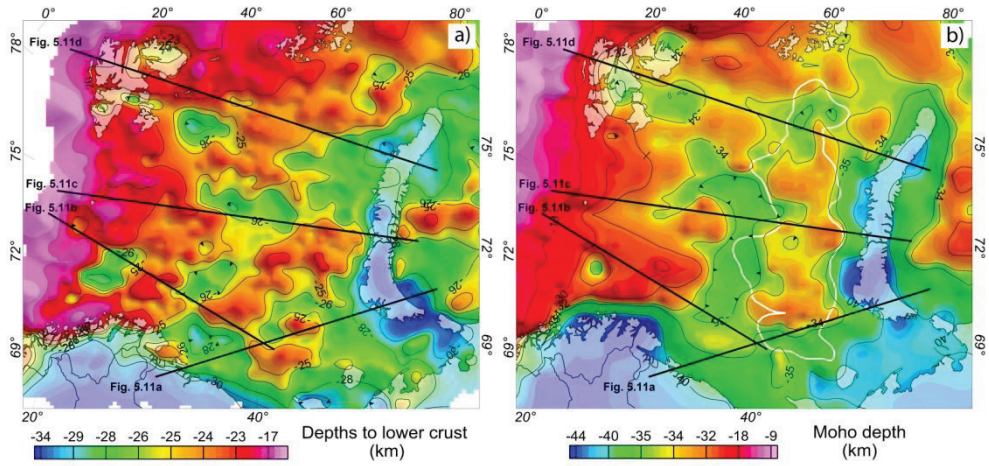


*Figure 5.8. Crustal model: a) upper-lower crust boundary; b) Moho depth. The white line shows the outline of the lower crustal body.*

### 5.5.5 Basement thickness (upper crustal thickness and total crystalline thickness)

Two different thickness maps have been calculated from the model. The first represents the thickness of the upper crust, which gives the strongest contribution to the magnetic anomalies (Fig. 5.9a). The second map represents the crystalline crustal thickness from top basement to Moho (Fig. 5.9b). The mean crystalline crustal thickness in the shelf is around 25 km with areas thinner than 20 km below the East Barents Basin, the Nordkapp and Sørkapp basins, and with areas thicker than 28 km beneath the Kong Karl Platform, Stappen High, Loppa High, Gardarbanken High, Sentralbanken High, Fedynisky High and the Central Barents High.

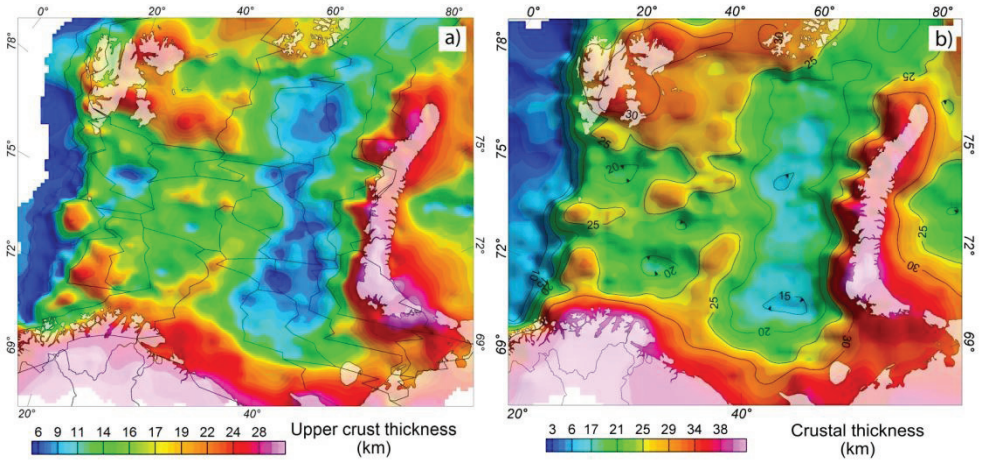


*Figure 5.9. Basement thickness maps. a) upper crust thickness map with the outline of the upper crustal blocks; b) total crystalline thickness map (from top basement to Moho)*

### 5.5.6 Top Basement and Moho geometries compared with previous models

The model results presented here are compared with previous top basement and Moho depth compilations in Fig. 5.10 and 5.11. Our modelled Moho depth is in quite good agreement with the Moho depth model of Grad et al. (2009); most of the differences are within ± 2 km, and thus smaller than the uncertainties estimated for the Grad compilation (Fig. 5.10c). Larger differences are found in the Moho depth beneath the Vestbakken volcanic province, the Sørvestsnaget Basin and northern Bjørnøya, here our crust mantle boundary is more than 8 km shallower (Fig. 5.10c, 5.11b, 5.11c). Our new estimates are constrained by the by new geoplysical results (Marello et al. 2010; Clark et al. 2009), not include in the compilation by Grad et al. (2009).The top basement in the West Barents Sea is slightly shallower compared with previous models (Fig. 5.10a, 5.10b, 5.11a, 5.11b), whilst in the East Barents Sea it is found to be about 4 km deeper (Fig. 5.10a, 5.10b, 5.11b, 5.11c). Some of the discrepancies may simply be a matter of basement definition and interpretation.

The basement concept is not unique and depends on the target of the study and on the methodology. Three definitions of the top basement are commonly used: geological, magnetic and acoustic basement (e.g. Neuendorf et al. 2005; Sheriff 2006). Goussev and Peirce (2010) have emphasised the importance of clarifying the top basement definition properly in order to avoid misinterpretations and miscorrelations. It is important to note that the magnetic basement does not necessarily coincide with the real geological basement (e.g. if the basement is not magnetic). Also, the acoustic basement, which is commonly used as an upper constraint for the magnetic basement interpretation, can be structurally close to or coincident with the magnetic basement, or it can be much shallower (e.g. in the case of metasediments producing a velocity jump but not necessarily an increase in magnetisation). If there is little velocity contrast between the lowermost sediments

and basement, then the seismic basement itself is unlikely to be clearly defined and does not coincide with the magnetic basement.

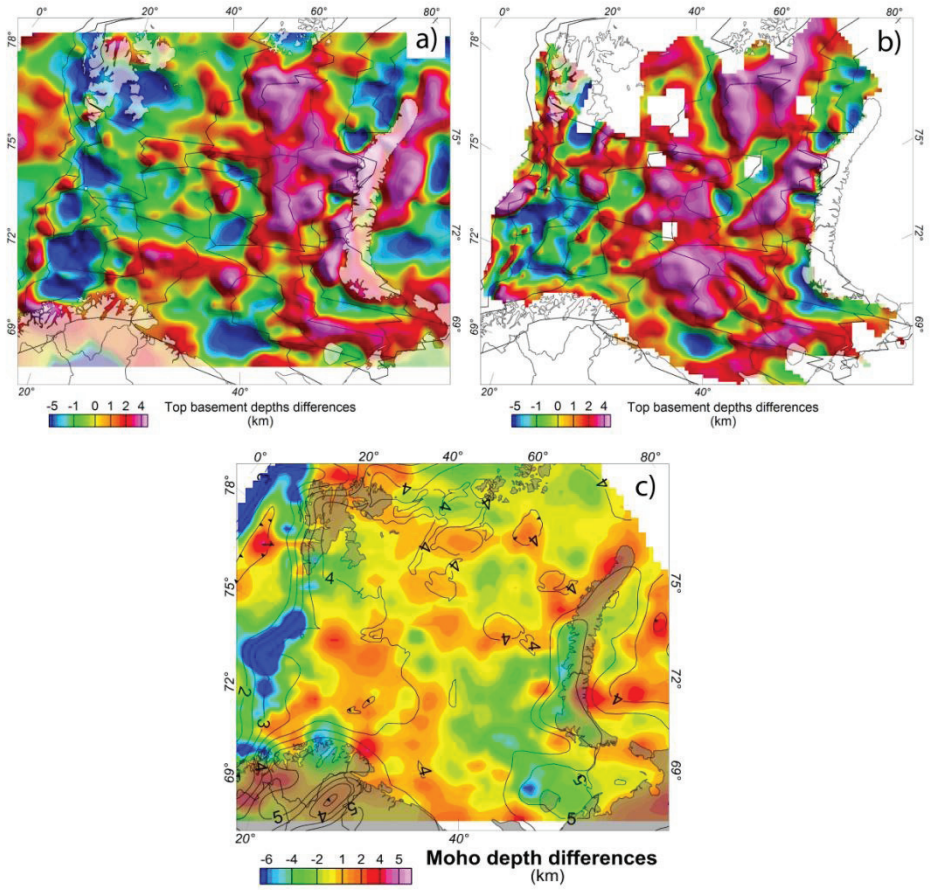


*Figure 5.10. Top basement and Moho geometry results compared with existing models: a) Differences between our top basement (Fig. 5.7a) and Barents50 top basement (Ritzmann et al. 2007). b) Differences between our top basement (Fig. 5.7a) and the Skilbrei et al (1990) basement for the West Barents Sea and Johansen et al. (1992) basement for the East Barents Sea. c) Moho differences between our model results (Fig. 5.8b) and the Moho map of Grad et al. (2009). The contours show the uncertainty in the Moho map of Grad et al. 2009, in km.*

In our model, we consider a basement which approximates the real geological basement but, even so, ambiguity in this definition remains. The Riphean metasedimentary succession (Ectasian, Stenian and Tonian time in the International Stratigraphy), for example, has been seismically differentiated from the underlying crystalline upper crust and has been considered as part of the sedimentary package by Ivanova et al. (2006). In our model, we include the Meso-Neoproterozoic rocks as part of the basement, since they have been involved in the Timanian orogenic

event and considered to be part of the Timanian basement terrane. Similarly, in the western Barents Sea, the pre-Devonian metasedimentary rocks that have been involved in Caledonian deformation are considered to be part of the Caledonian basement terrane. In general for the West Barents Sea, all pre-Carboniferous rocks have often been regarded as 'basement' rocks (Harland 1997). On the other hand, in the East Barents Sea the Late Palaeozoic and Mesozoic sedimentary successions that may have been involved in Uralian orogenesis have not been included in what we define as the Ural basement terrane.

## 5.6 Discussion

Our modelling approach allows us to identify basement units distinguished by densities and magnetic properties, and, correlated with first-order crustal geometries (top basement, Moho depth, crystalline crustal thickness), to propose a first-order geological interpretation of the Barents Sea crust, summarised in Fig. 5.11 and 5.12.

The basement units have been organised into four major terranes; pre-Carboniferous basement, Timanian, Caledonian and Uralian terranes.

Pre-Carboniferous basement has been traced and divided into three major units. One corresponds to the Archaean-Palaeoproterozoic complexes exposed in the Fennoscandian Shield, a second unit forms isolated, high-magnetic, thick crustal blocks recognised beneath the Loppa High and Stappen High, and a third unit constitutes the non-magnetic, thick crustal block that forms the Svalbard Platform.

The distinct magnetic properties of the low-magnetic Lower Allochthon, from the other, moderately magnetic Caledonian nappes and the high-magnetic Archaean-Palaeoproterozoic (Olesen at al. 2010; Barrère at al. 2011) allow us to interpret the basement in terms of Caledonian units. A prolongation of the different Caledonian nappes exposed in Finnmark into the southwestern Barents Sea has been proposed by several workers (Åm 1975; Olesen et al. 1990; Skilbrei 1995; Siedlecka and Roberts 1996; Barrère at al., 2011; Gernigon and Brönner 2012) and is reviewed here.

The Timanian terranes are distinguished by two units that represent a prolongation of the onshore geology: a high-magnetic domain which represents the aggregation of mafic and crystalline crustal blocks (island arcs, volcanosedimentary assemblages and magmatic rocks), and a non-magnetic domain which characterises the thick Meso-Neoproterozoic sedimentary successions (Fig. 5.12). The Timanian terranes are known to occur in the Southeast (Korago et al. 2004; Olovyanishnikov et al. 2010) and probably also in the Northeast Barents Sea.

The Uralian basement terrane is also subdivided into two units (Fig. 5.12). One corresponds to the continuation of the pre-Uralian domain (Kostyuchenko et al. 2006) that shows high-magnetic anomalies and may contain rocks of oceanic affinity. The other is composed of an agglomeration of non-magnetic units mostly comprising deformed Neoproterozoic and Early Palaeozoic complexes.

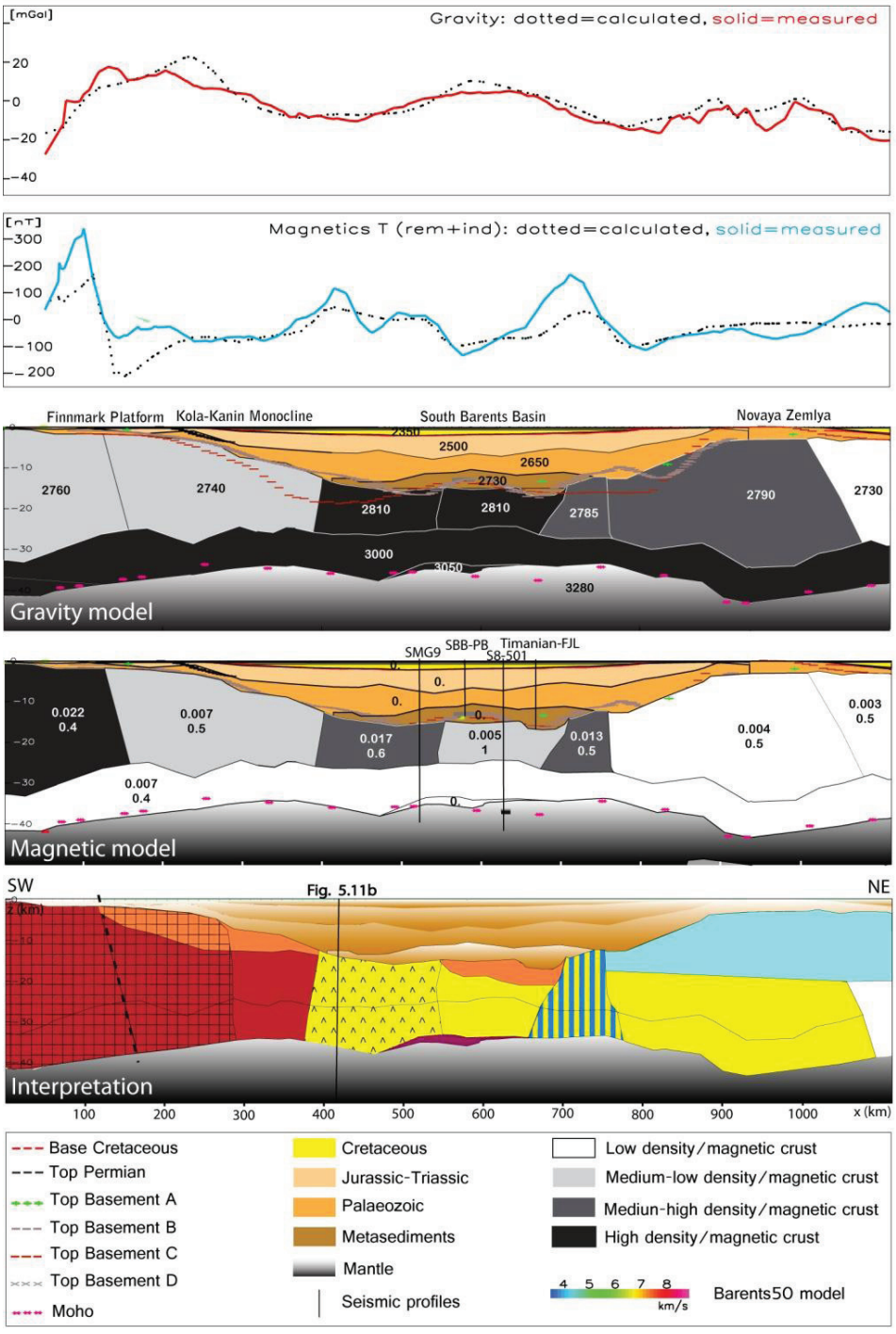


*Figure 5.11a. (continuing in the next pages).*

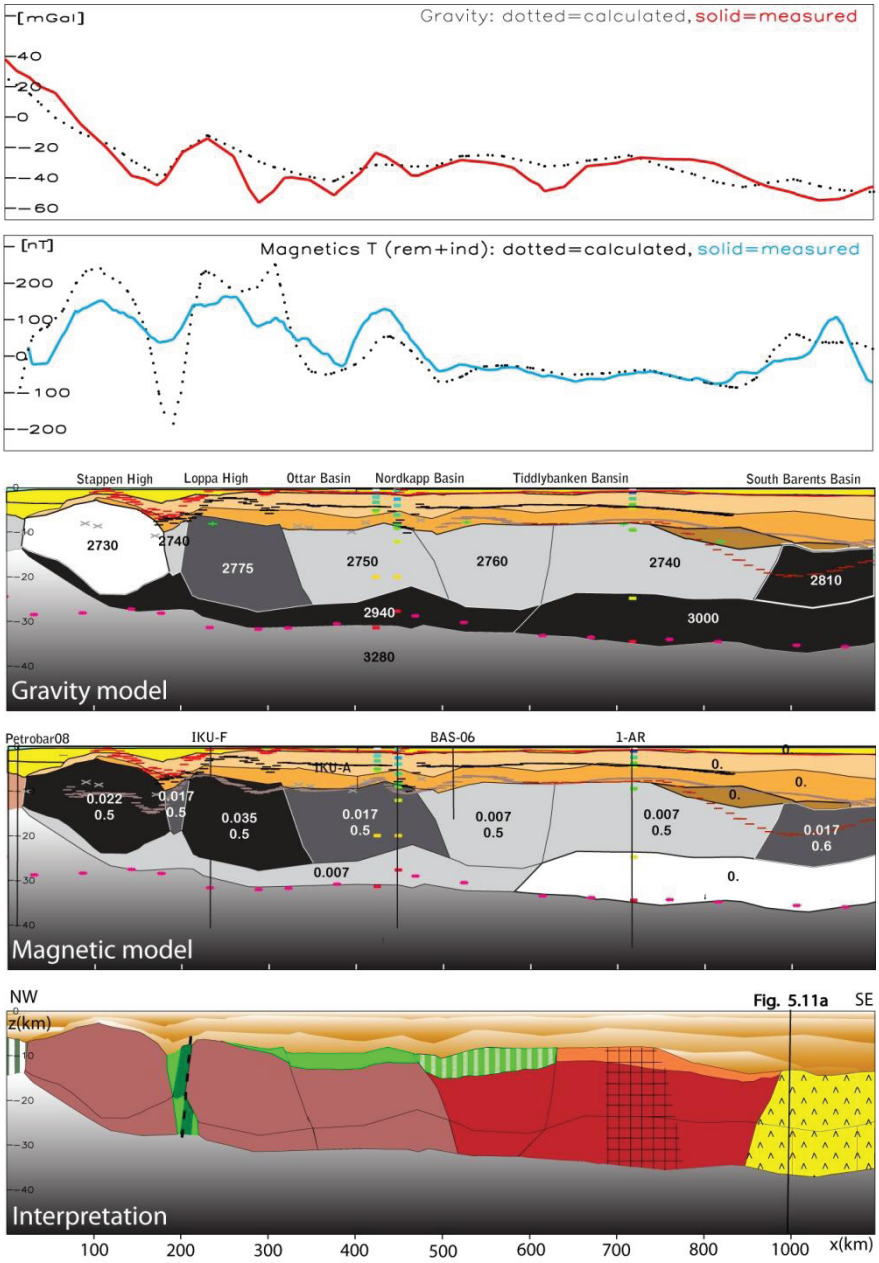


*Figure 5.11b. (continued from page 104).*

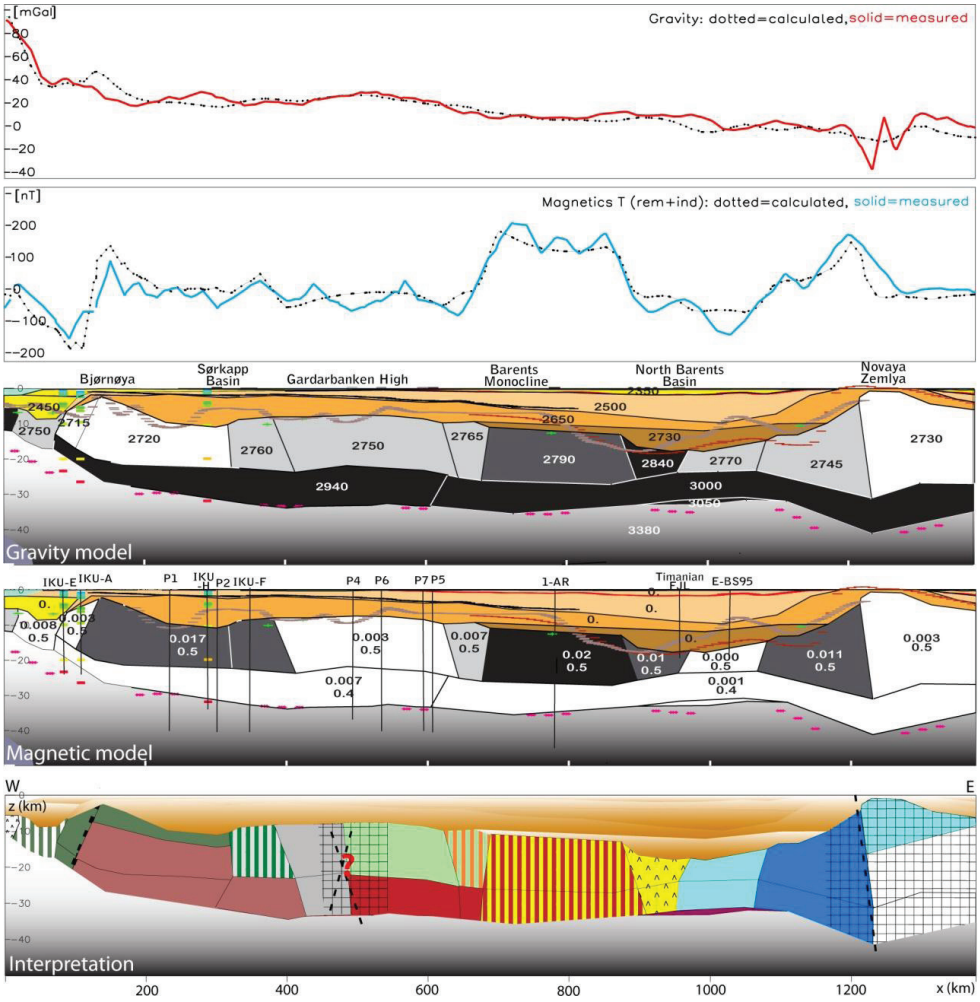


*Figure 5.11c. (continued from page 104).*

### 5.6.1 From the Archaean-Palaeoproterozoic Fennoscandian Shield to Timanian

The Southeast Barents Sea is distinguished from the rest of the Barents Sea shelf by having higher density in the upper crust (Fig. 5.7a). The basement surface beneath Kola Peninsula and the Timan Ridge dips steeply towards the South Barents Basin and the Pechora Basin (Fig. 5.1 and 5.6d). Moho depths vary from around 42 km in the onshore areas to 32 km under the South Barents Basin (Fig. 5.8b). In a previous study, Marello et al. (2010) supported the idea that the upper crust in the Southeast Barents Sea is most likely composed of Timanian complexes. Our crustal units are NW-SE oriented, like the Precambrian structures (Roberts and Siedlecka 2002), and have been interpreted as the prolongation of the onshore Pechora Basin Timanian terranes (Fig. 5.1 and 5.8).

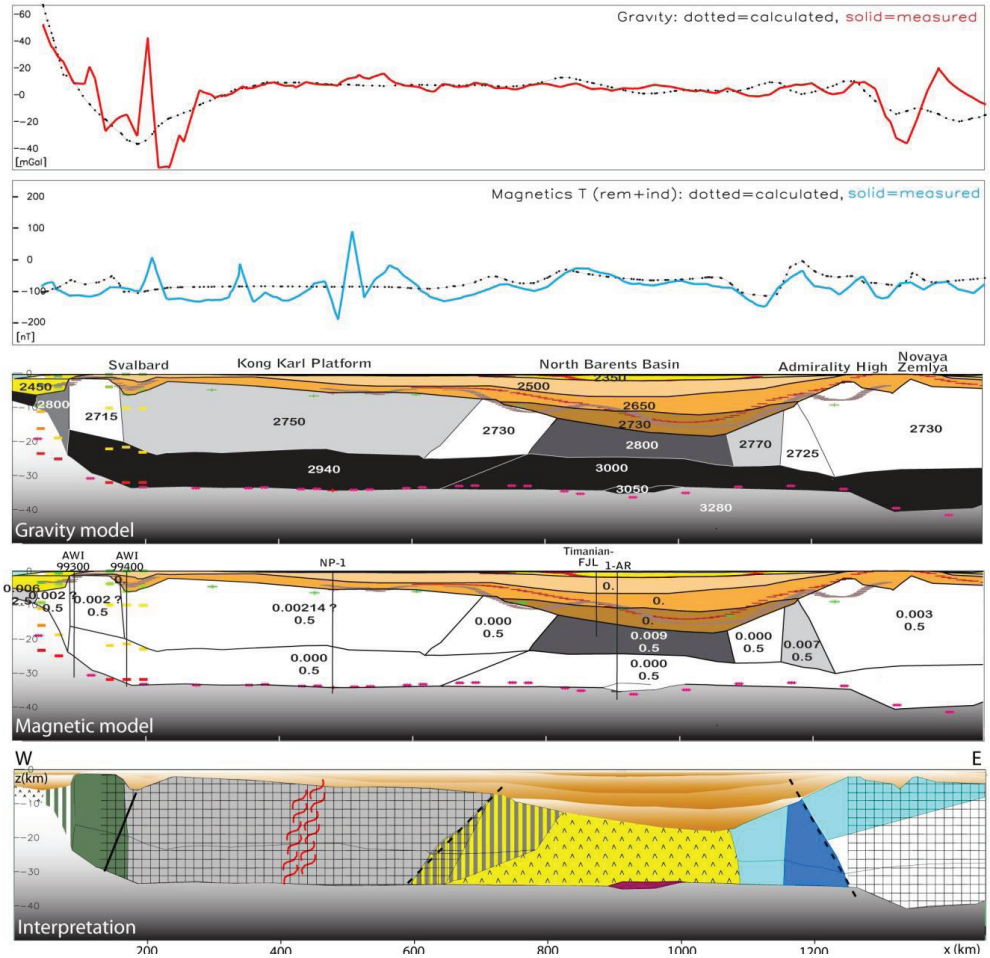


*Figure 5.11d* (continued from page 104). *Four profiles displaying the model results and the final interpretation: a) Southeast Barents Sea; b) Southwest Barents Sea; c) the Central-west and Central-east Barents Sea; and d) the North Barents Sea (see Fig. 5.12 for locations). The two upper panels show, respectively the gravity and magnetic field, calculated and observed. In the three lower panels the gravity model with the geographical locations (see Fig. 5.1 for geographical location) are displayed. The numbers in the model indicate the densities in kg/m$^3$. The underlying panel shows the magnetic model; the two numbers in the crust indicate the susceptibility (SI) and the Q (Königsberger) ratio. The names on top of the 2D crossing seismic line are plotted (for locations see also Fig. 5.2). The lowest panel shows the interpretation of the model (for the legend, see Fig. 5.12). In Fig. 5.11a, the legend for the additional information is displayed for all the four transects. The top basement models are: top basement A (Barents50, Ritzmann et al., 2007); top basement B (Skilbrei 1991 for the West Barents Sea, Johansen et al. 1992 for the East Barents Sea); top basement C (Gramberg et al. 2001); top basement D (Barrère et al. 2010). The Moho plotted is from Grad et al. (2009). The sediment boundaries were provided by Statoil (see Table 5.3)* (continuos in the previous pages).

The profile in Fig. 5.11a summarizes our model results and interpretation of the crustal geology in the Southeast Barents Sea.

The southwesternmost unit corresponds with the Archaean-Palaeoproterozoic crystalline basement which underlies large parts of the Fennoscandian Shield (Fig. 5.11a and 5.12). It is characterised by medium-low densities, very high susceptibilities, and an extremely thick continental crust. Such parameters have previously been associated with high-grade metamorphic rocks, including granulites (Barrère et al. 2010).

From the coast the basement changes to a low-magnetic and low-density domain (Fig. 5.11a). In this region, a thick Meso-Neoproterozoic mainly sedimentary succession (13 km in the Kola-Kanin Monocline) has been distinguished above the Archaean-Palaeoproterozoic basement (Verba and Sakolina, 2001; Ivanova et al. 2006). This sedimentary cover has been included in our model as part of the upper crust, a set-up which resulted in a decrease of densities and magnetic properties of our crustal block. The unit corresponds to the offshore prolongation of the Meso-Neoproterozoic successions exposed in the Kanin and Rybachi-Sredni Peninsulas which were deformed during the Timanian orogeny (Olovyanishnikov et al. 2000; Gee et al. 2006; Kostyuchenko et al. 2006).

Moving towards the South Barents Basin, the basement becomes highly magnetic and shows higher densities. This has been also interpreted as Timanian terranes consisting of deformed and transported island arc and ocean-floor magmatic assemblages with mafic to intermediate magmatism corresponding to a prolongation of the onshore Pechora Zone (Gee et al. 2006) (Fig. 5.12) Alternatively, it could represents an agglomeration of small microcontinental blocks and slivers (Getsen 1991) intruded by magmatic plutons of variable character and chemistry, and metamorphosed in amphibolite facies corresponding to the onshore Khoreyver Domain (Belyakova and Stepanenko 1991; Kostyuchenko et al. 2006).

Beneath the South Barents Basin we see a dense and low-magnetic crust (Fig. 5.11a). The low-magnetic properties are proposed to be the result of the Timanian terranes accretion reflecting a non-magnetic Meso-Neoproterozoic succession lying above magnetic crystalline metamorphic or magmatic rocks similar to those of the western units (Fig. 5.11a and 5.12). This scenario is similar to the one found in northwestern Kola Peninsula, where the gravity and magnetic signal of the crystalline basement is blurred by the Meso-Neoproterozoic sedimentary cover which was partly overthrust during the Timanian orogeny. Compared to the weakly deformed Riphean rocks found in the Fedynskiy High area (Ivanova et al. 2007), we think that under the South Barents Basin, the Riphean (Meso-Neoproterozoic) succession was first strongly deformed during the Timanian orogeny and later buried under a thick sedimentary cover (more than 15 km). This led to a metamorphism of the older Precambrian successions resulting in a significant increase of densities.

Farther east, the eastern flank of the South Barents Basin has a medium-high magnetic and medium-high dense crust (Fig. 5.11a and 5.12) and is interpreted to be the continuation of the pre-Urals Domain defined by Kostyuchenko et al. (2006). It consists of a Precambrian crust that contains rocks of oceanic affinity.

Most of the south island of Novaya Zemlya differs from the central and northern parts (Fig. 5.12). The Timanian orogeny is known to have affected this southern area (Pease and Scott 2009), as proposed from the analysis of outcopping Precambrian rocks (Korago et al. 2004) and from a study of the magnetic trends (Marello et al. 2010). The Late Permian-Triassic Uralian deformation reactivated the pre-existing Timanian terranes. The telescoped thrusted terranes could partly explain the thickening of the crust (Fig. 5.11a) and the formation of a wedge composed of Neoproterozoic and Late Palaeozoic metasedimentary units (Korango et al. 2004; Stoupakova et al. 2011) corresponding to low-magnetic units. This wedge of sedimentary assemblages overthrusts older high-magnetic basement (maybe Archaean-Palaeoproterozoic) similar to the crystalline basement below the Timanian Pechora Basin region (Fig. 5.11a and 5.12).

### 5.6.2 Southwest Barents Sea: from Caledonian to Timanian

The Southwest Barents Sea has medium- to high-magnetic upper basement units (Fig. 5.7) that correlate with the main structural elements (Gabrielsen et al. 1990) on top of a magnetic lower crust (Fig. 5.11b). In the West Barents Sea, the transition from the oceanic to the continental domain is characterised by a basinal province that originated during Late Mesozoic extension, which runs more or less parallel to the Senja Fracture Zone (SJZ in Fig. 5.1). In our model, the margin is defined by a basement block that extends under part of the Harstad and Sørvestsnaget Basins and ends at the Vestbakken volcanic province (Fig. 5.1 and 5.12) and is characterised by an extremely thinned, stretched crust (Fig. 5.11b). This unit has been interpreted as transitional crust of intermediate character between continental and oceanic crust.

The transect cuts two crustal blocks characterised by extremely high-magnetic crust, and by a crustal thickness thicker than the average shelf thickness and shallower top basement (Fig. 5.11b). These units correspond with the Loppa High and the Stappen High, and are interpreted as micro-blocks of a different basement type compared to their surroundings (Fig. 5. 11b and 5.12). The Loppa High basement is penetrated by wells and results reveal the presence of amphibolites with a significantly high magnetisation, which are possibly related either to the Seiland Igneous Province or to nappes in the Uppermost Allochthon (Slagstad et al. 2008). More recent information stems from seismic models that record anomalous high velocities in the mantle below the Loppa High, similar to the upper mantle velocities estimated for the Varanger Peninsula (Clark et al. 2009). This observation leads us to interpret the main crust of the Loppa High at being composed of high-grade metamorphic rocks, possibly granulites, similar to parts of the Archaean-Palaeoproterozoic basement in the Fennoscandian Shield, and with a thin cover of allochthonous terranes (Upper or Uppermost Allochthon) (Fig. 5.11b and 5.12). Similarly, the Stappen High is believed to be composed of comparable high-grade metamorphic rocks but its relationship to the Archaean-Palaeoproterozoic basement is doubtful. The crystalline crust of the Stappen High could be a basement block with Laurentian affinities (Breivik et al. 2005), or an independent microcrustal block initially located between Laurentia and Baltica and subsequently involved in the Caledonian orogeny.

Alternatively, Olesen et al. (2010) from interpretation of the magnetic anomalies associated the two units as the northward continuation of the TIB (Transscandinavian Igneous Belt).

Located between the two magnetic basement blocks, a thin crustal unit extends below the Bjørnøya Basin, Tromsø Basin and Hammerfest Basin. In the deepest part of the Bjørnøya Basin (which has a 12 km-thick sedimentary succession) the upper crust gets thinner, and a high-density and magnetic lower crust and Moho are rising up in this area (Fig. 5.11b). Our crustal geometry is in agreement with new refraction data (Clark et al. 2009) and could be an example of exhumation of a lower crust that developed during the Late Mesozoic thinning phase of the western Barents Sea, as already proposed by Barrère et al. (2009). More local studies (Barrère et al. 2011, Clark et al. 2009) also presented a different scenario, proposing the existence of a high-density lower crustal body under the Bjørnøya Basin and part of the Loppa High. The quite high susceptibility of the crust could be explained by the presence of magnetic gneisses comparable to the ones mapped and sampled onshore Norway (Olesen et al. 1990; 2010; Barrère et al. 2011), and with the medium-grade complexes, dolerite-intruded Neoproterozoic sandstones and Precambrian crystalline nappes that form most of the Middle Allochthon. An alternative explanation could involve ophiolites, island-arc and back-arc basin assemblages that occur in the Upper Allochthon in many parts of Norway (e.g. Furnes et al. 1985; Gee at al. 2008) (Fig. 5.11b and 5.12).

Moving southeast of the Loppa High, a crustal block extends from the southern part of the Nordkapp Basin, below the Ottar Basin and part of the Bjarmeland Platform (Fig. 5.11 and 5.12). Previous studies recognise a lateral deflection of the Caledonian structures at this location (Gernigon et al. 2007; Barrère et al. 2009; Gernigon and Brönner 2012). This corresponds to medium- to high-grade metamorphic Caledonian rocks that are part of the Middle and Upper Allochthons lying on top of the crystalline crust. The crust beneath is interpreted to be similar to the Archaean-Palaeoproterozoic crust forming the Fennoscandian Shield or the Loppa High (Fig. 5.11b and 5.12).

Beneath the Nordkapp Basin, another basement unit has been defined (Fig. 5.11b). It extends from the coastal zone of northern Norway mostly parallel to the Troms-Finnmark Fault Complex (TFFC) and the Måsøy Fault Complex (MFC) to the Bjarmeland Platform (Fig. 5.1 and 5.12). Similar to the western unit the petrophysical properties suggest that the crust could correspond to the extension of the basement unit defined by Barrère at al. (2011) and interpreted as Caledonian terrane including the Lower and Middle allochthons (dominated by lower densities and magnetic properties) overlying the older Archaean-Palaeoproterozoic crust (Fig. 5.11b and 5.12). Farther to the southeast the transect leaves the Caledonian domain and crosses into the Timanian basement units described in the previous section.

### 5.6.3 Transition between north and south Barents Sea

The central-west Barents Sea represents a transitional region from the southern high-magnetic crust dominated by structural basement highs and lows to the northern platform area characterised by non-magnetic crust (Fig. 5.7 and 5.12). The

transition between these northern and southern areas of the Barents Sea is summarised in Fig. 5.11c.

From the western margin, the transect is passing through a basement block that extends northeast of the Stappen High including a large part of Bjørnøya and the northeasten areas of the Barents Sea (Fig. 5.11c and 5.12). Pre-Ordovician dolomites, sandstones, shales and limestones exposed in the south of Bjørnøya are interpreted as basement with a northeastern Greenland affinity (Smith 2000). Our model suggests a top basement geometry that links the Stappen High with Bjørnøya (Fig. 5.6d). This observation, combined with the petrophysical parameters applied in the model (lower densities and lower magnetic properties compared to the Stappen High), leads to the interpretation that Bjørnøya is made up of two different basement types: a crystalline crust related to the Stappen High crustal block, and a cover of Caledonian nappes. During the Caledonian collision Late Neoproterozoic to Ordovician terranes with Laurentian affinities (Holtedahl 1920, Dallmann and Krasil'ščikov 1996; Smith and Rasmussen 2008) were thrusted above the deeper Precambrian crustal block, generating the complex that is exposed on Bjørnøya today. We correlate this Caledonian thrust cover with the Uppermost Allochthon unit of mainland Norway (Fig. 5.11c and 5.12).

Farther east, the transect crosses a basement unit that extends northward beneath the Sørkapp Basin and Edgeøya Platform (Fig. 5.12). The crustal geometry (Fig. 5.6d, 5.8 and 5.9) and petrophysical values applied suggest a transition from a crustal type composed of magnetic terranes, similar to those found in the Southwest Barents Sea, to a thick and non-magnetic crystalline crust as exposed in the Svalbard region (Fig. 5.12). Seismic records indicate an increase in P-velocity and Vp/Vs ratio in the crust northeastwards from the margin north of Bjørnøya, suggesting an increase in density and the average mafic rock composition (Breivik et al. 2003, 2005). This mafic composition and density increase could be explained as a transition from the Uppermost Allochthon, comprising shelf and slope-rise successions (Roberts et al. 2007; Gee et al. 2008), to the diverse Iapetus Ocean terranes of the Upper Allochthon (Fig. 5.11c and 5.12).

Under the Gardarbanken High (Fig. 5.1, 5.11c), the basement becomes non-magnetic and is thickening, correlating with a shallowing of the basement and a slight deepening of the Moho. Here, Breivik et al. (2002) proposed an interpretation involving a deep, eclogitised, crustal root associated with an inferred old Caledonian suture (see Fig. 5.12). We interpret the crust in the north of Gardarbanken to be composed of low-magnetic rocks that have affinities with the Svalbard block. On the other hand, the basement in the south is interpreted to be mostly composed of terranes linked with the Baltican platform and margin, which are now part of the Lower Allochthon (Fig. 5.11c and 5.12).

A sag basin with a sediment record that spans from the late Palaeozoic to the Mesozoic is present in the East Barents Sea. The lithology of the basement beneath the sedimentary succession is difficult to interpret due to the sparsity of data that reach the crust. The geometry of our modelled crustal unit reflects the arc-shaped geometry of the Novaya Zemlya Fold Belt observed farther to the east.

The western flank of the basin shows a high-magnetic basement. Two prominent magnetic units (susceptibility > 0.2 SI) are distinguished from the rest of the crust and produce the two central Barents Sea magnetic anomalies (Fig. 5.3b).

Both structures are corresponding with shallow Archaean-Palaeoproterozic basement but are not imaged as a different type of crust on crossing seismic-reflection data (1-AR profile, Ivanova et al. 2006). Our model suggests distinct properties for these two units compared with the surrounding crust (Fig. 5.7 and 5.11c). The shallow Archaean-Palaeoproterozoic basement could imply a thinning or total removal of the Neoproterozoic non-magnetic cover, which is included in the basement layer defined in our model. This results in crustal units with a higher average magnetisation entirely made up of granulite rocks. Another possible explanation is a relationship with mafic magmatic bodies, which could be part of older Timanian terranes observed beneath the Pechora Zone (Gee et al. 2006).

The eastern basement unit crossed by the transect still forms the western flank of the basin (Fig. 5.11c and 5.12). We explain this unit as a complex of island-arc, ocean-floor magmatic rock or volcano-sedimentary assemblage with mafic to intermediate magmatism considered to be the prolongation of the Pechora Zone described by Gee et al. (2006). This interpretation is based on the idea that the Timanian range extends farther north mimicking the arcuate shape of Novaya Zemlya. An alternative interpretation is that the crust is of oceanic origin. Aplonov et al. (1996) have argued that in the Devonian, during a pre-Uralian rifting phase, oceanic crust was generated and formed a precursor basin to the East Barents Basin. The higher densities are explained by sedimentary compaction and the gabbroic and basaltic rock compositions of the proposed oceanic domain.

Farther east buried under the East Barents Basin, an almost non-magnetic and low-density unit has been defined (Fig. 5.11c and 5.12). Its petrophysical properties are explained by an aggregation of Precambrian terranes most likely related to Neoproterozoic sedimentary successions and later affected by Uralian deformation. We suggest that the Uralian deformation ends in the proximity to this crustal block (Fig. 5.11c and 5.12).

West of Novaya Zemlya, the crustal geometry is variable but thinning is recognised towards the centre of the basin (Fig. 5.6c, 5.8 and 5.11c). The crust forming the eastern flank of the South and North Barents Basins is steep compared to the western flank of the basin. This geometry is an indication of the multi-phase evolution of the basin that evolved at one stage as a foreland basin. The intermediate magnetic properties and low-densities characterising this crust lead us to propose this unit as being part of the pre-Uralian domain as defined by Kostyuchenko et al. (2006). It may represent a crust that is Precambrian and may contain rocks of oceanic affinity obducted during the Uralian orogeny (Fig. 5.12).

The eastern unit encountered along the profile (Fig. 5.11c) is the analogue to the one described in the transect Fig. 5.11a in the south Novaya Zemlya region, with the difference that no Timanian deformation has been proposed for this area (Korago et al. 2004).

### 5.6.4 Northern Barents Sea: from Barentsia to the North Barents Basin

The transect displayed in Fig. 5.11d shows the setting of the northern Barents Sea. The Northwest Barents Sea is mainly a platform area where Mesozoic tectonism produced smaller structures (Grogan et al. 1998) compared to the

Southwest Barents Sea. One of the reasons for differentiating the Northwest from the Southwest Barents Sea is the different evolution of the margin north of the Stappen High compared to the south (Faleide et al. 2008). Moreover, the inherited Caledonian structures (Ziegler 1988; Doré 1991) and pre-Caledonian geology identified here play an important role.

The transect (Fig. 5.11d) shows a crustal unit in the west that extends along the Hornsund Fault Zone (HFZ) and Sørkapp Fault Zone (SKZ) (Fig. 5.1), and corresponds with a complex sheared and rifted margin (Faleide et al. 2008). In the northwest of Spitsbergen the continental crust thins rapidly towards the Svalbard margin (Fig. 5.11c). In the same way as for the southern margin (Fig. 5.11b), the unit has been interpreted as crust with an intermediate character between continental and oceanic crust. This might have been produced by the interaction of the continental crust with the mantle during extension and break up (Fig. 5.12).

The western Svalbard unit (Fig. 5.11c and 5.12) corresponds with exposed basement comprising an amalgamation of different terranes (Late Mesoproterozoic, Early Neoproterozoic) that differs from the rest of Svalbard. The unit has an affinity with the Pearya terrane of northernmost Ellesmere Island in northern Canada and with Laurentia (Harland 1997; Trettin 1998; Gee and Teben'kov 2004).

The eastern and central Svalbard unit differs from the west for two main reasons: (1) the low-magnetic crust (Fig. 5.11d) and (2) the crustal geometry characterised by a shallow basement and thick crust (Fig. 5.6d, 5.9a and 5.11d). An explanation for the low-magnetic crust is not easy to deduce. Pseudo-gravity transformation, which enhances the effect of large and deeper structures, indicates low-magnetic properties for the region (Marello et al. 2010). In Nordaustlandet (Northeast Svalbard), there are Neoproterozoic volcanic rocks, granites and migmatites, which thus make it difficult to explain such a low-magnetic crust. The low polarity and remanence of magmatic intrusions may be an explanation, but the modelling of remanent magnetisation was not sufficient to explain the magnetic anomaly. Moreover, the presence of large Early Cretaceous intrusions east of Svalbard (Grogan et al. 1998) correlates with the high-frequency magnetic pattern observed in the area. The presence of this young and shallow magmatism affects the magnetic signal and precludes the analysis of deeper and larger basement magnetic sources. The distribution of these intrusions has been interpreted to relate to an old basement weakness zone of Caledonian origin (Barrére et al. 2010). Besides these modelling difficulties, our results provide an indication of the existence of a thick crustal block characterised by very different and distinct magnetic properties. This may suggest a different origin for the Svalbard block and could support the notion of the existence of a Barentsia micro-crustal block (Fig. 5.11c and 5.12) as earlier suggested by Gudlaugsson et al. (1998).

The transition from the Svalbard block to the North Barents Basin is marked by a low-density and poorly magnetic basement unit (Fig. 5.11c and 5.12). This unit extends from southwest of Franz Josef Land and links the proposed Svalbard Craton (Barentsia) with the North Barents Basin. The basement consists of rocks similar to those found in the Svalbard block. Its thickness diminishes towards the North Barents Basin and this geometry could be the result of the initial rifting

(probably Late Devonian) that caused the crustal thinning and the formation of the early North Barents Basin.

Farther east, the profile displays the North Barents Basin which is dominated by a basement that represents the continuation of the domains described in the previous section (Fig. 5.11c and 5.12).

### 5.6.5 Caledonian- Timanian extension and interaction

The offshore extension of the Caledonian nappes and the location of the suture zone separating Baltica and Laurentia terranes has been matter of extensive discussion (e.g. Harland and Gayer 1972; Siedlecka 1975; Gudlaugsson et al. 1987, 1998; Ziegler 1988; Nikishin et al. 1996; Doré 1991; Johansen et al. 1994; Fichler et al. 1997, Breivik et al. 2002; Gee at al., 2006; Ritzmann et al, 2007; Barrère et al. 2011, Gernigon and Brönner 2012). Whilst we support the idea of the existence of two Caledonian branches (Siedlecka 1975, Gudlaugsson et al. 1998), we propose a different location than in previous studies.

One branch corresponds to the site of the Laurentia-Baltica collision and extends northwards from northern Norway, passing to the west of the Loppa High and also probably west of the Stappen High, and continuing to the east of the southwestern Svalbard terrane as defined by Gee et al. (2008). This location mostly coincides with the extension of the Upper Allochthon terranes (Fig. 5.12).

A second Caledonian branch occupies the Northwest Barents Sea. We support the idea that a microcrustal block (Barentsia), including the actual Svalbard platform area, was involved in the Caledonian orogeny and that the boundary between Baltica and Barentsia has to be in the central part of the Barents Sea. Barrère et al. (2009) proposed the existence of a more competent terrane to the north of Baltica to justify the contrasting tectonic setting between the northern and the southern Barents Sea and to create their proposed elbow-shape in the offshore extension of the Caledonian thrusts. We validate the existence of this competent block, suggesting it to be a thick crustal body distinct from the other crustal units, which we relate with Barentsia.

Ocean bottom seismic data denote the existence of a SE-dipping, inferred Caledonian suture extending beneath a ‘deep crustal root’ located in proximity to the Gardarbanken and Sentralbanken highs and Olga Basin (Fig. 5.12, Breivik et al. 2002). We agree with the possible location of the suture between Barentsia and Baltica in this area and extend this boundary north-northeastwards to the western part of Franz Josef Land.

The orientation of this inferred suture can be discussed. The profiles displayed in Fig. 5.11d show boundaries between the Svalbard crustal block and the eastern units which dip at depth toward the northwest. We can assume that these reflect the orientation and dip of the major thrusts and a link to the westward-dipping reflectivity interpreted as an eastward overthrust by Gudlaugsson et al. (1987) ( Fig. 5.12). On the contrary, in proximity to the Gardarbanken High (Fig. 5.11c) the crustal boundaries dip towards the southeast and simulate the major thrust geometry interpreted as a suture by Breivik et al. (2002).

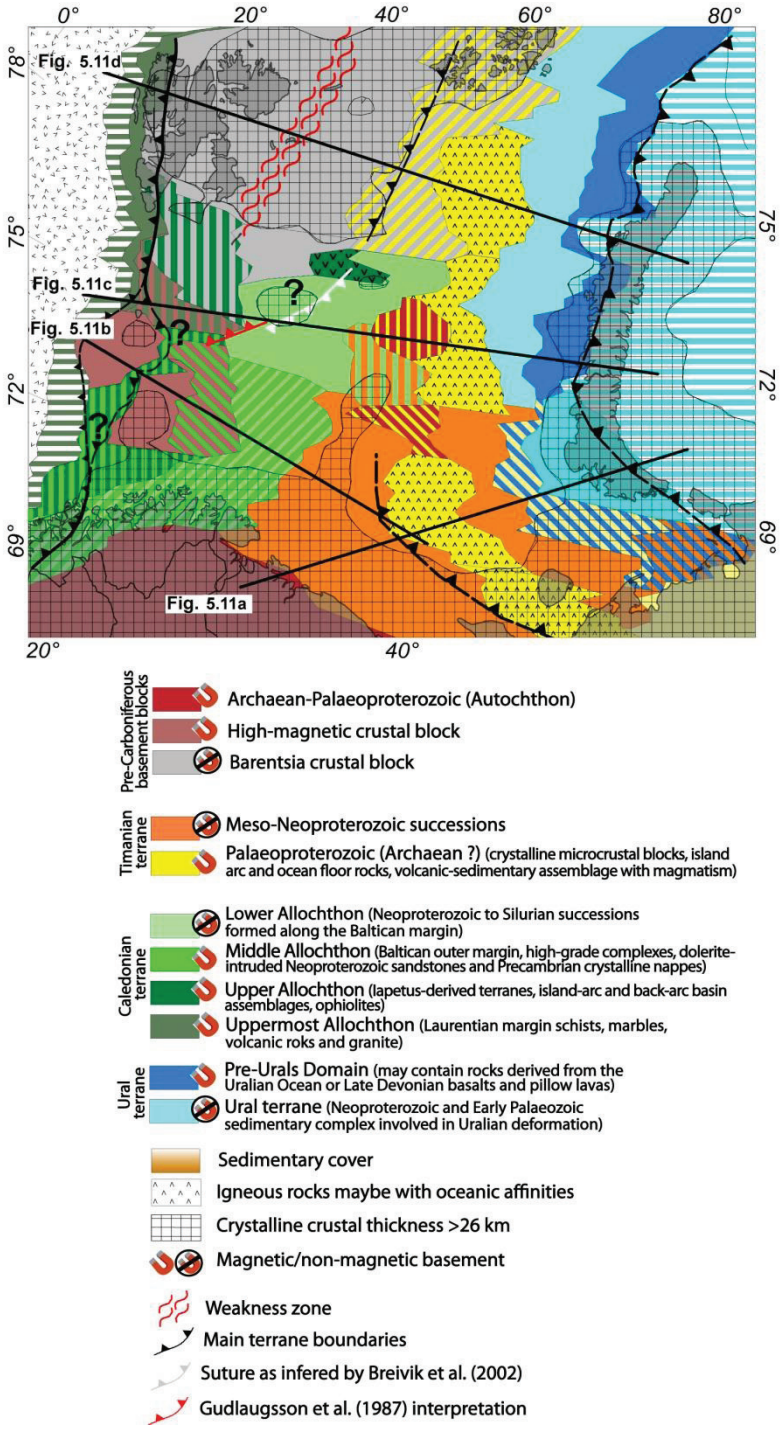


*Figure 5.12. Geological interpretation of the crustal setting for the Barents Sea Region.*

The observed increase in thickness of the crystalline basement, which coincides with the Fedynskiy and Central Barents highs (Fig. 5.10b, 5.11b and 5.12) could support the idea that the Fedynskiy and Central Barents highs are microcontinental blocks (Aplonov et al. 1996). A proper understanding of their existence and formation is important since these two blocks are located roughly at the Caledonian and Timanian deformation fronts. On Varanger Peninsula, the Caledonian structures are dying out eastwards and, conversely, the Timanian structures gradually disappear westwards (Roberts and Olovyanishnikov 2004, Herrevold at al. 2009). That situation could be extended offshore where the Caledonian nappes that swing around the Loppa High (Barrère et al. 2009, 2011; Gernigon and Brönner 2012) are separated by the Fedynskiy and Central Barents Highs from the Timanian terranes which swing in the opposite sense in an arc shape that mimics the geometry of Novaya Zemlya. That the Timanian terranes do not extend farther across the Barents Sea into the Svalbard Caledonides is supported by petrological observations (Gee and Teben'kov 2004).

In south Novaya Zemlya, interaction between Uralian and Timanian structures is also recorded, but not in the central and northern parts of the archipelago. We propose that the arcuate shape of the basement units under the eastern Barents Sea is a geometry that reflects the Timanian accretion of different crustal units and is not related to a Permo-Triassic, Uralian event.

## 5.7 Conclusions

We have developed a new model for the Barents Sea that integrates potential field modelling with pre-existing models. Our modelling refines the crustal architecture and provides density and magnetic distributions for the entire region. The final result improves our understanding of the Barents Sea geology in space and time.

Three major regions are distinguished in our model; (1) the Southwest Barents Sea, (2) the Northwest Barents Sea and (3) the eastern Barents Sea. Large differences between these areas are recognised in terms of top basement geometry, crustal thickness and crustal properties, which reflect their different tectonic histories.

Comparative observations of our crustal setting and properties results with previous models, allow us to propose a new interpretation for the basement beneath the Barents Sea.

- The Southwest Barents Sea crust is of high-magnetic character and is composed of Precambrian basement mostly covered by Caledonian terranes. The Caledonian units occurring along the Baltica-Laurentia margin correspond to aggregation series of nappes characterised by medium-magnetic (except for the Lower Allochthon which is non-magnetic) overlying older basement terranes (Fennoscandian Shield, Loppa High and Stappen High).
- The Caledonian basement in the Northwest Barents Sea comprises terranes formed at the margin between the Svalbard Craton (Barentsia) and Laurentia, and is dominated by medium-low densities and a non-magnetic basement. The central Barents Sea in proximity to the Sentralbanken High is distinguished from the

Southwest Barents Sea by its low-magnetic properties. It is composed of crustal terranes developed between the platform margin of Baltica and the Barentsia margin, which were thrust together during the Caledonian event. The existence of a second branch of Caledonian basement in this area is supported by our model.

- The basement beneath the North Barents Basin is dominated on its western flank by high-magnetic and high-density crust interpreted as Precambrian basement which may have been affected by Timanian deformation. The central part of the basin is underlain by a non-magnetic and less dense crust, including Meso-Neoproterozoic or younger successions lying close to the Uralian front. The steeper eastern flank with higher magnetic and less dense crust is considered to have oceanic or magmatic affinities and to have been strongly affected by the Uralian deformation.
- The crust of the Southeast Barents Sea represents an extension of the Timan-Pechora basement domains. This region is characterised by a high-density basement and by an alternation of high-magnetic and non-magnetic blocks. The non-magnetic crust is considered to represent the Meso-Neoproterozoic successions on top of older, magnetic, crystalline crust.

## *Acknowledgments*

*The study was carried out as part of the PETROBAR project (Petroleum-related regional studies of the Barents Sea region) funded by Statoil and the PETROMAKS programme of the Research Council of Norway. We thank Odleiv Olesen, Marco Brönner and Christine Fichler for sharing their knowledge about the Barents Sea. We are very grateful to David Roberts for editorial review before manuscript submission.*

# Chapter 6

# Thermal and compositional structure of the lithospheric mantle

*The content of this chapter is in preparetion for submission: Marello, L., Gradmann, S., Ebbing, J., Thermal and compositional structure of the lithospheric mantle in the Barents Sea.*

## 6.1 Introduction

Plate tectonics influence the structure and physical properties of the crust and lithospheric mantle (Artemieva et al. 2002). The lithospheric mantle is non-convecting, which means it does not mix and homogenise, and therefore carries a unique geochemical, thermal and chronological record of tectonic events (O'Reilly and Griffin 2006). The lithospheric mantle heterogeneities of the Barents Sea (Fig. 6.1) can be observed using different geophysical data sets reflecting the geological processes that affected the area. A recent surface wave tomography model of the Barents Sea shows lateral heterogeneities in shear wave velocities in the upper mantle across the region (Levshin et al. 2007) (Fig. 6.2). The data image a low-velocity anomaly that reflects the thermal field related to break-up of the North

Atlantic during the Cenozoic, and additionally a high velocity mantle has been detected mostly beneath the East Barents Sea. The shape of the anomaly exhibits a gentle dip to the east and thickens to more than 120 km beneath the East Barents Basin. The feature has been proposed to reflect a relict slab or cratonic root, but neither explanation is univocally accepted (e.g. Levshin et al. 2007; Ritzmann et al. 2009).

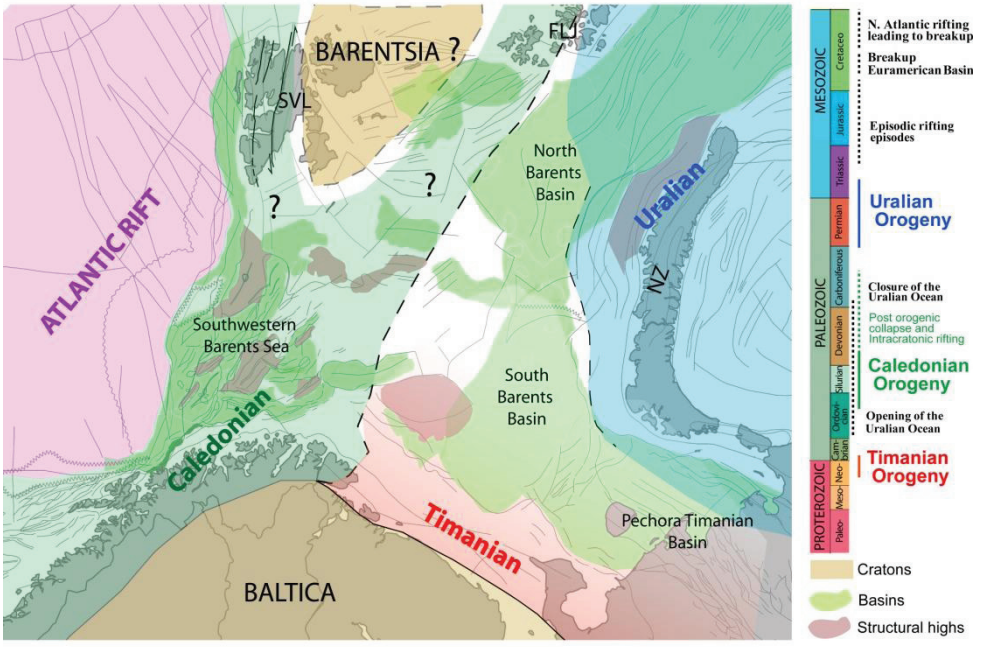


*Figure 6.1. Structural elements of the Barents Sea region. The chronology of the major geological events is displayed on the right. Labels on the map indicate: SVL, Svalbard archipelago; FJL, Franz Josef Land; NZ, Novaya Zemlya (modified after Gudlaugsson et al. 1998).*

Isostatic studies point out the existence of a high-density upper mantle, which spatially correlates with the tomographic velocity high (Ebbing et al. 2007). The influence of temperature on mantle densities below the west Barents Sea continental margin has been studied previously (e.g. Breivik et al. 1999; Ritzmann et al. 2009), and the decrease in velocity as observed for the Barents Sea is correlating with such lower densities towards the oceanic domain.

In this work, we present integrated models for the lithospheric mantle to address two major topics. Firstly, we investigate the origin of the high shear-wave velocities imaged under the East Barents Basin. Seismic velocities are studied with respect to compositional and thermal changes of the lithospheric mantle, which are simultaneously compared to the geoid and gravity field. Moreover we are interested to study the low-velocity, low-density domain at the continent-ocean transition. This study develops for the first time an integrated geophysical-petrological 3D lithospheric model for the Barents Sea region.

The models allow us to analyse the thermal, compositional and seismological structure of the upper mantle in the Barents Sea region and its relation with the regional geological evolution. E.g., different thermal and compositional setups have been tested in function of the assumed age of the Barents Sea lithosphere. Additional information of mantle heterogeneities is inferred from comparison to seismological, petrophysical and potential field data. Differences between the observed and calculated fields have been reduced by introducing thermal and compositional changes. The models results allow validation of different tectonic scenarios such as the existence of cratons, rifted areas and transition to oceanic domains.

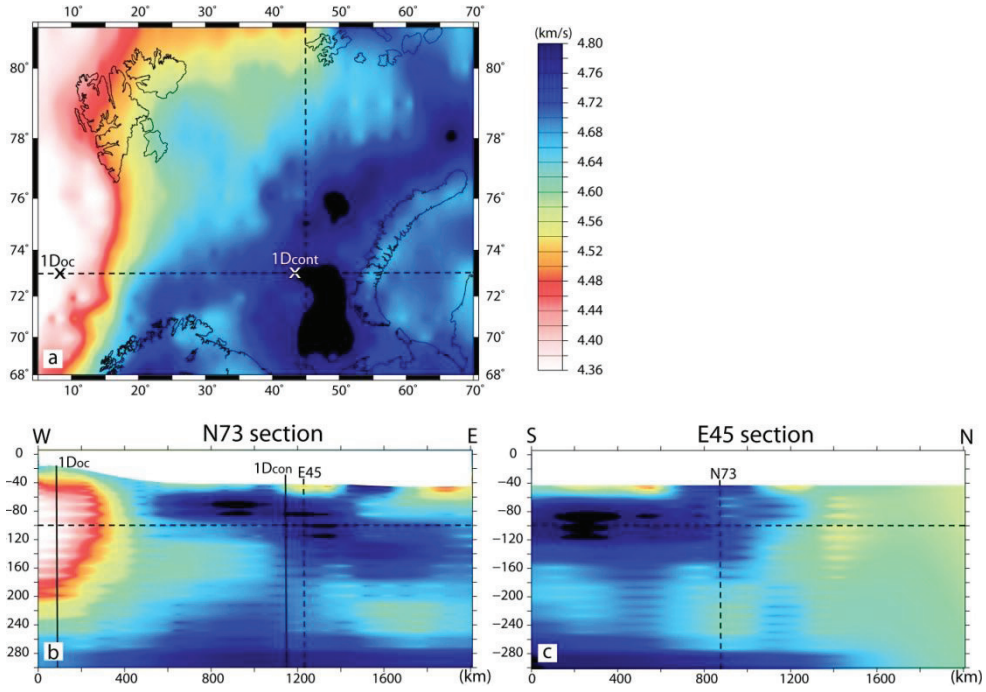


*Figure 6.2. Tomographic S-wave model from Levshin et al. (2007). Two vertical transects are displayed: (a) constant-depth slice of shear wave velocities at 100 km. The crosses show the location of two vertical profiles $1D_{oc}$ and $1D_{con}$ in the oceanic and continental areas, respectively (Figs 6.8, 6.12). Dotted lines display the intersection between the 3 panels. (b) N73 section at constant latitude of 73˚Nshows the low velocities anomaly of the oceanic domain to the west and the high-velocity anomaly in the continental domain to the east; (c) E45 section at constant longitude of 45˚E shows the northern edge of the high-velocity anomaly.*

## 6.2 Geological evolution and tectonothermal age

The Barents Sea geological history is characterized by repeated cycles of collision and extension stemming mainly from the interaction of three major plates: Baltica, Laurentia and Siberia. Three stages of major convergence are known for the region, related to the Timanian (600–545 Ma), Caledonian (440–410 Ma) and Uralian (280–240 Ma) orogenies (Faleide et al. 2006a, b) (Fig. 6.1).

The *latest Precambrian to early Cambrian* collision affected mostly the actual south east Barents Sea resulting in an accretion of various microcontinental blocks onto Baltica forming a much expanded terrane area in the Lower Paleozoic (Cocks and Torsvik, 2005).

Later in the *Silurian*, the Iapetus Ocean subducted under Laurentia. In early-mid Silurian the compressive phase culminated in a continental collision, between Baltica and Laurentia and in the formation of the Caledonian chain (Robert 2003; Cocks and Torsvik 2005) that propagated northwards and affected most of the western Barents Sea (e.g. Roberts and Olovyanishnikov 2004; Ritzmann and Faleide 2007; Barrère et al. 2011).

In the *Early Carboniferous* closure of the Uralian Ocean with eastward subduction under the Siberian craton started. The active margin phase propagated northward and reached the eastern Barents Sea in the Late Carboniferous to Early Permian (e.g. Puchkov 2002). At the same time (Late Permian and Early Triassic) a large flexural sag basin developed in the eastern part of the Barents Sea and was filled with molasse of the proto-Uralian Mountains (e.g. O'Leary et al. 2004; Petrov et al 2008).

The Late *Palaeozoic and Mesozoic* Barents Sea evolution was mostly dominated by a stable platform and extensional tectonics that culminated in the opening of the Norwegian Greenland Sea (Faleide et al. 1996; Gudlaugsson et al. 1998; Johansen et al. 1992).

This geological evolution created a continental shelf region characterised by Palaeozoic and Mesozoic sediments that cover older basement. The crustal structure in the southwest Barents Sea is dominated by a large number of graben and half-graben basins, in the northwest and the Central Barents Sea by a platform area, and in the entire East Barents Sea by a large sag basin (Johansen et al. 1992; Henriksen et al. 2011).

The buried basement is formed from an aggregation of different rock types consisting of microcontinental blocks with accreted margin terranes and intrusions, that pass into oceanic domain toward the west and toward the north (e.g. Johansen et al. 1992; Kostyuchenko et al. 2006; Ritzmann et al. 2007; Barrère et al. 2011; Marello et al. 2012).

At the continent-ocean transition, a strong contrast generally occurs between sub-oceanic lithospheric mantle (SOLM) and sub-continental lithospheric mantle (SCLM). The SCLM is usually cold and resistive but also more buoyant than the SOLM (Carlson et al. 2005). Estimates on the formation age of the SCLM are obtained from the tectonothermal history of the overlaying crust (Poudjom Djomani et al. 2001). For the Barents Sea, the crustal evolution suggests a large variation in SCLM age. Archaean lithospheric mantle is proposed under the Baltic Shield and probably extends offshore (e.g. Artemieva et al. 2006).

Palaeoproterozoic ages have been estimated in Timanian areas and large parts of the South Barents Basin (e.g. Olovyanishnikov et al. 2000). The youngest Phanerozoic age is expected in the proximity of the margin.

Compositional variations in the lithospheric mantle are well correlated with age and interpreted as an irreversible variation where the lithospheric mantle becomes colder, thicker and more depleted over time (e.g. O`Reilly and Griffin, 2006, Poudjom Djomani et al. 2001; Jordan 1988; Deschamps et al. 2002). Studies of xenoliths and xenocrysts in volcanic rocks and exposed massifs estimated the mean composition of the SCLM in relation to age (Griffin et al. 1998, 1999b). The removal of incompatibles elements, in particular iron, has important geophysical consequences as it results in higher seismic velocities and lower densities (Poudjom Djomani, et al. 2001, Artemieva et al. 2006, O'Reilly and Griffin, 2006). In general, *Archaean lithosphere (> 2.5 Ga)* is thick (180-350 km) and strongly depleted, leading to higher seismic velocities and lower densities. *Proterozoic SCLM* (2.5 - 1.0 Ga as commonly defined in lithospheric studies; e.g. Artemieva and Mooney 2001; Poudjom Djomani et al. 2001) is less depleted, less cold and thinner than Archaean lithosphere, leading to moderately fast mantle velocities and medium mantle densities with a thickness of 150-250 km. *Phanerozoic SCLM* (< 1.0 Ga, 100 to 180 km thick) is warmer and poorly depleted, leading to mantle of higher densities and lower seismic velocities with a thickness that ranges from 100 to 180 km (Artemieva and Mooney 2001; Poudjom Djomani et al. 2001).

## 6.3 LITMOD3D approach

Our models are developed using LitMod3D (LIThospheric MODelling in a 3D geometry), an interactive software for combined geophysical-petrological modelling of the lithosphere and sublithospheric upper mantle (Afonso et al. 2008; Fullea et al. 2009).

### 6.3.1 Model definition in *LITMOD3D*

The model consists of the crust, lithospheric mantle and sub-lithospheric mantle. Input parameters characterise each model domain via its geometry, density (for crustal material), thermal properties (e.g. thermal conductivity, heat production) and composition (for mantle material).

The entire SCLM is bounded by the Moho boundary at the top and the lithosphere/asthenosphere boundary (LAB) at the bottom. The material forming each SCLM domain is simplified to the most frequent oxide component CaO-FeO-MgO-$Al_2O_3$-$SiO_2$ (CFMAS system) that make up the 98% of the Earth's mantle (Palme and O'Neill, 2005). The CFMAS is considered to be a good representative system for modeling mantle phase equilibria (Afonso et al, 2009).

The model domains are divided into multiple prisms for the calculation of the thermal regime and of the different geophysical observables. LitMod3D for any given model is simultaneously able to calculate temperature, pressure, surface heat flow, density, seismic wave velocities, geoid and gravity anomalies and elevation.

### 6.3.2 Iterative P, T, density calculations

A fully iterative scheme couples pressure and temperature to densities and thermal properties (Fullea and Afonso, 2010). A first configuration is derived from initial thermophysical values of crust and SCLM, subsequent refinement occurs in the following way.

For the prevailing pressure-temperature conditions the respective stable mineral phases and assemblages in the SCLM are calculated from the CFMAS system using a Gibbs free-energy minimization algorithm. For this approach we use the thermodynamic database of Stixrude and Lithgow-Bertolloni (2005). The resulting thermodynamic tables are generated by Perple_X (see Connolly 2005) describing densities (third- or fourth-order Birch–Murnaghan equation), elastic moduli and thermophysical parameters of the end-member minerals.

In the crust, the pressure controls the densities via the compressibility (β). Thermal effects on the crustal physical properties are not incorporateed in our study.

The temperatures distribution in the lithospheric domain is calculated solving the heat transfer equation (Galerkin's ponderation methods: Zienkiewicz, 1977). Heat production rate and crustal thermal conductivity are explicitly defined as input parameters. The pressure- and temperature dependence of the thermal conductivity of the SCLM is constrained by additional input parameters (reference conductivity, Grüneisen parameter, isothermal bulk modulus and its pressure derivative). The base of the rigid and conductive layer (thermal and compositional LAB) (Afonso et al. 2008) is defined as the 1300˚C isotherm, below which the model extends down to 410 km where the temperature is defined at 1520˚C. In the sublithospheric domain the temperature distribution approximately follows an adiabatic gradient. Between the lithospheric and sublithospheric domain a buffer temperature layer is applied in order to assure a smooth transition of the different physical properties (Afonso et al. 2009). The pressure is calculated from the overall density distribution in the crust (pressure-dependent) and SCLM (as derived in the thermodynamic tables).

### 6.3.3 Geophysical fields and observables

In the next step, geophysical observables are computed and compared with observable data (e.g. topography, geoid, gravity and seismic velocities). Seismic velocities are obtained from the thermodynamic tables as a function of composition, pressure and temperature (Afonso et al. 2008; Fullea et al. 2009). Elevation and potential fields are calculated using the density structure derived in the previous step. The concept of local isostasy is applied to calculate the absolute elevation of any column forming the model (Afonso et al. 2008). Flexural isostatic compensation with a constant effective elastic thickness can additionally be calculated. Gravity and geoid anomalies are calculated for every surface point of the model by adding the effect of all individual prisms (Fullea et al. 2009).

The calculated geophysical data from the model are then compared with the observed data. The outputs can be used to modify the input parameters in order to simultaneously fit all available geophysical and petrological observables.

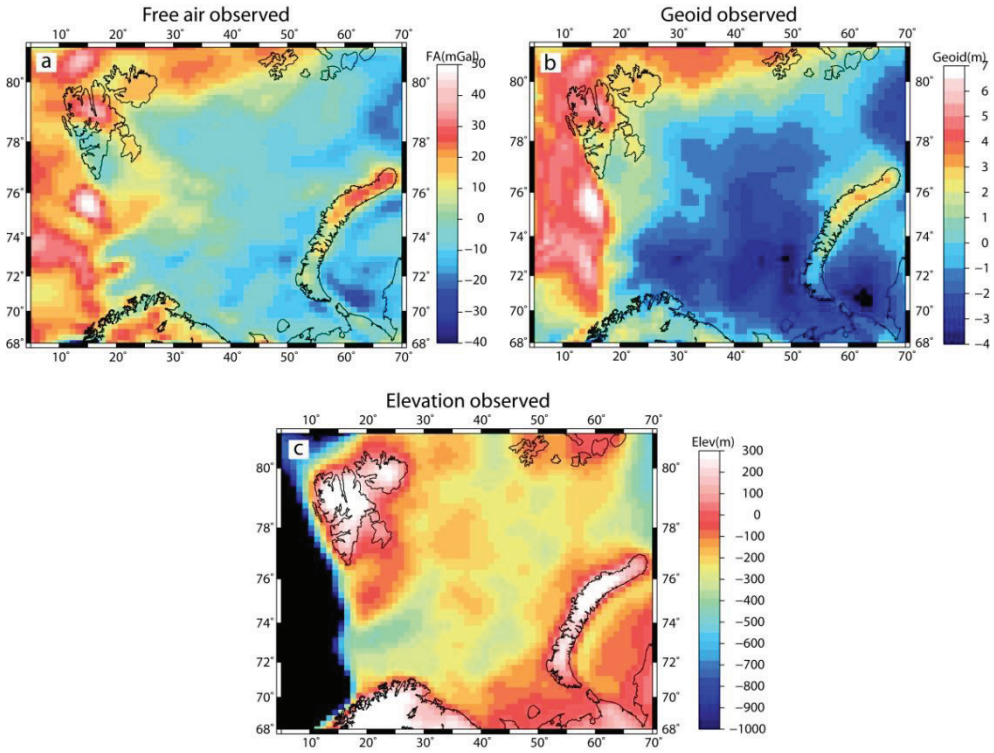


*Figure 6.3. Observed geophysical data: (a) Free air anomaly (FaArcGP); (b) Geoid filtered at spherical harmonical degree 11 (EGM2008); (c) Elevation (IBCAO). For references see Table 1.*

| | | | |
|---|---|---|---|
| Geometry | Topography | IBCAO | Jakobsson et al. 2008 |
| | Moho | | Grad et al. 2009; Marello et al. 2012 |
| | Lithosphere-asthenosphere boundary | LAB | Conrad et al. 2006; Artemieva et al. 2006 |
| Petrophysical parameters | Thermal conductivity | K | Afonso et al. 2008; Fullea et al. 2009; Hofmeister, 1999 |
| | Thermal Grüneisen parameter | γ | Afonso et al. 2008 and references therein |
| | Heat production rate | A | Afonso et al. 2008; Fullea et al. 2009; Kolstrup 2010; Pinet and Jaupart 1987; Rudnick et al. 1998 |
| | Thermal expansion | α | Afonso et al. 2008; Fullea et al. 2009; Turcotte and Schubert 2002 |
| | Compressibility | β | Afonso et al. 2008; Fullea et al. 2009 |
| Geophysical data | Free air gravity | FaArcGP | http://earth-info.nga.mil/GandG/wgs84/agp/; Forsberg et al. 2007 |
| | Geoid | EGM2008 | http://earth-info.nga.mil/GandG/wgs84/gravitymod/egm2008/egm08_wgs84.html |
| | Seismic tomography | BARMOD | Levshin et al. 2007 |

*Table 6.1. Data sets used for the models*

## 6.4 Input parameters and geophysical data

Geometrical, petrophysical and geophysical data have been used to build the thermal and compositional structure of the SCLM in the Barents Sea, as summarized in Table 6.1.

### 6.4.1 Geophysical observables

The simultaneous use of different observables (gravity, geoid, seismic tomography, elevation) reduces the uncertainties associated with modelling (Afonso et al. 2009). The tomographic shear wave velocities of Levshin et al. (2007) are used for comparison with the calculated velocities. Two large lateral heterogeneities in shear wave velocities are recorded in the upper mantle. Fig. 6.2 shows two vertical cross-sections and a horizontal slice of the model at 100 km depth. The 3 panels display the shape of the low velocity anomaly in the oceanic areas and the high velocity anomaly that underlies the East Barents Basin.

Gravity, geoid and elevation data (for references see Table 6.1) have been used to model the density structure of the SCLM. Fig. 6.3 shows the potential field data of the Barents Sea. A positive gravity anomaly and positive geoid are located at the margin of the shelf, while negative anomalies dominate the continental areas. The regional, sub-lithospheric contribution to the geoid has been removed at spherical harmonic degree eleven (~ 3600 km wavelength, Bowin 2000).

A first correlation is seen between the geoid low in the East Barents Sea (ranging from -1m to -4m) and the increased mantle velocity (Fig. 6.2 and 6.3b).

### 6.4.2 Geometry and model parameterization

Crustal geometry has been defined using the topography and Moho depth as given in Table 6.1 and Fig. 6.3c and 6.4b.

The lithosphere–asthenosphere boundary (LAB) is difficult to constrain as it is not a sharp boundary, but rather a transition zone. The definition of the LAB furthermore depends on the method used (e.g. McKenzie and Bickle, 1988; Wyllie, 1988; Anderson, 1989; Pavlenkova et al. 1997; O'Reilly and Griffin, 2006; Artemieva 2011): geochemically, the LAB is marked by the change from depleted SCLM to the fertile asthenospheric composition. Seismically, the LAB may be identified as a low-velocity zone or as a decrease in velocity with depth. Rheologically, the LAB is interpreted as a mechanical boundary layer at the base of the SCLM. Thermally, the lithosphere-asthenosphere transition is defined as the transition from conductive to convective heat flow (Turchotte and Schubert, 2002), and often chosen to coincide with the 1300 degree Celsius isotherm. LitMod3D uses a combined thermal and compositional definition of the LAB (Afonso et al. 2008).

For the Barents Sea region, the depth of the LAB is taken from global and regional studies. A global LAB model (see Fig. 6.4a) was released by Conrad et al. (2006); for oceanic areas the LAB was defined proportional to the square root of lithospheric age (Müller et al. 1997), while for the continents it follows the approach of Gung et al. (2003), who used the maximum depth for which the velocity anomaly is consistently greater than +2%.

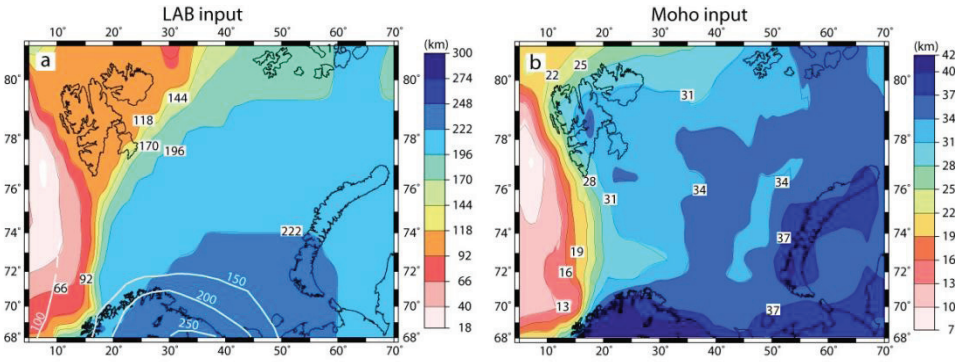


*Figure 6.4. Input geometry used in lithospheric models. (a) LAB of Conrad et al. (2006) as colour plot, LAB of by Artemieva et al. (2006) as white contour lines; (b) Compilation of Moho depth from Grad et al. (2009) for oceanic areas, from Marello et al. (2012) for the continental shelf region.*

Artemieva et al. (2006) compared different seismic models of the European continental upper mantle with magnetotelluric, thermal and gravity models and mantle xenolith data to constrain an integrated model (Fig. 6.4a). The vertical resolution of the model is limited to 50 km due to the diffuse character of the base of the seismic lithosphere together with the substantial thickness of the transition zone between purely conductive and purely convective heat transfer.

Three different SCLM compositions have been chosen as representative for the different degrees of depletion in relation to lithospheric age, and are defined by the CFMAS system as described above and in Table 6.2. The first type (Tecton-type) corresponds to an average Phanerozoic, fertile mantle. The second composition (Proterozoic-type) represents medium depleted mantle. The third (Archaean-type) represents strongly depleted mantle and is based on Archaean craton garnet SCLM. In addition to the three SCLM types, the sublithospheric mantle is characterized by the fertile composition of the primitive upper mantle (PUM).

The additional petrophysical parameters required to calculate pressure and temperature fields are summarized in Table 6.1.

| **Elements** | **Fertile[1] Tecton-type** | **Medium depleted[2] Proterozoic-type** | **Highly depleted[3] Archaean-type** | **sub-lithospheric mantle (PUM)** |
|---|---|---|---|---|
| $SiO_2$ | 44.5 | 44.6 | 45.7 | 45.0 |
| $Al_2O_3$ | 3.5 | 1.9 | 0.99 | 4.5 |
| FeO | 8.0 | 7.9 | 6.4 | 8.1 |
| MgO | 39.8 | 42.6 | 45.5 | 37.8 |
| CaO | 3.1 | 1.7 | 0.59 | 3.6 |
| [1] Average Tecton (Phanerozoic craton) Garnet SCLM<br>[2] Average Proterozoic craton SCLM<br>[3] Average Archaean craton Garnet SCLM | | | | |

*Table 6.2. Lithospheric mantle composition (CFMAS system) used in this study. The compositions correspond to average mantle composition estimated for different age (after Afonso et al. 2008; Griffin et al. 1996b).*

## 6.5 Modelling

This study of the thermal and compositional structure of the Barents Sea consists of two phases. First, we explore the sensitivity of our SCLM models to composition, geometry and temperature distribution. In the second more detailed phase we refine the models by changing the LAB structure (thermal and compositional boundary) and by introducing vertical and/or lateral compositional discontinuities in order to adjust the models to the observed seismic velocities and gravity fields.

The resolution in our models is defined by the size of the rectangular prisms of 25 km by 25 km by 4 km (length, width, depth).

The results of our analysis are summarised in 5 examples. The first model is the most simple and has a homogeneous lithospheric mantle. In model 2 and 3 lateral variations have been introduced to simulate the transition between SOLM and SCLM. In model 4 and 5 a further refinement is introduced by a vertical layering of the SCLM that differentiates the upper and lower part of the lithospheric mantle under the Barents Sea shelf.

The crustal geometry was constant for all models, simplified by two crustal layers. The densities in the upper part of the crust are increasing with depth controlled by the compressibility β (Table 6.3). The lower crust is represented by a 4.5 km thick layer characterised by constant density introduced to avoid unrealistically low crustal densities. Additional thermal inputs are summarised in Table 6.3.

| Layer | Density | α | K | A | β | γ | Pressure derivatives of isothermal bulk modulus | Isothermal bulk modulus |
|---|---|---|---|---|---|---|---|---|
| Crust | 2750 | 0.000E+00 | 2.2 | 0.110E-05 | 0.50E-10 | 0.00 | 0.00 | 0.00 |
| Lower crust | 2950 | 0.000E+00 | 2.3 | 0.110E-06 | 0.000E+00 | 0.00 | 0.00 | 0.0 |
| Mantle | | 0.310E-04 | 5.3 | 0.100E-07 | 0.000E+00 | 1.25 | 4.30 | 130.0 |

*Table 6.3 Thermal model inputs. For references and description see Table 6.1*

### 6.5.1 Homogeneous mantle (model 1)

As previously noted, the Barents Sea basement is an aggregation of different terranes, whose origin span from Archaean to Lower Palaeozoic. Considering the last major tectonothermal events in the area, the North Atlantic opening (around 65 Ma), Uralian orogeny (280-240 Ma), and the Caledonian Orogeny (410-440 Ma), a Phanerozoic age for the lithospheric mantle could be argued for. Therefore, our model 1 tests a homogenous lithospheric mantle composition corresponding to the Tecton-type (Table 6.2).

The geometry of the Moho interface and LAB are as given in Table 6.1 and displayed in Fig. 6.4. The input parameters used for each layer are summarised in Table 6.3.

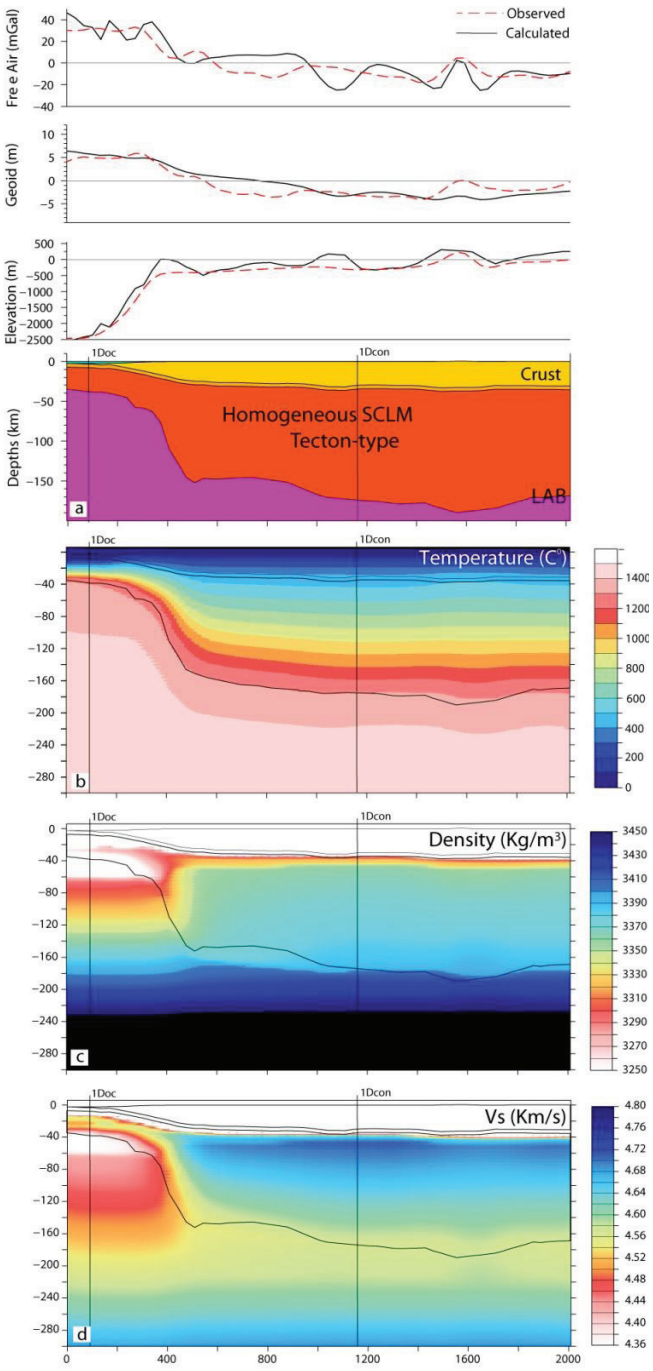


*Figure 6.5. Cross-section at 73˚N of model 1 (homogeneous SCLM composition). For location and comparison with observed velocities see Fig 6.2b. Observed and calculated free air anomaly, geoid and elevation, are displayed in the top panels. (a) Model geometry; (b) calculated temperature distribution; (c) calculated densities; (d) calculated shear-wave velocities. $1D_{oc}$ and $1D_{con}$ corresponding to the location of the 1D-depth profiles shown in Figure 6.8.*

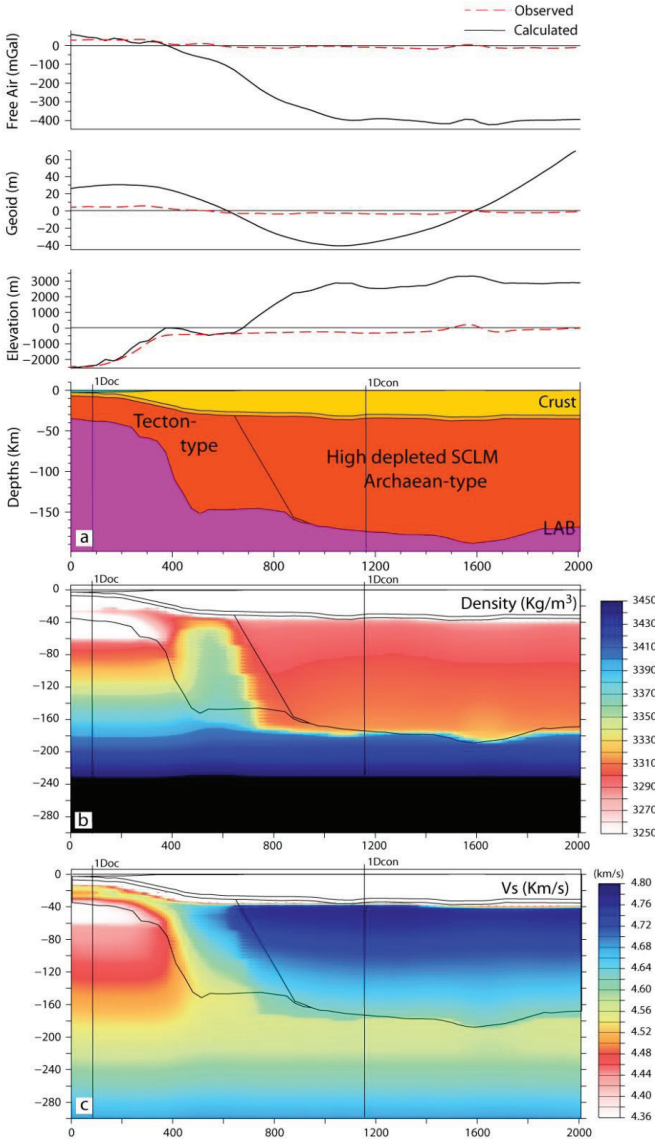


*Figure 6.6. Cross-section at 73˚N of model 2 with laterally varying lithospheric mantle composition from more fertile SOLM to highly depleted SCLM (Archaean-type). Observed and calculated free air anomaly, geoid and elevation, are displayed in the top panels. (a) Model geometry; (b) calculated densities; (c) calculated shear-wave velocities. $1D_{oc}$ and $1D_{con}$ corresponding to the location of the 1D-depth profiles shown in Figure 6.8.*

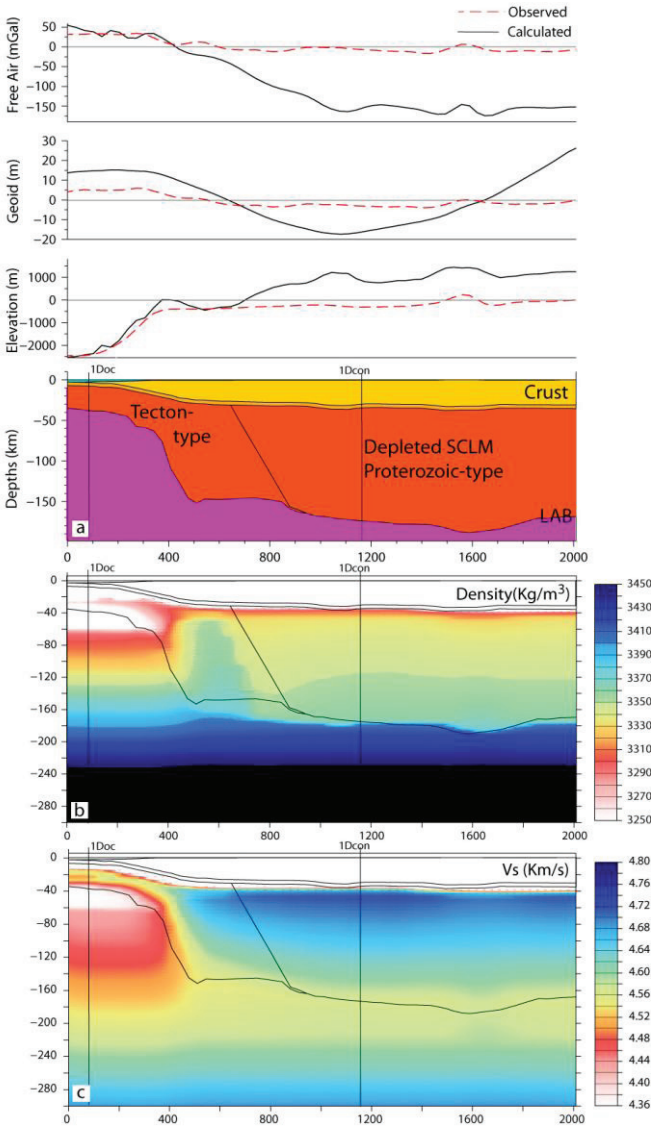


*Figure 6.7. Cross-section at 73˚N of model 3 with laterally varying lithospheric mantle composition from more fertile SOLM to more depleted SCLM (Proterozoic-type). Observed and calculated free air anomaly, geoid and elevation, are displayed in the top panels. (a) Model geometry; (b) calculated densities; (c) calculated shear-wave velocities. $1D_{oc}$ and $1D_{con}$ corresponding to the location of the 1D-depth profiles shown in Figure 6.8.*

The Moho depth geometry is considered to be well constrained and has been kept unchanged, except for small variations at the edges of the modelled area to minimise edge effects that strongly influence the model results, in particular the geoid. The base of the lithosphere has been defined as discussed above (Table 6.1, Fig 6.4a), but locally adjusted to study the thermal influence on the densities, and consequently to fit the gravity field and geoid.

### 6.5.2 Lateral mantle variations: highly depleted case (model 2) and depleted case (model 3)

In the following two models, we differentiate between the sub-oceanic and sub-continental lithospheric mantle to study the influence of depletion on the geophysically observed fields. The geometry of the models as well as the thermophysical parameters remain the same as in the model 1.

The lithospheric mantle of the oceanic domain and under the edge of the margin is represented by the Tecton-type. Under the Barents Sea, both Proterozoic and Archaean basements have been proposed, and we accordingly test two models with these two mantle types. In model 2, the composition of the SCLM under the Barents Sea shelf was defined as highly depleted, Archaean-type mantle (Fig 6.6, Table 6.2); in model 3 a medium depleted, Proterozoic-type mantle was defined (Fig. 6.7, Table 6.2).

We first compare resulting densities and velocities of models 2 and 3 with those of model 1 and with the tomography results. Subsequently we discuss changes of the LAB depth that would be necessary to match the gravity and geoid data for the latter two models.

### 6.5.3 Results of sensitivity tests (models 1, 2 and 3)

The densities of the SOLM are lower than for the SCLM (Figs 6.5c, 6.6b, 6.7b and 6.8) reflecting the higher temperatures created by a shallower LAB. A general decrease of densities with depth can be recognised in the SOLM (from approximately 3270 to 3230 kg/m$^3$). A jump in the density can be observed at 30 km depth in the SOLM corresponding to the plagioclase/spinel phase transition (Fig. 6.8).

In the model 1 an almost linear increase with depth is observed in the SCLM (from around 3320 kg/m$^3$ at the Moho to around 3390 kg/m$^3$ at the LAB) and a jump at 40 km depth in the SCLM is related to the spinel/garnet phase transition (Fig. 6.8).

The use of older and more depleted mantle generally results in lower densities. The decrease is around 70 kg/m$^3$ (2.1 %) in case of the Archaean-type, and around 25 kg/m$^3$ (0.75%) for the Proterozoic-type (Fig. 6.6, 6.7 and 6.8).

Gravity anomalies, geoid undulations and elevation produced by model 1 are in good agreement with the observed fields (Fig. 6.5). The residuals are characterised by short-wavelength which are probably related to crustal sources.

Models 2 and 3 show significant negative gravity, geoid anomalies and high elevation residuals (Fig. 6.6, 6.7). The gravity anomalies generated by the Archaean-type strongly depleted SCLM are around 300 mGal (model 2, Fig. 6.6) and -130 mGal for the medium depleted SCLM (model 3, Fig. 6.7). The geoid

undulations are -40 to -50 m for model 2 (Fig. 6.6) and -10 to -20 m for model 3 (Fig. 6.7), which is significantly different than the values of -4 m to 0 m model 1 (Fig. 6.5). The elevation exceeds 3000 m in model 2 and 1000 m in model 3 (Fig. 6.6 and 6.7).

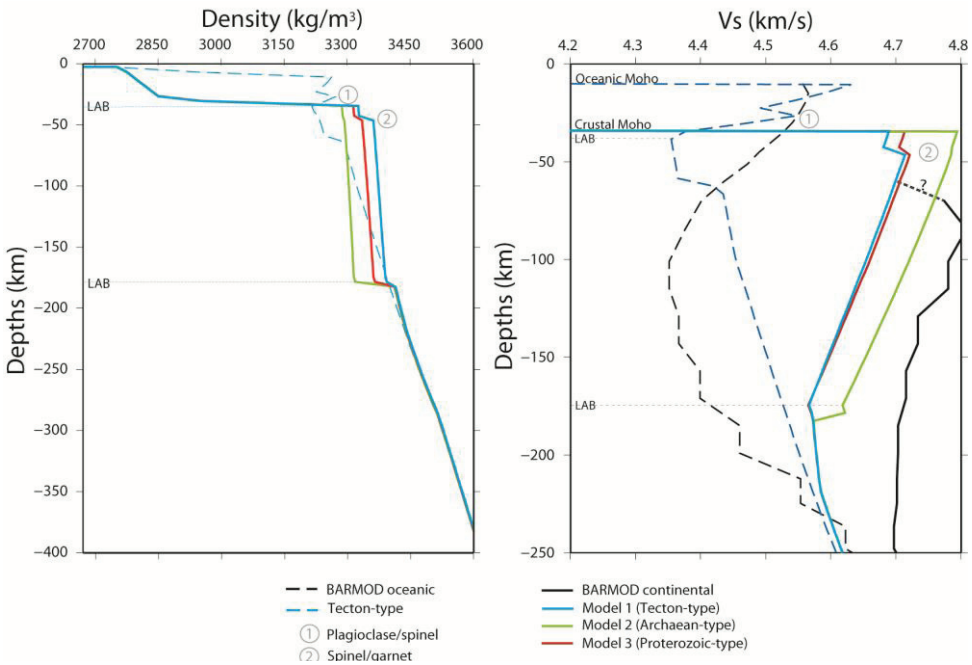


*Figure 6.8. 1D seismic and density profile summarising the model results. BARMOD denotes the tomography results from Levshin et al. (2007.) For the location of the profiles see Figs 6.2, 6.5, 6.6, 6.7.*

To compensate for this deviation, a deeper LAB in the continental shelf is needed, which defines a lower thermal gradient and thus results in higher densities. In models not shown here we estimated the required change. A LAB at 250-300 km depth (almost 100 km deeper than model 1) would be needed to explain the observed gravity and geoid of model 3. The estimated density of the Proterozoic-type SCLM at 175 km depth and at 1300° (LAB location) increases by 40 kg/m$^3$, if cooled by c. 400° (corresponding to a 100 km deeper LAB).

For model 2 (strongly depleted mantle) a reasonable fit to the gravity data cannot be achieved by cooling of the SCLM. A deepening of the LAB of around 100 km creates an increase of the anomaly of only 40 mGal.

The seismic velocity responses of models 1, 2 and 3 are summarised in Fig. 6.5d, 6.6c, 6.7c and 6.8. The velocities in the SOLM are generally decreasing with depth (from around 4.64 to 4.38 km/s) interrupted by a velocity jump owing to the plagioclase/spinel transition at around 30 km depth (Fig 6.8). The shear-wave velocities in the SCLM are higher and dominated by a continuous decrease with depth. The increased depletion in model 2 and 3 leads to higher velocities, in agreement with previous studies (0'Reilly and Griffin, 2006; Lee 2003). In the case of a highly depleted SCLM (model 2) the calculated velocities are around 2.1 %

higher than in model 1 above the spinel/garnet transition zone (increase ≈0,1 km/s), and around 1.5% higher below it (increase ≈0,07 km/s). In model 3 the shear wave velocities above the spinel/garnet transition zone are around 0.4% higher compared to model 1 (increase ≈0.02 km/s), below it the velocities are almost the same (Fig. 6.5d, 6.6c, 6.7c and 6.8).

Comparison of our velocity results with the tomography model for the SOLM shows a similar trend but with a wider velocity range (Fig 6.8). The modelled velocities decrease is around 0.25 km/s instead of the recorded 0.1 km/s. Below the LAB in the upper part of the sub-lithospheric mantle, the discrepancy observed (Fig 6.8) is attributed to modelling artefacts produced by the definition of the buffering layer (Fullea et al. 2009).

The model results for the continental domain shows no increase of velocities with depth as observed in the tomography model (Fig 6.8). The seismic velocities in model 1 are more than 0.1 km/s lower than in the tomography model. This difference is larger than it can be accounted for by an increase in LAB depth, which has been tested for.

The range of seismic velocities in model 2 using a strongly depleted mantle (4.75 – 4.8 km/s) is close to the observed high velocities anomaly (Fig 6.2, 6.6c and 6.8). Instead, the velocities of a medium depleted mantle (model 3) are again much lower than those observed (Fig. 6.2, 6.7c, 6.8). If the thermal structure of the Proterozoic composition is changed to match the potential fields (LAB around 100 km deeper than model 1) the resulting seismic velocities increase by only 0.04%, which is too small to approach the observed velocities. Besides the mismatch in velocity range, the shape of the imaged high-velocity anomaly under the East Barents Basin is not reproduced by our model (comparison Fig. 6.2b, 6.5d, 6.6c and 6.7c).

## Summary of sensitivity test

The results of model 1 show that the low-velocity anomaly under the western Barents Sea can be explained without compositional variations by a seaward LAB rise resulting in a high thermal gradient. The high-velocity anomaly in the continental domain, however, cannot be explained by changes in LAB depth (and related temperature changes) alone, but additional compositional changes are required.

Model 2 demonstrates the difficulty to satisfy gravity field, geoid and elevation using extremely depleted mantle. Nevertheless, the seismic response is closer to the observed seismic velocities. The difficulty of fitting the observed gravity and geoid above a highly buoyant and depleted mantle has been encountered in many previous works (e.g. Mooney and Vidale, 2003, Afonso et al. 2008).

Petrophysical studies show that the uppermost SCLM is commonly more depleted than its lower parts, and that the SCLM generally becomes more fertile with depth (e.g. Artemieva et al. 2002; Artemieva and Mooney 2002; O'Reilly and Griffin 2006). King (2005) proposed a model for cratons that attempts to reconcile petrological and geophysical evidence by composing the SCLM of two layers: an upper, buoyant SCLM characterized by being highly depleted with respect to primitive mantle; a lower, more fertile SCLM. Such models should be in agreement with both petrological and geophysical evidence but have so far been poorly

investigated (Afonso et al. 2008). We study the cases of a layered SCLM in the following models.

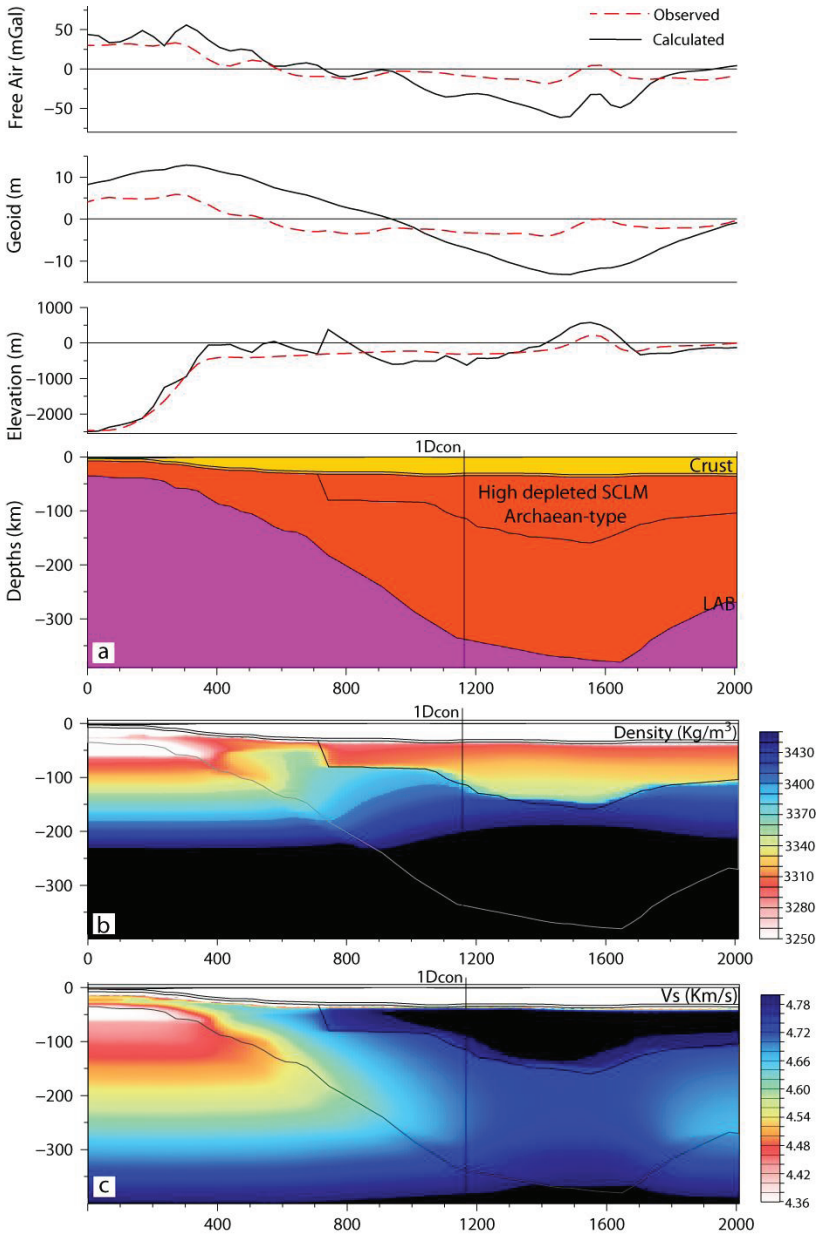


*Figure 6.9. Cross-section at 73˚N of model 4 with laterally and vertical varying lithospheric mantle composition from high depleted upper SCLM (Archaean-type) to fertile SOLM and lower SCLM. Observed and calculated free air anomaly, geoid and elevation, are displayed in the top panels. (a) Model geometry; (b) calculated densities; (c) calculated shear-wave velocities. $1D_{oc}$ and $1D_{con}$ corresponding to the location of the 1D-depth profiles shown in Figure 6.12.*

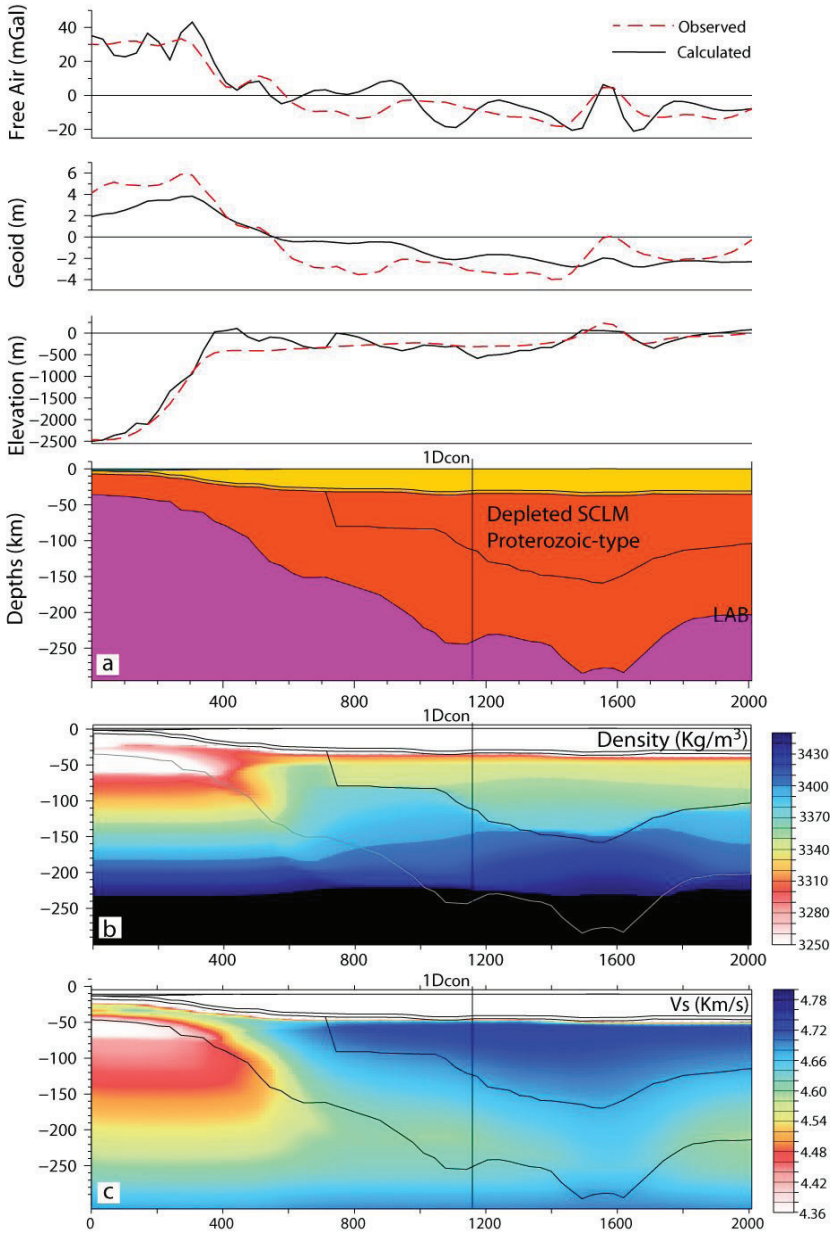


*Figure 6.10. Cross-section at 73˚N of model 5 with laterally and vertical varying lithospheric mantle composition from depleted upper SCLM (Proterozoic-type) to fertile SOLM and lower SCLM. Observed and calculated free air anomaly, geoid and elevation, are displayed in the top panels. (a) Model geometry; (b) calculated densities; (c) calculated shear-wave velocities. $1D_{oc}$ and $1D_{con}$ corresponding to the location of the 1D-depth profiles shown in Figure 6.12.*

## 6.6 Vertical layering in the SCLM

Improved models have been defined by implementing an additional vertical layering in the SCLM. Besides the lateral lithospheric mantle variations between SOLM and SCLM, a vertical change from a more depleted upper SCLM layer to a less depleted lower SCLM has been defined. Depending on the degree of depletion and on the fertilization, the contrast in density and seismic velocity between the upper and the lower SCLM changes. The lithospheric mantle of the oceanic domain and of the lower SCLM has been defined using a fertile mantle composition (Tecton-type). The depleted upper part of the SCLM has been defined either as strongly depleted Archaean-type (model 4, Fig. 6.9) or moderately depleted Proterozoic-type (model 5, Fig. 6.10).

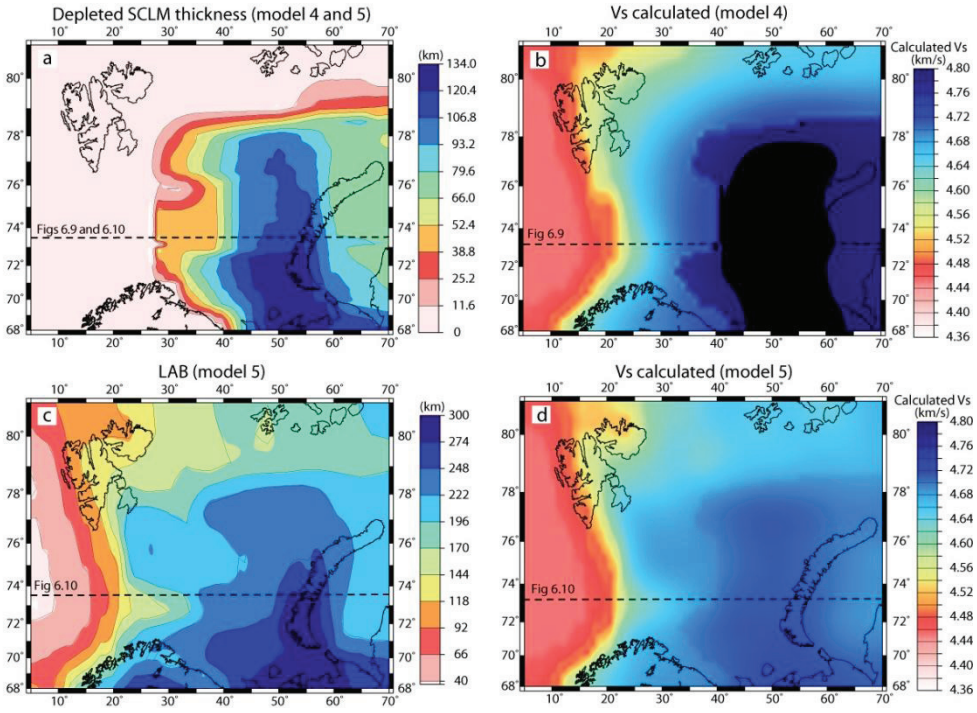


*Figure 6.11. Input and results of model 4 and 5. (a) Thickness of the upper, more depleted SCLM as defined from the tomographic velocity anomaly. (b) Seismic velocity distribution of model 4 (Archaean-type upper SCLM) at 100km depth. For comparison with tomographic results see Fig 6.2a. Corresponding LAB depth of model 4 is not shown because of unreasonable depth values. (c) LAB depth of model 5 (Proterozoic-type upper SCLM) that provides the best fit for observed gravity fields and elevation. For comparison with original LAB depth see Fig. 6.4a. (d) Seismic velocity distribution of model 5 at 100 km depth. For comparison with tomographic results see Fig 6.2c.*

The geometry of the upper SCLM was chosen to mimic the shape of the high velocity anomaly (Fig. 6.2 and 6.11a). The tomographic model is additionally used for comparison of the velocity fields. The depth and geometry of the LAB have been adjusted to fit gravity anomalies, geoid undulations and elevation.

### 6.6.1 Results of Model 4 (Archaean and Tecton SCLM)

Model 4, unlike all other models, shows overall velocity trends and values close to those in the tomography model. However, the adjustment of the LAB to fit the observed data produces results that exceed the range of reasonable depths.

The estimated densities in the model 4 show an increase with depth, with values in the upper part similar to those of the Archaean-type mantle of model 2. In the lower SCLM, significantly higher densities (20-40 kg/m$^3$) than in the Tecton-type mantle of model 1 are found (Fig. 6.9b and 6.12). This last effect is attributed to the thermal contribution as the adjustment for the potential field data requires a deep LAB resulting in a cold and dense lithosphere. The density jump at the transition from the upper depleted to the lower fertile SCLM is approximately 100 kg/m$^3$ (Fig. 6.9b and 6.12).

The upper SCLM is strongly buoyant and produces a negative gravity anomaly and geoid undulation. The presence of a more fertile and denser lower SCLM partly compensates the effect of the Archaean composition, but a good fit of gravity, geoid and elevation remain difficult to achieve, even if the LAB has been deepened to the maximum possible model depth (400 km, Fig. 6.9). LAB deeper than 380 km is out of the proposed depth range by Poudjom Djomani et al. (2001), and leads to a density increase that is still not sufficient to fit the observed anomalies. Remaining residuals are on the order of 60 mGal for the free air gravity anomaly, of 20 m for the geoid undulations and about 500 m for the elevation (Fig 6.9).

The low lithospheric temperatures produced by the deep LAB lead to much higher seismic velocities than in previous models (Fig. 6.5d, 6.6c, 6.9c and 6.12). The transition from the upper depleted to the fertilized SCLM is reflected in an abrupt decrease of velocity around 0.08 km/s (Fig. 6.9c and 6.12).

At about 70-80 km depth, the calculated velocities are within the range of those of the tomographic model. At shallower depth, the tomographic model is not well resolved but indicates lower velocities. The calculated velocities, however, are even higher here with highest values (>4.8 km/s) just below the Moho (Fig. 6.2, 6.9c and 6.12). The velocity decrease at 80-100 km depth is abrupt in the model (owing to the sharp boundary between upper and lower SCLM) but much more gradual in the tomographic data. In nature a compositional transition from upper, depleted SCLM to lower, fertile SCLM is generally gradual (e.g. Reilly and Griffin, 2006) but could not be modelled as such with the software used in this study. Yet, such a gradual transition from Archaean-type to Tecton-type SCLM will produce a velocity pattern closer to the one observed (Fig. 6.12).

A horizontal slice (100 km) of the calculated velocity distribution is displayed in Fig. 6.11b. The shape of the modelled velocity anomaly is resulting similar to the shape of the observed tomographic anomaly (Fig. 6.2c and 6.11b).

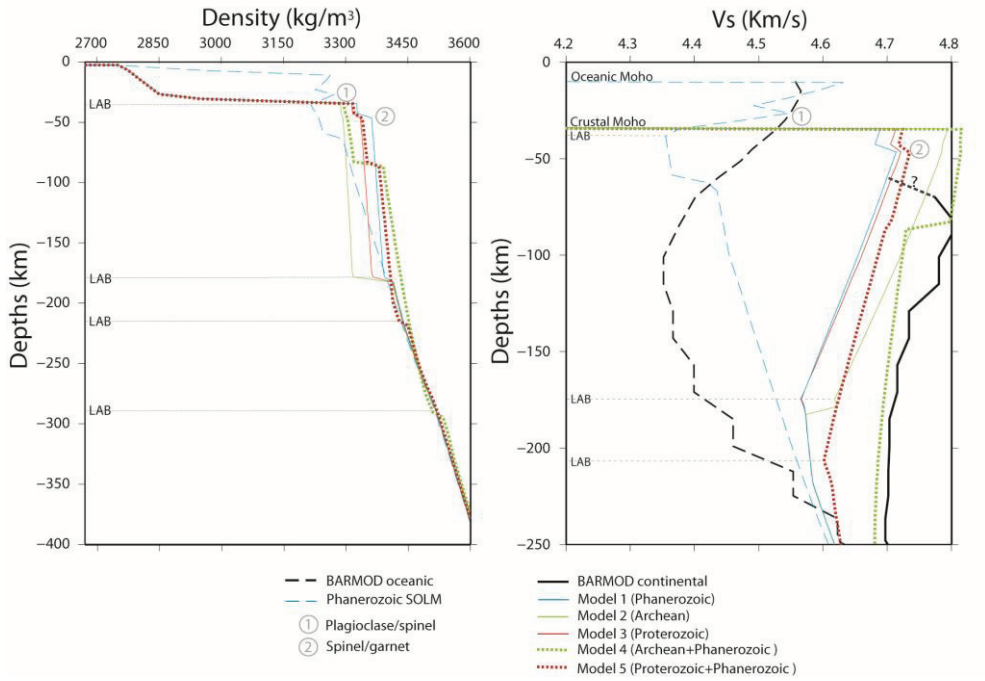


*Figure 6.12. 1D density and seismic profiles summarising the results of models 4 and 5. Results of models 1-3 shown in Figure 6.8 are depicted in light gray.*

### 6.6.2 Results of Model 5 (Proterozoic and Tecton SCLM)

Similar to model 4, the lower densities of the depleted upper SCLM need to be compensated by a thicker, hence colder, lithosphere and accordingly higher densities in the lower SCLM. The final LAB depth for model 5 is c. 130-190 km in the continental regions close to the margin and c. 190-290 in the southeast Barents Sea (Fig. 6.10 and 6.11c).

The final density structure is similar to model 3 (Proterozoic-type SCLM only) for the upper SCLM, and similar to model 1 (Tecton-type SCLM only) in the lower lithospheric mantle (Fig. 6.5c, 6.7b, 6.10b and 6.12). Slightly larger densities in model 5 (5-10 kg/m$^3$) are related to the thermal effect produced by the deeper location of LAB. The density contrast between upper and lower SCLM is calculated to be approx. 40 kg/m$^3$.

The fit of gravity anomaly, geoid and elevation is satisfying (Fig. 6.10) for model 5. The gravity residuals are generally smaller than 15 mGal and have wavelengths of less than 200 km. Geoid undulation residuals are generally around 2 m and elevation residuals less than 250 m (Fig 6.10).

The final velocity distribution in the SCLM shows a nearly linear decrease with depth (Fig. 6.10 and 6.12). The transition from the upper to the lower SCLM shows a small decrease in velocities of around 0.01 km/s. The SCLM in this model is faster than in model 3, which is mainly a consequence of the lower LAB and hence lower geothermal gradient. Compared with the tomography model, the calculated seismic velocities below 80 km depth have a similar trend but an offset

of about 0.8 km/s. The tomography velocity vertical increase above 80 km depth cannot be reproduced from our model, while the lateral velocity increase under the East Barents Sea is approximately simulated (Fig. 6.2a, 6.2b, 6.10 and 6.11d).

## 6.7 Discussion

### 6.7.1 Model response

Table 6.4 summarises the main results for the models presented above. Model 1 and 3 give a good representation of the gravity field, geoid and elevation, but fail to explain the seismic anomaly in the East Barents Sea. The first three models are used to test the model sensitivity regarding the LAB depth, potential fields and seismic velocity. Model 4 and 5 use one less degree of freedom since the geometry of the depleted mantle is forced to mimic the shape of the shear wave anomaly.

The absolute velocities of the tomography model are only reproduced by the models with an extremely depleted, Archean-type composition (model 2 and 4), but these fail to reproduce the geoid, gravity field and elevation with reasonable changes of the geometry of the lithosphere.

Only model 5 is able to create a high velocity anomaly in the mantle that has a shape similar to the tomography and simultaneously satisfy the observed geoid, gravity field and elevation.

| MODEL DESIGN | | | MODEL RESPONSE | | | | |
|---|---|---|---|---|---|---|---|
| | | | Free air gravity fit | Geoid fit | Elevation fit | Seismic anomaly range fit | Seismic anomaly shape fit |
| Model | SOLM | SCLM | | | | | |
| 1 | Tecton | Tecton | ***Yes*** | ***Yes*** | ***Yes*** | ***No*** | ***No*** |
| 2 | Tecton | Archaean | ***No*** | ***No*** | ***No*** | ***Yes*** | ***No*** |
| 3 | Tecton | Proterozoic | ***Yes*** | ***Yes*** | ***Yes*** | ***No*** | ***No*** |
| 4 | Tecton | Archaean<br>Tecton | ***No*** | ***No*** | ***No*** | ***Yes*** | ***Yes*** |
| 5 | Tecton | Proterozoic<br>Tecton | ***Yes*** | ***Yes*** | ***Yes*** | ***No*** | ***Yes*** |

*Table 6.4: Summary of the main model results.*

### 6.7.2 Implications of density results

Our models show that the density of the SCLM is increasing with depth below 50 km. The compositional heterogeneity due to depletion produces a density variation comparable with thermal induced density variations, as already described by Forte and Parry (2000). A more depleted SCLM leads to a density decrease of ~0.75% for the Proterozoic-type and ~2.1 % for the Archaean-type. These results are in good agreement with average densities summarised in Artemieva (2011; her Table 6.4).

Such low mantle densities can be expected to be reflected as lows in the gravity field and in particular in the geoid. However, such lows are not generally

observed over areas where depleted mantle is expected (Artemieva, 2011 and reference therein). Similarly, no geoid or gravity highs can be directly correlated to the Precambrian cratons, where the lithosphere is expected to be cooler than the younger continental or oceanic lithosphere (e.g. Kaban et al. 2003).

Jordan (1978, 1981, 1988) postulated that the temperature and compositional effects balance each other, so that the density increase caused by lower temperatures is compensated by a density decrease due to a compositional change to more depleted mantle (indicated by a linear relationship with Mg). This idea is the base for the later developed isopycnic hypothesis which validity is still debated (Artemieva et al. 2011).

Our results show that the isopycnic theory of Jordan (1978, 1981, 1988) cannot be satisfied for the case of Archaean-type SCLM. The high degree of depletion generates a very buoyant SCLM, which cannot be compensated by a decrease of temperature. Though, for less depleted mantle the mechanism may work, such as for the Proterozoic-type SCLM of models 2 and 5.

Furthermore, the calculated model densities show an increase at around 45 km depth under the Barents Sea shelf. This density jump corresponds to the spinel-garnet phase transition (Fig. 6.8 and 6.12) and it is larger for a more fertile mantle composition (~+40 kg/m$^3$ in model 1), moderate for a medium depleted mantle (~+25 kg/m$^3$, model 3 and 5) and small for highly depleted mantle (+10 kg/m$^3$, model 2 and 4).

### 6.7.3 Velocity-depth trends and high velocity anomaly

Directly beneath the Moho boundary to ~80 km depth, the modelled velocities are very high and decrease with depth, whereas the seismic tomography suggest lower shallow velocities, increasing with depth. The discrepancy could be attributed to the low accuracy of seismic tomography close to the Moho. The resolution of the tomography is here strongly reduced and the true velocity trends are not clear (e.g. Lebedev et al. 2009 and references therein). Lebedev et al. (2009) prefers an increase of shear-wave velocity between the Moho and 100-150 km, arguing that this is largely due to the transition from spinel-peridotite to garnet-peridotite.

Alternatively, the discrepancy could be attributed to the inaccuracy of the calculated model velocities, which are the effect of the mineralogical organization of just 5 elements (CFMAS, Afonso et al. 2008). At around 40 km depth the spinel-garnet transition occurs and produces a jump towards higher velocities (Fig. 6.8 and 6.12). This change is influenced by the CFMAS system; it is smoother for a more depleted SCLM. Other studies show that the phase transition is strongly affected by others elements not considered in the CFMAS model. Klemme (2004) showed that the addition of chromium would not only shift the phase transition to higher pressures (greater depths) but also make it spread over a broader depth interval. High Cr/(Cr+Al) values in samples from kimberlites also imply that the spinel peridotite–garnet peridotite transformation beneath cratons may occur over a broad depth interval, with spinel and garnet co-existing down to below 100 km (Klemme, 2004; Grütter et al. 2006). This additional effect, if included in our model, would produce results closer to the tomographic velocities, and could be a reasonable explanation for the discrepancies found in the first 80 km. Below 80 km

depth the vertical velocity changes are similar between the model and the seismic tomography (Fig. 6.2, 6.6, 6.9, 6.10 and 6.11b).

High-velocity anomalies as observed beneath the East Barents Sea are generally interpreted as either thick, cold cratonic lithosphere or as cold, sinking lithospheric slabs (e.g. Artemieva 2002). The interpretation of a cold sinking slab has already been rejected for the Barents Sea, because the last major tectonic activity happened 240 Ma ago, and a slab would be thermally equilibrated since then (e.g. Levshin et al. 2007). Levshin et al. (2007) support the idea that the high mantle velocities are the result of compositional variations related to the subduction of lithosphere during the Caledonian orogeny. This interpretation is based on the observation that the western boundary of the anomaly correlates with the Caledonian suture outlined by Breivik et al. (2002). The eastern part of the anomaly beneath the East Barents Basin is interpreted to originate from the Uralian collision. A different interpretation has been proposed by Faleide et al. (2006), who explain the anomaly as a continuous remnant of subducted lithosphere related to a late Neoproterozoic Timanian event at the eastern margin of the East European Craton. This idea is based on apparent correlation between the shape of the velocity anomaly and the outline of Timanian deformation.

The relation of the high seismic anomaly with a subduction zone is doubtful. The compositional imprint of an older and thermally re-equilibrated subduction zone is not well documented (Artemieva et al 2011). Compositional variations of the SCLM in a possible suture are inferred from petrophysical studies on Siberian kimberlites (Griffin et al. 1999b). These authors suggest that the mixing zone between Precambrian mantles would probably be less than 100 km wide; significantly smaller than our more than 500 km wide anomaly.

Most likely, the high velocity anomaly relates to cold, cratonic lithosphere. Ritzmann et al. (2009) already relate the observed high velocities to the cold thermal structure of a continental root. The suggested root below the Barents Sea-Kara Sea region was proposed to belong to the surrounding cratonic provinces (the Baltic Shield and the Siberian Craton). Our model results agree with this interpretation but at the same time show that very low temperatures, corresponding to a thick lithosphere, are not sufficient to reproduce the shape and amplitudes of the observed velocity anomaly. Our models nevertheless suggest that the portion of mantle that produces the anomaly is made of a more depleted mantle material. The degree of depletion is mostly related to the iron content (Artemieva 2011). Geodynamic studies on the variation of iron content in the SCLM show that the resulting effects on the seismic velocities either produce a velocity maximum at c. 150 km depth or a gradual velocity decrease from the Moho to the transition zone (Forte and Perry 2000). The Barents Sea is probably an example of the first case. We propose that the upper part of the lithospheric mantle is depleted in iron and the degree of depletion has is maximum at around 80-100 km, where the higher velocities are observed (Fig 6.2).

To estimate the degree of depletion and its relation with age from our models would be too speculative, but it would probably represent a type in between the Archaean- and Proterozoic-type. Our models suggest that the Archaean-type may be too depleted in iron and too buoyant, while a Proterozoic-type is not depleted enough to produce the amplitude of the observed shear wave velocities.

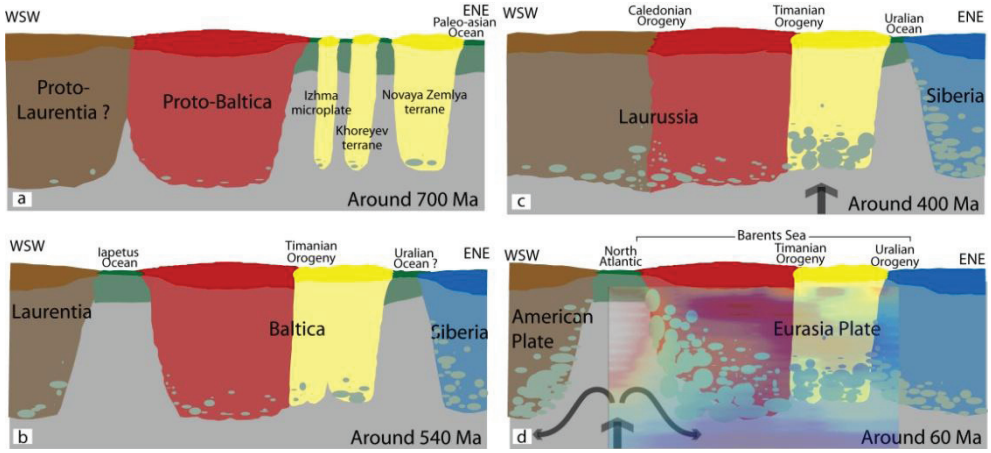


*Fig 6.13. Cartoon representing the proposed lithospheric evolution of the northeastern margin of the Fennoscandian Shield. Drawings are not to scale. (a) Tonian times scenario (800-600 Ma) showing the different lithospheric blocks involved in the lithospheric evolution of Baltica (modified after Olovyanishnikov et al. 2002); (b) Results of telescoping and accreting of diverse lithospheric blocks against the Baltica margin in late Ediacaran time (635-542 Ma), immediately following the Timanian orogenic event (Modified after Roberts and Siedlecka 2002). (c) Devonian setting showing the Laurussian plate, which formed by continent-continent collision between Baltica and Laurentia in the Silurian, generating the Caledonian mountains that propagate into the west Barents Sea. During Mid-Late Devonian the eastern part of the Laurussia plate (southeast Barents Basin/Timanian Pechora Basin) was dominated by rifting (e.g. O'Leary et al. 2004; Stephenson et al. 2006). Here the black arrow indicates the rising of hot asthenospheric material, resulting in metasomatism of the lithospheric root and/or its replacement by younger, more fertile mantle. The interaction between lithospheric and sublithospheric mantle is represented by the small grey blobs. (d) Cenozoic setting in which Laurussia and Siberia have collided in the east, generating the Uralian orogeny (today part of the Eurasian plate). In the west the North Atlantic opens, the rising of hot astenosphere creates crustal magmatism and metasomatism at the base of the lithosphere, followed by erosion of the craton's margin (Atemieva et al. 2002). Black arrows indicate the sublithospheric flow. The tomographic velocities are overlain (See figure 6.2b for description and comparison) and show the proposed correlation between the high velocity anomaly and the portion of the Precambrian SCLM not involved in the re-fertilization processes.*

### 6.7.4 LAB estimation

Our LAB geometry reflects the differences between the SOLM and the SCLM by shallower depth below the continental margin and in the oceanic domain (30-100 km) and greater depth under the shelf. The LAB in all five models had to be relatively deep to explain the gravity field and geoid. A relation between lithospheric thickness and age has been made based on thermal lithospheric structure and clearly distinguishes the Early Proterozoic from medium-late Proterozoic SCLM (Artemieva and Money 2001). Accordingly, model 5 with an LAB at 250 km depth could indicate a SCLM age closer to Palaeo-Proterozoic age. This is consistent with previous studies (Artemieva et al. 2006 and references therein) that indicate a lithospheric thickness of 250 - 300 km beneath the Archaean–early Proterozoic part of the Baltic Shield and its likely extension farther north into the Barents Sea.

### 6.7.5 Proposed lithospheric evolution of the Barents Sea

We propose that the highly depleted SCLM under the East Barents Sea shelf corresponds to the relict lithosphere of one or more old microplates, probably accreted to the Baltica margin during the Timanian orogeny. The age of this relict lithosphere is proposed to be Palaeo-Proterozoic.

In general, deeper lithosphere has a more fertile composition. The most simple and common process that explains a transition from an upper depleted SCLM to a lower, more fertile SCLM is metasomatism. This process changes the composition by enriching the lower SCLM in incompatible elements, leading to a decrease in Mg and an increase in Al, Cl, creating a rock with higher densities and lower seismic velocities (Artemieva, 2011). Artemieva et al. (2002) point out two major processes that cause strong interaction between lithosphere and sublithospheric mantle. The first is the rising of hot sublithosphere during the active phase of continental rifting. The second is related to plate motion and basal drag generated by mantle convection.

The geodynamic evolution of the Barents Sea is dominated by several compressive and extensional phases, which likely created alternating phases of plates accretion and re-fertilization by metasomatism. We discuss here the tectonothermal history of the region and summarize our interpretations in Fig. 6.13.

The Mesoproterozic Barents Sea region comprised a mosaic of microplates (Olovyanishnikov et al, 2000; Cocks and Torsvik, 2005; Kostyuchenko et al. 2006) (Fig. 6.13a). During the Edicarian (around 635-542 Ma), a compressive system occurred, leading to the Timanian orogeny and to the accretion of different blocks against Paleo-Baltica. This larger plate is later called Baltica and separated sometime between 570 and 550 Ma from Laurentia (Cocks and Torsvik, 2005) (Fig. 6.13b). During Late Ordovician-Silurian (440-410 Ma) another compressive phase led to the closure of the Iapetus Ocean at the western margin of Baltica and subsequent continental collision with Laurentia, creating the Caledonian orogen (Roberts and Gale 1978, Torsvik et al. 1996; Gee at al. 2006) (Fig. 6.13c). During the Mid-Late Devonian to Early Carboniferous (400 – 320 Ma) the northeastern margin of the Baltica craton, including the Timanian Pechora Basin, was subject to rifting. The underlying lithosphere must have been weak during this phase (and

perhaps even prior to it) as evidenced by the location of rifting and accompanying magmatism. The propagation of the rifting farther north under the East Barents Basin is not well known (Johansen et al. 1992; Olovyanishnikov et al. 2000; O'Leary et al. 2004; Stephenson et al. 2006), though the crust in this region is overall thinned (Ivanova et al. 2006, 2011; Marello et al. 2010, 2012). Controversial opinions exist about the crustal composition under the East Barents Sea Basin, in particular regarding the existence of an ancient oceanic crust (e.g. Artyushkov, 2005; Apolonov, 1996; Ivanova et al 2006, 2001). The existence of a Precambrian SCLM underlain by re-fertilized SCLM, as proposed here for explaining the high velocity anomaly, would be supportive evidence of this early-Paleozoic rifting. We propose that the Devonian rifting thinned the crust and created a Paleozoic basin, which is probably the precursor of the actual Barents Basin. It furthermore produced local magmatism as evidenced in the Pechora Basin. These processes have been accompanied by metasomatism and reworking of the deep lithosphere, creating the re-fertilized lower portion of the SCLM under the Barents Sea Basin (Fig. 6.13c).

During the Late Carboniferous, the tectonic regime in the East Barents Sea changed to a compressive setting related to the closure of the Uralian Ocean caused by its eastward subduction under the Siberian craton and the subsequent collision between Laurussia (Baltica and Laurentia) with western Siberia (e.g. Puchkov, 1997; Cocks and Torsvik, 2005) (Fig. 6.13d).

Late Paleozoic and Mesozoic rifting mostly affected the western Barents Sea and culminated in the opening of the North Atlantic. This large scale magmatic event is considered responsible for significant structural and compositional modification of the base of the lithospheric mantle. Griffin et al. (2005) argue based on petrological data that large-scale magmatic events can influence the SCLM up to several hundred kilometres away from the main magmatic centre. We suggest that the North Atlantic opening created re-fertilization and heating of the lithosphere for large parts of the Barents Sea. Close to the margin, the SCLM is strongly reflecting the interaction with the sublithosphere. The lower SCLM below 100-150 km has been metasomatized and partly removed by thermal erosion and/or by delamination of a dense lowermost lithosphere, which coincides in our models with a rise of the LAB. Farther away from the margin, the degree of interaction between SCLM and sublithosphere decreases. The 1300˚ isotherm does not deflect and the SCLM is not eroded chemically or mechanically. In this region the rifting creates re-fertilized SCLM characterised by higher densities, lower seismic velocities and a southeast dipping structure that reflects the boundary between the relict depleted mantle and the re-fertilised SCLM. This chemical change coincides with the dipping structure imaged by the seismic tomography (Fig. 6.13d).

In the northern part of the Barents Sea, the high velocity anomaly ends quite far from the continental shelf margin (~800 km) and the lithospheric thickness is decreasing (Fig. 6.2c and 6.11c). The observed transition toward higher velocities is proposed to be the result of magmatic-related mechanism that creates interaction between the SCLM and the sublithospheric mantle. The northern margin of the Barents Sea has been strongly affected by the formation of the Lomonosov Ridge (e.g. Minakov et al, 2012). This event is proposed to be responsible for the changes

in the SCLM toward more fertile composition and for destruction and replacement of the older lithosphere creating a thinner SCLM characterised by low velocities.

An additional melt-related lithosphere-sublithosphere interaction can be linked to the intensive magmatic activity occurred at the Cretaceous time in the northwest Barents Sea, interpreted by Maher (2001) as part of a Large Igneous Provence. The magmatic activity involved in particular the region between East Svalbard and Franz Josef Land, where slow shear wave velocities and thinned lithosphere are seen (Fig. 6.2a, 6.2c and 6.11c). The event is proposed to have strongly contributed to the reworking of the SCLM, causing large thermal and compositional destruction of the old SCLM and its replacement with new fertile and thinner SCLM. We propose that the observed slow velocities are caused by this fertile SCLM (Fig. 6.2).

## 6.8 Conclusions

This work presents a first integrated study of the lithospheric mantle in the Barents Sea region. The results presented here combine for the first time the velocity and density structure of the lithosphere with the geodynamic evolution of the Barents Sea region.

Different types of SCLM composition, reflecting different tectonic ages, have been used in the models and their influence on densities and velocities have been estimated. The compositional change from a young, poorly depleted mantle to an old, strongly depleted mantle can produce a density decrease of 2.1% and a velocity increase of 2.1%.

The transition from continental to oceanic mantle can be in a first approximation explained by a homogeneous mantle composition where density and velocity changes are primarily the effect of temperature variations, here evoked by changes in the lithospheric thickness.

However, the SCLM under the Barents Sea shows velocity anomalies that cannot be explained by a thermal effect alone but require a change in mantle composition. We relate the high-velocity anomaly under the East Barents Sea to the existence of a Palaeoproterozoic, depleted lithosphere. This old SCLM is proposed to be a portion of the Baltica plate formed by the accretion and aggregation of microplates during the Timanian event. Additionally, we suggest that there must be a vertical gradient in SCLM composition, here simplified by two layers: a more depleted upper SCLM overlying a more fertile lower SCLM. The latter is proposed to be the reworked portion of the old Baltica lithosphere that has been affected by the thermal anomaly related to the Devonian rifting. The induced metasomatic interaction between the old SCLM and the sublithospheric mantle produced a compositional change leading to a decrease in the magnesium content and an increase in incompatible elements.

The continental break-up and opening of the North Atlantic event generated a thermal, chemical and mechanical modification in the southwester Barents Sea SCLM. Today's observed SCLM is characterized by a LAB rising toward the margin and southeast dipping lower mantle anomaly with higher densities and lower seismic velocities consisting in the chemically re-fertilized SCLM.

In the northern part of the Barents Sea the thinner lithosphere and the slower velocities have been attributed to reworking of the SCLM due to magmatic event related with Large Igneous Provinces or with the evolution of the Amerasian Basin.

## *Acknowledgments*

*This study is part of the PETROBAR project (Petroleum-related regional studies of the Barents Sea region) funded by Statoil and the PETROMAKS programme of the Research Council of Norway. We particularly thank Bernard Steinberger and Joya Tetreault for helping with the understanding of tomography model. We are thankful to Javier Fullea for the LitMod3D support and to David Roberts and Laurent Gernigon for sharing their geological knowledge of the Barents Sea.*

# Chapter 7

# Concluding Remarks

The Barents Sea shelf is characterised by heterogeneous crust and structures resulting from the aggregation of different terranes during the Timanian, Caledonian and Uralian events. The models developed in this thesis allow defining the lithospheric properties and structures and to interpret them in the context of the geological history of the Barents Sea.

The integrated study applied in this work and the development of a large numbers of models that reflect different scenarios have been proven to be an efficient tool to understand the structures buried under thick sedimentary cover.

Inverse magnetic models represent a rapid approach and can provide a first indication of the magnetic crustal properties of the entire Barents Sea. The successive development of forward models, which integrate different geophysical data sets, refines and validates the inversion results. 3D forward modelling that simultaneously satisfies gravity and magnetic data, as well as local constraints, is an efficient way to test and/or extrapolate local information towards less studied areas. Such combined models resolve both the sediment/basement transition and provide structural and petrophysical informations about the crust and properties of the entire Barents Sea region. This permits to identify different crustal domains that are characterised by a similar geological evolution and to propose a new interpretation for the crustal terranes extension into the shelf.

The integration of crustal studies with a better understanding of the lithospheric mantle provides crucial information not only on the tectonic history, but also on how crust and upper lithosphere interact. Studying the lithospheric mantle provides

an explanation of geophysical anomalies in terms of their geodynamic evolution and confirms the existence of old cratons, the imprints of rifting and of larger magmatic events. In this thesis I interpret how the geodynamic evolution of the Barents Sea left its imprint in the lithosphere.

The Southwestern Barents Sea is dominated by high magnetic crust composed of Precambrian basement, covered by Caledonian terranes. The crustal setting is dominated by structural highs and a large number of basins as the result of different rifting phases. Evidence of these extensional events has been recorded also in the lithospheric mantle under the Southwestern Barents Sea, resulting in a thinned and fertile mantle.

The distinct low magnetic properties and structural setting of the Northwestern Barents Sea crust support the existence of a distinct microcrustal block (Barentsia Craton) attached to the rest of the Barents Sea during the Caledonian event. The lithospheric mantle model shows under the proposed block a subcontinental lithospheric mantle dominated by a composition and thermal setting typical of young lithosphere. This observation has been interpreted as a consequence of the magmatic events (part of a large igneous province ?) that involved the area.

A Timanian domain is proposed in the Southeastern Barents Sea from magnetic field analysis and inversion modelling. Its outline had been further refined by 3D forward modelling. The crustal units defined are dominated by high densities and an alternation of magnetic and non-magnetic NW oriented blocks. Those units are inferred to be the extension of the Timan-Pechora basement domains. Beneath the area lies a thick two-layered lithospheric mantle. The shallower layer is dominated by a depleted composition and has been interpreted as the relict of the Paleoproterozoic microplate/s accreted to proto-Baltica during the Timanian. The deeper SCLM layer is interpreted as a fertile mantle originated by lithosphere/sublithosphere interactions proposed to occur in Mid-Late Devonian.

The easternmost Barents Sea is dominated by Uralian terranes which extend mimicking the arc shape of Novaya Zemlya. A high magnetic terrane has been related to the Pre-Uralian onshore terrane and is proposed to contain rocks derived from the Uralian Ocean. The crustal setting resulting from this thesis shows crust thinning and asymmetric top basement. These geometries have been linked with the evolution of the Eastern Barents Basin, combining rifting basin evolution in a first phase (Mid-Late Devonian ?) and foreland basin development in a later stage (Permian-Jurassic).

My results support the bifurcated extension of the Caledonian into the western Barents Sea. The first branch is located on the west of Loppa High and is extending northwards to Svalbard. The second branch is suggested to run from north of the Bjarmeland Platform in the proximity to the Sentralbanken High and to propagate northwards between Svalbard and Franz Josef Land. This second is proposed to represent the old margin between Baltica and Barentsia.

The existence of the thick lithospheric block accreted on Baltica during the Timanian seems to control the later propagation of Caledonian and Uralian terranes. The presence of Barentsia and of the extension of Baltica with this aggregated Paleoproterozoic unit sets a new geodynamic context for the Barents Sea which needs to be further studied in the future.

Numerical models and plate reconstructions have been used previously to constrain horizontal movements in the Barents Sea, but focussing on the implications for the crustal structure in 2D (Buiter and Torsvik 2007). The enigmatic evolution of the Barents Sea requires 3D dynamic models to verify the link between the stable present-day proposed lithospheric structure and the geological evolution. As yet, such models are computational expensive and it will be a challenge to reconstruct the architecture and properties through time.

On a different scale, the results of this thesis provide valuable inputs for geothermal and basin modelling. The lithospheric results provide the background lithospheric temperature, while the results of the crustal studies allow distributing crustal properties in relation to geological formation. From this one can calculate the present day heat flow into the sedimentary basins and verify against surface heat-flow data or vitrinite reflectance.

In conclusion it is in my hope that the regional models I have developed will provide a useful framework for future focused studies and that will be farther updated with these latest results.

# Appendix

# Magnetic expression of salt diapir-related structures

*The content of this chapter is published in: Gernigon, L., M. Brönner, C. Fichler, L. Løvås, L. Marello, and O. Olesen, (2011), Magnetic expression of salt diapir-related structures in the Nordkapp Basin, western Barents Sea, Geology, 39, 135-138.*

Is not included due to copyright

# References


Afonso, J. C., Fernàndez, M., Ranalli, G., Griffin, W. L., and Connolly, J. A. D., 2008, Integrated geophysical-petrological modeling of the lithosphere and sublithospheric upper mantle: Methodology and applications: Geochemistry Geophysics Geosystems, v. 9, no. 5, p. doi:10.1029/2007GC001834.

Alexander, M., and Heintz, K. O., 1998, Sulfur exploration with core-hole and surface gravity, in Gibson, R. I., and Millegan, P. S., eds., Geologic applications gravity and magnetics: Case histories, Volume AAPG Studies in Geology, SEG Geophysical Reference Series 8 and American Association of Petroleum Geologists,, p. 113-119.

Andersen, M. S., 1988, Late Cretaceous and early Tertiary extension and volcanism around the Faeroe Islands, in Morton, A. C., and Parson, L. M., eds., Early Tertiary Volcanism and the Opening of the NE Atlantic, Volume 39, Geological Society, London, Special Publications, p. 115-122.

Andersen, T. B., 1998, Extensional tectonics in the caledonides of southern Norway, an overview.: Tectonophysics, v. 285, no. 3-4, p. 333-351.

Anderson, D. L., 1989, Theory of the Earth: Blackwell Scientific Publications, v. Cambridge, MA, USA, p. 366.

Andreasson, P. G., Svenningsen, O. M., and Albrecht, L., 1998, Dawn of Phanerozoic orogeny in the North Atlantic tract; evidence from the Seve-Kalak Superterrane, Scandinavian Caledonides: Journal of the Geological Society of Sweden (GFF), v. 120, p. 159-172.

Aplonov, S. V., Shmelev, G. B., and Krasnov, D. K., 1996, Geodynamics of the Barents-Kara Shelf: Geophysical Evidence: Geotectonics, v. 30, no. 4, p. 309-326.

Apolonov, S. V., Shmelev, G. B., and Krasnov, D. K., 1996, Geodynamica of the Barents-Kara Shelf:Geophysical Evidence.: Geotectonics, v. 30, no. 4, p. 309-326.

Artemieva, I. M., 2011, The lithosphere: An interdisciplinary approach, Cambridge University Press, 797 p.:

Artemieva, I. M., and Mooney, W. D., 2001, Thermal thickness and evolution of Precambrian lithosphere: a global study: Journal of geophysical Research, v. 106, p. 16,387-316,414.

Artemieva, I. M., Mooney, W. D., Perchuc, E., and Thybo, H., 2002, Processes of lithosphere evolution: new evidence on the structure of the continental crust and uppermost mantle: Tectonophysics, v. 358, p. 1-15.

Artemieva, I. M., Thybo, H., and Kaban, M. K., 2006, Deep Europe today: Geophysical synthesis of the upper mantle structure and lithospheric processes over 3.5 Ga, in Gee, D., and Stephenson, R., eds., Lithosphere Dynamics, Volume 32, Geological Society London Sp. Publ, p. 11-41.

Artyushkov, E. V., 2005, The formation mechanism of the Barents Basin: Russian Geology and Geophysics, v. 46, no. 7, p. 683-696.

Artyushkov, E. V., 2010, Mechanism of formation of superdeep sedimentary basins: lithospheric stretching or eclogitization?: Russian Geology and Geophysics (Geologiya i Geofizika), v. 51 no. 12, p. 1304-1313.

Athy, L. F., 1930, Density, porosity, and compaction of sedimentary rocks: AAPG Bull., v. 14, p. 1-24.

Bailey, J. C., and Rasmussen, M. H., 1997, Petrochemistry of Jurassic and Cretaceous tholeiites from Kong Karls Land, Svalbard, and their relation to Mesozoic magmatism in the Arctic.: Polar Res. , v. 16, p. 37–62.

Bain, J. E., Horscroft, T. R., Weyand, J., Saad, A. H., and Bulling, D. N., Complex salt features resolved by integrating seismic, gravity and Magnetics, in Proceedings 5th European Association of Petroleum Geophysicists (EAGP) Conference and technical Exhibition/ 55th European Association of Exploration Geophysicists (EAEG), Stavanger, Norway, June7-11 1993, p. abstract E006.

Baranov, V., 1957, A new method for interpretation of aeromagnetics maps: pseudo-gravimetric anomalies: Geophysics, v. 29, p. 359-383.

Barrère, C., Ebbing, J., and Gernigon, L., 2009, Offshore prolongation of Caledonian structures and basement charaterisation in the western Barents Sea from geophysical modelling.: Tectonophysics, v. 470 no. 1-2, p. 71-88.

Barrère, C., Ebbing, J., and Gernigon, L., 2011, 3D density and magnetic crustal characterisation of the southwestern Barents Shelf: Implications for the offshore prolongation of the Norwegian Caledonides.: Geophys. J. Int., v. 184, p. 1147-1166.

Belayakovla, T., and Stepanenkvo, I., 1991, Magmatism and geodynamics of the Baikalide basement of the Timan-Pechora syneclise: Izvestiya Akademii Nauk SSSR, Seriya Geologicheskaya, v. 12 [in Russian], p. 106- 101 117.

Belyakov, S. L., 1994, Structural complexes of the Timan–Pechora region sedimentary cover, in Leonov, Y., ed., Tectonics and Magmatism of the East-European Platform: Moscow, KMK, p. 134-144.

Bhattachatyya, B., 1966, Continuous spectrum of the total-magnetic field anomaly due to a rectangular prismatic body.: Geophysics, v. 31, p. 97-121.

Birch, F., 1961, The velocity of compressional waves in rocks to 10 kilobars, Part 2: Geophysical Research, v. 66, no. 7, p. 2199-2224.

Birch, F., 1996, Compressibility, elastic constants, in Clark, S. P., ed., Handbook of physical constants, Volume 97, Geological Sosciety of America, Memoir, p. 97-174.

Blakely, R. J., 1996, Potential theory in gravity and magnetic applications, Cambridge University Press, p. 464.

Blakely, R. J., and Simpson, R. W., 1986, Approximating edges of source bodies from magnetics or gravity anomalies: Geophysics, v. 51, no. 7, p. 1494-1498.

Bogatski, V. I., Bogdanov, N. A., Kostyuchenko, S. L., Senin, B. V., Sobolev, S. F., Shipilov, E. V., and Khain, V. E., 1996, Explanatory notes for the Tectonic Map of the Barents Sea and the Northern Part of European Russia, Maps and geologo-geophysical profiles., in Lithosphere, I. o. t., ed.: Moscow (in Russian).

Bogdanov, N. A., Khain, V. E., Bogatsky, V. L., Kostyuchenko, S. L., Senin, B. V., Shipilov, E. V., and Sobolev, S. F., 1996, Tectonic Map of the Barents Sea region and the northern parts of the European Russia. : Russian Academy of Sciences, Moscow.

Bogolepova, O. K., and Gee, D. G., 2004, Early Palaeozoic unconformity across the Timanides, NW Russia. , in Gee, D. G., and Pease, V. L., eds., The Neoproterozoic Timanide Orogen of Eastern Baltica., Volume Memoirs, 30: London, Geological Society, London, p. 145-157.

Bonatti, E., and Michael, J. P., 1989, Mantle peridotites from continental rifts to oceanic basins to subduction zones: Earth & Planetary Science Letters, v. 91, p. 297-311.

Bowin, C., 2000, Mass anomalies and structures of the Earth: Phys. Chem. Earth, v. 25, no. 4, p. 343-356.

Braathen, A., Nordugulen, Ø., Osmundsen, P. T., Andersen, T. B., Solli, A., and Roberts, D., 2000, Devonian, orogen-parallel, opposed extension in the Central Norwegian Caledonides.: Geology, v. 28, p. 615-618.

Breivik, A. J., Faleide, J. I., and Gudlaugsson, S. T., 1998, Southwestern Barents Sea margin: Late Mesozoic sedimentary basins and crustal extension.: Tectonophysics, v. 293, p. 21-44.

Breivik, A. J., Gudlaugsson, S. T., and Faleide, J. I., 1995, Ottar-Basin, SW Barents Sea: a Major Upper Palaeozoic rift basin containing large volumes of deeply buried salts: Basin Research., v. 7, no. 4, p. 299-312.

Breivik, A. J., Mjelde, R., Gorgan, P., Shimamura, H., Murai, Y., Nishimura, Y., and Kuwano, A., 2002, A possible Caledonide arm through the Barents Sea imaged by OBS data: Tectonophysics, v. 355, p. 67-97.

Breivik, A. J., Mjelde, R., Grogan, P., Shimamura, H., Murai, Y., and Nishimura, Y., 2003, Crustal structure and transform margin development south of Svalbard based on ocean bottom seismometer data: Tectonophysics, v. 369, no. 1-2, p. 37-70.

Breivik, A. J., Mjelde, R., Grogan, P., Shimamura, H., Murai, Y., and Nishimura, Y., 2005, Caledonide development offshore–onshore Svalbard based on ocean bottom seismometer, conventional seismic, and potential field data.: Tectonophysics, v. 410, p. 79-117.

Breivik, A. J., Verhoef, J., and Faleide, J. I., 1999, Effect of thermal contrasts on gravity modeling at passive margins: Results from the western Barents Sea: Journal of Geophysical Research-Solid Earth, v. 104, no. B7, p. 15293-15311.

Brown, D., Juhlin, C., and Puchkov, V., 2002, Mountain building in the Uralides: Pangea to the Present, Geophysical Monograph series, 286 p.:

Bugge, T., Elvebakk, G., Fanavoll, S., Mangerud, G., Smelror, M., Weiss, H. M., Gjelberg, J., Kristensen, S. E., and Nilsen, K., 2002, Shallow stratigraphic drilling applied in hydrocarbon exploration of the Nordkapp Basin, Barents Sea: Marine and Petroleum Geology, v. 19, no. 1, p. 13-37.

Bugge, T., Mangerud, G., Elvebakk, G., Mørk, A., Nilsson, I., Fanavoll, S., and Vigran, J. O., 1995, The Upper Palaeozoic succession on the Finnmark Platform, Barents Sea. : Norsk Geologisk Tidsskrift v. 75, p. 3-30.

Buiter, S. J. H., and Torsvik, T. H., 2007, Horizontal movements in the eastern Barents Sea constrained by numerical models and plate reconstructions: Geophys. J. Int., v. 171, p. 1376-1389.

Bungum, H., Ritzmann, O., Maercklin, N., Faleide, J. I., Mooney, W. D., and Detweiler, S. T., 2005, Three-dimensional model for the crust and upper mantle in the Barents Sea region.: EOS Trans. Am. geophys. Un., v. 86, p. 160-161.

Carlson, R. L., and Herrick, C. N., 1990, Densities and porosities in the oceanic-crust and their variations with depth and age: Journal of Geophysical Research-Solid Earth and Planets, v. 95, no. B6, p. 9153-9170.

Carlson, R. W., Pearson, D. G., and James, D. E., 2005, Physical, chemical, and chronological characteristics oc continental mantle: Reviews of geophysics, v. 43, no. RG1001, p. doi:10.1029/2004RG000156,002005.

Chorowicz, J., 1992, Gravity-Induced Detachment of Devonian Basin Sediments in Northern Svalbard. : Norsk Geologisk Tidsskrift, v. 71, no. 1, p. 21-25.

Christensen, N. I., and Mooney, W. D., 1995, Seismic velocity structure and composition of the continental crust: A global view: J. Geophys. Res, v. 100, p. 9761-9788.

Chroston, P. N., 1974, Geological interpretation of gravity data between Tromsø and Øksfjord (Finnmark): Norges geologiske undersøkelse Bulletin, v. 312, p. 59-90.

Churkin , M. J., Soleimani, G., Carter, C., and Robinson, R., 1981, Geology of the Soviet Arctic: Kola Peninsula to Lena river in Nairn, A. E. M., Churkin, M. J., and Stehli, F. G., eds., The ocean basins and margins, Volume 5; The Arctic Ocean: New York, Plenum Press, p. 331-375.

Clark, D. A., 1997, Magnetic petrophysics and magnetic petrology: aids to geological interpretation of magnetic surveys: AGSO Journal of Australian Geology and Geophysics, v. 17, no. 2, p. 83-103.

Clark, D. A., and Emerson, D. W., 1991, Notes on rock magnetisation in applied geophysical studies: Exploration Geophysics, v. 22, no. 4, p. 547-555.

Clark, S. A., Faleide, J. I., Ritzmann, O., and Mjelde, R., 2009, Multi-stage rift evolution of the SW Barents Sea from wide-angle seismic velocity modeling: Geophys. Res. Abs., v. 11, no. 12 559.

Cocks, L. R. M., and Fortey, R. A., 1982, Faunal evidence for oceanic separations in the Palaeozoic of Britain: Journal of the Geological Society London, v. 139, p. 465-478.

Cocks, L. R. M., and Torsvik, H. T., 2005, Baltica from the late Precambrian to mid-Palaeozoic times: The gain and loss of a terrane's identity: Earth-Science Review, v. 72, p. 39-66.

Cocks, L. R. M., and Torsvik, T. H., 2006, European geography in a global context from the Vendian to the end of the Palaeozoic, in Gee, D. G., and Stephenson, R. A., eds., European Lithosphere Dynamics, Geological Society of London, p. 83-95.

Cocks, L. R. M., and Torsvik, T. H., 2011, The Palaeozoic geography of Laurentia and western Laurussia: A stable craton with mobile margins: Earth-Science Reviews, v. 106, no. 1-2, p. 1-51.

Connolly, J. A. D., 2005, Computation of phase equilibria by linear programming: A tool for geodynamic modeling and its application to subduction zone decarbonation: Earth Planet. Sci. Lett., v. 236, p. 524-541.

Conrad, C. P., and Lithgow-Bertelloni, C., 2006, Influence of continental roots and asthenosphere on plate-mantle coupling: Geophysical Research Letters, v. 33, no. 5.

Corfu, F., Torsvik, T. H., Andersen, T. B., Ashwal, L. D., Ramsay, D. M., and Roberts, R. J., 2006, Early Silurian mafic-ultramafic and granitic plutonism in contemporaneous flysch, Magerøy, northern Norway: U-Pb ages and regional significance.: Journal of the Geological Society v. 163, p. 291-301.

Dallmann, W. K., and Krasil'ščikov, A. A., 1996, Geological map of Svalbard. 1:50000, sheet D20G. Bjørnøya. Temakart 27.

Dengo, C. A., and Røssland, K. G., 1992, Extensional tectonic history of the western Barents Sea, in Larsen, R. M., Brekke, H., Larsen, B. T., and Talleraas, E., eds., Structural and tectonic modelling and its applications to petroleum geology, Volume 1: Amsterdam, Norwegian Petroleum Society (NPF) Special Pubblication, p. 91-107.

Deschamps, F., Trampert, J., and Snieder, R., 2002, Anomalies of temperature and iron in the uppermost mantle inferred from gravity data and tomographic models: Physics of the Earth and Planetary, Interiors, v. 129, p. 245-264.

Dibner, V. D., 1998, Geology of Franz Josef Land, Norsk Polarinstitutt, 190 p.:

Dimakis, P., Braathen, B. I., Faleide, J. I., Elverhoi, A., and Gudlaugsson, S. T., 1998, Cenozoic erosion and the preglacial uplift of the Svalbard-Barents Sea region: Tectonophysics, v. 300, no. 1-4, p. 311-327.

Dobretsov, N. L., and Polyansky, O. P., 2010, On formation mechanisms of deep sedimentary basins: Is there enough evidence for eclogitization?: Russian Geology and Geophysics, v. 51, p. 1314-1321.

Dobretsov, N. L., and Sobolev, N. N., 1984, Glaucophane schists and eclogites in the folded systems of northern Asia: Ofioliti, v. 9, p. 401-424.

Doré, A., 1995, Barents Sea geology, petroleum resources and commercial potential.: Arctic, v. 48, no. 3, p. 207-221.

Doré, A. G., 1991, The structural foundation and evolution of Mesozoic seaways between Europe and the Arctic.: Palaeogeogr. Palaeoelimat., v. Palaeoeeol. , no. 87, p. 441-492.

Doré, A. G., and Vining, B. A., 2005, Petroleum Geology: North-West Europe and Global Perspectives - Proceedings of the 6th Petroleum Geology Conference: London, The Geological Society.

Drachev, S. S., Malyshev, N. A., and Nikishin, A. M., 2010, Tectonic history and petroleum geology of the Russian Arctic Shelves: an overview, in Vining, B. A., and Pickering, S. C., eds., Petroleum Geology: From Mature Basins to New Frontiers - Proceedings of the 7th Petroleum Geology Conference, Volume 7: London, Geological Society.

Ebbing, J., Braitenberg, C., and Wienecke, S., 2007, Insights into the lithospheric structure and tectonic setting of the Barents Sea region from isostatic considerations: Geophys. J. Int., v. 171, no. 3, p. 1390-1403.

Eckman, M., 1998, What is the geoid? In Coordinate Systems, GPS, and the Geoid, in Vermeer, M., ed., Report 95:5 of the Finnish Geodetic Institute: Masala, p. 49-51.

Eldholm, O., Faleide, J. I., and Myhre, A. M., 1987, Continent-ocean transition at the western Barents Sea/Svalbard continental margin: Geology, v. 15, p. 1118-1122.

Euweina, M. C., and Van Eminerik, I. J. H., 2007, Intercultural competencies and conglomerated conflict behaviors in intercultural conflicts: International Journal of Intercultural Relations, v. 31, no. 4, p. 427-441.

Faleide, J. I., Gudlaugsson, S. T., Eldholm, O., Myhre, A. M., and Jackson, H. R., 1991, Deep seismic transects across the sheared western Barents Sea-Svalbard margin.: Tectonophysics, v. 189, p. 73-89.

Faleide, J. I., Ritzmann, O., Weidle, C., and Levshin, A., 2006a, Geodynamical aspects of a new 3-D geophysical model of the greater Barents Sea region—linking sedimentary basins to the upper mantle structure: Geophys. Res. Abstr, v. 8, 08640.

Faleide, J. I., Ritzmann, O., Weidle, C., Levshin, A., and Gee, D., 2006b, Linking Eastern Barents Sea basin formation to the deep crustal and upper mantle structure: AGU Fall Meeting, abstract.

Faleide, J. I., Solheim, A., Fiedler, A., Hjelstuen, B. O., Andersen, E. S., and Vanneste, K., 1996, Late Cenozoic evolution of the western Barents Sea-Svalbard continental margin. Impact of glaciations on basin evolution; data and models from the Norwegian margin and adjacent areas.: Global and Planetary Change, v. 12, p. 53-74.

Faleide, J. I., Tsikalas, F., Breivik, A. J., Mjelde, R., Ritzmann, O., Engen, O., Wilson, J., and Eldholm, O., 2008, Structure and evolution of the continental margin off Norway and Barents Sea: Episodes, v. 31, no. 1, p. 82-91.

Faleide, J. I., Vagnes, E., and Gudlaugsson, S. T., 1993, Late Mesozoic-Cenozoic evolution of the southwestern Barents Sea in a regional rift-shear tectonic setting.: Marine and Petroleum Geology, v. 10, p. 186-214.

Featherstone, W. E., 1997, On the Use of the Geoid in Geophysics: A Case Study Over the North-West Shelf of Australia: Exploration Geophysics, v. 28, no. 1, p. 52-57.

Fichler, C., Rueslåtten, H., Gram, C., Ingebrigtsen, A., and Olesen, O., Salt interpretation with special focus on magnetic data, Nordkapp Basin, Barents Sea, in Proceedings 2007 International workshop Innovation in EM, Grav and Mag Methods (EGM 2007): A new perspective for exploration. Capri, Italy, 16-18 April 20072007.

Fichler, C., Rundovde E., Johansen S., and Saether, B. M., 1997, Barents Sea tectonic structures visualized by ERS1 satellite gravity with indications of an offshore Baikalian trend.: First Break v. 15, p. 582-585.

Forsberg, R., Skourup, H., Andersen, O. B., Knudsen, P., Laxon, S. W., Ridout, A., Johannesen, J., Siegismund, F., Drange, H., Tscherning, C. C., Arabelos, D., Braun, A., and Renganathan, V., 2007, Combination of Spaceborne, Airborne and In-situ Gravity Measurements in Support of Arctic Sea Ice Thickness Mapping: Danish National Space Center, Technical Report, v. 7, p. 136 pp.

Forte, a. M., and Perry, H. K. C., 2000, Geodynamic Evidence for a Chemically Depleted Continental Tectosphere: Science, v. 290, p. 1940-1944.

Fossen, H., 2000, Extensional tectonics in the Caledonides: Synorogenic or postorogenic?: Tectonics, v. 19, no. 2, p. 213-224.

Fossen, H., 2010, Extensional tectonics in the North Atlantic Caledonides: a regional view, in Law, R. D., Butler, R. W. H., Holdsworth, R. E., Krabbendam, M., and Strachan, R. A., eds., Continental Tectonics and Mountain Building: The Legacy of Peach and Horne, Volume 335, Geological Society, London, Special Publications, p. 767-793.

Fossen, H., Odinsen, T., Færseth, R. B., and Gabrielsen, R. H., 2000, Detachments and low-angle faults in the northern North Sea rift system, in Nøttvedt, A., ed., Dynamics of the Norwegian Margin, Volume 167, Geological Society of London, Special Publications, p. 105-131.

Fossum, B. J., Schmidt, W. J., Jenkins, D. A., Bogatsky, V. L., and Rappoport, B. I., 2001, New frontiers for hydrocarbon production in the Timan–Pechora Basin, Russia, in Downey, M. W., Threet, J. C., and Morgans, W. A., eds., Petroleum Provinces of the Twenty-first Century, Volume Memoirs, 74, American Association of Petroleum Geologists, Tulsa,OK, p. 259-279.

Fullea, J., Afonso, J. C., Connolly, J. A. D., Fernàndez, M., García-Castellanos, D., and Zeyen, H., 2009, LitMod3D: An interactive 3-D software to model the thermal, compositional, density, seismological, and rheological structure of the lithosphere and sublithospheric upper mantle: Geochemistry Geophysics Geosystems, v. 10, no. 8, p. doi:10.1029/2009GC002391.

Furnes, H., Ryan, P. D., Grenne, T., Roberts, D., Sturt, B. A., and Prestvik, T., 1985, Geological and geochemical classification of the ophiolitic fragments in the Scandinavian Caledonides, in Gee, D. G., and Sturt, B. A., eds., The Caledonide Orogen - Scandinavia and Related Areas, John Wiley & Sons p. 1266.

Gabrielsen, R. H., Færseth, R. B., Jensen, L. N., Kalheim, J. E., and Riis, F., 1990, Structural elements of the Norwegian continental shelf. Part1: the Barents Sea Region: Norwegian Petroleum Directorate Bulletin, v. 6, p. 33.

Gabrielsen, R. H., Klovjan, O. S., Rasmunssen, A., and Stolan, T., Interaction between halokinesis and faulting; structuring of the margins of the Nordkapp Basin, Barents Sea region, in Proceedings Structural and tectonic modelling and its implication to petroleum geology; proceedings1992, Volume 1, Norwegian Petroleum Society (NPF) Special Publications, p. 121-131.

Gale, G. H., and Roberts, D., 1974, Trace element geochemistry of Norwegian Lower Palaeozoic basic volcanics and its tectonic implications: Earth Planet. Sci. Lett., v. 22, p. 280-390.

Galitchanina, L. D., Glaznev, V. N., Mitrofanov, F. P., and O., O., 1995, Surface density characteristics of the Baltic Shield and adjacent territories: Norwegian Journal of Geology, v. Special Publication, p. 349-354.

Gallardo-Delgado, L. A., Pérez-Flores, M. A., and Gómez-Treviño, E., 2003, A versatile algorithm for joint 3D inversion of gravity and magnetic data: Geophysics, v. 68, p. 949-959. doi:910.1190/1191.1581067.

Gardner, G. H. F., Gardner, L. W., and Gregory, A. R., 1984, Formation velocity and density -The diagnostic basics for stratigraphic traps: Geophysics, v. 39, p. 770-780.

Gautier, D. L., Bird, K. J., Charpentier, R. R., Grantz, A., Houseknecht, D. W., Klett, T. R., Moore, T. E., Pitman, J. K., Schenk, C. J., Schuenemeyer, J. H., Sorensen, K., Tennyson, M. E., Valin, Z. C., and Wandrey, C. J., 2009, Assessment of undiscovered oil and gas in the arctic: Science, v. 324, no. 5931, p. 1175-1179.

Gee, D. G., 1975, A tectonic model for the central part of the Scandinavian Caledonides: American Journal of Science, v. 275A, p. 468-515.

Gee, D. G., 2005, Scandinavian Caledonides (with Greenland), in Selly, R. C., Cocks, L. R. M., and Primer, I.-R., eds., Encyclopedia of Geology, Volume 2: Amsterdam, Elsevier, p. 64-74.

Gee, D. G., Belyakova, L. T., Pease, V., Larionov, A., and Dovshikove, L., 2000, New, single zircon (Pb-evaporation) ages from Vendian intrusions in the basement beneath the Pechora Basin, Northeastern Baltica: Polarforschung, v. 68, p. 161-170.

Gee, D. G., Bogolepova, O. K., and Lorenz, H., 2006, The Timanian, Caledonian and Uralide orogens in the Eurasian high Arctic, and relationship to paleo-continents Laurentia, Baltica and Siberia., in Gee, D. G., and Stephenson, R. A., eds., European Lithosphere Dynamics, Geological Society London, Memoir 32, p. 507-520.

Gee, D. G., Fossen, H., Henriksen, N., and Higgins, A. K., 2008, From the Early Paleozoic Platforms of Baltica and Laurentia to the Caledonide Orogen of Scandinavia and Greenland: Episodes, v. 31, no. 1, p. 44-51.

Gee, D. G., and Laurence, M. P., 1994, Caledonian terrane assembly on Svalbard; new evidence from 40Ar/39Ar dating in Ny Friesland Am J Sci v. 294, no. 1, p. 1166-1186.

Gee, D. G., and Pease, V. L., 2004, The Neoproterozoic Timanide Orogeny of Eastern Baltica., Geological Society London, Memoir 30.

Gee, D. G., and Teben'kov, A. M., 2004, Svalbard: a fragment of the Laurentian margin, in Gee, D. G., and Pease, V., eds., The Neoproterozoic Timanide Orogeny of Eastern Baltica: London, Memoirs, 30, Geological Society, p. 191-206.

Geissler, W. H., 2001, Marine seismishe Untersuchngen am nördlichen Kontinentalrand von Svalbard (Spitzbergen), Diploma thesis, Institut für Geophysik der Thechnishen Universität Bergakademie Freiberg: Freiberg.

Geosoft, 2005b, Montaj MAGMAP filtering, 2-D frequency domain processing of potential field data, Extension for Oasis Montaj v6.1., Geosoft Incorporated, p. 66.

Gernigon, L., and Brönner, M., 2012 in press, Late Palaeozoic architecture and evolution of the southwestern Barents Sea: Insights from a new generation of aeromagnetic data: Journal of the Geological Society of London.

Gernigon, L., Brönner, M., Fichler, C., Løvås, L., Marello, L., and Olesen, O., 2011, Magnetic expression of salt diapir-related structures in the Nordkapp Basin, western Barents Sea: Geology, v. 39, p. 135-138.

Gernigon, L., Marello, L., Barrére, C., Skilbrei, J. R., and Roberts, D., 2008, Significance of the new BAS-06 aeromagnetic survey for a better understanding of salt tectonics and basin structure in the Barents Sea, 33rd IGC International Geological Congress Oslo, Norway.

Gernigon, L., Marello, L., Moigaard, O. J., Werner, S. C., and Skilbrei, J. R., 2007, Barents Sea Aeromagnetic Survey BAS-06 - Acquisition - processing report and preliminary interpretation: Geological Survey of Norway 035.

Getsen, V. G., 1987, Tectonics of Timan.: Nauka, Leningrad, p. 170 (in Russian).

Getsen, V. G., 1991, Geodynamic reconstruction of the northeastern European part of the USSR in the Late Proterozoic: Geotectonics, v. 25, no. 5, p. 391-400.

Gibson, R. I., and Millegan, P. S., 1998, Geologic applications of gravity and magnetics: case histories, American Association of Petroleum Geologists, 170 p.:

Godfrey, N. J., Beaudoin, B. C., Klemperer, S. L., and The Mendocino Working Group USA, 1997, Ophiolitic basement to the Great Valley forearc basin, California, from seismic and gravity data: Implications for crustal growth at the North American continental margin: Geol.Soc. Am. Bull, v. 108 no. N12, p. 1536-1562.

Goussev, S. A., and Pierce, J. W., 2010, Magnetic basement: gravity-guided magnetic source depth analysis and interpretation: Geophysical Prospecting, v. 58, no. 2, p. 321-334.

Grad, M., Tiira, T., and Group, E. W., 2009, The Moho depth map of the European Plate: Geophys. J. Int., v. 176 p. 279-292. doi: 210.1111/j.1365-1246X.2008.03919.x. .

Gramberg, I. S., 1988, The Barents Shelf Platform. Nedra, Leningrad [in Russian].

Gramberg, I. S., Glebovsky, V. Y., Grikurov, G. E., Ivanov, V. L., Korago, E. A., Kos'ko, M. K., Maschenkov, S. P., Piskarev, A. L., Pogrebitsky, Y. E., Shipelkevitch, Y. V., and Suprunenko, O. I., 2001, Eurasian Arctic Margin: Earth Science Problems and Research Challenges: Polarforschung, v. 69, p. 3-25.

Griffin, W. L., O'Reilly, S. Y., Doyle, B. J., Pearson, N. J., Kivi, K., Malkovets, V., Coopersmith, H., and Pokhilenko, N. V., 2004, Lithosphere mapping beneath the North American plate: Lithos, v. 77, p. 873-922.

Griffin, W. L., O'Reilly, S. Y., and Ryan, C. G., 1999a, The composition and origin of sub-continental lithospheric mantle, in Mantle Petrology: Field Observations and High-Pressure Experimentation, in Fei, Y., Berkta, C. M., and Mysen, B. O., eds., A Tribute to Francis R. (Joe) Boyd,, Volume 6, Spec. Publ. Geochem. Soc, p. 13-45.

Griffin, W. L., Ryan, C. G., Kaminsky, F. V., O'Reilly, S. Y., Natapov, L. M., Win, T. T., Kinny, P. D., and P, I. I., 1999b, The Siberian lithosphere traverse: mantle terranes and the assembly of the Siberian Craton: Tectonophysics, v. 310, no. 1-4, p. 1-35.

Griffin, W. L., Zhang, A., O'Reilly, S., and C., R., 1998, Phanerozoic evolution of the lithosphere beneath the Sino-Korean Craton, in M. Flower, and et al., eds., Mantle Dynamics and Plate Interactions in East Asia, Volume 27, Geodyn. Ser,.AGU, Washington, D. C, p. 107-126.

Grogan, P., Nyberg, K., Fotland, B., Myklebust, R., Dahlgren, S., and Riis, F., 1998, Cretaceous Magmatism South and East of Svalbard. Evidence from Seismic Reflection and Magnetic Data: Polarforschung, v. 68, p. 25-34.

Grütter, H., Latti, D., and Menzies, A., 2006, Cr-saturation arrays in concentrate garnet compositions from kimberlite and their use in mantle barometry: Journal of Petrology, v. 47, no. 801-820.

Gubaidulin, M. G., Zhuravlev, V. A., and Koifman, L. I., 1993, Profiles along the northeastern and eastern framing of the shield, in: The structure of lithosphere of the Baltic Shield.: Moscow, USSR Acad Sci.

Gudlaugsson, S. T., and Faleide, J. I., 1994, The continental margin between Spitsbergen and Bjørnøya, in Eiken, O., ed., Seismic Atlas of Western Svalbard, Volume 130: Nor. Polarinst. Med, p. 11-13.

Gudlaugsson, S. T., Faleide, J. I., Fanavoll, S., and Johansen, B., 1987, Deep seismic reflection profiles across the western Barents Sea: Geophysical Journal of the Royal Astronomical Society, v. 89, p. 273-278.

Gudlaugsson, S. T., Faleide, J. I., Johansen, S. E., and Breivik, A. J., 1998, Late Palaeozoic structural development of the South-western Barents Sea: Marine and Petroleum Geology, v. 15, no. 1, p. 73-102.

Guggisberg, B., Kaminski, W., and Prodehl, C., 1991, Crustal structure of the Fennoscandian Shield; a traveltime interpretation of the long-range FENNOLORA seismic refraction profile: Tectonophysics, v. 195, p. 105-137.

Gung, Y., Panning, M., and Romanowicz, B., 2003, Global anisotropy and the thickness of continents.: Nature, v. 422, p. 707-711.

Gunn, P. J., 1997, Application of aermagnetic surveys to sedimentary basin studies: AGSO Journal of Australian Geology and Geophysics, v. 17, no. 2.

Götze, H. J., and Lahmeyer, B., 1988, Application of 3-Dimensional Interactive Modeling in Gravity and Magnetics: Geophysics, v. 53, no. 8, p. 1096-1108.

Hacker, B. R., Abers, G. A., and Peacock, S. M., 2003, Subduction factory - 1. Theoretical mineralogy, densities, seismic wave speeds, and H2O contents: Journal of Geophysical Research-Solid Earth, v. 108, no. B1.

Hager, B., 1984, Subducted slabs and the geoid: constraints on mantle rheology and flow: Journal of Geophysical Research, v. 89, p. 6003-6015.

Harland, W. B., 1985, Caledonide Svalbard, in Gee, D. G., and Sturt, B. A., eds., The Caledonide Orogen-Scandinavia and related Areas: Chichester, John Wiley & Sons, p. 999-1016.

Harland, W. B., Anderson, L. M., and Manasrah, D., 1997, The geology of Svalbard: Geological Society of London Memoir, v. 17, p. 1-521.

Harland, W. B., and Gayer, R. A., 1972, The Arctic Caledonides and earlier oceans: Geological Magazine, v. 109, p. 289-314.

Harland, W. B., and Stephens, C. F., 1997, Neogene-Quaternary history: Memoir Geological Society of London, v. 17, p. 418-435.

Hartz, E. H., and Torsvik, T. H., 2002, Baltica upside-down: A new plate tectonic model for Rodinia and the Iapetus Ocean: Geology, v. 30, p. 255-258.

Heiskanen, W. A., and Moritz, H., 1967, Physical Geodesy, San Francisco.

Henriksen, E., Ryseth, A. E., Larssen, B. G., Heide, T., Rønning, K., and Stoupakova, A. V., 2011, Tectonostratigraphy of the greater Barents Sea: implication for petroleum

systems, in Spencer, A. M., Embry, A. F., Gautier, D. L., Stoupakova, A., and Sorensen, K., eds., Arctic Petroleum Geology, Geological Society, London.

Herrevold, T., Gabrielsen, R. H., and Roberts, D., 2009, Structural geology of the southeastern part of the Trollfjorden-Komagelva Fault Zone, Varanger Peninsula, Finnmark, North Norway: Norwegian Journal of Geology, v. 89, p. 305-325.

Hofmeister, A. M., 1999, Mantle values of thermal conductivity and the geotherm from phonon lifetimes: Science, v. 283, p. 1699-1706.

Holtedahl, O., 1920, On the Paleozoic series of Bear Island, especially the Hecla Hoek System: Norsk Geologisk Tidsskrift, v. 5, p. 121-148.

Hudec, M. R., and Jackson, M. P. A., 2007, Terra infirma: Understanding salt tectonics: Earth-Science Reviews, v. 82, no. 1-2, p. 1-28.

Huismans, A., Finestone, J., Hauptfleisch, T., and de Wet, R., 1999, Unwilling champion - An interview with Reza de Wet: Contemporary Theatre Review, v. 9, p. 53-63.

Huismans, R. S., Podladchikov, Y. Y., and Cloetingh, S. A. P. L., 2001, Transition from passive to active rifting: Relative importance of asthenospheric doming and passive extension of the lithosphere: j. Geophys. Res., v. 106, no. 11, p. 11,271-211,292.

Hunt, C. P., Mosckowitz, B. M., and Banerjee, S. K., 1995, Magnetic Properties of Rocks and Minerals (Vol. 3). Rock physics and phase relations. A handbook of physical constants.: AGU Reference Shelf, American Geophysical Union, p. 189-204.

Huston, D. C., Huston, H. H., and Johnson, E., 2004, Geostatistical integration of velocity cube and log data to constrain 3D gravity modeling, deepwater Gulf of Mexico: The Leading Edge, v. 23, p. 842-846.

Høgden, S., 1999, Seismotectonics and crustal structure of the Svalbard Region. [Master Thesis: Geological Department, University of Oslo, 142 p.

Ivanova, N. M., Sakoulina, T. S., and Roslov, Y. V., 2006, Deep seismic investigation across the Barents–Kara region and Novozemelskiy Fold Belt (Arctic Shelf): Tectonophysics, v. 420, p. 123-140.

Ivanova, N. M., Sakulina, T. S., Belyaev, I. V., Matveev, Y. I., and Roslov, Y. V., 2011, Depth model of the Barents and Kara seas according to geophysical surveys results, in Spencer, A. M., Embry, A. F., L., G. D., Stoupakova, A., and Sørensen, K., eds., Arctic Petroleum Geology, Volume 35: London, Geological Society, p. 209-221.

Jacoby, W., and Smilde, P. L., 2009, Gravity Interpretation: Fundamentals and Application of Gravity Inversion and Geological Interpretation Springer, 395 p.:

Jacques, J. M., Parsons, M. E., Price, A. D., and Schwartz, D. M., 2003, Improving geologic understanding with gravity and magnetic data: Examples from Gabon, Nigeria and the Gulf of Mexico: First Break, v. 21, no. 11, p. 57-62.

Jakobsson, M., Macnab, R., Mayer, L., Anderson, R., Edwards, M., Hatzky, J., Schenke, H. W., and Johnson, P., 2008, An improved bathymetric portrayal of the Arctic Ocean: Implications for ocean modeling and geological, geophysical and oceanographic analyses: Geophys. Res. Lett., 35, Doi: 10.1029/2008gl033520.

Jeffrey, D. P., 2000, Locating magnetic contacts: a comparison of the horizontal gradient, analytic signal, and local wavenumber methods: SEG Expanded Abstracts, v. 19, no. 402, p. doi:10.1190/1191.1816078

Jimenez-Munt, I., Fernandez, M., Verges, J., Afonso, J. C., Garcia-Castellanos, D., and Fullea, J., 2010, Lithospheric structure of the Gorringe Bank: Insights into its origin and tectonic evolution: Tectonics, v. 29.

Johansen, S. E., Henningsen, T., Rundhovde, E., Saether, B. M., Fichler, C., and Rueslatten, H. G., 1994, Continuation of the Caledonides north of Norway - Seismic reflectors within the basement beneath the Southern Barents Sea: Marine and Petroleum Geology, v. 11, no. 2, p. 190-201.

Johansen, S. E., Ostisty, B. K., Birkeland, Ø., Fedorovsky, Y. F., Martirosjan, V. N., Christensen, O. B., Cheredeev, S. I., Ignatenko, E. A., and Margulis, L. S., 1992, Hydrocarbon potential in the Barents Sea region: play distribution and potential., in Vorren, T. O., Bergsager, E., Dahl-Stamnes, Ø. A., Holter, E., Johansen, B., Lie, E., and Lund, T. B., eds., Arctic Geology and Petroleum Potential, Volume vol2, Norwegian Petroleum Society (NPF), Special Publication, p. 273-320.

Jordan, T. H., 1978, Composition and development of the continental tectosphere: Nature, v. 274, p. 544-548.

Jordan, T. H., 1981, Continents as a Chemical Boundary Layer: Phil. Trans. Roy. Soc., v. 301, no. 1461, p. 359-373.

Jordan, T. H., 1988, Structure and formation of the continental tectosphere: Journal of Petrology, v. Special Lithosphere Issue, p. 11-37.

Kaban, M. K., Schwintzer, P., Artemieva, I. M., and Mooney, W. D., 2003, Density of the continental roots: compositional and thermal contributions: Earth and Planetary Science Letters, v. 209, p. 53-69.

Karpychev, M., and Fleitout, L., 2000, Long-wavelength geoid: The effect of continental roots and lithosphere thickness: Geophysical Journal International, v. 143, no. 3, p. 945-963.

Kimbell, G. S., Gatliff, R. W., Ritchie, J. D., Walker, A. S. D., and Williamson, J. P., 2004, Regional three-dimensional gravity modelling of the NE Atlantic margin: Basin Research, v. 16, no. 2, p. 259-278.

Kimbell, G. S., Ritchie, J. D., and Henderson, A. F., 2010, Three-dimensional gravity and magnetic modelling of the Irish sector of the NE Atlantic margin: Tectonophysics, v. 486, p. 36-54.

King, S. D., 2005, Archean cratons and mantle dynamics: Earth Planet. Sci. Lett., v. 234, p. 1-14.

Klemme, S., 2004, The influence of Cr on the garnet–spinel transition in the Earth's mantle: Experiments in the system MgO–Cr203–5i02 and thermodynamic modelling.: Lithos, v. 77, p. 639-946.

Kolstrup, M. L., 2010, The lithospheric mantle below southern Norway: University of Oslo.

Korago, E. A., Kovaleva, G. N., Il'in, V. F., and Platonov, L. G., 1992, Tectonics and Matallogeny of the Early Kimmeridgian of Novaya Zemlya.: Nedra St. Petersburg (in Russian).

Korago, E. A., Kovaleva, G. N., Lopatin, B. G., and Origo, V. V., 2004, The Precambrian rocks of Novaya Zemlya., in Gee, D. G., and Pease, V. L., eds., The Neoproterozoic Timanide Orogeny of Eastern Baltica., Volume 30, Geological Society London Memoir, p. 135-145.

Kostyuchenko, S., Egorkin, A., and Solodilov, L., 1999, Structure and genetic mechanism of Precambrian rift of the East-European Platform in Russia by integrated study of seismic, gravity and magnetic data.: Tectonophysics, v. 313, p. 9-28.

Kostyuchenko, S., Sapozhnikov, A., Egorkin, A., Gee, D. G., Berzin, R., and Solodilov, L., 2006, Crustal structure and tectonic model of northeastern Baltica, based on deep seismic and potential field data, in Gee, D. G., and Stephenson, R. A., eds., European Lithosphere Dynamics, Volume 32, Geological Society London Memoir, p. 521-539.

Koyi, H., Talbot, C. J., and Torudbakken, B. O., 1993, Salt Diapirs of the Southwest Nordkapp Basin - Analog Modeling: Tectonophysics, v. 228, no. 3-4, p. 167-187.

Larsen, H. C., Saunders, A. D., and Cliff, P. D., 1994, (and the Shipboard Scientific Party). Proceeding of the Drilling Program Initial Report: Ocean Drill. Program, College Station, Tex., v. 152.

Larssen, G. B., Elvebakk, G., Henriksen, L. B., Kristensen, S. E., Nilsson, I., Samuelseberg, T. J., Svåna, T. A., Stemmerik, L., and Worsley, D., 2005, Upper Palaeozoic lithostratigraphy of the southern part of Norwegian Barents Sea.: Norges geologiske undersøkelse Bulletin v. 444, p. 43.

Lauritsen, T., Blomstrand, L. B., Olesen, and Mørk, A., 2007, OSRAM II - Origin of Sediment-Related AeroMagnetics II: Magnetic susceptibility measurements on shallow stratigraphic cores from the Finnmark Platform, Nordkapp Basin and Svalis Dome: Geological Survey of Norway.

Le Stunff, Y., and Ricard, Y., 1995, Topgraphy and geoid due to lithospheric mass anomalies: Geophysical Journal International, v. 122, no. 3, p. 982-990.

Lebedev, S., Boonen, J., and Trampert, J., 2009, Seismic structure of Precambrian lithosphere: New constraints from broad-band surface-wave dispersion: Lithos, v. 109, p. 96-111.

Lee, C.-T. A., 2003, Compositional variation of density and seismic velocities in natural peridotites at STP conditions: Implications for seismic imaging of compositional heterogeneities in the upper mantle: Journal of geophysical Research, v. 108, no. doi:10.1029/2003JB002413, p. 2441, 2420 PP.

Levshin, A. L., Schweitzer, J., Weidle, C., Shapiro, N. M., and Ritzwoller, M. H., 2007, Surface wave tomography of the Barents Sea and surrounding regions: Geophys. J. Int., v. 170, no. 1, p. 441-459.

Li, X., 2001, Vertical resolution: Gravity versus vertical gravity gradient: The Leading Edge, v. 20, p. 901-904.

Lindsay, T., 1998, Introduction to Geophysical Exploration, University of Melbourne, http://www.earthsci.unimelb.edu.au/ES304/.

Ljones, F., Kuwano, A., Mjelde, R., Breivik, A., Shimamura, H., Murai, Y., and Nishimura, Y., 2004, Crustal transect from the North Atlantic Knipovich Ridge to the Svalbard margin west of Hornsund: Tectonophysics, v. 378, no. 1-2, p. 17-41.

Lobokovsky, L. I., Cloetingh, S., Nikishin, A. M., Volosh, Y. I. A., Lankreijer; A.C., Belvakov, S. L., Groshev, V., Fokin, P., Milanovsky, E., Pevzner, L., Gorbachov, V., and Korneev, M. A., 1996, Extensional basins of the former Soviet Union—structure, basin formation mechanisms and subsidence history: Tectonophysics, v. 266, p. 251-285.

Ludwig, W. J., Nafe, J. E., and Drake, C. L., 1970, Seismic refraction. In: Maxwell, A.E. (ed) The Sea: Wiley-interscience, New York, v. 4, p. 53-84.

Lønne, W., and Sellevoll, M. A., 1975, A reconnaissance gravity study of Magerøy, Finnmark, northern Norway.: Norges geologiske undersøkelse, v. 319, p. 1-15.

Maher, H. D., 2001, Manifestations of the Cretaceous High Arctic Large Igneous Province in Svalbard: Journal of Geology, v. 109, no. 1, p. 91-104.

Manby, G., and Lyberis, N., 1992, Tectonic evolution of the Devonian Basin of Northern Svalbard. : Norsk Geologisk Tidsskrift, v. 72, no. 1, p. 7-19.

Marello, L., Ebbing, J., and Gernigon, L., 2010, Magnetic basement study in the Barents Sea from inversion and forward modelling: Tectonophysics, v. 493, p. 153-171.

Marello, L., Ebbing, J., and Gernigon, L., 2012, Basement inhomogeneities and crustal setting in the Barents Sea from a combined 3D gravity and magnetic model: Geophys. J. Int. (submitted).

Martinec, Z., 1994, The density contrast at the Mohorovičić discontinuity: Geophys. J. Int., v. 117, p. 539-544.

Mauring, E., Beard, L. P., Kihle, O., and Smethurst, M. A., 2002, A comparison of aeromagnetic levelling techniques with an introduction to median levelling: Geophysical Prospecting, v. 50, no. 1, p. 43-54.

McKenzie, D., and Bickle, M. J., 1988, The volume and composition of melt generated by extension of the lithosphere: Journal of Petrology, v. 29, p. 625-679.

Mendonca, C. A., 2004, Inversion of gravity-field inclination to map the basement relief of sedimentary basins: Geophysics, v. 69, no. 5, p. 1240-1251.

Meyer, R., Wijk, V. J., and Gernigon, L., 2007, North Atlantic Igneous Province: A Review of Models for its Formation, in Foulger, G. R., and Jurdy, D. M., eds., Planets, Plumes, and Planetary Processes, Volume 430, The Geological Society of America, p. 525-552.

Miller, H. G., and Singh, V., 1994, Potential-field tilt - a new concept for location of potential-field sources: Journal of Applied Geophysics, v. 32, no. 2-3, p. 213-217.

Minakov, A., Faleide, J. I., Glebovsky, V. Y., and Mjelde, R., 2012, The structure and evolution of the Northern Barents-Kara Sea continental margin from integrated analysis of potential field, bathymetry and sparse seismic data: Geophys. J. Int., v. 188, p. 79-102.

Minakov, A., Mjelde, R., Faleide, J. I., Flueh, E. R., Dannowski, A., and Keer, H., 2011 (submitted), Mafic intrusion east of Svalbard imaged by active-source seismic tomography.: Tectonophysics.

Mitrovica, J. X., Wahr, J., Matsuyama, I., and Paulson, A., 2005, The rotational stability of an ice age Earth: Geophysical Journal International, v. 161, p. 491-506.

Mjelde, R., Breivik, A. J., Elstad, H., Ryseth, A. E., Skilbrei, J. R., Opsal, J. G., Shimamura, H., Murai, Y., and Nishimura, Y., 2002, Geological development of the Sørvestsnaget Basin, SW Barents Sea, from ocean bottom seismic, surface seismic and potential field data.: Norwegian Journal of Geology, v. 82, p. 183-202.

Monnereau, M., and Cazenave, A., 1990, Depth and geoid anomalies over oceanic hotspot swells: A global survey: Journal of Geophysical Research, v. 95, p. 15429-15438.

Mooney, W. D., and Vidale, J. E., 2003, Thermal and chemical variations in Subcrustal cratonic lithosphere: Evidence from crustal isostasy: Lithos, v. 71, p. 185-193.

Moritz, H., 1980, Geodetic Reference System: Journal of Geodesy, v. 54, p. 395-405.

Morozova, E. A., Pavlenkova, N. I., and Herbst, R., 1995, Ambiguity problems in constructing a seismic crustal model for the southeastern Barents Sea: Physics of the solid Earth, v. 35, no. 2, p. 164-174.

Murray, W., Telford, W. M., Geldart, L. P., and Sheriff, R. E., 1990, Applied geophysics, Cambridge university Press, 792 p.:

Mussett, A. E., and Khan, M. A., 2000, Looking into the Earth: An Introduction to Geological Geophysics, Cambridge University Press, 496 p.:

Myhre, A. M., Eldholm, O., and Sundvor, E. S., 1982, The margin between Senja and Spitsbergen fracture zone: implications from plate tectonics.: Tectonophysics, v. 89, p. 1-32.

Müller, R. D., Roest, W. R., Royer, J. Y., Gahagan, L. M., and Sclater, J. G., 1997, Digital isochrons of the world's ocean floor: J. Geophys. Res, v. 102, p. 3211-3214.

Mørk, M. B. E., 1999, Compositional variation and provenance of triassic sandstone from the Barents Shels: Journal of Sedimentary Research, v. 69, no. 3, p. 690-710.

Mørk, M. B. E., McEnroe, S. A., and Olesen, O., 2002, Magnetic susceptibility of Mesozoic and Cenozoic sediments off Mid Norway and the role of siderite: implications for interpretation of high-resolution aeromagnetic anomalies.: Marine and Petroleum Geology, v. 19, p. 1115-1126.

Nabighian, M. N., Ander, M. E., Grauch, V. J. S., Hansen, R. O., LaFehr, T. R., Li, Y., Pearson, W. C., Peirce, J. W., Phillips, J. D., and Ruder, M. E., 2005b, 75th Anniversary - Historical development of the gravity method in exploration: Geophysics, v. 70, no. 6, p. 63-89.

Nabighian, M. N., Grauch, V. J. S., Hansen, R. O., LaFehr, T. R., Li, Y., Peirce, J. W., Phillips, J. D., and Ruder, M. E., 2005a, 75th Anniversary - The historical development of the magnetic method in exploration: Geophysics, v. 70, no. 6, p. 33-61.

Nafe, J. E., and Drake, C., 1957, Variation in depth in shallow and deep water sediments of porosity, density and the velocities of compressional and shear waves: Geophysics, v. 22, p. 523-552.

Neprochnov, Y. P., Semenov, G. A., Sharov, N. V., Yliniemi, J., Komminaho, K., Luosto, U., and Heikkinen, P., 2000, Comparison of the crustal structures of the Barents Sea and the Baltic Shield from seismic data: Tectonophysics, v. 321, no. 4, p. 429-447.

Neuendorf, K. K. E., Mehl, J. P., and Jackson, J. A., 2005, Glossary of Geology, 5th ed., in Institute, A. G., ed., p. 57.

Nikishin, A. M., Ziegler, P. A., Abbott, D., Brunet, M.-F., and Cloetingh, S., 2002, Permo-Triassic intraplate magmatism and rifting in Eurasia: implication for mantle plumes and mantle dynamics: Tectonophysics, v. 351, p. 3-39.

Nikishin, A. M., Ziegler, P. A., and Stephenson, R. A., 1996, Late Precambrian to Triassic history of the East European Craton: dynamics of sedimentary basin evolution: Tectonophysics, v. 268, p. 23-63.

Nilsen, K. T., Vendeville, B. C., and Johansen, J. T., 1995, Influence of Regional Tectonics on Halokinesis in the Nordkapp Basin, Barents Sea, in Jackson, M. P. A., Robert, D. G., and Snelson, S., eds., Salt tectonics: a global perspective, Volume 65, AAPG Memoir, p. 413-436.

Nystuen, J. P., Andresen, A., Kumpulainen, R. A., and Siedlecka, A., 2008, Neoproterozoic basin evolution in Fennoscandia, East Greenland and Svalbard: Episodes, v. 31, no. 1, p. 35-43.

O`Reilly, S. Y., and Griffin, L. W., 1996, 4D lithospheric mapping: a review of the methodology with examples: Tectonophysics, v. 262, p. 3-18.

O'Leary, N., White, N., Tull, S., Bashilov, V., Kuprin, V., Natapov, L., and Macdonald, D., 2004, Evolution of the Timan-Pechora and South Barents Sea basins: Geological Magazine, v. 141, no. 2, p. 141-160.

Olesen, O., Brönner, M., Ebbing, J., Gellein, J., Gernigon, L., Koziel, J., Lauritsen, T., Myklebust, R., Pascal, C., Sand, M., Solheim, D., and Usov, S., 2010, New aeromagnetic and gravity compilations from Norway and adjacent areas – methods and applications., in Vining, B. A., and Pickering, S. C., eds., Petroleum Geology: From mature basins to new frontiers. Proceedings of the 7th Petroleum Geology Conference., Geological Society of London, p. 559-586.

Olesen, O., Henkel, H., Kaada, K., and Tveten, E., 1991, Petrophysical properties of a prograde amphibolite – granulite facies transition zone at Sigerfjord, Vesterålen,

northern Norway, in Wasilewski, P., and Hood, P., eds., Magnetic Anomalies - Land and Sea., Tectonophysics,192, p. 33-39.

Olesen, O., Roberts, D., Henkel, H., Lile, O. B., and Torsvik, T. H., 1990, Aeromagnetic and gravimetric interpretation of regional structural features in the Caledonides of West Finnmark and North Troms, northern Norway: Norges geologiske undersøkelse Bulletin, v. 419, p. 1-24.

Olovyanishnikov, V., Roberts, D., and Siedlecka, A., 2000, Tectonics and Sedimentation of the Meso- to Neoproterozoic Timan-Varanger Belt along the Northeastern Margin of Baltica: Polarforschung, v. 68, p. 267-274.

Olovyanishnikov, V. G., Siedlecka, A., and Roberts, D., 1997, Aspects of Geology of the Timans, Russia and linkage with Varanger Peninsula, NE Norway: Bulletin of the Geological Survey of Norway, no. 433, p. 28-29.

O'Reilly, B. M., Readman, P. W., and Hauser, F., 1998, Lithospheric structure across the western Eurasian plate from a wide-angle seismic and gravity study: evidence for a regional thermal anomaly: Earth and Planetary Science Letters, v. 156, no. 3-4, p. 275-280.

O'Reilly, S. Y., and Gruffin, W. L., 2006, Imaging global chemical and thermal heterogeneity in the subcontinental lithospheric mantle with garnets and xenoliths: Geophysical implications: Tectonophysics, v. 416, p. 289-309.

Osmundsen, P. T., Andersen, T. B., Markussen, S., and Svendby, A. K., 1998, Tectonics and sedimentation in the hanging wall of a major extensional detachment: the Devonian Kvamshesten basin, western Norway. : Basin Res., v. 10, p. 213-234.

Osmundsen, P. T., Braathen, A., Nordugulen, Ø., Roberts, D., Meyer, G., and Eide, E., 2003, The Devonian Nesna Shear Zone, north-central Norwegian Caledonides, and its regional implications.: J. Geol. Soc. Lond., v. 160, p. 137-150.

Ostisty, B. K., and Fedorovsky, Y. F., 1993, Main results of oil and gas prospecting in the Barents and Kara Sea inspire optimism, in Vorren, T. O., Bergsager, E., Dahl-Stamnes, Ø. A., Holter, E., Johansen, B., Lie, E., and Lund, T. B., eds., Arctic Geology and Petroleum Potential, Volume vol2, Norwegian Petroleum Society (NPF), Special Publication, p. 243-252.

Otto, S. C., and Bailey, R. J., 1995, Tectonic Evolution of the Northern Ural Orogen: Journal of the Geological Society, London, v. 152, p. 903-906.

Palme, H., and O'Neill, H. S., 2005, Cosmochemical estimates of mantle composition, in in Carlson, R. W., Holland, H. D., and Turekian, K. K., eds., The Mantle and Core. Treatise on Geochemistry, vol 2.: New York, Elsevier, p. 1-38.

Parker, R. L., 1972, The rapid calculation of potential anomalies: Geophysical Journal of the Royal Astronomical Society, v. 31, p. 447-455.

Paterson, N. R., and Reeves, C. V., 1985, Applications of gravity and magnetic surveys:The state-of-the-art in 1985: Geophysics, v. 50, p. 2558-2594.

Pavlenkova, N. I., 1997, General features of the upper mantle structure from seismic data, in Fuchs, K., ed., Upper Mantle Heterogeneities from Active and Passive Seismology: The Netherlands, Kluwer Academic Publishers, p. 225– 236.

Pavlis N.K., Holmes S.A., Kenyon S.C., and J.K., F., 2008, An Earth Gravitational Model to Degree 2160: EGM 2008, presented at Session G3: "GRACE Science Applications", EGU: Vienna.

Pease, V., and Scott, R. A., 2009, Crustal affinities in the Arctic Uralides, northern Russia: significance of detrital zircon ages from Neoproterozoic and Palaeozoic sediments in

Novaya Zemlya and Taimir.: Journal of the Geological Society, London v. 166, p. 517-527.

Pedersen, R. B., Furnes, H., and Dunning, G. R., 1988, Some Norwegian ophiolite complexes reconsidered: norges geologiske undersøkelse, v. Spec.Publ. 3, p. 80- 85.

Petrov, O. V., Sobolev, N. N., Koren, T. M., Vasiliev, V. E., Petrov, E. O., Larssen, G. B., and Smelror, M., 2008, Palaeozoic and Early Mesozoic evolution of the East Barents and Kara Seas sedimentary basins: Norwegian Journal of Geology, v. 88, p. 227-234.

Pinet, C., and Jaupart, C., 1987, The Vertical-Distribution of Radiogenic Heat-Production in the Precambrian Crust of Norway and Sweden - Geothermal Implications: Geophysical Research Letters, v. 14, p. 260-263.

Popowski, T., Connard, G., Tull, S., and Bashilov, V., 2006, GMSYS-3D Gravity and Magnetic Modeling for OasisMontaj- User Guide.: Northwest Geophysical Associates, v. Corvallis Oregon.

Poudjom Djomani, Y. H., O'Reilly, S. Y., Griffin, W. L., and Morgan, P., 2001, The density structure of subcontinental lithosphere through time: Earth and Planetary Science Letters, v. 184, no. 3-4, p. 605-621.

Pratsch, J. C., 1998, Gravity data define basin structure and the location of major oil and gas reserves: Examples from Subandean basins, Tunisia, and the U. S. Rocky Mountain region, in Gibson, R. I., and Millegan, P. S., eds., Geologic applications of gravity and magnetics: Case histories, Volume 43, SEG Geophysical Reference Series 8 and AAPG Studies in Geology, p. 28-31.

Prestvik, T., 1978, Cenozoic plateau lavas of Spitsbergen: a geochemical study, v. Arbok-Norsk Polarinstitutt no. v.1977, p. 129-142.

Prieto, C., 1993, Gulf of Mexico continental slope-undersanding the magnetic response due to salt intrusion, Footnotes on interpretation, Volume 1 Integrated geophysics corporation.

Puchkov, V. N., 1997, Structure and geodynamics of the Uralian orogen, in Burg, J. P., and Ford, M., eds., Orogeny Through Time (Spec. Publ.): London, Geol. Soc. of London., p. 201-236.

Puchkov, V. N., 2002, Paleozoic evolution of the east European continental margin involved in the Uralide orogeny, in Brown, D., Juhlin, C., and Puchkov, V., eds., Mountain Building in the Uralides: Pangea to the Present, Volume 132, Geophysical Monograph series, p. 9-31.

Ramberg, I. B., Bryhni, I., Nottvedt, A., and Rangnes, K., 2008, The Making of a Land - The Geology of Norway, Geological Society of Norway, 624 p.:

Reeves, C., 2009, Aeromagnetic Surveys: Principles, Practice and Interpretation e-Published by GEOSOFT, p. 155.

Reid, A. B., Allsop, J. M., Granser, H., Millett, A. J., and Somerton, I. W., 1990, Magnetic Interpretation in 3 Dimensions Using Euler Deconvolution: Geophysics, v. 55, no. 1, p. 80-91.

Reynisson, R. F., Ebbing, E., and Skilbrei, J. R., 2009, The use of potential field data in revealing the basement structure in sub-basaltic settings. An example from the Møre margin, offshore Norway, v. 57, p. 753-771.

Reynolds, J. M., 1997, An Introduction to Applied and Environmental Geophysics, 796 p.:

Ritsema, J., van Heijst, H. J., and Woodhouse, J. H., 2004, Global transition zone tomography: J. Geophys. Res., v. 109, no. B02302, p. doi:10.1029/2003JB002610,.

Ritzmann, O., 2003, Architecture and geodynamic evolution of the Svalbard Archipelago, the Yermak Plateau and the Fram Strait oceanic province, from deep seismic experiments.: Reports on Polar Research, v. 439, no. Alfred Wegener Institute for Polar and Marine Research, Bremerhaven.

Ritzmann, O., and Faleide, J. I., 2007, Caledonian basement of the western Barents Sea: Tectonics, v. 26, no. 5, p. TC5014, doi:5010.1029/2006TC002059.

Ritzmann, O., and Faleide, J. I., 2009, The crust and mantle lithosphere in the Barents Sea/Kara Sea region: Tectonophysics, v. 470, p. 89-104.

Ritzmann, O., and Jokat, W., 2003, Crustal structure of northwestern Svalbard and the adjacent Yermak Plateau: evidence for Oligocene detachment tectonics and non-volcanic breakup: Geophysical Journal International, v. 152, no. 1, p. 139-159.

Ritzmann, O., Jokat, W., Czuba, W., Guterch, A., Mjelde, R., and Nishimura, Y., 2004, A deep seismic transect from Hovgård Ridge to northwestern Svalbard across the continental-ocean transition: A sheared margin study: Geophysical Journal International, v. 157, no. 2, p. 683-702.

Ritzmann, O., Jokat, W., Mjelde, R., and Shimamura, H., 2002, Crustal structure between the Knipovich Ridge and the Van Mijenfjorden (Svalbard): Marine Geophysical Researches, v. 23, no. 5-6, p. 379-401.

Ritzmann, O., Maercklin, N., Faleide, J. I., Bungum, H., Mooney, W. D., and Detweiler, S. T., 2007, A three-dimensional geophysical model of the crust in the Barents Sea region: model construction and basement characterization: Geophys. J. Int., v. 170, no. 1, p. 417-435.

Roberts, D., 1983, Devonian tectonic deformation in the Norwegian Caledonides and its regional perspectives: Norges geologiske undersøkelse Bulletin, v. 380, p. 85-96.

Roberts, D., 2003, The Scandinavian Caledonides; event chronology, palaeogeographic settings and likely modern analogues: Tectonophysics, v. 365, p. 283-299.

Roberts, D., 2007, Palaeocurrent data from the Kalak Nappe Complex, northern Norway: a key element in models of terrane affiliation: Norwegian Journal of Geology, v. 87, no. 3, p. 319-328.

Roberts, D., and Gale, G. H., 1978, The Caledonian-Appalachian Iapetus Ocean, in Tarling, D., ed., The evolution of the Earth's crust, p. 255-341.

Roberts, D., and Gee, D. G., 1985, An introduction to the structure of the Scandinavian Caledonides, in Gee, D. G., and Sturt, B. A., eds., The Caledonide Orogen - Scandinavia and Related Areas, John Wiley & Sons Chichester, p. 55– 68.

Roberts, D., Nordgulen, Ø., and Melezhik, V., 2007, The Uppermost Allochthon in the Scandinavian Caledonides: From a Laurentian ancestry through Taconian orogeny to Scandian crustal growth on Baltica, in Hatcher, R. D. J., Carlson, M. P., McBride, J. H., and Artinez Catalán, J. R., eds., 4D Framework of Continental Crust::Geological Society of America Memoir, Geological Society of America, p. 357-377.

Roberts, D., and Olovyanishnikov, V., 2004, Structural and tectonic development of the Timanide orogen, in Gee, D. G., and Pease, V., eds., The Neoproterozoic Timanide Orogen of Eastern Baltica., Volume 30, Geological Society, London, Memoirs, p. 47-57.

Roberts, D., and Siedlecka, A., 2002, Timanian orogenic deformation along the northeastern margin of Baltica, Northwest Russia and Northeast Norway, and Avalonia-Cadomian connections.: Tectonophysics, v. 352, p. 169-184.

Roberts, D., Siedlecka, A., and Olovyanishnikov, V. G., 2004, Neoproterozoic, passive-margin, sedimentary systems of the Kanin Peninsula, and northern and central Timan,

NW Russia., in Gee, D. G., and Paese, V. I., eds., The Neoproterozoic Timanide Orogen of eastern Baltica., Volume 30, Geological Society, London, Memoirs, p. 5-17.

Roberts, D. G., and Lippard, S., 2005, Inferred Mesozoic faulting in Finnmark: current status and offshore links: Norges Geologiske Undersøkelse Bulletin, v. 443, p. 55-60.

Roberts, R. J., Corfu, F., Torsvik, T. H., Ashwal, L. D., and Ramsay, D. M., 2006, Short-lived mafic magmatism at 560–570 Ma in the northern Norwegian Caledonides: U-Pb zircon ages from the Seiland Igneous Province: Geological Magazine v. 143, p. 887-903.

Robins, B., and Gardner, P. M., 1975, The magmatic evolution of the Seiland Province and Caledonian plate boundaries in northern Norway.: Earth and Planetary Science Letters, v. 26, p. 167-178.

Roest, W. R., Verhoef, J., and Pilkington, M., 1992, Magnetic Interpretation Using the 3-D Analytic Signal: Geophysics, v. 57, no. 1, p. 116-125.

Roslov, Y., Matveev, Y., Belyaev, I., Ivanova, N., and Sakoilina, T., Deep model of the Barents-Kara Region by results of geophysical investigations along regional lines 1-4 AR, in Proceedings International Geological Congress, AAA-05 Arctic petroleum provinces (ii): Petroleum geoscience of Russian Arctic basins (Abstract), August 6-14, Oslo, 2008., 2008.

Roslov, Y. V., Sakoulina, T. S., and Pavlenkova, N. I., 2009, Deep seismic investigation in the Barents and Kare Seas: Tectonophysics, v. 472, p. 301-308.

Rudnick, R. L., McDonough, W. F., and O'Connell, R. J., 1998, Thermal structure, thickness and composition of continental lithosphere: Chemical Geology, v. 145, p. 395-411.

Ryseth, A., Augustson, J. H., Charnock, M., Haugerud, O., Knutsen, S. M., Midbøe, P. S., Opsal, J. G., and Sundsbø, G., 2003, Cenozoic stratigraphy and evolution of the Sørvestsnaget Basin, southwestern Barents Sea: Norwegian Journal of Geology, v. 83, p. 107-130.

Saad, A. H., 1993, Interactive integrated interpretation of gravity, magnetic and seismic data-tools and examples, Offshore Technology Conference, Paper 7079-MS: Houston, Texas, p. 35-44.

Saalmann, K., and Thiedig, 2001, Tertiary West Spitsbergen fold and thrust belt on Brøggerhalvøya, Svalbard: Structural evolution and kinematics: Tectonics, v. 20, no. 6, p. 976-998.

Sakoulina, T. S., Telegin, A. N., and Tikhonova, I. M., 1999, Deep seismic studies on the geophysical Zapolyarnyi-Heisa reference profile: Izvestiya. Physics of Solid Earth, v. 35, p. 760-769.

Saltus, R. W., and Blakely, R. J., 2011, Unique geologic insights from “non-unique” gravity and magnetic interpretation: GSA Today, v. 21, no. 12, p. 4-11.

Sanner, S., 1995, Et seismisk hastighetsstudium i Barentshavet, Master Sc. Thesis, Geologicy Department, University of Oslo: Oslo, p. 149.

Schatsky, N. S., 1935, On tectonics of the Arctic. Geology and Economic Deposits in northern USSR,, v. 1,, p. 476-509 (in Russian).

Schlinger, C. M., 1985, Magnetization of lower crust and interpretation of regional magnetic anomalies: example from Lofoten and Vesterålen, Norway: Journal of Geophysical Research, v. 90, p. 11484-11504.

Schmidt, S., and Götze, H. J., 1998, Interactive visualization and modification of 3D models using GIS functions: Physics and Chemistry of the Earth, v. 23, no. 3, p. 289-295.

Schmidt, S., and Götze, H. J., 1999, Integration of data constraints and potential field modelling - an example from southern lower Saxony, Germany: Physics and Chemistry of the Earth, v. 24, no. 3, p. 191-196.

Semprich, J., Simon, N. S. C., and Podladchikov, Y. Y., 2010, Density variations in the thickened crust as a function of pressure,temperature, and composition: J. Earth Sci (Geol Rundsch), v. DOI 10.1007/s00531-010-0557-7.

Séranne, M., and Séguret, M., 1987, The Devonian basins of western Norway: tectonics and kinematics of extending crust. , in Dewey, J. F., and Hanckock, P. L., eds., Continental Extensional Tectonics, Geological Society, London, Special Publications 28, p. 537-548.

Sheriff, R. E., 2006, Encyclopedic Dictionary of Applied Geophysics,. SEG. ISBN 1560801182, 4th ed., p2.

Shipilov, E. V., and Vernokovsky, V. A., 2010, The Svalbard–Kara plates junction: structure and geodynamic history: Russian Geology and Geophysics, v. 51, p. 58-71.

Siedlecka, A., 1975, Late Precambrian stratigraphy and structure of the northeastern margin of the Fennoscandian Shield (East Finnmark - Timan region): Norges Geologiske Undersøkelse, v. 316, p. 313-348.

Siedlecka, A., and Roberts, D., 1995, Neoproterozoic sedimentation and subsequent tectonic deformation in the northern coastal areas of Norway and Russia: Norges geologiske undersøkelse, v. Special Publication.

Siedlecka, A., Roberts, D., Nystuen, J. P., and Olovyanishnikov, V. G., 2004, Northeastern and northwestern margins of Baltica in Neoproterozoic time: evidence from the Timanian and Caledonian orogens, in Gee, D. G., and Pease, V., eds., The Neoproterozoic Timanide Orogen of Eastern Baltica: London, Geological Society, Memoirs, 30, p. 169-190.

Sigmond, E. M. O., and Roberts, D., 2007, Geology of the Land and Sea areas of Northern Europe, Volume Special publication 10, Norges geologiske undersøkelse, p. 100.

Simon, N. S. C., and Podladchikov, Y. Y., 2008, The effect of mantle composition on density in the extending lithosphere: Earth and Planetary Science Letters, v. 272, no. 1-2, p. 148-157.

Skilbrei, J. R., 1991, Interpretation of Depth to the Magnetic Basement in the Northern Barents Sea (South of Svalbard). Tectonophysics, v. 200 no. 1-3, p. 127-141.

Skilbrei, J. R., 1993, Interpretation of geophysical data from the northwestern Barents Sea and Spitzbergen [Doktor Ingeniøravhandling: Universitetet I trondheim Norges Tekniske Høgskole, 192 p.

Skilbrei, J. R., 1995, Aspect of the geology of the southwestern Barents Sea from aeromagnetic data: Norges Geologiske Undersøkelse Bulletin, v. 427, p. 64-67.

Slagstad, T., Barrère, C., Davidsen, B., and Ramstad, R. K., 2008, Geophysical and thermal properties of pre-Devonian basement rocks on the Norwegian continental margin: Norges Geologiske Undersøkelse Bulletin, v. 448.

Smelror, M., 2011, ....en sten løftet fra mitt hjerte... En reise over Polhavet i Nansens og Frams geologiske fotefar, Tapir akademisk forlag.

Smelror, M., Petrov, O. V., Larssen, G. B., and Werner, S. C., 2009, Geological history of the Barents Sea, Norges geologiske undersøkelse, p. 1-135.

Smith, M. P., 2000, Cambro-Ordovician stratigraphy of Bjørnøya and North Greenland: constraints on tectonic models for the Arctic Caledonides and Tertiary opening of the Greenland Sea: Journal of the Geological Society, London, v. 157, p. 459-470.

Smith, M. P., and Rasmussen, J. A., 2008, Cambro-Silurian development of the Laurentian margin of the Iapetus Ocean in Greenland and related areas: Geological Society of America Memoir, v. 202, p. 137-167.

Spector, A., and Grant, F. S., 1970, Statistical models for interpreting aeromagnetic data: Geophysics, v. 35, p. 293-302.

Stadtler, C., Fichler, C., Hokstad, K., Fotland, B., Gram, C., Hanssen, P., Myrlund, E. A., and Wienecke, S., 2010, Salt imaging with Gravity Gradiometry and Magnetic Data-Nordkapp Basin, Barents Sea, 72nd EAGE Conference & Exhibition incoporating SPE EUROPEC 2010: Barcelona, Spain, p. 14-17 June.

Steel, R. J., and Worsley, D., 1984, Svalbard's post-Caledonian strata – an atlas of sedimentational patterns and palaeogeographic evolution, in Spencer, A. M., ed., Petroleum geology of the North European Margin: London, Graham and Trotman, p. 109-135.

Stemmerik, L., and Worsley, D., 2005, 30 years on – Arctic Upper Palaeozoic stratigraphy, depositional evolution and hydrocarbon prospectivity: Norwegian Journal of Geology, v. 85, p. 151-168.

Stephens, M. B., and Gee, D. G., 1985, A tectonic model for the evolution of the eugeoclinal terranes in the central Scandinavian Caledonides, in Gee, D. G., and Sturt, B. A., eds., The Caledonide Orogen–Scandinavia and Related Areas, John Wiley & Sons, Chichester p. 953– 970.

Stephens, M. B., and Gee, D. G., 1989, Terranes and polyphase accretionary history in the Scandinavian Caledonides: Geol. Soc. Am., v. Spec. Paper 230, p. 17- 30.

Stephenson, R. A., Yegorova, T., Brunet, M.-F., Stovba, S., Wilson, M., Starostenko, V., Saintot, A., and Kusznir, N., 2006, Late Palaeozoic intra- and pericratonic basins on the East European Craton and its margins, in Gee, D. G., and Stephenson, R. A., eds., European Lithosphere Dynamics: London, Geological Society, Memoirs, 32, p. 463–479.

Stixrude, L., and Lithgow-Bertelloni, C., 2005, Mineralogy and elasticity of the oceanic upper mantle: Origin of the lowvelocity zone: J. Geophys. Res., v. 110, no. B03204, doi:10.1029/2004JB002965.

Stoupakova, A. V., Henriksen, E., Burlin, Y. K., Larsen, G. B., Milne, J. K., Kiryukhina, T. A., Golynchik, P. O., Bordunov, S. I., Ogarkova, M. P., and Suslova, A. A., 2011, The geological evolution and hydrocarbon potential of the Barents and Kara shelves, in Spencer, A. M., Embry, A. F., Gautier, D. L., Stoupakova, A., and sorensen, K., eds., Arctic Petroleum Geology, Volume 35: London, Gelogical Society, p. 325-344.

Strand, T., and Kulling, O., 1972, Scandinavian Caledonides, John Wiley and Sons, Interscience, London, p. 302.

Talwani, M., 1973, Computer Usage in the Computation of Gravity Anomalies: Methods in Computational Physics, v. 13, p. 343-389.

Terry, M. P., Robinson, P., Hamilton, M. A., and Jercinovic, M. J., 2000, Monazite geochronology of UHP and HP metamorphism, deformation, and exhumation, Nordøyane, Western Gneiss Region, Norway: American Mineralogist, v. 85, p. 1651-1664.

Tomoo, K., 1995, Thermal diffusivity of olivine under upper mantle conditions: Geophysical Journal International, v. 122, no. 1, p. 63-69.

Torsvik, T. H., and Andersen, T. B., 2002, The Taimyr fold belt, Arctic Siberia: timing of prefold remagnetisation and regional tectonics: Tectonophysics, v. 352, p. 335-348.

Torsvik, T. H., Smethurst, M. A., Meert, J. G., Van der Voo, R., McKerrow, W., Brasier, M. D., Sturt, B. A., and Walderhaug, H. J., 1996, Continental break-up and collision in tha Neoproterozoic and Palaeozoic- A tale of Baltica and Laurentia.: Earth Science Reviews, v. 40, no. 3-4, p. 229-258.

Torsvik, T. H., Smethurst, M. A., Van der Voo, R., Trench, A., Abrahamsen, N., and Halvorsen, E., 1992, Baltica. A synopsis of Vendian-Permian Paleomagnetic data and their Palaeotectonic implications. : Earth Sci. Rev., v. 33, p. 133-152.

Torsvik, T. H., and Steinberger, B., 2008, From continental drift to mantle dynamics, in Slagstad, T., and Dahl, R., eds., Geology for society for 150 years., Norges geologiske undersøkelse.

Trettin, H. P., 1987, Pearya: a composite terrane with Caledonian affinities in northern Ellesmere Island: Canadian Journal of Earth Sciences, v. 24, p. 224-245.

Trettin, H. P., 1998, Pre-Carboniferous geology of the northern part of the Arctic islands: Chapter 4: Geology of Pearya: Geological Survey Canada Bulletin, v. 425, p. 108-192.

Tsikalas, F., 1992, A study of seismic velocity, density and porosity in the Barents Sea wells (N. Norway): (Unpublished Master Thesis), University of Oslo, Norway.

Tulina, Y. V., Shemeleva, I. B., Sokolov, B. V., Sakulina, T. S., Nechkaev, S. A., Pavlenkin, A. D., Verba, M. L., and Nardov, N. M., 1988, Chief peculiarities of the southern part of the Barents Sea deep structure from DSS data.: Geophysical Fields of Atlantic Ocean. URSS Acad. Sci. Moscow, p. 34-51 (in Russian).

Turcotte, D. L., and Schubert, G., 2002, Geodynamics, Cambridge University Press, 472 p.:

Van Roermund, H., 2009, Recent progress in Scandian ultrahigh-pressure metamorphism in the northernmost domain of the Western Gneiss Complex, SW Norway: continental subduction down to 180–200 km depth Journal of geological Society, v. 166, p. 739-751.

Van Roermund, H., and Drury, M. R., 1998, Ultra-high pressure (P > 6 GPa) garnet peridotites in Western Norway: exhumation of mantle rocks from > 185 km depth Terra Nova, v. 10, no. 6, p. 295-301.

Vanicek, P., and Christou, N. T., 1994, Geoid and its geophysical interpretations:, CRC Press, Florida., 368 p.:

Vendeville, B., ongxing, G., and ackson, M. P. A., 1995, Scale models of salt tectonics during basement-involved extension: Petroleum Geosciences, v. 1, p. 179-183.

Verba, M. L., and Sakoulina, T. S., 2001, The Reconstruction of the Early Paleozoic Structure of the Barents Sea Sedimentary Basin Inferred from Geophysical Surveys along Profile 1-AR: Polarforschung, v. 69, p. 85-94.

Verduzco, B., Fairhead, J. D., Green, C. M., and MacKenzie, C., 2004, New insights into magnetic derivatives for structural mapping.: The Leading Edge, v. 23, p. 116-119.

Werner, S. C., Ebbing, J., Litvinova, T. P., and Olesen, O., 2011, Structural interpretation of the Barents and Kara Seas from gravity and magnetic data, in Spencer, A. M., Embry, A. F., L., G. D., Stoupakova, A., and Sørensen, K., eds., Arctic Petroleum Geology, Volume 35: London, Geological Society, p. 197-208.

Wijns, C., Perez, C., and Kowalczyk, P., 2005, Theta map: Edge detection in magnetic data: Geophysics, v. 70, p. 39-43.

Worsley, D., 2006, The post-Caledonian geological development of Svalbard and the Barents Sea: Norsk Geologisk Førening, Abstracts and Proceedings, v. 3, p. 5-21.

Wyillie, P., 1995, Experimental petrology of upper mantle materials, processes and products: Petrology v. 20, no. 4, p. 429-468.

Wyllie, P. J., 1988, The origin of kimberlite: Journal of Geophysical Research, v. 85, p. 6902-6910.

Young, I., 1995, Huismans to retire from Courtaulds: Chemical Week, v. 157, no. 23, p. 22-22.

Ziegler, P. A., 1988 Evolution of the Arctic-North Atlantic and the Western Tethys: Memoir American Association of Petroleum Geologists, v. 43, p. 1-198.

Ziegler, P. A., 1989, Evolution of Larussia: a study in Late Paleozoic Plate Tectonics., Dordrecht, The Netherlands, Kluwer Academic Publishers, 102 p.:

Zienkiewicz, O. C., 1977, The Finite Element Method: McGraw-Hill, New York.

Zonenshain, L. P., Kuzmin, M. I., and Natapov, L. M., 1990, Geology of the USSR: a plate tectonic sythesis.: Geodynamic Series, American Geophyisical Union, Washington DC, v. 21, p. 242.

Åm, K., 1975, Aeromagnetic basements complex mapping north of latitude 62N. Norway: Norges Geologiske Undersøkelse, v. 316, p. 351-374.